Selected Papers in the Hydrologic Sciences 1986

December 1986

United States
Geological
Survey
Water-Supply
Paper 2310

Selected Papers
in the
Hydrologic Sciences
1986

Edited by Seymour Subitzky

December 1986

U.S. GEOLOGICAL SURVEY WATER-SUPPLY PAPER 2310

DEPARTMENT OF THE INTERIOR

DONALD PAUL HODEL, Secretary

U.S. GEOLOGICAL SURVEY

Dallas L. Peck, Director

PREFACE

This is the fourth issue of the Water-Supply Paper series *Selected Papers in the Hydrologic Sciences* comprising 13 topical papers that address a broad range of topics including model simulations of ground- and surface-water systems, hydrogeochemistry, limnology, and selected physical and chemical techniques for hydrologic studies. It is aimed at meeting widespread public and professional needs for results of broad-based integrated hydrologic studies derived from the Federal research program, Federal-State cooperative program, and, to some extent, work done on behalf of other Federal agencies.

As a Survey-managed journal-type publication, *Selected Papers* is intended to serve as a forum that encourages dialogue between readers and authors. Participation in such dialogue among hydroscientists within and outside the Federal sector would be beneficial. Discussion papers by *all* members of the hydroscience community is desired. A discussion section for readers' comments and authors' replies will be included in each issue. Such discussion papers for this issue will be open until October 1987. Address comments to Editor, *Selected Papers in the Hydrologic Sciences*, U.S. Geological Survey, 444 National Center, Reston, VA 22092.

Seymour Subitzky

SI and Inch-Pound Unit Equivalents

International System of Units (SI), a modernized metric system of measurement. All values have been rounded to four significant digits. Use of hectare (ha) as an alternative name for square hectometer (hm^2) is restricted to measurement of land or water areas. Use of liter (L) as a special name for cubic decimeter (dm^3) is restricted to the measurement of liquids and gases.

Multiply SI units	By	To obtain inch-pound units
Length		
micrometer (μm)	0.000 039 37	inch (in)
millimeter (mm)	0.039 37	inch (in)
centimeter (cm)	0.393 7	inch (in)
meter (m)	3.281	foot (ft)
	1.094	yard (yd)
kilometer (km)	0.621 4	mile (mi)
Area		
centimeter^2 (cm^2)	0.155 0	inch^2 (in^2)
meter^2 (m^2)	10.76	foot^2 (ft^2)
	1.196	yard^2 (yd^2)
	0.000 247 1	acre
hectometer^2 (hm^2)	2.471	acre
kilometer^2 (km^2)	0.386 1	mile^2 (mi^2)
Volume		
centimeter^3 (cm^3)	0.061 02	inch^3 (in^3)
milliliter (mL)	0.061 02	inch^3 (in^3)
liter (L)	61.02	inch^3 (in^3)
	0.035 31	foot^3 (ft^3)
	33.82	ounce, fluid (oz)
	2.113	pint (pt)
	1.057	quart (qt)
	0.2642	gallon (gal)
meter^3 (m^3)	35.31	foot^3 (ft^3)
	1.308	yard^3 (yd^3)
	264.2	gallon (gal)
	0.000 810 7	acre-foot (acre-ft)
kilometer^3 (km^3)	0.239 9	mile^3 (mi^3)
Volume per unit time (includes flow)		
gram per minute (g/min)	0.035 27	ounce (avoirdupois) per minute (oz/min)
milliliter per minute (mL/min)	0.033 82	ounce (fluid) per minute (oz/min)
	0.035 31	foot^3 per second (ft^3/s)
liter per second (L/s)	15.85	gallon per minute (gal/min)
meter per second (m/s)	3.281	foot per second (ft/s)
meter per day (m/d)	3.281	foot per day (ft/d)
meter^2 per day (m^2/d)	10.76	foot^2 per day (ft^2/d)

Multiply SI units	By	To obtain inch-pound units
Volume per unit time (includes flow)—Continued		
meter^3 per second (m^3/s)	35.31	foot^3 per second (ft^3/s)
	15 850	gallon per minute (gal/min)
Mass		
microgram (μg)	0.000 015 43	grain (gr)
gram (g)	0.035 27	ounce, avoirdupois (oz avdp)
kilogram	0.002 205	pound, avoirdupois (lb avdp)
Mass per unit volume		
microgram per liter (μg/L)	0.000 058 41	grain per gallon (gr/gal)
milligram per liter (mg/L)	0.058 41	grain per gallon (gr/gal)
Transmissivity		
meter^2 per day (m^2/d)	10.76	foot^2 per day (ft^2/d)
Force per unit area		
kilopascal (kPa)	0.145 03	pound-force per inch^2 (lbf/in^2)
kilogram per meter^2 (kg/m^2)	0.204 8	pound-force per foot^2 (lbf/ft^2)
kilogram per meter^3 (kg/m^3)	0.624 6	pound-force per foot^3 (lbf/ft^3)
Temperature		
degree Celsius (°C)	Temp °F = 1.8 temp °C + 32	degree Fahrenheit (°F)
Specific conductance		
microsiemens per centimeter at 25 degrees Celsius (μS/cm at 25°C)	1.000	micromho per centimeter at 25 degrees Celsius (μmho/cm at 25°C)
millisiemens per meter at 25 degrees Celsius (mS/m at 25°C)	1.000	millimho per meter at 25 degrees Celsius (mmho/m at 25°C)

Any use of trade names and trademarks in this publication is for descriptive purposes only and does not constitute endorsement by the U.S. Geological Survey.

CONTENTS

Evaluation of Size-Distribution Effects and Laboratory Precision in the Analysis of Bottom Materials

By Dennis R. Helsel *and* Gregory F. Koltun

Abstract

Bottom materials may be useful in evaluating areal and temporal changes in concentrations of certain chemical constituents in the overlying waters. They are particularly useful for detecting hydrophobic compounds that may be present in the stream waters at low concentrations or at intermittent intervals. The particle-size distribution in the bottom materials must be considered when areal or temporal changes in sediment chemistry are interpreted.

Bottom-material samples were collected at two sites on the Cuyahoga River in Cuyahoga and Portage Counties, Ohio. Multiple samples were collected from one cross section at each site and separated into three fractions based on particle size (less than 2 millimeters to 63 micrometers, less than 63 micrometers to 20 micrometers, and less than 20 micrometers). Each fraction was then separately analyzed for six trace metals (chromium, copper, iron, lead, manganese, and zinc).

Significant differences in metal concentrations were observed within cross sections as well as between sites. The coefficient of variability within the cross sections decreased as the particle size decreased in the analyses for chromium, copper, iron, and lead, whereas the variability remained constant for manganese and zinc. Metals concentrations, however, generally increased as particle size decreased. An "index of discrimination" indicated that the less than 20-micrometer fraction was superior for detecting between-site differences in concentrations of metals in the bottom materials; the less than 63 to 20-micrometer fraction ranked second, and the less than 2 millimeter to 63-micrometer fraction ranked third. Replicate laboratory analyses were generally found to be unnecessary because differences in metal concentrations due to laboratory extraction and analysis were small.

INTRODUCTION

Bottom materials compose the upper part of a lakebed or streambed. They are derived primarily from material washed into the stream from the basin or are eroded from the river or lakebed itself. Because bottom materials interact with overlying waters, they may sorb certain chemical constituents (metals, nutrients, and pesticides and other organic chemicals) that might otherwise be carried away by moving water.

Bottom materials may be useful as long-term integrators of water quality. They may also be used to detect short-term contaminant discharges that may go unnoticed in intermittent surface-water sampling programs. Many of the hydrophobic compounds in stream waters are at low concentrations that are difficult to detect, yet these compounds may accumulate to large concentrations in the underlying sediments. Chemical analysis of compounds sorbed to bottom materials may therefore provide a rapid, reliable, and relatively inexpensive method for indirectly comparing long-term water quality at different sites. However, such comparisons are not without difficulty because factors other than upstream inputs can influence chemical concentrations in bottom materials. Particle-size distribution is the most significant of these.

Clay particles have greater surface areas per unit weight than do larger size grains; thus, clay particles are an excellent substrate for adsorption (surface-coating) reactions. Clay-rich sediments can be expected to have greater concentrations of adsorbed chemicals than sandy or gravel-rich sediments if all other conditions are identical. Concentration variations due to differences in the particle-size distribution of sediments could be mistakenly attributed to differences in water quality. Conversely, real differences in water-quality could be masked by differences in the particle-size distributions between samples. Particle-size effects should therefore be taken into account when bottom-sediment data are collected and interpreted.

Purpose and Scope

The first objective of the study described in this paper is to document differences in the concentrations of metals in bottom-material samples collected at several stations along a single cross section of a stream. The second objective is to determine whether analysis of one size fraction, rather than of an entire sample, will reduce

the variability in metals concentrations for samples taken at a single site. If the second objective is proved, any differences between sites should be more easily discerned.

The third and final objective of the study is to provide better estimates of laboratory precision for the U.S. Geological Survey's bottom-material extraction method (Skougstad and others, 1979, p. 19-20). Current precision estimates for the extraction of chromium, copper, iron, lead, manganese, and zinc, the six metals investigated in this report, are either unavailable or poorly defined (Skougstad and others, 1979).

Previous Studies

Numerous investigators have found correlations between decreasing particle size and increasing metals concentrations in bottom materials. Shimp and others (1971) and Thomas and others (1975) reported this for Great Lakes sediments. Fitchko and Hutchinson (1975) found this relationship for a number of metals in rivers emptying into the Great Lakes. Haushild and others (1975) found differences in radionuclide concentrations within the same channel section of the Columbia River. They demonstrated that these differences were due primarily to the different particle sizes of the bottom materials. Gibbs (1977) related particle size to the weight percentage (concentration) of metals in Amazon and Yukon Rivers sediments. Highest percentages were found associated with particles 10 to 20 μm and smaller. Shuman and others (1977) found that concentrations of metals increased as particle size decreased in sediments from Haw and New Hope Rivers in North Carolina.

Isolating a single particle-size fraction is one common technique used to remove the influence of particle size on the concentrations of metals in bottom materials. Rickert and others (1977) isolated the <20-μm fraction (clay and fine silt) and showed that by using this procedure, they eliminated concentration differences due to particle size for Willamette River sediments. Helmke and others (1977) used the clay size (<20-μm) fraction only, and demonstrated that this allowed detection of anomalous metals values. Bopp and Biggs (1981) chose the sand-silt break (<63 μm), whereas Leland and McNurney (1974) used a <100-μm separation.

Location of Study Sites

Bottom-material samples were collected at an urban site and at a rural headwater site on the Cuyahoga River in northeastern Ohio. Because of the unusual U-shaped channel configuration, these sampling sites were within the same soil association, approximately 30 miles from each other (fig. 1).

The urban site selected was the Cuyahoga River at the Harvard Avenue bridge in Cleveland, lat 41°26′51″N., and long 81°41′05″W., U.S. Geological Survey station number 04208503. This site was chosen because it is within a highly industrialized area, is downstream of all major tributaries to the river, and yet is above backwater influences from Lake Erie.

The rural site selected was the Cuyahoga River near Hiram, in Portage County, Ohio, lat 41°18′37″N., and long 81°11′42″W. Samples were taken at the State Route 82 bridge, 1.3 mi east of Mantua Corners and 2.7 mi west of Hiram.

METHODS OF STUDY

Sampling Techniques

Three stations along a cross section were sampled at each of the two sampling sites. Either a BMH-60 TM (trace-metal compatible) sampler or a linear polyethylene freezer container (capped at the bottom to prevent loss of fine particles while the sample was brought to the surface) was used to collect the bottom-material samples. The location of all except one of the stations were chosen at random. One station at the Harvard Avenue site was selected because of the noticeably different particle-size distribution of the bottom materials at the surface of the streambed.

The experimental design is outlined in table 1. Three parallel experiments should be done, one for each of the three size fractions discussed below. Each experiment tests a series of influences to determine whether they significantly affect the metals concentrations observed. Note that the laboratory influence was split into two components—one for subsampling and digestion procedures within the lab, and the other for analytical measurement.

Replicate observations were obtained so that the variability within each influence could be assessed. Our choice of the number of repetitions per influence was guided by a review of current literature.

Size-Separation Methods

After the sample was sieved through a 2-mm plastic screen in the field, a portion of the sample was reserved for particle-size distribution analysis. Particle-size distribution was later determined at the Columbus, Ohio, district office of the U.S. Geological Survey by means of sieves and bottom-withdrawal tubes. Most of each original sample was frozen in dry ice at the site and was kept frozen until size separation. Samples were freeze-dried and separated into sand (<2 mm to 63 μm), coarse silt (<63 μm to 20 μm), and fine silt and clay
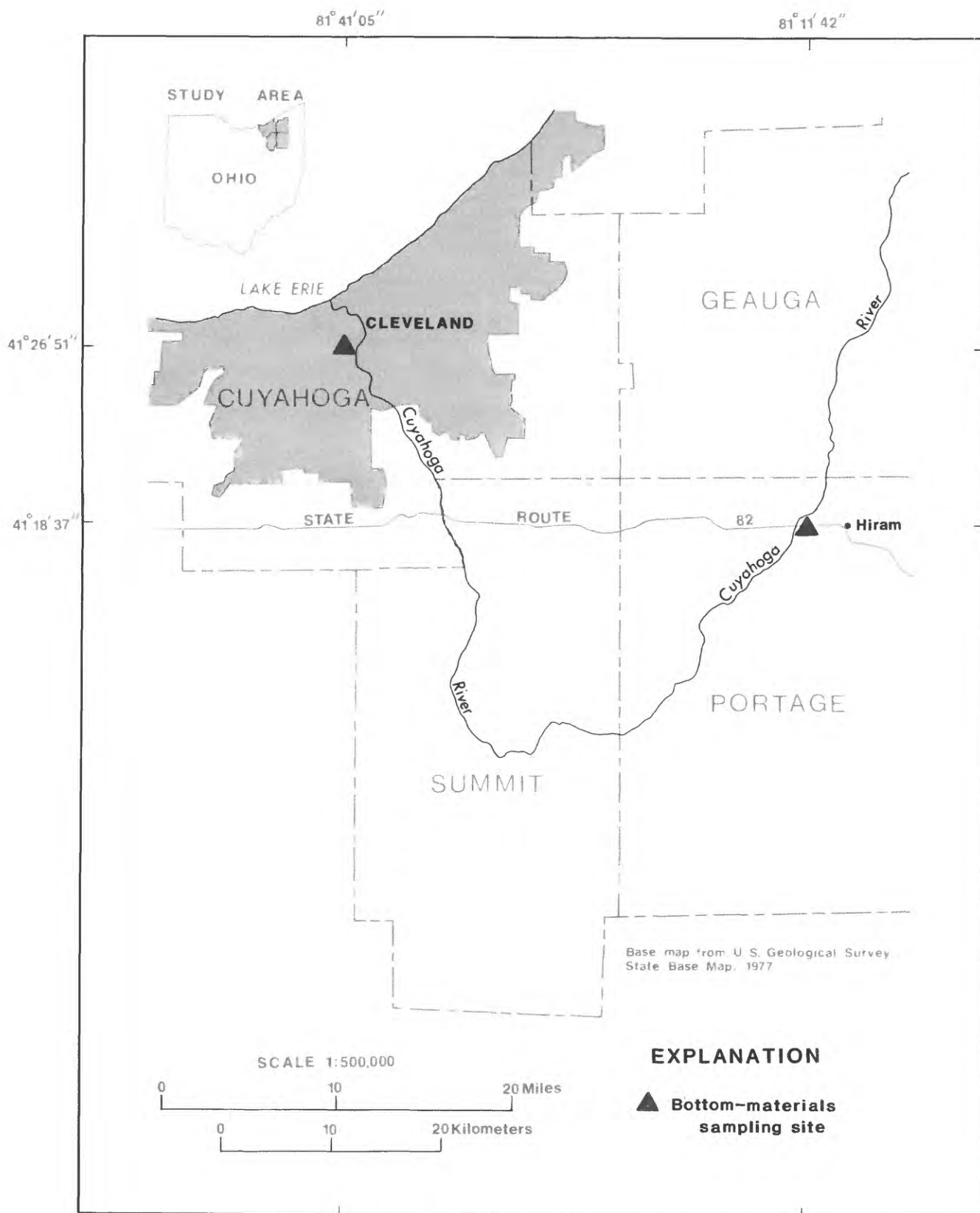
Figure 1. Location of sampling sites.

Table 1. Experimental design

Influence	Repetitions
Particle size	3 particle sizes.
Site	2 sites.
Station (cross section)	3 stations per site.
Laboratory:	
Digestion	3 digestions per station.
Measurement (error)	3 measurements per digestion.

(<20 μm) fractions by means of a microparticle classifier at the U.S. Geological Survey district office in Madison, Wis.

Laboratory Analysis

Laboratory precision is determined by differences in concentration among replicate analyses of the same sample. Imprecise analyses are not primarily a result of operator error, but are due to variation in such things as sample homogeneity, chemical reagents, digestion efficiency, and instrument performance. A large amount of analytical variability (imprecision) may obscure real and important differences in sample concentrations caused by other influences in the experimental design. Laboratory precision must therefore be known in order to assess the magnitude of influence effects.

Eighteen size-fractioned samples, labeled only as A through R, were sent to the U.S. Geological Survey Central Laboratory in Doraville, Ga. Each sample was split into three portions and digested separately by means of techniques discussed by Skougstad and others (1979). Triplicate atomic-absorption spectrophotometric (AAS) analyses of the liquid digestate were performed for each of the 54 digestions. Concentrations of iron, manganese, lead, zinc, copper, and chromium were determined.

DATA ANALYSIS

The following terms and definitions are used in presenting the data analysis.

1. In referring to the particle-size fractions collected and analyzed:
size fraction 1 = <2 mm to 63 μm (sand),
size fraction 2 = <63 μm to 20 μm (coarse silt), and
size fraction 3 = <20 μm (fine silt and clay).

2. A "response" is a numerical result observed for a particular experiment.

Comparison of Concentrations

Average metal concentrations obtained for each size fraction are listed in table 2. In general, the highest mean metal concentrations were found in size fraction 3. Mean concentrations of copper, lead, and zinc, however, were found to be higher in size fraction 2 at the Harvard Avenue site. These results are similar to those obtained by other researchers. (See the "Previous Studies" section of this report.)

The increasing metal concentrations as particle size decreases suggest that the metals are attaching to particle surfaces. Sediments that have different particle-size distributions will therefore have different "whole-sample" concentrations.

Determination of Significant Influences

Analysis of variance is used to determine whether an observed response due to the influence being tested is large enough to be distinguished above the background variability of the data. The total variation of the data is separated into the amount due to each influence, and to measurement error. An F statistic is computed in order to determine whether the response due to each influence is significant.

A two-way factorial analysis of variance (ANOVA) was performed to investigate the variation in metal concentrations with the main influence "site" and "particle size" and the nested subordinate influences "station" and "digestion" (fig. 2). This ANOVA tested (1) whether there are statistically significant differences in average metal concentrations between size fractions, sites, stations, and digestions and (2) whether the site and particle-size effects showed dependency on one another.

Many chemical analyses result in increasing variability as concentrations increase. This heterogeneity of variance violates the assumption of constant variance of experimental errors required for meaningful interpretation of the ANOVA test.

Plots of total laboratory variance (which is composed of the subsampling-digestion and measurement variances) as a function of average station concentration (within each cross section) were prepared in order to test for heterogeneity of variance. Laboratory variance should show no trend in relation to concentration to be considered homogeneous. Laboratory variances of chromium, lead, and iron concentrations were found to be homogeneous. Zinc, copper, and manganese, however, had laboratory variances with increasing linear trends in relation to concentration, as determined by ordinary least squares (OLS) regression. Therefore, base 10 logarithms of concentrations were used in the ANOVA for these three metals. The fact that no hetero-

Table 2. Mean metal concentrations by site and size fraction

Metal	Size fraction	Concentration (μg/g) at site Cleveland[1]	Concentration (μg/g) at site Hiram[2]
Chromium	<2 mm-63 μm	12	3.0
	<63 μm-20 μm	20	9.0
	<20 μm	65	14
Copper	<2 mm-63 μm	64	5.3
	<63 μm-20 μm	1,200	23
	<20 μm	570	84
Iron	<2 mm-63 μm	4,700	7,900
	<63 μm-20 μm	10,000	10,000
	<20 μm	15,000	18,000
Lead	<2 mm-63 μm	41	26
	<63 μm-20 μm	310	55
	<20 μm	260	120
Manganese	<2 mm-63 μm	170	1,000
	<63 μm-20 μm	320	1,000
	<20 μm	520	3,100
Zinc	<2 mm-63 μm	200	32
	<63 μm-20 μm	1,800	170
	<20 μm	1,300	220

[1]Cuyahoga River at Cleveland, Ohio (Harvard Avenue Bridge).
[2]Cuyahoga River near Hiram, Ohio (State Route 82 Bridge).
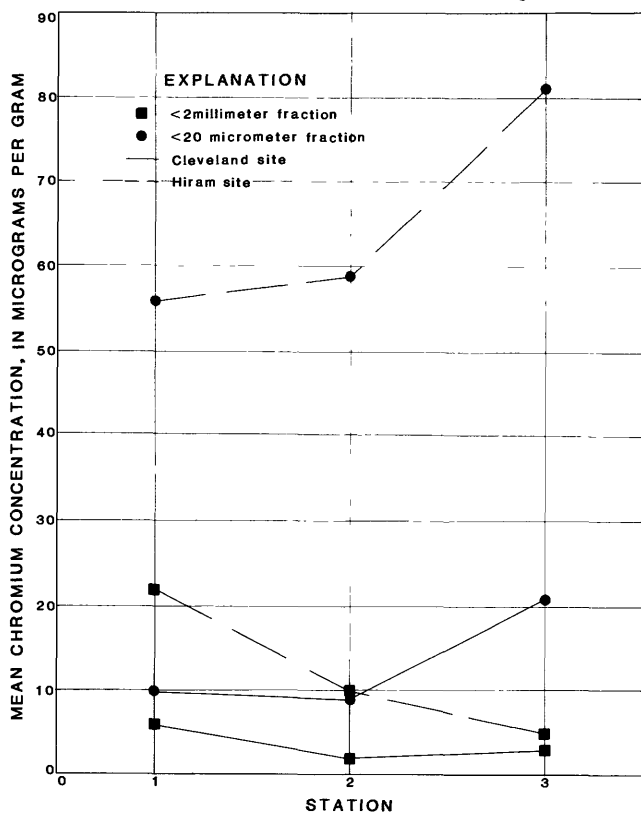
Figure 2. Comparison of mean chromium concentrations in the <2-mm and <20-μm fractions of the stream-bottom materials.

geneity of the laboratory variance was observed with the log-transformed concentrations indicated that the variances had been stabilized.

Results of the ANOVA are given below. An "X" indicates that the influence identified in the left-hand column had a significant (95-percent confidence level) effect on the metal concentration.

Influences	Copper[1]	Chromium	Iron	Lead	Manganese[1]	Zinc[1]
Site	X	X		X	X	X
Particle size	X	X	X	X	X	X
Site, size interaction						
Station	X	X		X	X	X
Digestion		X	X	X	X	X

[1]Base 10 logarithm of concentration used.

Significant differences in metal concentrations were observed between bottom materials of differing particle size for all metals analyzed. Metal concentrations differed significantly between sites and between stations for all metals except iron. However, no significant interaction effect was observed between the site and particle-size factors. The lack of an interaction effect indicates that the site and particle-size effects are inde-

pendent of one another. Finally, concentrations differed significantly between repetitive digestions for all metals except copper. However, although there may be statistically significant differences in metal concentrations due to an influence, the magnitude of these differences may be quite small and therefore be of little consequence from a practical standpoint.

Comparison of Size Fractions

Metal concentrations differed among the three size fractions as determined by means of the two-way ANOVA. Separate ANOVAs were performed for each of three size fractions to determine whether one fraction provided superior discrimination between samples obtained at the urban and rural sites.

The ANOVA procedure produces estimates of the variance attributable to each factor. Thus, metal concentrations that differed significantly between sites would ideally have a large percentage of the variance due to the site factor, and low percentages due to station and laboratory differences. Table 3 reports the variance and percent variance attributable to each influence for the three size fractions. Note that some influences previously found to be statistically significant contribute only a very small percentage of the total data variance. The square root of the variance, divided by the mean concentration, results in the coefficient of variability (CV). This is a relative measure of the data variation expressed as a percentage of their mean. Table 4 shows the CV attributable to each influence.

An "index of discrimination" was devised to compare the adequacy of each size fraction for detecting differences in metal concentrations between the two sites. We computed the index by dividing the site CV by the cross-section CV, and dividing that quantity by the laboratory CV. Thus, a size fraction having a large site CV and low cross-section and laboratory CV would result in a large index of discrimination. The size fraction having the largest index value should provide the greatest discrimination between sites. Table 5 lists the indices for the six metals. On the basis of this index, size fraction 3 ($<20\,\mu$m) provided superior discrimination for chromium, copper, and zinc, and was as effective as size fraction 2 for manganese and lead. All three size fractions were equally effective for iron.

A second method of rating the size fractions involved comparisons of significance levels obtained in the ANOVA test of the null hypothesis that mean metal concentrations are equal at the two sites. To make this comparison, we computed expected concentrations for <2 mm and $<63\,\mu$m fractions from the concentration and particle-size data. The concentrations observed for each size fraction were multiplied by the percentage of that size fraction in the sample (table 6) and summed to obtain the concentrations for the <2 mm fraction. Similar computations were made in computing concentrations for a sample composed entirely of particles $<63\,\mu$m in diameter, but here the percentage of sample in a given size range was divided by the total percentage of sample composed of particles $<63\,\mu$m in diameter before multiplying and summing the concentrations. These computed concentration data were then compared with the actual concentration data observed for the $<20\,\mu$m fraction.

For each actual or computed fraction, the significance of the site discrimination was based on the F statistic (the ratio of the between-site to within-site variance). Table 7 lists the significance probabilities associated with the null hypothesis that the mean metals concentrations are equal at the two sites. A smaller value indicates that there is a lower probability that the mean concentrations are equal at the two sites. Those fractions that provide a superior level of discrimination should also show low significance probabilities. Table 7 suggests that the $<63\,\mu$m and $<20\,\mu$m fractions usually discriminated between samples collected at the two sites with more certainty than the <2 mm fraction. Illustration of this can be seen in figure 2, where mean chromium concentrations at each station are plotted for the <2 mm and $<20\,\mu$m size fractions. The $<20\,\mu$m size fraction shows greater separations between lines representing the two sites. .

The high ANOVA significance probabilities associated with each size fraction for iron supports the previous conclusion that mean iron concentrations were virtually the same at both sites.

Precision

Precision is the repeatability of a measurement. The standard deviation of repeated concentration measurements is taken here as the measure of precision. The ANOVA design of this study divided laboratory precision into two components—subsampling-digestion, and repetitive analysis of a single digestate (error). The variances associated with each of these components were added to produce the total laboratory variance for a sample.

To calculate the precision for chromium, iron, and lead analyses, we transformed the total laboratory variance to a standard deviation by taking the square root. These metals did not show heterogeneity of variance; thus, one precision (standard deviation) value is presented in table 8 for each size fraction and metal.

Laboratory variance had a linear relationship to sample concentration for copper, manganese, and zinc. This is consistent with a lognormal distribution of concentration data. Given a lognormal distribution, equations from Aitchison and Brown (1957) can be used to

Table 3. Variance and percentage of variance in metals concentration by size fraction and source of variation

Metal	Size fraction	Variance, by source			
		Site	Station	Digestion	Error
Chromium	<2 mm-63 μm	2.67×10^1	3.05×10^1	2.28×10^{-1}	3.52×10^{-1}
	<63 μm-20 μm	5.22×10^1	1.52×10^1	2.46×10^0	1.55×10^1
	<20 μm	1.29×10^3	1.05×10^2	2.70×10^1	3.07×10^1
Copper[1]	<2 mm-63 μm	6.54×10^{-1}	5.9×10^{-2}	8.43×10^{-3}	1.80×10^{-3}
	<63 μm-20 μm	1.20×10^0	1.37×10^{-1}	.0	5.35×10^{-3}
	<20 μm	3.01×10^{-1}	3.0×10^{-2}	.0	1.27×10^{-3}
Iron	<2 mm-63 μm	4.55×10^4	1.53×10^7	1.47×10^6	9.13×10^4
	<63 μm-20 μm	.0	1.62×10^4	1.87×10^6	2.96×10^5
	<20 μm	.0	1.67×10^7	6.60×10^6	5.64×10^5
Lead	<2 mm-63 μm	.0	4.21×10^2	1.37×10^2	2.50×10^0
	<63 μm-20 μm	2.66×10^4	1.97×10^4	2.71×10^2	2.06×10^2
	<20 μm	6.24×10^3	7.05×10^3	2.12×10^2	1.61×10^2
Manganese[1]	<2 mm-63 μm	3.20×10^{-1}	5.37×10^{-2}	1.43×10^{-3}	9.04×10^{-5}
	<63 μm-20 μm	1.14×10^{-1}	1.87×10^{-2}	2.50×10^{-4}	1.30×10^{-4}
	<20 μm	2.47×10^{-1}	4.23×10^{-2}	5.60×10^{-4}	1.07×10^{-4}
Zinc[1]	<2 mm-63 μm	2.90×10^{-1}	1.69×10^{-2}	4.28×10^{-3}	1.57×10^{-4}
	<63 μm-20 μm	4.62×10^{-1}	7.73×10^{-2}	2.77×10^{-2}	3.30×10^{-4}
	<20 μm	2.87×10^{-1}	3.44×10^{-2}	3.17×10^{-3}	5.40×10^{-4}

Metal	Size fraction	Percentage of variance, by source			
		Site	Station	Digestion	Error
Chromium	<2 mm-63 μm	46.21	52.79	0.39	0.61
	<63 μm-20 μm	61.15	17.81	2.88	18.16
	<20 μm	88.80	7.23	1.86	2.11
Copper[1]	<2 mm-63 μm	90.43	8.15	1.17	.25
	<63 μm-20 μm	89.40	10.20	.0	.40
	<20 μm	90.59	9.03	.0	.38
Iron	<2 mm-63 μm	.27	90.51	8.68	.54
	<63 μm-20 μm	.0	.74	85.70	13.56
	<20 μm	.0	69.94	27.69	2.37
Lead	<2 mm-63 μm	.0	75.13	24.42	.45
	<63 μm-20 μm	56.85	42.13	.58	.44
	<20 μm	45.67	51.60	1.55	1.18
Manganese[1]	<2 mm-63 μm	85.27	14.33	.38	.02
	<63 μm-20 μm	85.69	14.02	.19	.10
	<20 μm	85.15	14.62	.19	.04
Zinc[1]	<2 mm-63 μm	93.15	5.43	1.37	.05
	<63 μm-20 μm	81.44	13.63	4.87	.06
	<20 μm	88.27	10.58	.98	.17

[1]Log (base 10) transformed.

Table 4. Coefficients of variability by size fraction and source of variability

| Metal | Size fraction | Coefficient of variability (in percent) by source | | | |
| | | Site | Station | Laboratory | |
				Digestion	Error
Chromium	<2 mm-63 μm	71	76	7	8
	<63 μm-20 μm	51	27	11	28
	<20 μm	91	26	13	14
Copper[1]	<2 mm-63 μm	67	20	8	4
	<63 μm-20 μm	52	17	0	3
	<20 μm	24	7	0	2
Iron	<2 mm-63 μm	3	62	19	5
	<63 μm-20 μm	0	1	13	5
	<20 μm	0	24	15	4
Lead	<2 mm-63 μm	0	61	35	5
	<63 μm-20 μm	88	77	9	8
	<20 μm	42	44	8	7
Manganese[1]	<2 mm-63 μm	22	9	1	0
	<63 μm-20 μm	12	5	1	0
	<20 μm	16	7	1	0
Zinc[1]	<2 mm-63 μm	29	7	3	1
	<63 μm-20 μm	25	10	6	1
	<20 μm	20	7	2	1

[1]Log (base 10) transformed.

Table 5. Indexes of discrimination
[For a given metal, larger numbers indicate greater discrimination]

| Metal | Size fraction | | |
| | 1 | 2 | 3 |
	<2 mm-63 μm	<63 μm-20 μm	<20 μm
Chromium	0.09	0.06	0.18
Copper[1]	.42	1.03	1.7
Iron	.003	0	0
Lead	0	.095	.095
Manganese[1]	1.22	2.4	2.3
Zinc[1]	1.035	.42	1.45

[1]Log (base 10) transformed

calculate concentration precision from the mean and variance of the logarithms of concentration.

For $Y = \log(x)$

$$CV_x = \sqrt{10^{2.303 S_y^2} - 1}$$

and from the definition of CV,

$$S_x | \mu_x = (CV_x)\mu_x$$

where
- x = concentration data,
- y = base 10 logarithm of x,
- CV_x = coefficient of variability for x,
- S_y^2 = laboratory variance of y,
- $S_x|\mu_x$ = standard deviation of x given the true mean of x is μ_x.

Precision was determined for copper, manganese, and zinc as a function of concentration (table 8).

Implications for Future Project Design

In a small pilot study, replicate analyses from single bottom-material samples may be independently analyzed in the laboratory. If concentrations show a large amount of variability, discerning differences between stations along a cross section or between different sites would be difficult. To compensate for this imprecision in future studies, the investigator could divide the samples into several subsamples and have each subsample analyzed independently. Similarly, if the variability in metals concentrations along a single cross section were large, discerning differences between sites would be difficult. Taking more samples per cross sec-

Table 6. Particle size analyses

Site	Station	Particle-size range	Percentage of sample in size range
Cuyahoga River at the Harvard Avenue Bridge (Cleveland, Ohio)	1	<2 mm-63 μm	71.8
		<63 m-20 μm	19.2
		$<20\,\mu$m	9.0
	2	<2 mm-63 μm	99.4
		<63 m-20 μm	.46
		$<20\,\mu$m	.14
	3	<2 mm-63 μm	99.3
		<63 m-20 μm	.6
		$<20\,\mu$m	.1
Cuyahoga River at the State Route 82 bridge (near Hiram, Ohio)	1	<2 mm-63 μm	72.6
		<63 m-20 μm	12.6
		$<20\,\mu$m	14.8
	2	<2 mm-63 μm	98.3
		<63 m-20 μm	1.1
		$<20\,\mu$m	.6
	3	<2 mm-63 μm	98.9
		<63 m-20 μm	.72
		$<20\,\mu$m	.38

Table 7. Significance probabilities associated with the null hypothesis that the mean metal concentration at the urban and rural sites are equal

Metal	Size fraction		
	<2 mm[1]	$<63\,\mu$m[1]	$<20\,\mu$m
Chromium	0.162	0.002	0.004
Copper[2]	.021	.010	.005
Iron	.457	.283	.452
Lead	.415	.085	.130
Manganese[2]	.012	.006	.013
Zinc[2]...............	.010	.012	.007

[1]Concentrations mathematically determined

[2]Log (base 10) transformed.

tion would then help compensate for the imprecision and improve the chances of detecting between-site differences. From such a pilot study, the estimates of variances associated with each influence of interest may be used to project an optimum number of future replicates, which, at little cost, maximizes the probability of detecting between-site differences.

Sokal and Rohlf (1969) presented the equations necessary to determine the optimum number of replicates per influence for a given cost. For bottom-materials analyses of metals concentration, the optimum number of replicates is a function of the variance due to digestion, measurement, and station influences and also the costs for sample collection and analysis. Specifically,

$$n = (C_C S_L^2 / C_L S_C^2)^{1/2}$$

where n = optimum number of replicate laboratory analyses per sample (where n is greater than or equal to 1),

C_C = cost of sampling at additional stations in the cross section,

C_L = cost for laboratory analysis of one sample,

S_L^2 = variance in concentration observed with replicate laboratory analyses of a single sample,

S_C^2 = variance in concentration observed between stations located along one cross section.

Table 8. Laboratory precision by particle size

Metal	Size fraction	Standard deviation
Chromium	<2 mm-63 μm	0.76
	<63 μm-20 μm	4.24
	<20 μm	7.59
Iron	<2 mm-63 μm	1,248
	<63 μm-20 μm	1,472
	<20 μm	2,676
Lead	<2 mm-63 μm	11.8
	<63 μm-20 μm	21.8
	<20 μm	19.3
Copper[1]	<2 mm-63 μm	.23(C)
	<63 μm-20 μm	.17(C)
	<20 μm	.08(C)
Manganese[1]	<2 mm-63 μm	.09(C)
	<63 μm-20 μm	.04(C)
	<20 μm	.06(C)
Zinc[1]	<2 mm-63 μm	.15(C)
	<63 μm-20 μm	.40(C)
	<20 μm	.14(C)

[1] Standard deviations for this metal are calculated by multiplying the listed coefficients by the concentrations (C), in micrograms per gram, at which the standard deviations are desired.

Replicate analyses are indicated where the ratio of laboratory variance (digestion plus measurement variance) to cross-section variance is large. As an example, if laboratory costs for analysis of the six metals of interest (C_L) were $100 per sample, and the cost for sampling at an additional station within a cross section (C_C) were $25, the variances listed in table 3 would result in a computer optimum sample size (n) greater than 1 for only one metal. Therefore, only one analysis per sample is appropriate for all size fractions and metals, except size-fraction 2 of iron, which would require approximately six replicates. Iron concentrations, as previously noted, are not significantly different at the two sites. However, if one seriously desired to use size-fraction 2 to detect the small differences in mean iron concentrations at the two sites, six replicate analyses would have to be performed per sample.

As a result of this experiment, in future analyses of metals in the sediments of these streams only one laboratory analysis per sample need be requested; the money saved on replicate analyses could be used to collect and analyze samples from additional stations within the cross sections.

CONCLUSIONS

1. In general, metals concentrations increased as particle size decreased.
2. On the basis of ANOVA significance levels and an "index of discrimination," the <20 μm fraction provided a level of discrimination between the urban and rural bottom-material samples that was superior to the other size fractions. The <63- to 20-μm fraction ranked second, and the <2-mm to 63-μm fraction ranked third.
3. The results of ANOVAs involving actual and computer size-fraction data indicated that, where differences were detected, a <63-μm fraction and <20-μm fraction discriminated between the two sites with a higher degree of certainty than did a <2-mm fraction.
4. Calculations of optimum sample size indicated that replicate laboratory analyses were unnecessary, unless iron was to be measured in the <63- to 20-μm size fraction.
5. A significant linear relationship existed between laboratory variance for a sample and sample concentrations of zinc, copper, and manganese. This was not found for iron, lead, or chromium.
6. Statistically significant variations in concentrations were observed with the site, size, station, and digestion factors for the metals zinc, lead, manganese, and chromium. Site, size, and station were significant for copper. Only size and digestion were significant for iron.
7. The site-size interaction, which was found to be insignificant in all cases, indicated that these two influences operated independently.

SELECTED REFERENCES

Aitchison, J., and Brown, J.A.C., 1957, The lognormal distribution: Cambridge, Cambridge University Press, 176 p.

Bopp, Frederick, and Biggs, R.B., 1981, Metals in estuarine sediments—factor analysis and its environmental significance: Science, v. 214, p. 441-443.

Fitchko, J., and Hutchinson, T.C., 1975, A comparative study of heavy metal concentrations in river mouth sediments around the Great Lakes: Journal of Great Lakes Research, v. 1, no. 1, p. 46-78.

Freund, R.J., and Littell, R.C., 1981, SAS for linear models—a guide to the ANOVA and GLM procedures: Cary, North Carolina, SAS Institute, 231 p.

Gibbs, R.J., 1977, Transport phases of transition metals in the Amazon and Yukon Rivers: Geological Society of America Bulletin, v. 88, p. 829-843.

Haushild, W.L., Dempster, G.R., Jr., and Stevens, H.H., Jr., 1975, Distribution of radionuclides in the Columbia River streambed, Hanford Reservation to Longview, Washington: U.S. Geological Survey Professional Paper 433-O, 35 p.

Helmke, P.A., Koons, R.D., Schomberg, P.J., and Iskandar, I.K., 1977, Determination of trace element contamination of sediments by multielement analysis of clay-size fractions: Environmental Science and Technology, v. 11, p. 984-989.

Leland, H.V., and McNurney, J.M., 1974, Lead transport in a river ecosystem, in Proceedings of the International Conference on Transport of Persistent Chemicals in Aquatic Ecosystems: Ottawa, Canada, p. III.27-III.23.

Rickert, D.A., Kennedy, V.C., MacKenzie, S.W., and Hines, W.G., 1977, A synoptic survey of trace metals in bottom sediments of the Willamette River, Oregon: U.S. Geological Survey Circular 715-F, 27 p.

Shimp, N.F., Schleicher, J.A., Ruch, R.R., Heck, D.B., and Leland, H.V., 1971, Trace element and organic carbon accumulation in the most recent sediments of southern Lake Michigan: Illinois Geological Survey Environmental Geology Note 41, 25 p.

Shuman, M.S., Smock, L.A., and Haynie, C.I., 1977, Metals in the water, sediments and biota of the Haw and New Hope Rivers, North Carolina: North Carolina State University, Water Resources Research Institute Report 124, 127 p.

Skougstad, M.W., Fishman, M.J., Friedman, L.C., Erdman, D.E., and Duncan, S.S., 1979, Methods for determination of inorganic substances in water and fluvial sediments: U.S. Geological Survey Techniques of Water-Resources Investigations, Book 5, Chapter A1, 626 p.

Sokal, R.R., and Rohlf, F.J., 1969, Biometry—the principles and practices of statistics in biological research: San Francisco, W.H. Freeman, 776 p.

Thomas, R.L., Jaquet, J.M., and Mudrochova, A., 1975, Sedimentation processes and associated changes in surface sediment trace metal concentrations in Lake St. Clair, 1970-1974, in International Conference for Heavy Metals in the Environment: Toronto, Canada, v. II, p. 691-708.

Evaluation of the Slope-Area Method for Computing Peak Discharge

By Robert D. Jarrett

Abstract

An evaluation of 70 slope-area measurements on higher gradient streams (stream slopes greater than 0.002) throughout the United States showed that peak discharge measurements were affected by *n*-values, scour, expansion and contraction losses, viscosity, velocity distribution, unsteady flow, number of cross sections, state of flow, and stream slope. In many places, measurement error can be as great as, or can exceed, 100 percent, which leads to overestimation of the actual peak discharge. This can result in misleading maximum flood values, flood-frequency analyses, and overdesign of flood-plain structures.

A brief discussion of these problems, tentative solutions, and research needs is presented. The critical-depth method of computing peak discharge provides the most reasonable results in higher gradient streams.

INTRODUCTION

The U.S. Geological Survey and other agencies often are required to determine the peak discharge of floods. On rivers where response time is slow, peak discharge usually can be determined by direct discharge measurement or by a short extension of the rating curve. However, at remote sites, during widespread flooding, or at those sites where debris, high velocity, or rapidly changing stage is present, peak discharge is computed by means of indirect methods, which are costly and time consuming.

In the slope-area method, discharge is computed on the basis of a uniform-flow equation involving channel characteristics, water-surface profiles, and a roughness coefficient based on the Manning equation (Barnes and Davidian, 1978; Dalrymple and Benson, 1967). The Manning equation was developed for uniform-flow conditions. For nonuniform-flow conditions in natural channels, the friction or energy slope in the Manning equation is computed from the energy equation. Selection of a slope-area reach is very important (Barnes and Davidian, 1978; Dalrymple and Benson, 1967). A good reach requires good high-water marks to define the water slope, the channel must be straight and uniform enough so that three to five cross sections can be made, and scour or deposition should be minimal.

The slope-area method is the most often used indirect method of computing peak discharge (Dalrymple and Benson, 1967). In Colorado and in Texas, 76 percent and 67 percent, respectively, of all indirect measurements were made by means of the slope-area method. Most users of the data assume that flood-measurement accuracy is within 25 percent, and many measurements have that accuracy or better. However, some of the flood measurements actually may be in error by as much as 100 percent or more. The measurement rating implies that the computed discharge is within some range that brackets the true discharge. However, because of problems associated with making the slope-area measurements under certain conditions, peak discharge values may consistently show positive bias greater than the true discharge. The possibility of errors in determining peak discharge by means of the slope-area method has been noted previously (Flaxman, 1974; Randall and Humphrey, 1984).

Peak discharges of large floods typically are used in flood-frequency analyses and often are the high outliers that are difficult to incorporate into the flood-frequency analysis. These flood measurements also are used in developing envelope curves of maximum-recorded discharge for various sizes of drainage areas (Crippen and Bue, 1977; Hoyt and Langbein, 1955; Matthai, 1969). Designers of flood-plain structures take into account these curves of large floods. If the peak-discharge measurements are typically greater than the actual discharges, flood frequencies may be overestimated and structures overdesigned. The problems associated primarily with higher gradient streams discussed here are widespread in the United States. The purposes of this paper are to evaluate the application and accuracy of slope-area measurements, to discuss the problems associated with these measurements, and to outline the needs for research into these problems.

EVALUATION OF SLOPE-AREA MEASUREMENTS

The development and verification of the slope-area method were made on relatively tranquil, mild-gradient streams (Dalrymple and Benson, 1967). However, many measurements actually are made for extremely turbulent floods on higher gradient streams. The author has had extensive experience in the collection, computation, and review of indirect measurements and in studies of hydraulics of streams with gradients greater than 0.002 (slopes in ft/ft) (Jarrett, 1984). Also, 1 reviewed 40 large-flood measurements from several areas in the United States that were made by means of the slope-area method. These slope-area measurements followed established procedures and were well documented. In Colorado, where many streams can be categorized as hydraulically steep, only 15 percent of all indirect measurements were rated "good."

In the United States, a review of 70 slope-area measurements indicated that the common problems associated with the making of slope-area measurements on higher gradient streams are related to such factors as n-values, scour, expansion and contraction losses, viscosity, velocity distribution, unsteady flow, number of cross sections, state of flow, and stream slope. Similar problems associated with indirect flood measurements also have been noted in other countries such as Great Britain (Dobbie and Wolf, 1953). Usually, not all these factors are significant in a single reach. However, they may all be significant during extreme floods such as the Big Thompson River, Colo., flood of 1976 (McCain and others, 1979) or floods resulting from dam failures such as the flood at Lawn Lake, Colo., in 1982 (Jarrett and Costa, 1985). These problems often cannot be avoided by better or additional site selections because they are common to the entire stream system.

A brief discussion follows on the various problems associated with these factors and tentative solutions to these problems. However, these factors are to some extent interrelated.

n-Values

Guidelines are available to aid in the selection of Manning's roughness coefficient, n (Chow, 1959; Barnes, 1967; Benson and Dalrymple, 1967; Limerinos, 1970); however, most of the n-values verified are for sites on relatively low-gradient streams. Data collected by Jarrett (1984) indicate that n-values are much greater on higher gradient cobble- and boulder-bed streams than on low-gradient streams having similar relative smoothness values (hydraulic radius divided by the median intermediate particle diameter).

Factors other than streambed characteristics also affect roughness and energy loss, particularly obstructions, debris, vegetation, and irregular banks, all of which can produce much turbulence; hence, roughness and energy loss may not be completely accounted for. As flow increases, these factors cause an increase of eddy losses and roughness (Aldridge and Garrett, 1973). Similarly, as stream slope increases, turbulence increases; as a result, energy losses and flow resistance increase (Barnes, 1967; Jarrett, 1984). Photographic comparisons of a lower and a higher gradient stream for similar conditions are shown in figure 1. Most of the slope-area measurements reviewed were made on higher gradient streams where slopes are greater than 0.01 (a few have slopes greater than 0.20) and n-values used were low compared with n-values computed by means of an equation for higher gradient streams (Jarrett, 1984). The n-values for the reviewed slope-area reaches also did not appear to have n-values increased sufficiently for effects of bank vegetation, obstructions, debris, and irregular banks (Dobbie and Wolf, 1953; Herbich and Shulits, 1964; Aldridge and Garrett, 1973; Richards, 1973; Flaxman, 1974).

A similar comparison of the n-values of relatively low-gradient sand-bed channels was made using the corresponding guidelines for the estimation of n-values (Benson and Dalrymple, 1967). However, a few of the reviewed measurements were on higher gradient sand-bed streams (slopes as much as 0.08), well beyond the range and conditions of the n-verifications. Simons and Richardson (1966) reported chutes and pools on higher gradient streams that result in great increases in channel roughness and flow alternating between subcritical and supercritical, or basically critical flow.

Wormleaton and others (1982) indicated that the traditional methods of calculating the discharge in compound channels (main channel with subdivided overbank flow) do not fully account for energy losses, and that channel discharge capacity is considerably overestimated. Their study indicates that the tendency is further exaggerated where overbank roughness is greater than main channel roughness. No guidelines are presently available for determining the effects of varying roughness in compound channels or these effects on n-values, although most floods occupy the overbanks.

The solution to the problem of underestimating n-values is to fully account for the increased energy losses and resistance on the higher gradient streams due to factors (such as obstructions, vegetation, and irregular banks) other than bed roughness (Chow, 1959; Benson and Dalrymple, 1967). Jarrett (1984) studied the main channel roughness of mountain streams; all slopes in that study were greater than 0.002. An overview of this work is presented below and is an aid in selecting n-values on higher gradient streams.

A

B

Figure 1. Characteristic turbulence. *A*, Lower gradient stream. Upstream view of Rio Grande at Wagonwheel Gap, Colo. (Discharge is 4,040 cubic feet per second, water slope is 0.004, hydraulic radius is 3.98 feet, mean velocity is 5.94 feet per second, Froude number is 0.52, Manning's *n* is 0.035 (verified), and the intermediate diameter of bed material is 0.3 feet.) (Jarrett, 1984). Note the relatively smooth water surface. *B*, Higher gradient stream. Upstream view at Arkansas River above Buena Vista, Colo. (Discharge is 4,530 cubic feet per second, water slope is 0.023, hydraulic radius is 5.51 feet, mean velocity is 8.65 feet per second, Froude number is 0.60, Manning's *n* is 0.086 (verified), and the intermediate diameter of bed material is 1.4 feet.) (Jarrett, 1984). Note the extremely turbulent water surface.

Onsite surveys and 75 measurements of discharge were made on 21 streams that have slopes greater than 0.002 for the purposes of computing the Manning roughness coefficient, *n*, and collecting data on the hydraulics of these streams. These data show that (1) *n* varies inversely with depth, (2) *n* varies directly with slope, and (3) streams thought to be in the supercritical flow range were actually in the subcritical range. Because *n*-values varied drastically with depth of flow, a simple objective

method was used to develop an equation for predicting the *n* of higher gradient streams by means of multiple-regression techniques and measurements of the slope and hydraulic radius.

Most equations used to predict channel roughness, such as those by Chow (1959) and Limerinos (1970), require streambed particle-size information. Studies by Golubtsov (1969), Riggs (1976), and Ayvazyan (1979) indicate that channel roughness is related directly to channel gradient in natural stable channels. For similar bed-material size, channels with low gradients have much lower *n*-values than channels with higher gradients. Values of *n* as small as 0.032 have been obtained for channels having very low gradients, shallow depths, and large boulders (Barnes, 1967). This relation of resistance and slope is due, in part, to the interrelation between slope and particle size. As slope increases, finer material is removed and larger particles remain in the channel. The effect of increased turbulence and resistance results in increased friction slope.

Multiple-regression analyses were performed on the data of the 21 sites. The equation developed for predicting Manning's *n* in higher gradient natural channels is

$$n = 0.39S^{0.38}R^{-0.16} \tag{1}$$

The hydraulic characteristics used in equation 1 are defined below.

Friction slope, *S*, or energy gradient, is the slope of the energy line of a body of flowing water. The slope should be representative of the channel and can be estimated by averaging the slope over a length of several channel widths. The data indicate that the water and friction slopes were approximately the same and can be used interchangeably in equation 1.

Hydraulic radius, *R*, is a measure of the boundary area causing friction per unit of flow and is computed as the perpendicular cross-sectional area of a stream of water divided by the channel wetted perimeter. Cross-section area and wetted perimeter are obtained from field surveys. Hydraulic depth, *D*, the cross-sectional area divided by the top width, could also be used in place of hydraulic radius in equation 1 because the data indicated that the two depths are approximately equal for all but very small streams or deep narrow channels.

Testing with Colorado data showed that the average standard error of estimate of the prediction equation was 28 percent. The equation had the same accuracy when other data on higher gradient (slopes as much as 0.052) streams were used, including data from Barnes (1967) and Limerinos (1970).

The following restrictions should be observed when equation 1 is used to predict Manning's *n* for higher gradient streams:

1. Equation 1 is applicable to natural main channels having stable bed and bank materials (gravels, cobbles, and boulders) and minimal bank vegetation, irregular banks, or obstructions.

2. Equation 1 can be used for slopes from 0.002 to 0.052 and for hydraulic radii from 0.5 to 7 ft. The upper limit on slope is due to a lack of verification data available for the slopes of higher gradient streams. Equation 1 has been applied to other streams (Barnes, 1967; Judd and Petersen, 1969; Limerinos, 1970) and has a standard error of 22 percent. Results of the regression analyses indicated that, for a hydraulic radius greater than 7 ft, n did not vary significantly with depth and should be applicable as long as the bed and bank material remain fairly stable.

3. Equation 1 should not be used for reaches of streams affected by backwater from downstream obstructions.

4. Equation 1 is applicable to streams having relatively clear water and low suspended sediment.

A comparison was made for six representative mountain streams of the main-channel n-values of slope-area measurements reviewed that met the above criteria and the n-values computed from the hydraulic properties of the measurement using equation 1, as shown in table 1. In these measurements, n-values were consistently lower typically by an average of 59 percent. Equation 1 does not include additional energy losses from factors such as bank vegetation, rough banks, and obstructions; hence, these n-value differences would be considered minimum. However, for streams with higher slopes, many measurement n-values were often lower than the predictive-equation n-values by more than 100 percent. This discrepancy implies that the computed discharges could be overestimated by as much as 100 percent or more.

Although no studies of higher gradient sand-bed streams have been made, it seems that roughness and energy losses are underestimated. On the basis of the study by Simons and Richardson (1966), flow resistance on higher gradient sand-bed streams having chutes and pools should be increased to reflect flow near critical (discussed later) to provide more accurate results.

Scour

The passage of a flood can cause dramatic changes in a channel in a very short time. Probably the most common problem noted in the review of measurements was the unknown amount of scour in the slope-area reach. (None of the measurements reviewed indicated problems associated with deposition because slope-area measurements are generally in uniform or contracting reaches.) Sites were selected in reaches having the least

amount of scour. One criterion for site selection is that the reach be uniform to slightly contracting in a downstream direction. Unfortunately, contracting reaches are the reaches most susceptible to scour because of high-flow velocities in the reach. Scour is a function of flow, channel geometry, and soil properties; the most dominant factor seems to be stream slope. As slope increases, particularly to more than 0.03 to 0.04, scour increases greatly (Jarrett and Costa, 1985). In many higher gradient streams, almost their entire length can be scoured or filled. This is not meant to imply that erosion and channel enlargement cannot take place on flatter slope streams. A check for erosion and channel enlargement should be made on all measurements.

Indications of a scoured reach are straight, nearly vertical, and raw banks, and exposed bedrock surface. Photographs of most of the reviewed measurements indicated that extensive scour had occurred during the flood. High-water marks set during the flood may not be representative of the actual cross-sectional area of flow at the flood peak. First, eyewitnesses have stated that in floods on small streams that are densely vegetated, floating debris dams the flow and causes backwater or flows of higher than normal depths (Jarrett and Costa, 1985). This exaggerates flow depths. Second, subsequent erosion of valley fill could lower the water surface as sediment was being scoured, and high-water marks that were set before erosion could be left as a false indicator of the top of the flow area during the peak discharge, as shown in figure 2. Depth Y_1 represents the depth of water that set high-water marks early in the flood. As discharge increases, valley fill is eroded, and the water surface drops. However, depth Y_2 from the high-water marks to the new channel bottom (in many places, the bedrock valley floor) may be used to compute cross-sectional area in the slope-area calculations. Exaggerated cross-sectional areas and the resulting computations can yield extremely overestimated and many record-breaking discharges (by a factor of 2 or more) for a watershed of a given size.

Where measurement of a scoured reach cannot be avoided, two solutions are suggested. First, attempt to reconstruct the preflood ground level of the eroded cross section using the remaining preflood ground. This method assumes that the erosion took place after the peak discharge because the peak occurred so rapidly. The evaluation of the measurement should incorporate the percentage difference between the preflood and postflood computed discharge. The smaller the difference, the more confidence in the measurement.

Second, assume that the flow is at or very near critical flow, which is supported by Dobbie and Wolf (1953) and Jarrett (1984). See the discussion on this assumption under "State of Flow." Critical flow is represented by the Froude number (F) (Chow, 1959):

Table 1. Comparison of Manning's n values

| Location | Year of flood | Peak discharge (ft³/s) | Slope (ft/ft) | Main Channel | | | Percent differences in n values |
				Hydraulic radius (ft)	Manning n (field selected)	Manning n (equation 1)	
Big Thompson River tributary below Loveland Heights, Colo.	1976	8,700	0.066	7.0	0.040	0.102	-155
Big Thompson River above Drake, Colo.	1976	28,000	.022	8.5	.045	.065	-44
Canacadea Creek at Alfred Station, N.Y.	1972	6,080	.012	5.0	.040	.057	-42
Chenunda Creek at Stannards, N.Y.	1972	9,200	.008	6.7	.037	.046	-24
Cataract Creek near Basin, Mont.	1981	3,160	.046	5.0	.070	.094	-34
Cleghorn Canyon at Rapid City, S. Dak.	1972	12,600	.019	7.0	.041	.063	-54
						Average	-59

$$F = \frac{V}{\sqrt{gD}}; \quad F = 1.0 , \qquad (2)$$

where V = the mean velocity;
 g = acceleration due to gravity; and
 D = mean depth of flow.

If high-water marks above a steep drop or fall (preferably bedrock) are assumed to represent critical depth, then the solution for peak discharge Q, based on one cross section, is:

$$Q = A \sqrt{gD} , \qquad (3)$$

where A = cross-sectional area.

Because the flow is at or near critical throughout the higher gradient channel, the exact location of the critical depth section is not that important, although it is best to locate the cross section immediately upstream from the drop. Also, because the least scour generally is at or just upstream from a bedrock drop, problems associated with scour are minimized. One can obtain improved results from equation 3 by surveying a second cross section located a minimum of 2 1/2 times the mean depth upstream (Barnes and Davidian, 1978) and by balancing the energy equation for the cross sections for the observed water-surface elevations. Step-back-

water analysis (Bailey and Ray, 1966) is then made to develop a rating curve at the upstream (approach) cross section. The discharge then can be determined from the observed approach water-surface elevation and the rating curve.

For example, the critical-depth method (equation 3) was applied to two higher gradient sites in the Big Thompson River basin for which slope-area measurements were made after the 1976 flood (McCain and

EXPLANATION
Y_1 DEPTH BEFORE EROSION
Y_2 DEPTH AFTER EROSION
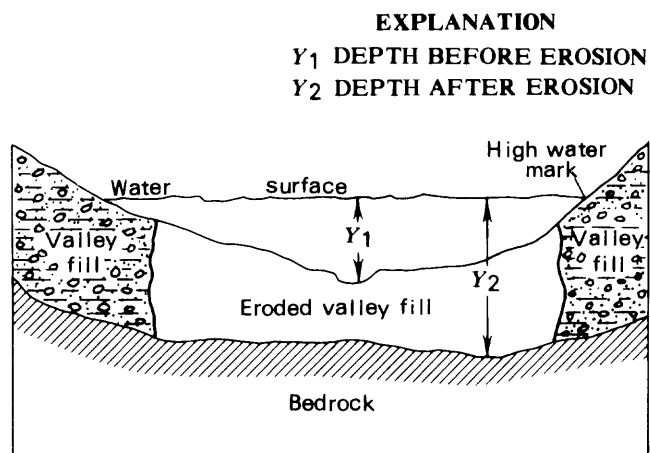
Figure 2. Hypothetical cross section showing how high-water marks could be set before extensive erosion of valley fill. This erosion would result in excessive slope-area discharge measurements.

others, 1979). These sites were Big Thompson River tributary below Loveland Heights, Colo., and Dark Gulch at Glen Comfort, Colo., which have good critical depth sites and minimal scour. The computed discharges for each method and other pertinent information are given in table 2. Assuming that the critical-depth measurement gives the true discharge, slope-area discharges are 85 percent greater for Big Thompson River tributary and 112 percent greater for Dark Gulch.

Two other completely different methods of estimating peak discharge suggest that the critical-depth measurement provides the more reasonable estimate in terms of velocity, Froude number, and precipitation data. Miller and others (1978) reconstructed flood peaks based on rainfall-runoff analyses to evaluate the storm precipitation for the two sites given in table 2. These investigators found it difficult or impossible to reconcile the slope-area peak discharges with rainfall measurements. However, point rainfall data are not good indicators of basinwide rainfall for localized storms. Reconstructed peaks based on rainfall-runoff analyses were generally 25 to 50 percent lower than the slope-area measurements for the higher gradient streams. However, they chose to accept that the peak discharges were correct and increased the rainfall (intensities and volumes) for the storm. Costa (1983) developed a paleohydraulic technique for computing velocity, depth, and peak discharge on small steep watersheds from remaining channel flood deposits (boulders) and cross sections. His estimated peak discharges also are given in table 2.

Other applications of the critical-depth method also have yielded more hydraulically and hydrologically sound results than slope-area results. In one Utah stream, the slope-area method indicated a peak discharge of 16,000 ft^3/s, whereas a critical-depth measurement indicated a peak discharge of 3,700 ft^3/s. Randall and Humphrey (1984) indicated that a slope-area measurement in Alaska showed peak discharge of 12,000 ft^3/s, whereas they demonstrated that a critical-depth method value of 4,700 ft^3/s was a more accurate assessment of the true discharge. They noted similar problems to those described here.

The purpose of comparing the different methods is that for these sites, as well as for other sites in other comparisons, the slope-area method appears to give overestimated peak discharges for the adverse conditions on higher gradient streams. Slope-area measurements should not be made where scour is evident unless the flood-ground surface can be reasonably reconstructed. The critical-depth method results in better peak discharges than slope-area measurements on higher gradient streams with or without channel scour. Critical-depth measurement sites are common on higher gradient streams.

Expansion and Contraction Losses

The energy loss due to contraction or expansion of the channel in the reach is assumed equal to a coefficient times the difference in velocity heads between two sections. The value of the coefficient proportionality factor used is 0 for contracting reaches and 0.5 for expanding reaches (Dalrymple and Benson, 1967). Other agencies recommend other values for these coefficients; however, both the procedure and the coefficient are based on limited flume and siphon studies (Hinds, 1928).

One common problem is that energy losses due to turbulence may not be fully accounted for. Jarrett (1984) noted that even minor channel expansions on higher gradient streams resulted in greatly increased energy losses. This review of flood measurements indicates that an expanding subreach can greatly increase the computed discharge. Even contracting reaches can have energy losses, but these are not accounted for because the coefficient generally is assumed equal to 0. Many investigators allow for positive contraction coefficients in hydraulic analyses. An evaluation of the values of the contraction- and expansion-loss coefficients is needed to help evaluate their effect on the computed peak discharge.

The problem of expansion and contraction losses requires additional research. Meanwhile, the measurement sites should be located in the most uniform reaches.

Viscosity

Sediment can alter the fluid characterstics of flowing water by increasing its viscosity and density. Presently, measurements are made assuming clear-water flow and no sediment in transport. During floodflows (and on some streams during normal flow conditions), large amounts of sediment are transported. About 60,600 tons of sediment were eroded from the valley floor of the Loveland Heights tributary to the Big Thompson River, Colo., during the 1976 flood (Andrews and Costa, 1979). Substantial but unknown amounts of energy are required to transport this material. The Manning equation is suited for all fully rough water flow. For sediment-laden flows, the Manning equation is no longer suitable unless the coefficient n is modified according to its dependence on the Reynold's Number (Henderson, 1966).

Flume studies by Li and Simons (1982) indicate that, during the passage of a flood wave, a sufficient supply of sand-size sediment can submerge rocks and cobbles making up the channel bed and function as an upper regime sand-bed channel having n-values as low as 0.015, or a decrease in roughness by a factor of 2 to 3 or more. In most mountain channels, this is not reasonable because the supply of sand probably is not sufficient. Also, the question remains as to why the sand is

Table 2. Comparison of peak discharge using different methods

Location	Drain-age area (mi^2)	Slope (ft/ft)	Estimated peak discharge (ft^3/s)			
			Slope-area method (McCain and others, 1979)	Critical-depth method	Rainfall-runoff method (Miller and others, 1978)	Paleo-hydraulic method (Costa, 1983)
Big Thompson River tributary below Loveland Heights, Colo.	1.35	0.077	8,700	4,700	5,400	3,740
Dark Gulch at Glen Comfort, Colo.	1.0	.125	7,200	3,390	3,880	4,630

subsequently eroded after the peak flow, and a cobble- and boulder-covered streambed is left. According to Henderson (1966), suspended sediment reduces flow resistance, but that effect is small compared with the increases in flow resistance due to bedforms induced by sediment motion.

Costa and Jarrett (1981) stated that very high sediment-laden streams or debris flows have been misinterpreted as waterfloods. Debris flows (one type of mudflow) are a heterogeneous mixture of sediment sizes and contain sufficient clay or silt to form a cohesive non-Newtonian fluid mass. The main difference between mudflows and debris flows is that debris flows have larger size material than mudflows. The slope-area method was developed for Newtonian fluids. Some investigators have misapplied the slope-area method and have computed world-record-breaking waterfloods where, in fact, the debris flows were initiated by only moderate rainfall or, in some places, snowmelt on steep unstable slopes. Five of seven documented large waterfloods investigated in Colorado were, in fact, debris flows (Costa and Jarrett, 1981).

The important point to remember is that no information is available at present for adjusting the velocity of flow or for estimating roughness coefficients of flows having large concentrations of sediment. However, it is doubtful that sediment-laden streams have no effect on flow. Mudflows and debris flows take place in many parts of the country, although they are most common in the western third of the United States. In most events, slope-area measurements should not be used if the event may have been a mudflow or debris flow because the method may not be applicable, as there are no verified n-values, and because of debris damming that affects the flow hydraulics (velocity, depth, and slope) in the channel. An indication of a mudflow is a thick (1/4-1 in.) veneer of mud on the ground surface, obstructions, and

vegetation. Evidence used to identify debris flows includes coarse lobate, poorly sorted, unstratified, pebbly mudstonelike unconsolidated deposits having well-defined levees and terminal lobes, and the extent of ground-litter disruption below high-water marks. Also, debris flows generally end where slope decreases and, from that point downstream, channel shows minimal or no evidence of disruption. If the slope-area method is used to compute the peak debris discharge, all assumptions and a qualification as to the unknown accuracy needs to be incorporated in the report on the debris flow.

If no mudflow and debris-flow features are found, then the slope-area method can be cautiously applied, but the evaluation should note that sediment concentrations are great. Because of the need for more information on mudflows and debris flows, hydraulic and sediment data should still be collected for these events. This documentation should include the source area and cause of debris flow, length of reach affected, site characteristics (width, depth, slope, and apparent roughness), depositional and sediment characteristics, and photographs.

Velocity Distribution

The vertical-velocity distribution in fully developed turbulent flow has been shown to be approximately logarithmic (Chow, 1959). The logarithmic vertical-velocity distribution for a stream is shown graphically in figure 3 and is considered applicable in computing the mean velocity of a slope-area measurement. Measurements of streamflow velocity are normally made by means of a current meter, which measures the velocity of water flowing through incremental subareas of a channel cross section. The mean velocity of the flow through each subarea is obtained by measuring the velocity at 0.6 of the depth of flow ($V_{0.6}$) if the depth is less than 2.5 ft, or by

RATIO OF OBSERVATION DEPTH TO DEPTH OF WATER (y/Y)

0

0.2

0.4

0.6

0.8

1

● Lake Creek data point

▲ Clear Creek data point

——— Logarithmic curve

—·—·— Clear Creek
Station = 14 feet
Depth of water = 4.1 feet
Discharge = 765 cubic feet
per second

——— Lake Creek
Station = 28 feet
Depth of water = 3 feet
Discharge = 830 cubic feet
per second

0   0.2   0.4   0.6   0.8   1   1.2   1.4   1.6   1.8   2   2.2

RATIO OF POINT VELOCITY TO MEAN VELOCITY IN THE VERTICAL (v/V)

Figure 3. Relation of ratio of observation depth to depth of water and ratio of point velocity to mean velocity in the vertical.

measuring the velocities at the 0.2 and 0.8 depths and averaging the results ($V_{0.2+0.8}$) if the depth of flow is equal to or greater than 2.5 ft. For example, the 0.6 distance below the water surface corresponds to the mean velocity in the logarithmic vertical-velocity distribution shown in figure 3. The discharge at the cross section is computed by summing the products of velocity and area.

Multiple-point vertical-velocity measurements were randomly taken at several depths of flow at several sites to determine whether the vertical-velocity distribution of higher gradient streams is logarithmic. The velocity-profiles at two of the sites are shown in figure 3.

All the vertical-velocity curves for different flow depths and at different sites had this general shape. This shape probably is a result of roughness caused by the larger bed particles protruding into the total depth of flow. Near the channel bottom, the flow is retarded, and the curve shifts to the left of the logarithmic curve; near the surface, the flow accelerates, and the curve shifts to the right of the logarithmic curve. The differences between the integrated (measured) velocity, the velocity at the 0.6 depth ($V_{0.6}$), and the mean of the velocities at the 0.2 and 0.8 depths ($V_{0.2+0.8}$) are shown in table 3. These few vertical-velocity data indicate that the mean velocity

Table 3. Comparison of mean velocities in two Colorado streams

[All velocities are in feet per second; V, integrated (measured) velocity; $V_{0.6}$, velocity at 0.6 depth; $V_{0.2+0.8}$, mean of velocities at 0.2 and 0.8 depths]

Location	Depth (ft)	V	$V_{0.6}$	Percent differ- ence	$V_{0.2+0.8}$	Percent differ- ence
Clear Creek at Lawson, Colo..............................	4.1	6.81	6.29	-7.6	6.92	1.6
Lake Creek above Twin Lakes, Colo..............................	3.0	7.03	3.80	-45.9	4.62	-34.3

may occur at less than 0.6 the depth and that, for certain flow conditions, the 0.6-depth method underestimates the mean velocity in the vertical for higher gradient streams. A study in progress of 11 additional higher gradient sites corroborates these data and results (Marchand and others, 1984). Theoretically, if the flow on these streams were deep enough, the vertical-velocity distribution would approach a logarithmic relation. However, such depths of flow typically are not found in higher gradient streams. The discrepancy between the measured vertical-velocity distributions and the logarithmic curve becomes less as the depth of flow increases.

At present, no criteria are available for making adjustments for nonlogarithmic vertical-velocity profiles in the slope-area method. The assumption of a logarithmic vertical-velocity profile may lead to erroneous indirectly computed peak discharge. Similarly, for direct velocity measurements during large floods, a point velocity often is taken just below the water surface. The mean velocity is estimated by dividing by a coefficient of 1.15 taken from the logarithmic-velocity profile. Velocity-profile data on higher gradient streams (Marchand and others, 1984) indicate that the coefficient is closer to 1.5 (fig. 3); hence, the mean velocity and flood discharge would be overestimated.

Unsteady Flow

Most of the flood measurements reviewed were made after intense short-duration thunderstorms that resulted in rapid runoff or flash floods. Also, several dam-failure floods were investigated. The flow in these types of floods is classified "unsteady." The slope-area method was developed for conditions of steady flow. Flume studies by Koloseus and Davidian (1966) indicate that flow resistance increases for unsteady nonuniform flow conditions. V.R. Schneider (U.S. Geological Survey, written commun., 1982) indicated that where the slope-area method was used to determine the flow of an unsteady wave on the flood plain at National Space and Technology Laboratory Station, Miss., the true discharge was overestimated by as much as 21 percent. These results were obtained under relatively controlled

conditions and for low-gradient conditions. There are no present means to evaluate the effects of unsteady flow in less ideal steeper natural channels.

Number of Cross Sections

A slope-area measurement should be made with a minimum of three cross sections and preferably four or five (Dalrymple and Benson, 1967; Barnes and Davidian, 1978). More cross sections and greater spacing generally minimize some of the errors associated with the method, particularly the definition of energy slope. A number of the slope-area measurement sites reviewed had a minimum of three cross sections. However, some had only two cross sections, and a few had only one, commonly called a slope-conveyance measurement (Barnes and Davidian, 1978). It must be emphasized that, in most reviewed measurements, channel length was not sufficient to establish a minimum of three cross sections. However, the measurements having the fewest cross sections had the highest (record breaking) unit discharges. The accuracy of these measurements is extremely questionable.

To minimize the error associated with the number of cross sections, one must select a minimum of 3 cross sections at a site. Slope-conveyance measurements and two-section slope-area measurements should be avoided. If adequate reach length is not available, a critical-depth site, as discussed previously, should be located.

State of Flow

Flow is classified as subcritical, critical, or supercritical depending on whether the Froude number is less than 1, 1, or greater than 1, respectively. Most of the measurements reviewed had Froude numbers much greater than 1, and several were greater than 3. Studies by Dobbie and Wolf (1953), Jarrett (1984), and others indicated that supercritical flow can occur, and has occurred, in sand, smooth bedrock, and concrete channels but is only very localized in boulder-bed channels typical of the stream reaches reviewed. All streamflow data collected by the author and other data in the literature on boulder-bed streams (even on slopes greater than 0.05) showed Froude numbers of less than 1, indicating

subcritical flow. These high Froude numbers of the peak discharge computed by means of the slope-area method indicate that the measurements are overestimated. During flood flows, the combined effects of channel and cross-section variations, obstructions, transport of large-size bed material, and form roughness create extreme turbulence and large energy losses (often as localized hydraulic jumps) that result in increased flow resistance and larger expansion and contraction coefficients. The resulting flow is usually subcritical or critical, but rarely supercritical for any extent of the stream.

The state of flow generally is not known until the computations are made. The results should be questioned if the Froude number is much greater than 1 on steep-gradient boulder-bed streams or sand-bed streams. Relatively high Froude numbers, based on the computed discharge, probably indicate that not all the energy losses have been fully accounted for, as is also indicated by the extremely high velocities.

Stream Slope

Except for sand-bed streams, the channel bottom is not uniform but is a series of steps or drops whose spacing and height are controlled by the slope (Judd and Petersen, 1969). As slope increases, spacing decreases and height increases. These drops are formed by deposits of boulders across the channel or by natural bedrock outcrops and have been noticed on most higher gradient boulder-bed streams. These steplike features appear to be formed during extremely rare and large floods and usually remain stable during lesser flows. One should use extreme care in making a slope-area measurement that spans one or more of these steps, because the flow usually passes through critical depth. Manning's and Bernoulli's equations require a hydraulically connected water surface and do not apply where flow passes through critical depth in a computational reach. The slope-area method might be applicable at greater depths that drown out the drops.

Errors associated with peak discharge computed by means of the slope-area method generally become significant as stream slope exceeds about 0.01. Once stream slope exceeds a certain value, say 0.05, most of the problems discussed severely affect the computations. However, in many of the slope-area measurements reviewed, stream slopes were greater than 0.05, and one was 0.24. These measurements had the most problems discussed and had the highest unit discharges. Once stream slope exceeds a given value, say 0.08, which probably varies from stream to stream, slope-area measurements may be completely invalid and result in totally incorrect and overestimated peak discharges.

The most accurate measurements on higher gradient streams should result from a critical-depth measurement for which the boulder or bedrock steps are used as the control. Slope-area measurements made under adverse conditions should be viewed with suspicion as they violate several hydraulic limitations and assumptions.

RESEARCH NEEDS

This paper has presented a compilation of currently recognized problems associated with making valid slope-area measurements. The number and nature of the problems demonstrate the critical need for research to improve flood-measuring capabilities in higher gradient streams. Improvement of the slope-area method for application on higher gradient streams can be obtained through a combination of mathematical and physical modeling and field studies. Flume studies could be specifically designed to evaluate the effects of obstructions, expanding reaches, scalloped banks, viscosity, unsteady flow, stream slope, and vertical velocity on the energy losses, channel roughness, and flow velocity. Mathematical modeling could be used to evaluate the relative changes and to perform sensitivity analyses of processes, such as scouring, that cannot be physically modeled owing to their complexity and the interaction of the problems identified. Field studies could be made at or near streamflow-gaging stations where good rating curves are available. Physical and mathematical models of flow at these sites could be made and refined. Examples include the selection of a reach of a higher gradient stream near a gage to evaluate the critical-depth method of computing discharge, an evaluation of the effects of expanding reaches, and an evaluation of flow in very steep reaches.

Additional studies are needed to evaluate other methods for computing peak discharge. This paper addresses only the problems of the slope-area method; however, other indirect discharge methods (in which the same basic equations are used), including measurements in contracting openings, culverts, and supercritical flow flumes, and of embankment overflow need an evaluation for accuracy. A brief review of several applications of these techniques has yielded questionable results because the actual coefficients exceeded the range of verification.

There is also a need to evaluate alternative measuring techniques, such as superelevation around bends (Apmann, 1973). This method holds considerable promise, particularly for channels that are extremely sinuous and lack adequate reach length and for measurements of mudflows and debris flows. Research is needed to determine at what viscosity and density of flow, reconstructed from analysis of depositional features, present techniques are not.applicable or what modifications should be incorporated in these techniques to make them applicable.

DISCUSSION AND SUMMARY

The slope-area method, which requires substantial cost and effort, is widely used in determining peak discharge. The method has been verified on relatively tranquil flow in low-gradient streams with good results, but it is often applied to extremely turbulent flow in higher gradient streams in many parts of the United States. Large-flood measurements from different areas of the country were reviewed to determine whether there are common problems in the application of the slope-area method. This review indicated that there are common problems; for many higher gradient streams, measurement error is great and biased to yield larger than actual peak discharges. This can result in misleading maximum flood values and flood-frequency analyses, and in the overdesign of flood-plain structures.

The use of these overestimated peak-discharge values (often the cause of a flood being identified as a high outlier in flood-frequency analysis) results in overestimated discharges for a given frequency. Similarly, these large peak-discharge measurements also have been used to revise envelope curves of maximum recorded discharge for various sizes of drainage area. The Committee on Geology and Public Policy (1978) showed that, since 1890, increasingly larger floods have been recorded, particularly for drainages of less than 50 mi². For a 10-square-mile basin, the envelope curves indicated a maximum discharge of 4,000 ft³/s in 1890, 30,000 ft³/s in 1948, and 60,000 ft³/s in 1978 (Committee on Geology and Public Policy, 1978). The study indicates that this increase in discharge is a result of additional data collection as well as a longer timespan of recorded events. Three peak discharges that define that part of the envelope curve are probably overestimated. One of the sites used was the Big Thompson River tributary below Loveland Heights, Colo. (table 1). These overestimated flood discharges explain much of the increase in the envelope curves.

Errors in applying the slope-area method are associated with n-values, scour, expansion and contraction losses, viscosity, velocity distribution, unsteady flow, number of cross sections, state of flow, and stream slope. These problems are most common on higher gradient small-size drainage basins and generally become significant at stream slopes greater than about 0.01. Where slopes exceed about 0.08, hydraulic theory may not be applicable and may produce erroneous results. A brief discussion of these problems, tentative solutions, and research needs have been presented. The critical-depth method of computing peak discharge provides the most reasonable peak discharges in higher gradient streams. This paper addresses only the accuracy of slope-area measurements; however, the same general problems probably affect other indirect measurement methods and should be investigated. Research would provide the most benefits if physical, mathematical, and field studies were undertaken concurrently.

REFERENCES CITED

Aldridge, B.N., and Garrett, J.M., 1973, Roughness coefficients for streams in Arizona: U.S. Geological Survey Open-File Report, 87 p.

Andrews, E.D., and Costa, J.E., 1979, Stream channel changes and estimated frequency of a catastrophic flood, Front Range of Colorado: Geological Society of America Abstracts with Programs, v. 11, no. 7, p. 379.

Apmann, R.P., 1973, Estimating discharge from superelevation in bends: American Society of Civil Engineers, Journal of the Hydraulics Division, v. 98, HY1, p. 65-79.

Ayvazyan, O.M., 1979, Comparative evaluation of modern formulas for computing the Chezy coefficient: Soviet Hydrology, v. 18, no. 3, p. 244-248.

Bailey, J.F., and Ray, H.A., 1966, Definition of stage-discharge relation in natural channels by step-backwater analysis: U.S. Geological Survey Water-Supply Paper 1869-A, 24 p.

Barnes, H.H., Jr., 1967, Roughness characteristics of natural channels: U.S. Geological Survey Water-Supply Paper 1849, 213 p.

Barnes, H.H., Jr., and Davidian, Jacob, 1978, Indirect methods, in Herschy, R.W., ed., Hydrometry: Principles and Practices: New York, Wiley, p. 189-190.

Benson, M.A., and Dalrymple, Tate, 1967, General field and office procedures for indirect discharge measurements: U.S. Geological Survey Techniques of Water-Resources Investigations, Book 3, Chapter A1, 30 p.

Chow, V.T., 1959, Open channel hydraulics: New York, McGraw-Hill, 680 p.

Committee on Geology and Public Policy, 1978, Floods and people—a geological perspective: Geological Society of America Report, 7 p.

Costa, J.E., 1983, Paleohydraulic reconstruction of flash-flood peaks from boulder deposits in the Colorado Front Range: Geological Society of America Bulletin, v. 94, p. 986-1004.

Costa, J.E., and Jarrett, R.D., 1981, Debris flows in small mountain stream channels of Colorado and their hydrologic implications: Bulletin of the Association of Engineering Geologists, v. XVIII, no. 3, p. 309-322.

Crippen, J.R., and Bue, C.D., 1977, Maximum floodflows in the conterminous United States: U.S. Geological Survey Water-Supply Paper 1887, 52 p.

Dalrymple, Tate, and Benson, M.A., 1967, Measurement of peak discharge by the slope-area method: U.S. Geological Survey Techniques of Water-Resources Investigations, Book 3, Chapter A12, 12 p.

Dobbie, C.H., and Wolf, P.O., 1953, The Lynmouth Flood of August 1952: London, Proceedings of the Institution of Civil Engineers, v. 2, Part 3, p. 522-588.

Flaxman, E.M., 1974, Potential errors in peak discharge estimates obtained by indirect methods: Portland, Oregon,

U.S. Soil Conservation Service, West Technical Service Center, Engineering Technical Note no. 5, 15 p.

Golubtsov, V.V., 1969, Hydraulic resistance and formula for computing the average flow velocity of mountain rivers: Soviet Hydrology no. 5, p. 500-510.

Henderson, F.M., 1966, Open channel flow: New York, MacMillan Publishing Company, Inc., 522 p.

Herbich, J.B., and Shulits, Sam, 1964, Large-scale roughness in open-channel flow: American Society of Civil Engineers, Journal of the Hydraulics Division, no. HY6, p. 203-230.

Hinds, Julian, 1928, The hydraulic design of flumes and siphon transitions: American Society of Civil Engineers Transactions, v. 92, p. 1423-1459.

Hoyt, W.G., and Langbein, W.G., 1955, Floods: Princeton, N.J., Princeton University Press, 469 p.

Jarrett, R.D., 1984, Hydraulics of high-gradient streams: American Society of Civil Engineers, Journal of Hydraulics Division, v. 110, HY11, p. 1519-1539.

Jarrett, R.D., and Costa, J.E., 1985, Hydrology, geomorphology, and dam-break modeling of the July 15, 1982, Lawn Lake Dam and Cascade Lake Dam failure, Larimer County, Colorado: U.S. Geological Survey Open-File Report 84-612, 109 p.

Judd, H.E., and Petersen, D.F., 1969, Hydraulics of large bed element channels: Logan, Utah, Utah State University, Utah Water Research Laboratory, Report no. PRWG17-6, 115p.

Koloseus, H.J., and Davidian, Jacob, 1966, Free-surface instability correlations: U.S. Geological Survey Water-Supply Paper 1592-C, 72 p.

Li, R.M., and Simons, D.B., 1982, Geomorphological and hydraulic analysis of mountain streams, in Hey and others, ed., Gravel bed rivers: New York, Wiley, p. 425-441.

Limerinos, J.T., 1970, Determination of the Manning coefficient from measured bed roughness in natural channels: U.S. Geological Survey Water-Supply Paper 1898-B, 47 p.

Marchand, J.P., Jarrett, R.D., and Jones, L.L., 1984, Velocity profile, water-surface slope, and bed-material size for selected streams in Colorado: U.S. Geological Survey Open-File Report 84-733, 82 p.

Matthai, H.F., 1969, Floods of June 1965 in South Platte River basin, Colorado: U.S. Geological Survey Water-Supply Paper 1850-B, 64 p.

McCain, J.F., Hoxit, L.R., Maddox, R.A., Chappell, C.F., and Caracena, Fernando, 1979, Meteorology and hydrology in Big Thompson River and Cache la Poudre River basins, Larimer and Weld Counties, Colorado, Part A of Storm and flood of July 31-August 1, 1976, in The Big Thompson River and Cache la Poudre River basins, Larimer and Weld Counties, Colorado: U.S. Geological Survey Professional Paper 1115-A, p. 1-85.

Miller, D.L., Everson, C.E., Mumford, J.A., and Bertle, F.A., 1978, Peak discharge estimates used in refinement of the Big Thompson storm analysis, in Conference on flash floods, Hydrometeorological aspects: American Meteorological Society, May 2-3, 1978, p. 135-142.

Randall, M.L., and Humphrey, J.H., 1984, Estimating peak flows in unstable channels using indirect methods, in Elliott, C.M., River meandering—Conference Rivers '83, New Orleans, Louisiana, October 24-26, 1983, Proceedings: American Society of Civil Engineers, p. 574-585.

Richards, K.S., 1973, Hydraulic geometry and channel roughness—a non-linear system: American Journal of Science, v. 273, p. 877-896.

Riggs, H.C., 1976, A simplified slope-area method for estimating flood discharges in natural channels: U.S. Geological Survey, Journal of Research, v. 4, no. 3, p. 285-291.

Simons, D.B., and Richardson, E.V., 1966, Resistance to flow in alluvial channels: U.S. Geological Survey Professional Paper 422-J, 61 p.

Wormleaton, P.R., Allen, John, and Hadjipanos, Panos, 1982, Discharge assessment in compound channel flow: American Society of Civil Engineers, Journal of Hydraulics Division, v. 108, HY9, p. 975-994.

Correlations Between Basin Development Parameters and Water-Quality Characteristics of the Cape Fear River at Lock 1 Near Kelly, North Carolina

By J. Kent Crawford *and* Douglas A. Harned

Abstract

Water-quality data from long-term (24 years), fixed-station monitoring at the Cape Fear River at Lock 1 near Kelly, N.C., and various measures of basin development are correlated. Subbasin population, number of acres of cropland in the subbasin, number of people employed in manufacturing, and tons of fertilizer applied in the basin are considered as measures of basinwide development activity. Linear correlations show statistically significant positive relations between both population and manufacturing activity and most of the dissolved constituents considered. Negative correlations were found between the acres of harvested cropland and most of the water-quality measures. The amount of fertilizer sold in the subbasin was not statistically related to the water-quality measures considered in this report. The statistical analysis was limited to several commonly used measures of water quality including specific conductance, pH, dissolved solids, several major dissolved ions, and a few nutrients. The major dissolved ions included in the analysis were calcium, sodium, potassium, magnesium, chloride, sulfate, silica, bicarbonate, and fluoride. The nutrients included were dissolved nitrite plus nitrate nitrogen, dissolved ammonia nitrogen, total nitrogen, dissolved phosphates, and total phosphorus.

For the chemicals evaluated, manufacturing and population sources are more closely associated with water quality in the Cape Fear River at Lock 1 than are agricultural variables.

INTRODUCTION

Purpose and Scope

Decisionmakers frequently must determine management practices that best achieve water-quality improvement. Often, available water-quality data from long-term, fixed-station sampling sites document the need for additional management action, but clearcut appropriate choices may not be evident. In this report, prepared in cooperation with the North Carolina Department of Natural Resources and Community Development, water quality and subbasinwide development characteristics are examined and correlated for the Cape Fear River at Lock 1 near Kelly, N.C. (fig. 1); thus, likely target areas may be identified for effective implementation of management practices. Correlation analyses are used to make the comparisons.

Water-quality data are available from the Cape Fear River at Lock 1 from 1956 through 1980 water years. These data represent three data-collection efforts. First, data for 1956 through 1973 were collected from the station on the Cape Fear River near Acme, N.C. (Station 02105771), which was operated by the U.S. Geological Survey. This station was approximately 2 miles below the present station at Lock 1, and in both places water quality is considered to be the same. No effluent enters the stream between the two stations and both stations are above the point of maximum upstream saltwater intrusion (Giese and others, 1979). Second, data were collected at Lock 1 (Station 02105769) by the Survey from 1974 through 1980, when the station was operated as part of the National Stream Quality Accounting Network (NASQAN). Water-quality data from Lock 1 for 1974 through 1980 collected by the North Carolina Department of Natural Resources and Community Development (NRCD) are also included in the analyses. NRCD data are limited to measurements of pH, nitrite plus nitrate nitrogen, total phosphorus, and dissolved phosphates.

The complete water-quality data base available for this study contains concentrations of the major dissolved ions, including calcium, sodium, potassium, magnesium, chloride, sulfate, silica, bicarbonate, and fluoride. Dissolved solids, specific conductance, total hardness, and total alkalinity are also included along with concentrations of the nutrients—dissolved nitrite plus nitrate nitrogen, dissolved ammonia nitrogen, total nitrogen, dissolved phosphates, pH, and total phosphorus. Sampling was distributed fairly evenly among the different seasons throughout the entire 24-year sampling period.

The population of the subbasin, the number of acres of harvested cropland, the tons of fertilizer used, and the number of persons employed in manufacturing
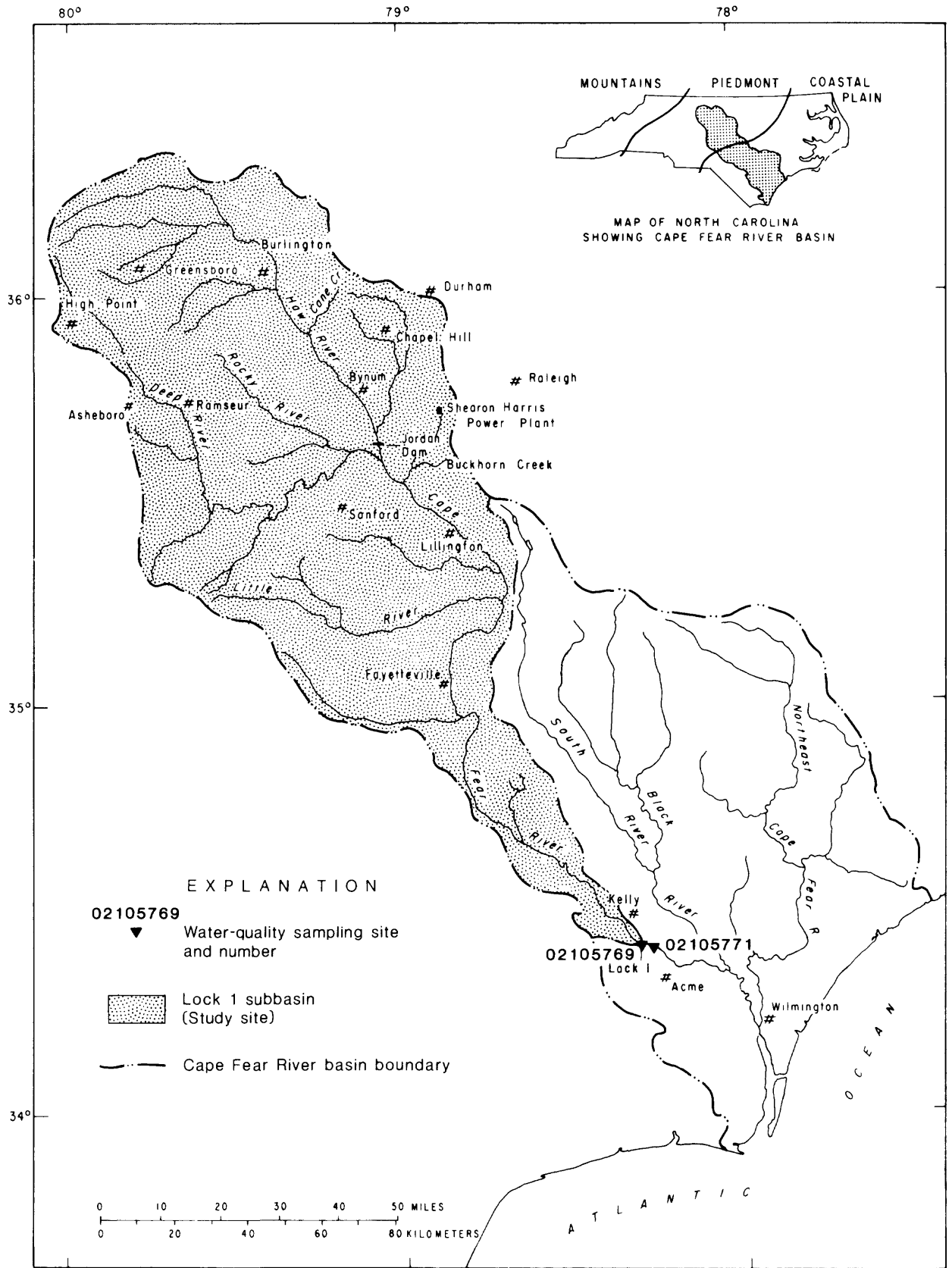
Figure 1. The Cape Fear River basin, Lock 1 subbasin, and location of sampling stations.

were measures of subbasin development. These were calculated from published records as detailed in the "Methods of Study" section of this report.

These two kinds of data, (1) long-term, fixed-station water-quality data and (2) information on development activities in the basin, are necessary for developing the relations presented in this report.

Basin Description

The Cape Fear River and its tributaries drain 9,010 mi^2 of the Piedmont and Coastal Plain provinces of North Carolina (fig. 1). The basin is the largest in the State and includes parts or all of 29 counties. The population of the basin is more than 1 million and is concentrated in several small cities (Greensboro, Burlington, Chapel Hill, Fayetteville, Durham, High Point, Sanford, and Wilmington). The topography consists of rolling hills, where the highest altitudes are slightly more than 1,000 feet. Hot, humid summers and mild winters characterize the climate of the basin. Two new impoundments in the basin, the B. Everett Jordan Reservoir and the cooling reservoir at the Shearon Harris Nuclear Power Plant, will affect the quality of the river, but neither impoundment was in place at the time data for this study were collected.

The study area (5,255 mi^2) consists of the subbasin upstream from Lock 1 (fig. 1) and contains 80 percent of the population of the Cape Fear basin. Approximately 156 Mgal/d (241 ft^3/s) of treated wastewater enters the Cape Fear above Lock 1 and constitutes about 4 percent of the average flow (5,740 ft^3/s) past Lock 1. Most of the study area is in the Piedmont of North Carolina and is underlain by metamorphic rocks, including relatively insoluble gneiss and schist in the west and more soluble metamorphosed volcanic and sedimentary rocks farther east. The low solubility of these underlying formations accounts for the low-ionic-strength water of the Cape Fear River. The river flows through quartz sand, clay, and marl in the Coastal Plain.

Acknowledgments

This report is an outgrowth of a major study addressing water-quality variability, pollution loads, and long-term trends in the major rivers of North Carolina; the study was conducted from 1979 to 1983 by the U.S. Geological Survey and NRCD, without whose support this report would not have been possible.

METHODS OF STUDY

Adjustments for Discharge

Interpretation of water-quality data from streams is complicated by the effects of stream discharge. In-creased discharge serves to dilute the concentrations of many dissolved substances. Conversely, decreased flow rates may concentrate substances in the water. Thus, a series of wetter than normal or drier than normal years can create the appearance of a change in water quality that may be only a consequence of variations in flow. Therefore, efforts to analyze water-quality data should first adjust for the influence of discharge.

Techniques adapted from Hirsch and others (1982) were used to adjust the Cape Fear River concentration data for effects of discharge on water quality. Five functions (linear, inverse, hyperbolic, logarithmic, and log-log) were used to model the relation of concentration versus discharge. Residuals from the fit of each function were squared and summed. The function with the smallest sum of squared residuals was chosen as the best fit. Residuals from this best fitting line were considered to have the effects of discharge removed. Next, residuals were adjusted by adding the long-term period-of-record average concentration to each residual. This makes the adjusted residuals positive and results in values near those of normal concentrations. Adjusted residual concentrations were then used for further analysis.

Measures of Development

Data on population, agriculture, and manufacturing were aggregated from available sources. Population data were taken from official census counts (U.S. Department of Commerce, 1971; 1981). These data are available for each county at 10-year intervals. Linear-interpolation was used to calculate populations for years between official census counts. County totals were adjusted to include only the part of each county that actually lies within the Cape Fear River basin. This adjustment was based on county-by-county subbasin populations (North Carolina Department of Water and Air Resources, 1972, unpublished data) calculated from detailed census maps for 1970 census data. Adjusted county populations were summed to obtain a total basin population.

Harvested cropland (row crops) was used as an indicator of agricultural activity. Information concerning the number of acres of cropland harvested annually from 1953 through 1976 for each county was available from the U.S. Department of Agriculture (1978). On the basis of the percentage of total land area of each county that is in the basin, countywide cropland figures were adjusted to include only the amount of cropland in the basin above Lock 1. Harvested cropland data from 1977 through 1980 are not available.

The amount of fertilizer sold annually by manufacturers to retailers and consumers in each county was used as an indicator of fertilizer applied in the county (North Carolina Department of Agriculture, 1973-1980). Again, data were adjusted according to the percentage

of land in each county lying within the basin. Four different chemical measures were included in the fertilizer analysis: (1) mixed fertilizers (mixtures of nitrogen, phosphorus, and potassium in various combinations); (2) fertilizer materials (fertilizers containing one primary ingredient such as nitrogen solutions or superphosphate); (3) lime (calcium and magnesium carbonates); and (4) land plaster (calcium sulfate). The sum of these four measures constitutes a fifth variable, total fertilizer usage. Fertilizer data are available from 1973 through 1980.

The number of people employed in manufacturing was used as an indicator of industrial activity. Manufacturing employment data from the Employment Security Commission of North Carolina (1973; 1980) were compiled annually beginning in 1962, by county. Again, population-distribution data were used to adjust countywide manufacturing employment data to values representative of the part of the county within the basin. County data were summed to give an overall value representing the entire study area. Manufacturing employment data from 1957 to 1961 are not available.

RESULTS AND DISCUSSION

To assess the effect of population, cropland, fertilizer usage, and manufacturing on water quality, linear correlations were calculated between measures of each of these development indicators and various water-quality constituents. Annual averages, rather than individual observations, were used in the analysis because cropland and fertilizer data for the basin are available only on an annual basis and, therefore, could not be related directly to individual water-quality observations.

The correlations were calculated for both pH and hydrogen-ion concentration. These two water-quality parameters are simply different expressions of the same chemical constituent, hydrogen ion. pH is the negative logarithm of the hydrogen-ion concentration. Because pH is a negative function of the hydrogen ion, correlations of these two parameters will have opposite signs. Because pH is a logarithmic function, the magnitude of the correlation coefficient between pH and a given basin characteristic will not be the same as between hydrogen-ion concentration and the same basin characteristic.

Population

Specific conductance and dissolved solids are useful indicators of broad changes in water quality. Both are significantly correlated with population in the basin (table 1). Variation of population and specific conductance with time is shown in figure 2.

Significant positive correlations were also found for hydrogen-ion concentration and dissolved magnesium, sodium, potassium, sulfate, and nitrite plus nitrate nitrogen with population (table 1). Dissolved constituents such as these are not normally removed by wastewater-treatment plants. It is, therefore, not surprising to see high correlations between population and these dissolved materials.

Manufacturing Employment

Specific conductance and dissolved solids also are significantly correlated with manufacturing employment in the basin (table 1). Variation of manufacturing employment and specific conductance with time is shown in figure 3.

Significant positive correlations with manufacturing employment were also found for total hardness and pH and for dissolved magnesium, potassium, sulfate, nitrite plus nitrate nitrogen, and silica.

Agricultural Effects

Specific conductance and dissolved solids are negatively correlated with the amount of cropland harvested and are not significantly related to any of the fertilizer measures (table 1). The variation of specific conductance and harvested cropland with time is shown in figure 4. The variation of specific conductance and mixed fertilizer with time is shown in figure 5. Significant negative correlations were also found between harvested cropland and hydrogen-ion concentration, dissolved sodium, potassium, sulfate, chloride, and total nitrogen (table 1).

Only two significant positive correlations were found for any of the measures of fertilizer usage. Positive relations were found between silica concentration and land plaster and between pH and mixed fertilizer tonnage (table 1). Fertilizer materials, lime, and the sum of all fertilizers were all negatively correlated with hardness and calcium, and bicarbonate concentrations. Land plaster was negatively correlated with total phosphorus. The relation of animal husbandry to chemical constituents and physical parameters of water was not investigated.

Cross Correlations

Cross correlations between independent variables can cloud the analysis and make it difficult to assess the relative effect of each variable individually. The cross correlation matrix for this study (table 2) shows a strong positive correlation between population and manufacturing employment. Thus, it is not possible to assess the relative importance of the individual effect that these two independent variables may have on the water quality of the Cape Fear River.

In addition, negative correlations are seen between acres of cropland harvested and population, and between acres of cropland harvested and number of people employed in manufacturing. In other words, as population and manufacturing employment increase, the number of acres of cropland decreases—an expected consequence of development.

Discussion

The positive correlations of specific conductance and dissolved solids with population and industrial activity are not surprising. Increases in population and manufacturing bring predictable deterioration in water quality. The unexpected negative correlation between harvested cropland and water quality may be attributed to the strong effect of industrial activity and population on water quality. The degradation of water quality from population increases and manufacturing activity apparently overshadows any improvements in water quality coming from decreasing acreages of cropland harvested. Therefore, from the water-quality characteristics that we examined, management options directed at controlling effluents from population and manufacturing sources appear to be the best means for achieving improvements in water quality.

The negative relations between calcium and lime and between bicarbonate and lime were unexpected because agricultural lime is composed of calcium and magnesium carbonate. Perhaps as more lime is applied on cropland, concentrations of calcium, hardness, and bicarbonate in receiving waters will increase.

Two alternative explanations can account for the apparent anomaly. First, agricultural lime applied in the Cape Fear basin may not be a dominate influence on water quality at Lock 1. This explanation is plausible because positive correlations of water-quality measures with both population and manufacturing indicate that these basin variables are important determinants of water-quality constituents in the river and probably overshadow any effect of lime. Also, although almost 150,000 tons of lime were sold in the basin in 1980, the total acreage in the basin is about 3.4 million. This amounts to an average of 90 pounds of lime per acre. Thus, the amount of calcium applied in agricultural liming is relatively small.

Second, the powdered lime that is applied to agricultural land is relatively insoluble and is not easily transported through the soils to the ground water. It is also not readily washed overland to receiving streams because much of it is probably quickly bound by the soils of the basin. Soils in this part of North Carolina have high cation-exchange capacities. Calcium is held very tightly by these soils, but sodium is held relatively loosely. Therefore, application of lime may result in more calcium bound to the soils as sodium is released

to the soil water. The positive, although weak, correlation between sodium and lime shown in table 1 gives support to this explanation.

The hydrogen ion and pH correlations again suggest that development in the basin has been associated with higher hydrogen-ion concentrations or lower pH in the stream. Conversely, the agricultural measures indicate that more cropland and greater fertilizer use are associated with higher pH and lower hydrogen-ion concentrations. However, these correlations do not imply causation. In fact, decreasing pH and increasing sulfate concentrations over time measured in streams have been related to acid rain (Altshuller and Linthurst, 1984). Acid rain is caused by factors related to population and industry, but, on a large scale, these factors may not be confined within the borders of a single river basin. Therefore, the measures of development within the Cape Fear Lock 1 subbasin may be only indirectly related to the true causes of water-quality changes.

Spurious correlations can also confuse interpretation of results. A correlation between two logically unrelated measures may be due simply to chance. For example, why land plaster shows a significant correlation with dissolved silica (table 1) is not at all clear.

Finally, the magnitude of population and industrial changes within the basin may mask effects of changing agricultural practices. The 1957 to 1980 growth in population in the subbasin of 50 percent and the increase in manufacturing employment of 40 percent may overshadow effects of a 20-percent reduction in cropland or 50-percent increase in fertilizer used.

SUMMARY

Changes in water-quality conditions at Lock 1 are statistically related to changes in the population, cropland harvested, and the amount of industrial activity in the basin. Specific conductance and concentrations of dissolved magnesium, sodium, potassium, sulfate, nitrite plus nitrate nitrogen, and dissolved solids are all positively correlated with population. Magnesium, potassium, sulfate, nitrite plus nitrate nitrogen, dissolved solids, specific conductance, pH, dissolved silica, and total hardness are positively correlated with manufacturing employment. Sodium, potassium, sulfate, chloride, specific conductance, and dissolved solids are all negatively correlated with the amount of cropland (row crops only) harvested. Somewhat surprisingly, calcium, hardness, and bicarbonate are negatively correlated with lime.

In sum, dissolved water-quality constituents at Lock 1 generally vary positively with population and industrial activity, and inversely with the acres of cropland harvested. Water quality at Lock 1 appears to be largely unrelated to the amount of fertilizer applied in the subbasin. However, causation cannot be assumed from correlation. The actual causes of changes in water quality

Table 1. Correlation coefficients, with significance probabilities and number of observations, between water-quality constituent concentrations, adjusted for discharge, and population, agriculture, and industry in the Lock 1 subbasin

Constituent	Correlation coefficients							
	Acres of cropland harvested	Subbasin population	Number of people employed in manufacturing	Mixed fertilizer tonnage	Fertilizer materials tonnage	Land plaster tonnage	Lime tonnage	Total fertilizer tonnage
Specific conductance	-0.45 .048 20	0.51 .010 24	0.58 .012 18	0.65 .083 8	0.29 .478 8	0.06 .882 8	0.13 .752 8	0.07 .870 8
Dissolved solids	-.58 .007 20	.72 <.001 24	.77 <.001 18	.46 .247 8	.11 .792 8	.28 .508 8	.43 .294 8	.33 .424 8
Total hardness	-.41 .073 20	.14 .519 24	.54 .020 18	.14 .735 8	-.86 .007 8	.43 .286 8	-.74 .036 8	-.80 .017 8
pH	.34 .147 20	-.30 .151 24	.55 .019 18	.72 .046 8	.15 .726 8	.06 .884 8	-.50 .202 8	-.30 .471 8
Hydrogen ion	-.46 .041 20	.41 .049 24	-.16 .519 18	-.62 .099 8	.23 .580 8	-.40 .325 8	.63 .096 8	.49 .222 8
Total alkalinity	-.08 .758 16	-.22 .360 20	.08 .769 17	.45 .264 8	-.68 .065 8	.57 .137 8	-.63 .092 8	-.59 .123 8
Bicarbonate	.07 .769 20	-.27 .199 24	.01 .980 18	.21 .615 8	-.86 .006 8	.39 .336 8	-.73 .040 8	-.78 .023 8
Dissolved calcium	-.28 .228 20	-.17 .424 24	.27 .271 18	.24 .574 8	-.86 .006 8	.42 .299 8	-.72 .044 8	-.76 .029 8
Dissolved magnesium	-.41 .069 20	.49 .016 24	.65 .004 18	-.61 .105 8	-.32 .439 8	.17 .684 8	-.26 .538 8	-.44 .271 8

Water-quality characteristic								
Dissolved sodium	.54 .013 20	.41 .046 24	.35 .154 18	.60 .115 8	.69 .058 8	-.54 .165 8	.16 .703 8	.39 .345 8
Dissolved potassium	-.61 .005 20	.86 <.001 24	.77 <.001 18	-.03 .944 8	.37 .369 8	-.11 .799 8	.53 .179 8	.56 .148 8
Dissolved sulfate	-.79 <.001 20	.85 <.001 24	.74 .001 18	.01 .983 8	.65 .083 8	-.37 .361 8	.26 .537 8	.34 .416 8
Dissolved chloride	-.66 .002 20	.30 .160 24	.29 .241 18	.47 .240 8	.40 .322 8	-.50 .211 8	-.04 .926 8	.12 .783 8
Dissolved fluoride	-.30 .194 20	-.14 .515 24	<.01 .986 18	.51 .193 8	-.29 .485 8	.20 .642 8	-.57 .144 8	-.47 .244 8
Dissolved silica	.22 .343 20	-.13 .530 24	.55 .017 18	-.43 .290 8	-.47 .239 8	.85 .008 8	-.06 .889 8	-.20 .630 8
Dissolved nitrite plus nitrate nitrogen	-.14 .574 18	.61 .003 22	.80 <.001 18	-.03 .939 8	-.26 .527 8	.02 .964 8	-.43 .286 8	-.47 .240 8
Dissolved ammonia nitrogen	.38 .755 3	.27 .564 7	.27 .607 6	-.29 .530 7	-.19 .679 709	.44 .321 7	-.04 .936 7	-.12 .796 7
Total nitrogen	-.95 .049 4	-.28 .507 8	.42 .349 7	.12 .784 8	-.18 .674 8	-.20 .632 8	-.19 .657 8	-.19 .656 8
Total phosphorus	.78 .068 6	.51 .130 10	-.33 .381 9	.35 .396 8	.42 .300 8	-.74 .034 8	.24 .560 8	.36 .378 8
Dissolved phosphates	[1]	-.13 .805 6	.78 .123 5	.10 .846 6	-.69 .130 6	.44 .381 6	-.08 .880 6	-.13 .799 6

[1]Only two data points available.
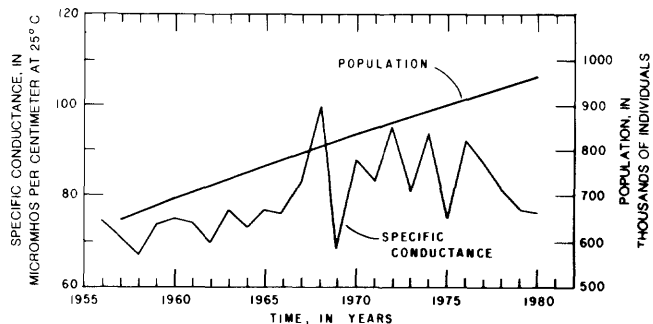
Figure 2. Annual variations of specific conductance, adjusted for discharge, with population.
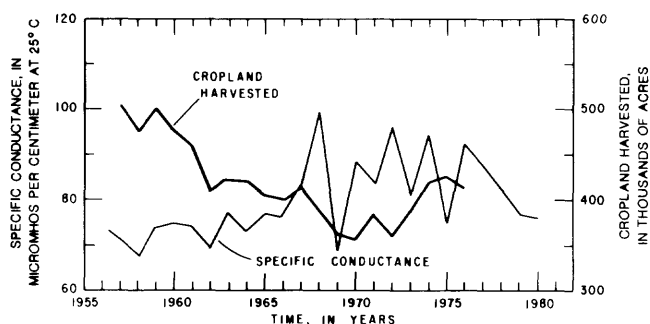
Figure 4. Annual variations of specific conductance, adjusted for discharge, with cropland harvested.
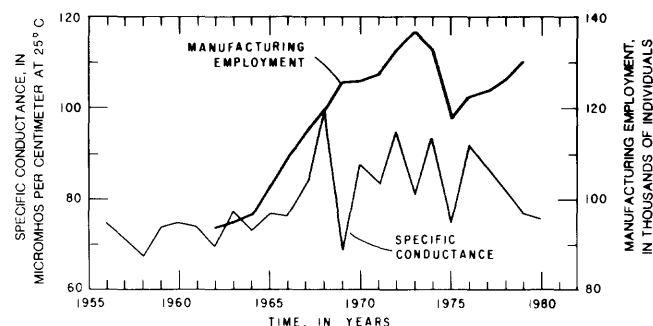
Figure 3. Annual variations of specific conductance, adjusted for discharge, with manufacturing employment.
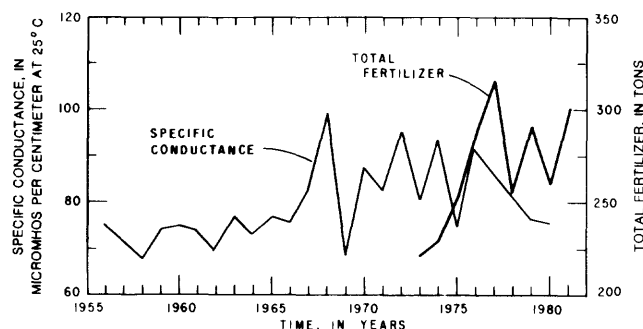
Figure 5. Annual variations of specific conductance, adjusted for discharge, with total fertilizers sold.

Table 2. Cross-correlation matrix for basin development characteristics

Constituent	Correlation coefficients[1]						
	Subbasin population	Number of people employed in manufacturing	Mixed fertilizer tonnage	Fertilizer materials tonnage	Land plaster	Lime	Grand total fertilizer
Acres of .... cropland harvested	-0.74 .0002 20	-0.54 .0369 15	-0.045 .955 4	0.50 .498 4	-0.13 .871 4	0.63 .371 4	0.63 .367 4
Subbasin .... population		0.81 <.001 18	-0.88 .004 8	0.33 .428 8	-0.063 .883 8	0.78 .0225 8	0.60 .118 8
Number of people .... employed in manufacturing			0.148 .752 7	-0.65 .114 7	0.78 .038 7	-0.56 .193 7	-0.59 .167 7
Mixed fertilizer .... tonnage				-0.17 .656 9	-0.19 .624 9	-0.52 .152 9	-0.30 .43 9
Fertilizer .... materials tonnage					-0.091 .816 9	0.73 .027 9	0.83 .006 9
Land plaster						-0.12 .77 9	-0.14 .720 9
Lime							0.97 <.001 9

[1] Numbers presented are the correlation coefficient, the significance probability, and the number of observations.

include a long chain of related variables such as effects of specific types of manufacturing and wastewater-treatment practices for which data are not readily available. On the basis of the available data and the constituents considered in this report, these results suggest that improving municipal and industrial effluents may improve water quality.

REFERENCES CITED

Altshuller, A.P., and Linthurst, R.A., eds., 1984, The acidic deposition phenomenon and its effects: Critical assessment review papers: U.S. Environmental Protection Agency, 600/8-83-016BF, v. II, Chapters 1 to 7, 690 p.

Employment Security Commission of North Carolina, 1973, North Carolina labor force estimates by county, area, and state: Raleigh, N.C., Bureau of Employment Security Research, 274 p.

———1980, North Carolina labor force estimates by county, area, and state: Raleigh, N.C., Bureau of Employment Security Research, 274 p.

Giese, G.L., Wilder, H.B., and Parker, G.G., Jr., 1979, Hydrology of major estuaries and sounds of North Carolina: U.S. Geological Survey Water-Resources Investigations Report 79-46, 175 p.

Hirsch, R.M., Slack, J.R., and Smith, R.A., 1982, Techniques of trend analysis for monthly water quality data: Water Resources Research, v. 18, no. 1, p. 107-121.

North Carolina Department of Agriculture, 1973-1980, North Carolina fertilizer tonnage report: Raleigh, N.C., Crop and Livestock Reporting Service, 153 p.

U.S. Department of Agriculture, 1978, Summary of North Carolina 1977 land utilization survey: Raleigh, N.C., North Carolina Crop and Livestock Reporting Service, 5-FR78-7, 7 p.

U.S. Department of Commerce, 1971, 1970 census of population, number of inhabitants, North Carolina: Bureau of the Census, 43 p.

———1981, 1980 census population and housing—North Carolina: Bureau of the Census, PHC80-V-35, 30 p.

Synthesis of Hydraulic Properties of Rocks with Reference to the Basin and Range Province, Southwestern United States

By Marion S. Bedinger, William H. Langer, and Joe E. Reed

Abstract

Hydraulic properties of rock types common in the Basin and Range province were synthesized. Field and laboratory hydraulic-conductivity measurements for many rock types having granular and fracture permeability have a log-normal distribution. For material that is granular and well sorted consisting of particles of approximately the same size and uniformly packed, the intrinsic permeability is a function of the square of the median grain size. For granular well-graded material with a broad range of grain sizes and argillaceous material, permeability may be an exponential function of the porosity. For fractured unweathered crystalline rock, the permeability is an exponential function of the porosity if the fracture density and geometry is uniform.

Beneath the zone of weathering, the average bulk-rock intrinsic permeability decreases as depth increases, owing to overburden pressure. The least permeable rocks in the Basin and Range province are argillaceous rocks and deeply buried, unweathered crystalline rocks that have hydraulic-conductivity values ranging from about 10^{-9} to 10^{-4} meters per day. The most permeable rocks include fractured karstic carbonate rocks that have hydraulic-conductivity values ranging from 10^{-1} to 10^5 meters per day, coarse-grained basin fill that has hydraulic conductivities from 10^{-1} to 10^3 meters per day, and fractured basalt that has hydraulic-conductivity values as great as 10^3 meters per day. Other rock types of importance in the province with intermediate hydraulic-conductivity values include weathered crystalline rocks, tuffaceous rocks, dense carbonate rocks, indurated clastic rocks, and dense lava flows.

Porosity values for granular materials generally are normally distributed and vary from a few percent to, at most, a few tens of percent. For greatly weathered fractured crystalline rock that has fracture and intergranular porosity, the porosity has a log-normal distribution; for unweathered fractured crystalline rock without intergranular porosity, the porosity probably is log-normally distributed.

INTRODUCTION

This report presents results of a synthesis of hydraulic rocks, which was part of a study of the Basin and Range province (fig. 1) to identify geohydrologic environments and characteristics favorable for the isolation of high-level radioactive waste. The study was designed to screen the Basin and Range province by a process in which successively smaller land units are considered in increasing detail. An introduction to the study and the results of the characterization and evaluation of the province are given in reports by Bedinger, Sargent, and Reed (1984); Sargent and Bedinger (1985); and Bedinger, Sargent, and Brady (1985).

Hydraulic properties of rocks in a region cannot be predicted without site-specific in situ, or laboratory tests. However, it was not practicable at the second step of the study to determine site-specific values of hydraulic properties for estimating traveltimes of water particles or waste. The literature, which contains considerable data on measurements of hydraulic conductivity and porosity has been searched for data from the Basin and Range province and data for rocks of similar characteristics elsewhere. We reviewed and synthesized these data in order to derive ranges of values for hydraulic conductivity and porosity applicable to rocks in the Basin and Range province. Because site-specific criteria were not considered at the regional phase of study, ranges of hydraulic properties in a region were adequate for estimating relative traveltimes of water particles (see, for example, Bedinger, Langer, and Reed, 1985).

PERMEABILITY AND POROSITY OF EARTH MATERIALS

The hydraulic conductivity, K, of a rock is a function of the density of the water, ρ, and the dynamic viscosity of the water, μ, in the rock matrix, the acceleration of gravity, g, and the intrinsic permeability of the rock, k.

$$K = \rho g k / \mu \qquad (1)$$
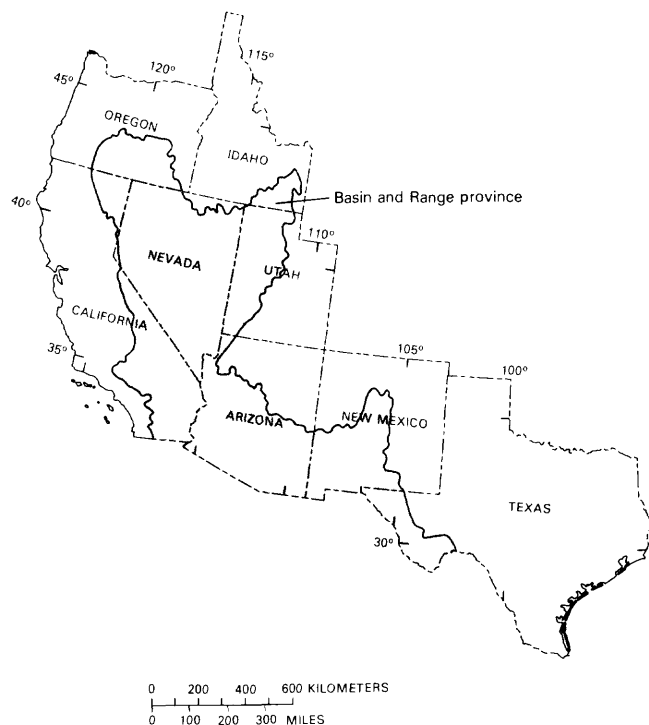
Figure 1. Location of Basin and Range province.

The hydraulic conductivity is thus a function of the field of gravity, the properties of the rock, and the properties of the water. Intrinsic permeability is solely a property of the rock that is dependent upon the size and shape of the pores.

In porous media consisting of grains of mean diameter, d, the intrinsic permeability is given by Hubbert, (1940, p. 819):

$$k = Cd^2 \qquad (2)$$

where C is a constant that depends on the distribution of grain sizes, the sphericity and roundness of grains, and the nature of their packing which in turn determines porosity. The diameter, d, of the mean grain size is taken as being proportional to the size of the typical pore. This relationship was demonstrated theoretically by Slichter (1899) for spheres of uniform packing. The relationship also has been found to be true (Bedinger, 1961) for natural granular materials that are relatively well sorted, that is, composed of particles having approximately the same size, and well rounded. Olsen (1962, p. 137) attributed the lack of a similar grain size-permeability relationship for clays to unequal pore sizes due to grouping arrangements of particles. It is also significant that in equation 2, the mean grain diameter, d, is used as a surrogate for the mean void aperture of sand- and gravel-sized materials. For clay, whose particles are typically characterized as plates, the mean grain diameter is not a measure of the mean void aperture.

Flow through a fracture has been analyzed by many investigators on the assumption of flow between two parallel plates. If we use this assumption for a single set of parallel fractures with uniform aperture width, ω, and uniform spacing between fractures, Δ, intrinsic permeability and porosity for this fracture set are (Snow, 1968a, p. 80)

$$k = \frac{\omega^3}{12\Delta}$$

and

$$\phi = \frac{\omega}{\Delta} \qquad (3)$$

Flow through multiple sets of uniform fractures, based on the above relations for each set, also indicates that the intrinsic permeability varies as a power function of the fracture aperture and the direct relation between fracture aperture and porosity. For example, for three sets of uniform fractures, each set at right angles to the others, and all three having the same aperture width and fracture spacing (Snow, 1968a, p. 80),

$$k = \frac{\omega^3}{6\Delta}$$

and

$$\phi = \frac{3\omega}{\Delta} \qquad (4)$$

This fracture system, termed a "cubic system" by Snow (1968a, p. 80), separates the dense medium into uniform cubes.

In nature, the extremely variable fracture geometry and aperture are extremely variable resulting in marked anisotropy of fractured rocks. The great variability in fracture distribution creates problems in scale of measuring hydraulic properties and mapping areal distribution of hydraulic properties in fractured rocks.

Davis (1969, 1980), Freeze (1975), and Neuman (1982) cited investigators who have concluded that large numbers of hydraulic-conductivity measurements from a single rock type having intergranular or fracture permeability are probably log-normally distributed. Davis (1969) also cited studies that suggest that specific capacity and well yield, which are indirect measures of hydraulic conductivity, have log-normal distributions when measurements are limited to single rock types.

Davis (1969) and Freeze (1975), in reviewing work of several investigators, indicated that porosity values from a single formation have a normal distribution. Most of the work cited by Davis and Freeze refers to porosity of clastic material. In well-sorted granular material, reported values of porosity range within a few percent, from about 34 to 42 percent for sand and from about 45 to 52 percent for silt. In contrast, porosity of a poorly sorted or well-graded granular material may

range from several to 10 or 20 percent accompanied by a change in permeability of 1 or 2 orders of magnitude. Fracture porosity, however, may range within several orders of magnitude and appears to have a log-normal distribution.

Slichter (1899) showed that there is no relationship between permeability and porosity for media composed of spheres in which the diameter and arrangement of grains are uniform and identical. Thus, in sand-sized granular materials that are very well sorted and have uniform shape, packing, and a small range in porosity values, the intrinsic permeability may not vary greatly with the relatively small range in porosity.

Many natural granular materials differ in sorting, packing, and uniformity of grains and, as a result, show wide ranges in porosity values. Particularly important in affecting porosity is the degree to which the voids between the coarser particles are filled by finer particles. Such materials may have a discernible relation between porosity and permeability. An increase in permeability with increase in porosity was shown by Davis (1980, p. 7) for lower Mesozoic Navajo Sandstone and by Davis (1969) for oil-bearing sands. Chilingarian and others (1975) determined the relation between permeability and porosity for very well graded coarse-grained to clayey sandstone. The relationship indicated in each of the works cited above is that permeability is an exponential function of the porosity.

RELATION OF HYDRAULIC PROPERTIES TO DEPTH

Many studies have shown that the permeability and porosity of crystalline rocks decrease as depth increases. Well yields, an indirect measure of permeability, have been shown to decrease as well depth increases (LeGrande, 1954; Dingman and others, 1956; Davis, 1969; and Davis and Turk, 1964). Many investigators ascribe the greater values of permeability and porosity near the surface to increased jointing owing to release of stress by erosional unloading (Jahns, 1943; Davis and Turk, 1964; and Snow, 1968b, p. 168) and to weathering of the rock (Davis and Turk, 1964). Porosities of unweathered crystalline rocks generally are less than 1 percent; but weathering commonly produces porosities ranging from 30 to 50 percent (Davis and Turk, 1964; Morris and Johnson, 1967).

Most available data for hydraulic properties, well yield, and specific capacity are for relatively shallow depths, that is, several tens of meters; few data are for depths of greater than 150 m. Ground-water flow analyses for studies pertaining to the isolation of high-level radioactive waste require knowledge of hydraulic properties at depths of as much as several thousand meters. At depths below about 30 to 150 m, weathering and

fractures due to release of confining pressures by erosional unloading probably are not significant. At increased depth below the land surface, overburden pressures tend to decrease the apertures of joints or fractures and the size of pores and, therefore, tend to decrease the porosity and intrinsic permeability. Chemical changes, such as solution and deposition of minerals, also may affect porosity and permeability of rocks to depths as great as a few thousand meters (Keys and Sullivan, 1979). Solution-type voids and relict-cavernous conditions in carbonate rocks have been penetrated by boreholes at depths of more than 2,000 m.

Vertical effective stress is the difference between the pressure exerted downward by the weight of rock and liquids above a point and the liquid pressure at the same point. Relative permeability decreased 20 to 40 percent in response to effective stress in laboratory tests of a sandstone (Fatt and Davis, 1952). Olsen (1972) reported that intrinsic permeability in kaolinite as a function of effective stress decreased 3 orders of magnitude (from about 10^{-11} to 10^{-14} cm^2) under a consolidation load change of less than 3 orders of magnitude (from 100 to less than 10^5 kPa). Laboratory measurements of intrinsic permeability of granite under effective pressures ranging from 10^4 to 4×10^5 kPa ranged from 350×10^{-17} to 4×10^{-17} cm^2 (Brace and others, 1968). Hydraulic-conductivity values from laboratory-consolidation tests of Cretaceous Pierre Shale had a tendency to substantially decrease with effective stress (Bredehoeft and others, 1983, fig. 23). Thus, laboratory data indicate that an increase in overburden pressure is accompanied by a decrease in hydraulic conductivity.

The studies of fracture distribution in wells as deep as a few thousand meters (Seeburger and Zoback, 1982; Davison and others, 1982; Keys and Sullivan, 1979) indicate that numerous fractures are found throughout the wells. The change in fracture density with depth ranged from a slight decrease to an increase related to a change in lithology. In some wells to depths of several thousand meters, fractures were relatively uniformly distributed, whereas in others they were concentrated primarily in densely fractured intervals. In the wells examined by Seeburger and Zoback (1982) near Palmdale, Calif., fractures were steeply dipping. Observed horizontal fractures were few; fracture density differed significantly, and fracture orientation showed considerable difference within an area. They concluded that surface-fracture patterns probably are a good indication of the orientation of fractures in the upper 1 kilometer of crust, and that there was no simple, genetic relationship between fracture sets and regional stress field or structure. Logging of holes to depths of 1,000 m in crystalline rocks in Ontario and Manitoba, Canada (Davison and others, 1982), indicated that fractures intersected the boreholes at all depths, although there were intervals of a few tens of meters that appeared to be relatively free of fractures.

Although fractures may be common to depths of several thousand meters, fractures must be open to possess permeability; fractures must be interconnected for the rock to transmit water. Because fractures may be closed or sealed, the presence of fractures alone is not an indication of permeability. The studies of Davison and others (1982) Keys and Sullivan (1979), however, indicate contrarily that zones with substantial permeability were found at great depth, and permeability was more variably distributed than fracture density. Direct evidence from boreholes indicates that significant permeability occurs locally at depths of a few thousand meters (Keys, 1979, and Keys and Sullivan, 1979). Borehole data may provide little or no indication of the regional extent of permeable zones at depth. Regional fracture permeability is dependent not only on the presence of open fractures, but also on the intersection of fractures within different sets. Indirect evidence for significant regional permeability at depths of as much as a few thousand meters is gained from studies of groundwater flow systems in igneous rock terrane in geothermal areas (Sorey and others, 1978) and in consolidated sedimentary rock terrane of low permeability (Bedinger and others, 1979).

Data from in-place measurements in one or a few boreholes may not reveal a decrease in hydraulic conductivity with vertical effective stress (Davison and others, 1982). The observed variability of fracture permeability with depth in a borehole has led some investigators to place little credence on establishing a consistent relation between thickness of overburden and fracture permeability. The relationship is complex and affected by other factors, including rock type (Davison and others, 1982), fracture orientation (Gale, 1982), and the history of tectonic stress in a region. However, analysis of data having regional significance shows a decrease in hydraulic conductivity with depth. The study of Snow (1968) showed a relationship between permeability and overburden for relatively shallow depths. Using data on permeability of crystalline rocks from four damsites in the Front Range of Colorado, Snow found that the logarithm of hydraulic conductivity decreased in proportion to the logarithm of depth from near the surface to a depth of about 100 m. Hydraulic conductivity decreased more than 3 orders of magnitude within the 100 m. Regional values of hydraulic conductivity obtained from flow simulations for confining layers in the northern Great Plains clearly indicate a decrease in hydraulic conductivity with increase in the vertical effective stress (Bredehoeft and others, 1983, fig. 23). Johnson (1981) and Davis (1984) plotted the decreasing trend of hydraulic conductivity in metamorphic and plutonic igneous rocks with depth for localities in California and Sweden. Results of recent tests in boreholes to depths of 800 m in Sweden show a decrease in hydraulic conductivity with depth (Ahlbom,

Albino, Carlsson, Nilsson, and others, 1983; Ahlbom, Carlsson, Gentzschein, and others, 1983; Ahlbom, Albino, Carlsson, Danielson, and others, 1983; Ahlbom, Carlsson, Carlsten, and others, 1983). The Swedish tests distinguish between hydraulic conductivities of the rock mass and local fracture zones (Ahlbom, Albino, Carlsson, Gentzschein, and others, 1983) and between hydraulic conductivities of the rock mass, local fracture zones, and regional fracture zones (Ahlbom, Carlsson, Gentzschein, and others, 1983). The data from Sweden show a great decrease in hydraulic conductivity with depth to about 300 m and less decrease in hydraulic conductivity with greater depth.

Few data are available for porosity of crystalline rocks below the zone of weathering. Snow (1968b) estimated that porosity decreased from 0.0004 near the land surface to 0.00001 at 60 m. Davis (1980), recognizing the paucity of data, estimated that the effective porosity might decrease with depth from an average of 0.002 at a depth of 50 m, 0.001 at 200 m, to perhaps less than 0.0005 at 500 m. We have assumed a decrease in effective porosity with depth and with decreasing hydraulic conductivity.

SYNTHESIS OF HYDRAULIC PROPERTY DATA

The following generalizations are made from the preceding discussions and were followed in synthesizing the data from the literature for determining values of hydraulic conductivity and porosity:

1. Field and laboratory hydraulic-conductivity measurements for many rock types having granular and fracture permeability predominantly have a log-normal probability distribution.
2. Porosity values for granular materials are generally normally distributed and range from a few to several tens of percent. For granular materials that are well sorted, that is, composed of particles having approximately the same size, and uniformly packed, the porosity is large and varies only slightly; permeability is a function of the square of the median-grain size. For granular, well-graded material, that is, having a gradation through a broad range of particle size material, the porosity ranges from a few to several tens of percent; for these materials permeability may be an exponential function of the porosity.
3. For fractured crystalline rock that is greatly weathered, with fracture and intergranular porosity, the porosity is assumed to have a normal distribution; but, for a fractured crystalline rock that is relatively unweathered, the porosity probably has a log-normal distribution. For fractured, unweathered crystalline rock, the permeability is an exponential function of the porosity where fracture density and geometry are uniform.

4. Beneath the zone of weathering, average bulk-rock intrinsic permeability of crystalline rock decreases as depth increases owing to overburden pressure. Commonly, a systematic or uniform decrease with depth is not obvious from data from a single test hole. However, larger data sets from several localities in the world at depths to less than 1,000 m indicate a decrease in permeability with depth. The decrease in permeability appears to be greater for depths less than 300 m and the decrease is less for greater depths. The occurrences of zones of significant permeability generally decrease, but localized zones of significant permeability have been penetrated at depths as great as a few thousand meters.

Values of hydraulic conductivity and porosity for rock types common in the Basin and Range province were compiled from the literature. Many such values of hydraulic conductivity are reported without corresponding data on the viscosity and density of the water; conversion of the values to intrinsic permeability could, therefore, not be made uniformly. Accordingly, hydraulic-conductivity values, as reported in the literature, are used in this synthesis. Figure 2 shows a general-ized log-normal plot of hydraulic conductivity for the 14 rock types present in the Basin and Range province in this plot; we have used the generalizations stated above and a great deal of judgment. The hydraulic-conductivity values show a log-normal distribution because we plotted the distribution as a straight line on log-probability coordinates. We drew the distribution for a rock type, for which there were many reported values of hydraulic conductivity, using the spread from 1 to 99 percentiles, the range of values reported in the literature. The approximate mean of the majority of the values of hydraulic conductivity was placed at the 50-percentile value and the majority of the values were included within about 1 standard deviation on each side of the mean (16.5 to 83.5 percentiles).

We estimated porosity values, wherever possible, by using pair values of porosity and hydraulic conductivity from individual samples. Lacking pair values, we estimated porosities from the relations between porosity and hydraulic conductivity expressed in the preceding paragraphs. The values of hydraulic conductivity and its associated porosity for the mean and 16.5 and 83.5 percentiles for each rock type are presented in table 1.

HYDRAULIC CONDUCTIVITY, K, IN METERS PER DAY

EXPLANATION

BASALT
  1-Moderately dense to dense lava flows
  2-Fractured cavernous basalt

BASIN FILL
  1-Fine-grained basin-fill
  2-Coarse-grained basin-fill

CARBONATE ROCKS
  1-Dense to moderately dense carbonate rocks
  2-Fractured, karstic carbonate rocks

CLASTIC ROCKS
  1-Fine-grained clastic rocks
  2-Coarse-grained clastic rocks

METAMORPHIC ROCKS
  1-Unweathered metamorphic and intrusive rocks with fracture permeability, greater than 300 meters below land surface
  2-Metamorphic and intrusive rocks with fracture permeability, less than 300 meters below land surface
  3-Weathered metamorphic and intrusive rocks

TUFF
  1-Nonwelded to partially welded, bedded tuff
 2-Welded, moderately fractured to dense tuff
  3-Fractured, welded tuff

Figure 2. Hydraulic-conductivity distributions estimated for rock types.

Table 1. Hydraulic properties of rocks in the Basin and Range province

Rock type	Description	16.5-percentile Hydraulic conductivity (K) (m/d)	16.5-percentile Effective porosity (Φ)	16.5-percentile K/Φ (m/d)	Mean Hydraulic conductivity (K) (m/d)	Mean Effective porosity (Φ)	Mean K/Φ (m/d)	83.5-percentile Hydraulic conductivity (K) (m/d)	83.5-percentile Effective porosity (Φ)	83.5-percentile K/Φ (m/d)	References (see list below)
Metamorphic rocks, felsic and mafic intrusive rocks	Weathered	2×10^{-3}	0.03	6×10^{-1}	3×10^{-2}	0.05	6×10^{-1}	4×10^{-1}	0.07	6×10^{0}	1, 4, 6, 9, 10, 14, 18, 20, 21, and 22
	Fracture permeability; depth more than 300 m.	1×10^{-5}	.002	5×10^{-3}	5×10^{-4}	.003	2×10^{-1}	2×10^{-2}	.005	4×10^{0}	
	Fracture permeability; depth less than 300 m.	2×10^{-8}	.00004	5×10^{-4}	3×10^{-7}	.0001	3×10^{-3}	6×10^{-6}	.0003	2×10^{-2}	
Lava flows; includes basalt, rhyolite, and trachyte	Fractured and cavernous.	2×10^{-2}	.11	2×10^{-1}	5×10^{-1}	.15	3×10^{0}	1×10^{1}	.19	5×10^{1}	3, 6, 8, 12, 14, and 22
	Moderately dense to dense.	5×10^{-5}	.004	1×10^{-2}	4×10^{-4}	.01	4×10^{-2}	4×10^{-3}	.03	1×10^{-1}	
	Welded and fractured.	3×10^{-1}	.02	2×10^{1}	1×10^{0}	.03	3×10^{1}	5×10^{0}	.04	1×10^{2}	
	Welded and moderately fractured to dense.	3×10^{-5}	.0004	8×10^{-2}	4×10^{-4}	.001	4×10^{-1}	5×10^{-3}	.003	2×10^{0}	4, 10, 12, 16, 18, 20, 21, and 22
Tuff	Nonwelded, partially welded, friable, pumiceous, zeolitized, and bedded friable.	2×10^{-5}	.33	6×10^{-5}	4×10^{-5}	.35	1×10^{-3}	5×10^{-3}	.37	1×10	

Rock type										References
Clastic sedimentary rocks (consolidated)										
Coarse-grained (sandstone and conglomerate).	5×10^{-3}	.12	4×10^{-2}	3×10^{-2}	.18	2×10^{-1}	3×10^{-1}	.23	1×10^{0}	2, 3, 6, 7, 11, 13, and 23
Fine-grained (argillite and shale).	3×10^{-8}	.10	3×10^{-7}	5×10^{-7}	.22	2×10^{-6}	1×10^{-5}	.30	3×10^{-5}	
Carbonate rocks; includes limestone, dolomite, and marble										
Fractured, karstic, cavernous.	4×10^{0}	.09	4×10^{1}	6×10^{1}	.12	5×10^{2}	1×10^{2}	.16	6×10^{3}	4, 6, 14, 15, 17, 21, and 22
Dense to moderately dense.	5×10^{-4}	$.005^{-1}$	1×10^{-1}	3×10^{-3}	.01	3×10^{-1}	2×10^{-2}	.02	1×10^{0}	
Basin fill (unconsolidated)										
Coarse-grained (sand and gravel).	1×10^{0}	.12	8×10^{0}	1×10^{1}	.18	6×10^{1}	7×10^{1}	.23	3×10^{2}	3, 5, and 19
Fine-grained (clay and silt).	1×10^{-5}	.29	3×10^{-5}	2×10^{-4}	.32	6×10^{-4}	2×10^{-3}	.36	6×10^{3}	

References:

1. Brace, 1980.
2. Brown and Silvey, 1973.
3. Davis, 1969.
4. Davis, 1980.
5. Davis and DeWiest, 1966.
6. Freeze and Cherry, 1979.
7. Gondouin and Scala, 1958.
8. Isherwood, 1981.
9. Jamieson and Freeze, 1983.
10. Keller, 1960.
11. Lin, 1978.
12. Morris and Johnson, 1967.
13. Muskat, 1937.
14. Rasmussen, 1964.
15. Rove, 1947.
16. Rush, Thordarson, and Bruckheimer, 1983.
17. Sanyal, Kvenvolden, and Marsden, 1971.
18. Thordarson, 1965.
19. Trauger, 1972.
20. Winograd, 1971.
21. Winograd and Thordarson, 1975.
22. Wolff, 1982.
23. Wyckoff and others, 1934.

Table 1 also includes a K/ϕ value for each hydraulic conductivity-porosity pair; K/ϕ is a measure of the relative velocity of ground-water flow. Strictly interpreted, the K/ϕ value is the ground-water velocity under a hydraulic gradient of 1.

REFERENCES CITED

Ahlbom, K., Albino, B., Carlsson, L., Danielson, J., Nilsson, G., Olsson, O., Sehlstedt, S., Stejskal, V., and Stenberg, L., 1983, Evaluation of the geological, geophysical, and hydrogeological conditions at Kamlunge: Swedish Nuclear Fuel Supply, Co./Division KBS, SKBF/KBS Technical Report 83-54, 66 p.

Ahlbom, K., Albino, B., Carlsson, L., Nilsson, G., Olsson, O., Stenberg, L., and Timje, H., 1983, Evaluation of the geological, geophysical, and hydrogeological conditions at Gidea: Swedish Nuclear Fuel Supply, Co./Division KBS, SKBF/KBS Technical Report 83-53, 70 p.

Ahlbom, K., Carlsson, L., Carlsten, L-E., Duran, O., Larsson, N-A., and Olsson, O., 1983, Evaluation of the geological, geophysical, and hydrological conditions at Fjallveden: Swedish Nuclear Fuel Supply, Co./Division KBS, SKBF/KBS Technical Report 83-52, 72 p.

Ahlbom, K., Carlsson, L., Gentzschein, B., Jamtlid, A., Olsson, O., and Tiren, S., 1983, Evaluation of the geological, geophysical, and hydrogeological conditions at Svartboberget: Swedish Nuclear Fuel Supply, Co./Division KBS, SKBF/KBS Technical Report 83-55, 69 p.

Bedinger, M.S., 1961, Relation between median grain size and permeability in the Arkansas River Valley, Arkansas: U.S. Geological Survey Professional Paper 424-C, p. 31-32.

Bedinger, M.S., Langer, W.H., and Reed, J.E., in press, Ground-water hydrology, in Bedinger, M.S., Sargent, K.A., and Langer, W.H., eds., Studies of geology and hydrology in the Basin and Range province, southwestern United States, for isolation of high-level radioactive waste—Characterization of the Trans-Pecos region, Texas: U.S. Geological Survey Professional Paper 1370-B.

Bedinger, M.S., Pearson, F.J., Jr., Reed, J.E., Sniegocki, R.T., and Stone, C.G., 1979, The waters of Hot Springs National Park, Arkansas—Their nature and origin: U.S. Geological Survey Professional Paper 1044-C, 33 p.

Bedinger, M.S., Sargent, K.A., and Brady, B.T., 1985, Geologic and hydrologic characterization and evaluation of the Basin and Range province relative to the disposal of high-level radioactive waste—Part III, Geologic and hydrologic evaluation: U.S. Geological Survey Circular 904-C, 27 p.

Bedinger, M.S., Sargent, K.A., and Reed, J.E., 1984, Geologic and hydrologic characterization and evaluation of the Basin and Range province relative to the disposal of high-level radioactive waste—Part 1, Introduction and guidelines: U.S. Geological Survey Circular 904-A, 67 p.

Brace, W.F., 1980, Permeability of crystalline and argillaceous rocks: International Journal of Rock Mechanics and Mining Sciences and Geomechanics Abstracts, v. 17, no. 5, p. 241-251.

Brace, W.F., Walsh, J.B., and Frangos, W.T., 1968, Permeability of granite under high pressure: Journal of Geophysical Research, v. 73, no. 6, p. 2225-2236.

Bredehoeft, J.D., Neuzil, C.E., and Milly, P.C.D., 1983, Regional flow in the Dakota Aquifer—A study of the role of confining layers: U.S. Geological Survey Water-Supply Paper 2237, 45 p.

Brown, D.L., and Silvey, W.D., 1973, Underground storage and retrieval of fresh water from a brackish-water aquifer, in Braunstein, J., ed., Underground waste management and artificial recharge: American Association of Petroleum Geologists, v. 1, p. 379-419.

Chilingarian, G.V., Wolf, K.H., and Allen, D.R., 1975, Compaction of coarse-grained sediments, 1—Chapter 1, Introduction: Developments in Sedimentology, v. 18A, p. 1-42.

Davis, R.W., 1984, Review of buried crystalline rocks of eastern United States in selected hydrogeologic environments potentially suitable for isolating high-level radioactive wastes: U.S. Geological Survey Water-Resources Investigations Report 84-4091, 20 p.

Davis, S.N., 1969, Porosity and permeability of natural materials, in DeWiest, R.J.M., ed., Flow through porous media: New York, Academic Press, p. 54-89.

———1980, Hydrogeologic effects of natural disruptive events on nuclear waste repositories: Richland, Washington, Pacific Northwest Laboratory Battelle Memorial Institute, Office of Nuclear Waste Isolation, PNL-2858, UC-70, 33 p.

Davis, S.N., and DeWiest, R.J.M., 1966, Hydrogeology: New York, John Wiley, 463 p.

Davis, S.N., and Turk, L.J., 1964, Optimum depth of wells in crystalline rock: Groundwater, v. 2, no. 2, p. 6-11.

Davison, C.C., Keys, W.S., and Paillet, F.L., 1982, Use of borehole-geophysical logs and hydrologic tests to characterize crystalline rock for nuclear-waste storage, Whiteshell nuclear research establishment, Manitoba, and Chalk River nuclear laboratory, Ontario, Canada: Atomic Energy Canada Limited and U.S. Geological Survey Office of Nuclear Waste, Battelle Memorial Institute Technical Report, ONW1-418, UC-70, 103 p.

Dingman, R.J., Ferguson, H.F., and Martin, R.O.R., 1956, The water resources of Baltimore and Harford Counties: Maryland Department of Geology, Mines, and Water Resources Bulletin 17, 233 p.

Fatt, I., and Davis, D.H., 1952, Reduction in permeability with overburden pressure: Petroleum Transactions of the American Institute of Mining and Metallurgical Engineers, v. 195, p. 329.

Freeze, R.A., 1975, A stochastic-conceptual analysis of one-dimensional groundwater flow in nonuniform homogeneous media: Water Resources Research, v. 11, no. 5, p. 725-741.

Freeze, R.A., and Cherry, J.A., 1979, Groundwater: Englewood Cliffs, N.J., Prentice-Hall Inc., 604 p.

Gale, J.E., 1982, Assessing the permeability characteristics of fractured rock, in Narasimhan, T.N., ed., Recent trends in hydrology: Geological Society of America Special Paper 189, p. 163-181.

Gondouin, M., and Scala, C., 1958, Streaming potential and the SP log: Transactions of the American Institute of Mining Metalurgical and Petroleum Engineers, T.P. 8023, p. 170-179.

Hubbert, M.K., 1940, The theory of ground water motion: Journal of Geology, v. 48, no. 8, pt. 1, p. 785-944.

Isherwood, Dana, 1981, Geoscience data base handbook for modeling a nuclear waste repository, volume 2: Livermore, Calif., Lawrence Livermore Laboratory, 331 p.

Jahns, R.H., 1943, Sheet structure in granite, its origin and use as a measure of glacial erosion in New England: Journal of Geology, v. 51, no. 2, p. 71-98.

Jamieson, G.R., and Freeze, R.A., 1983, Determining hydraulic conductivity distributions in a mountainous area using mathematical modeling: Ground Water, v. 21, no. 2, p. 168-177.

Johnson, K.L., 1981, Permeability-depth relationships in crystalline rocks with applications to low-level waste repositories: Tucson, Ariz., University of Arizona, unpublished M.S. thesis, 112 p.

Keller, G.V., 1960, Physical properties of tuffs of the Oak Spring Formation, Nevada: U.S. Geological Survey Professional Paper 400-B, p. 396-400.

Keys, W.S., 1979, Borehole geophysics in igneous and metamorphic rocks: 20th Annual Well Logging Symposium, Transactions, Society of Professional Well Log Analysts, Tulsa, Oklahoma, p. 1-26.

Keys, W.S., and Sullivan, J.K., 1979, Role of borehole geophysics in defining the physical characteristics of the Raft River geothermal reservoir, Idaho: Geophysics, v. 44, no. 6, p. 1116-1141.

LeGrande, H.E., 1954, Geology and ground water in the Statesville area, North Carolina: North Carolina Department of Conservation and Development, Division of Mineral Resources Bulletin 68, 68 p.

Lin, W., 1978, Measuring the permeability of Eleana argillite from area 17, Nevada Test Site, using the transient method: Livermore, Calif., Lawrence Livermore Laboratory, UCRL 52604, 11p.

Morris, D.A., and Johnson, A.I., 1967, Summary of hydrologic and physical properties of rock and soil materials, as analyzed by the Hydrologic Laboratory of the U.S. Geological Survey, 1948-1960: U.S. Geological Survey Water-Supply Paper 839-D, 42 p.

Muskat, M., 1937, The flow of homogeneous fluids through porous media: New York, McGraw-Hill, 763 p.

Neuman, S.P., 1982, Statistical characterization of aquifer heterogeneities—An overview, in Narasimhan, T.N., ed., Recent trends in hydrogeology: Geological Society of America Special Paper 189, p. 81-102.

Olsen, H.W., 1962, Hydraulic flow through saturated clays, in Clays and Clay Minerals, volume 9, National Conference of Clays and Clay Minerals, 9th, 1960, Proceedings: New York Permagon Press Earth Sciences Series Monograph 11, p. 131-161.

————1972, Liquid movement through kaolinite under hydraulic, electric, and osmotic gradients: American Association Petroleum Geologists Bulletin, v. 65, no. 10, p. 2022-2028.

Rasmussen, W.C., 1964, Permeability and storage of heterogeneous aquifers in the United States: Paris, International Association of Scientific Hydrology Publication 64, p. 317-325.

Rove, O.N., 1947, Some physical characteristics of certain favorable and unfavorable ore horizons, Part 1: Economic Geology, v. 42, no. 1, p. 57-77.

Rush, F.E., Thordarson, William, and Bruckheimer, Laura, 1983, Geohydrologic and drill-hole data for test well USW H-1, adjacent to Nevada Test Site, Nye County, Nevada: U.S. Geological Survey Open-File Report 83-141, 38 p.

Sanyal, S.K., Kvenvolden, D.A., and Marsden, S.S., 1971, Permeabilites of Precambrian Onverwacht cherts and other low permeability rocks: Nature, v. 232, no. 5309, p. 325-327.

Sargent, K.A., and Bedinger, M.S., 1985, Geologic and hydrologic characterization and evaluation of the Basin and Range province relative to the disposal of high-level radioactive waste—Part II, Geologic and hydrologic characterization: U.S. Geological Survey Circular 904-B, 30 p.

Seeburger, D.A., and Zoback, Mark, 1982, The distribution of natural fractures and joints at depth in crystalline rock: Journal of Geophysical Research, v. 87, no. B7, p. 5517-5534.

Slichter, C.S., 1899, Theoretical investigation of the motion of ground water: U.S. Geological Survey 19th Annual Report pt. 2, p. 305-328.

Snow, D.T., 1968a, Rock fracture spacings, openings, and porosities: Journal of Soil Mechanics and Foundations Division, Proceedings of the American Society of Civil Engineers, v. 94, no. SM-1, p. 73-91.

————1968b, Hydraulic character of fractured metamorphic rocks of the front range and implications to the Rocky Mountain arsenal well: Colorado School of Mines Quarterly, v. 63, no. 1, p. 167-199.

Sorey, M.L., Lewis, R.E., and Olmsted, F.H., 1978, The hydrothermal system of Long Valley Caldera, California: U.S. Geological Survey Professional Paper 1044-A, 60 p.

Thordarson, William, 1965, Perched ground water in zeolitized-bedded tuff, Rainier area and vicinity, Nevada Test Site, Nevada: U.S. Geological Survey Trace Elements Investigations 862, 90 p.

Trauger, F.D., 1972, Water resources and general geology of Grant County, New Mexico: New Mexico Bureau of Mines and Mineral Resources Hydrologic Report 2, 211 p.

Winograd, I.J., 1971, Hydrogeology of ash flow tuff—A preliminary statement: Water Resources Research, v. 7, no. 4, p. 994-1006.

Winograd, I.J., and Thordarson, William, 1975, Hydrogeologic and hydrochemical framework, south-central Great Basin, Nevada-California, with special reference to the Nevada Test Site: U.S. Geological Survey Professional Paper 712-C, 126 p.

Wolff, R.C., 1982, Physical properties of rocks—Porosity, permeability, distribution coefficients, and dispersivity: U.S. Geological Survey Open-File Report 82-166, 118 p.

Wyckoff, R.D., Botset, H.G., Muskat, M., and Reed, D.W., 1934, Measurement of permeability of porous media: American Association of Petroleum Geologists, v. 18, no. 2, p. 161-190.

Selected Soda Springs of Colorado and Their Origins

By William C. Evans, Theresa S. Presser, *and* Ivan Barnes

Abstract

Soda springs of Colorado are composed chiefly of meteoric water. Other identifiable waters in these springs include brines of marine origin. The soda springs contain much higher concentrations of dissolved carbon dioxide species than typical ground waters. Most of the carbon dioxide is generated at depth. Likely sources of carbon in the carbon dioxide are the mantle and from the metamorphism of marine carbonate rocks possibly by local igneous bodies. Hydrocarbon gases constitute less than 1 percent of the gas phase in all but one of the springs sampled.

INTRODUCTION

Recent work has shown that springs discharging water rich in carbon dioxide (CO_2) generally are found in regions of historic seismicity (Irwin and Barnes, 1975; Irwin and Barnes, 1980; Barnes and others, 1984). Central and western Colorado are moderately active seismically (Tarr, 1974) and have CO_2-rich spring discharges. The CO_2-rich waters from 12 selected springs and an artesian well have been studied along with two hot springs for comparison. Sampling sites were chosen from the comprehensive work by George and others (1920) on the mineral springs of Colorado. Some of the mineral springs reported by George and others (1920) could not be resampled. Road and canal construction and ground-water withdrawals have so changed the hydrology that some springs no longer exist as such.

Earlier work using the isotopic compositions of carbon in CO_2 discharges in other areas, and the isotopic and chemical compositons of the associated waters have allowed the identification of the sources of both the CO_2 and associated waters (Barnes and O'Neil, 1974). The isotopic composition of carbon in CO_2 from the mantle is known to include the range from -4.7 per mil to -8.0 per mil from the findings of Pineau and others (1976) and Moore and others (1977). The ranges of ^{13}C isotopic compositions of organic matter and marine carbonates were given by Craig (1953). The deuterium and ^{18}O compositions of meteoric waters were reported by Craig (1961), and the ^{18}O shifts of geothermal waters reacting with rocks were reported by Craig and others (1956). The chemical characteristics of waters from var-ious geologic sources were described by White and others (1963). A comparison of the properties of fluids in the springs sampled in Colorado and the properties given in the above references should permit the identification of the sources of the fluids.

METHODS

The methods used for collection and analysis of water samples were summarized by Presser and Barnes (1974). Water used for hydrogen and oxygen isotopic analyses was collected in tightly stoppered glass bottles and analyzed on a mass spectrometer by L.D. White, U.S. Geological Survey. The gases were collected in previously evacuated glass bulbs and analyzed by means of gas chromatography and mass spectrometry. Dissolved CO_2 species were precipitated as strontium carbonate ($SrCO_3$) by ammoniacal strontium chloride at the time the samples were collected. The $SrCO_3$ precipitate was washed, dried, and ground finely to homogenize it before analyzing for the ^{13}C composition.

GEOLOGY

The locations of the springs sampled are shown in figure 1. The names of the springs and the inferred or known bedrock geology are given in table 1. The CO_2-rich springs discharge from a large variety of rock types. Many, such as granite, biotite gneiss, and mio-geosynclinal sandstone, are poor sources of CO_2. The general geology may be misleading, however. For example, although Yellow Soda Spring issues from Proterozoic biotite gneiss (Epis and others, 1979), lenses of impure marble are present in the gneiss (Douglas Sheridan, oral commun., 1977).

RESULTS AND DISCUSSION

The chemical compositions of the gases from the springs sampled in this study are given in table 2. Chemical compositions and temperatures of the waters are given in table 3. CO_2 (aqueous) values were calculated from the values of pH and alkalinity determined in the field Isotopic compositions of the waters are given in
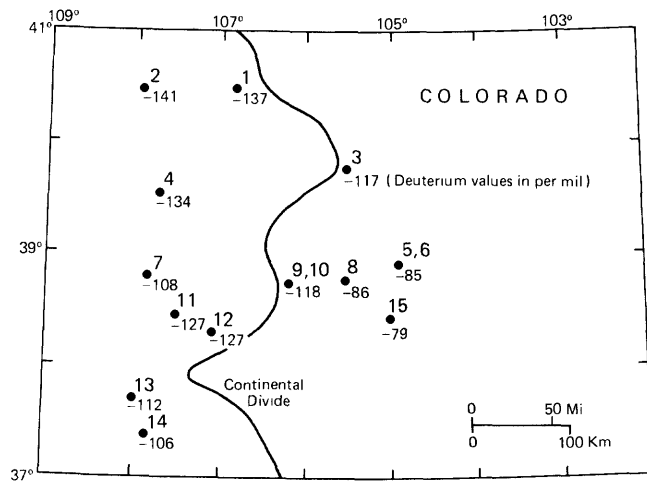
Figure 1. Location of selected soda springs of Colorado and the deuterium values in per mil. Larger numbers refer to map numbers listed in table 1.

table 3 and plotted in figure 2. The meteoric water line (Craig, 1961) is also shown in figure 2. The deuterium values are also plotted next to the geographical locations in figure 1. Carbon-isotope compositions of CO_2 species dissolved in the waters are shown in table 3. Where the spring gases contained sufficient CO_2 for isotopic analysis, the ^{13}C values are shown in table 3. All isotopic values are reported in the standard δ notation (Friedman and O'Neil, 1977).

With the exception of Mineral Spring (map number 7), figure 2 indicates that the waters may be regarded as composed almost exclusively of meteoric water. The differences in ^{18}O between the meteoric water line and

the analyzed values are small, and, even for Princeton and Hortense Hot Springs, are much smaller than the ^{18}O shifts typical of geothermal areas (Craig and others, 1956). The large spread in the isotopic compositions along the meteoric water line reflects the climatic effects of the Rocky Mountains (see fig. 1). Colorado lies in the belt of the prevailing westerlies. The eastward airflow from the Pacific Ocean and Bering Sea leads to marked depletions in ^{18}O and D by the time the air masses reach northwestern Colorado. Recharge from the winter snows from the prevailing westerlies results in ground waters depleted in ^{18}O and D as at Juniper, Glenwood, and Steamboat Springs, map numbers 2, 4, and 1 (fig. 2). Little precipitation occurs from eastward airflow over the eastern Rocky Mountains because of adiabatic compression of the air on its flow down the east side of the Rocky Mountains. Precipitation on the eastern Rocky Mountains is largely from summer thunderstorms resulting from the northward flow of humid air from the Gulf of Mexico (Rufner, 1977, p. 385). Consequently, the meteoric waters of Manitou Springs (map numbers 5 and 6), Yellow Soda Spring (map number 8), and the Dean artesian well (map number 15) are much less depleted in D and ^{18}O (figure 1 and table 3) than the meteoric waters of northwestern Colorado.

Mineral Spring plots well off the meteoric water line (fig. 2). This position cannot be due to high-temperature ^{18}O exchange with rocks because the temperature of the spring (15 °C) is the mean annual temperature of nearby Delta, Colo. (National Oceanic and Atmospheric Administration, 1974, p. 604). The isotopic shift is not due to present-day evaporation; the spring discharges into a channel, and the water immediately flows away

Table 1. Names of springs and rock types and ages of known or inferred bedrock
[See figure 1 for location of map numbers]

Map no.	Name	Known or inferred bedrock	Age	Reference
1	Steamboat Springs	Limestone and sandstone	Jurassic	Tweto (1976a).
2	Juniper Hot Spring	Sandstone	Mesozoic	Tweto (1976a).
3	Idaho Springs	Biotite gneiss	Proterozoic	Tweto (1976b).
4	Glenwood Springs	Sandstone	Pennsylvanian	Tweto and others (1976).
5	Manitou Springs	Granite	Proterozoic	Scott and Wobus (1973).
6	Manitou Springs Seven Minute Spring .	Fountain Formation	Permian and Pennsylvanian	Scott and Wobus (1973).
7	Mineral Spring	Dakota Sandstone	Cretaceous	Hail (1972).
8	Yellow Soda Spring	Biotite gneiss	Proterozoic	Epis and others (1979).
9	Princeton Hot Spring	Quartz monzonite—inferred	Oligocene and Eocene	Scott and others (1975).
10	Hortense Hot Spring	Quartz monzonite	Oligocene and Eocene	Scott and others (1975).
11	Cimarron Spring	Mancos Shale	Cretaceous	Hansen (1971).
12	Powder Horn Hot Spring	Ash flow on felsite— inferred.	Oligocene, Precambrian	Hedlund and Olson (1975).
13	Rico, Iron Draw	Hermosa Formation— inferred (marine clastic sediments and limestone).	Pennsylvanian	McKnight (1974).
14	Trimble Spring	Sandstone	Permian and Pennsylvanian	Steven and others (1974).
15	Dean artesian well	Niobrara Formation (calcareous shale and limestone).	Cretaceous	Scott and others (1976).

Table 2. Chemical compositions of gases from selected CO_2-rich springs of Colorado
[Concentrations are in percent volume. The gases from two hot springs (Hortense and Princeton) are given for comparison]

Map no.	Name	Field number	He	H_2	Ar	O_2	N_2	CH_4	CO_2	C_2H_6	H_2S	Total
1	....Steamboat Springs...........	CQ75IB77	<0.02	<0.01	<0.02	0.04	0.20	0.02	98.00	<0.05	0.4[1]	98.66
2	...Juniper Spring..........	CQ74IB77	0.22	0.01	0.38	<0.02	20.53	77.18	1.41	0.05		99.78
3	...Idaho Springs	CQ77IB77	<0.02	<0.01	0.06	0.11	2.60	<0.005	96.73	<0.05		99.50
4	....Glenwood Springs	CQ76IB77	0.90	<0.01	0.78	<0.02	35.57	0.27	61.56	<0.05		99.08
5	....Manitou Iron Geyser	CQ80IB77	0.02	0.02	0.03	<0.02	1.58	0.005	98.04	<0.05		99.69
6	....Manitou 7-Minute Spring	CQ81IB77	<0.02	<0.01	0.02	0.30	0.75	<0.005	98.88	<0.05		99.95
7	....Mineral Spring	CQ86IB77	<0.02	<0.01	0.02	<0.02	0.45	0.01	97.85	<0.05		98.33
8	....Yellow Soda Spring	CQ78IB77	0.06	<0.01	0.17	0.38	7.04	0.005	91.97	<0.05		99.62
9	....Princeton Hot Spring	CQ82IB77	0.02	<0.01	1.31	8.53	88.48	<0.01	0.16	<0.05		98.50
10	....Hortense Hot Spring	CQ83IB77	0.06	<0.01	2.10	0.05	96.60	<0.01	0.28	<0.05		99.09
11	....Cimarron Spring	CQ85IB77	0.07	<0.01	0.21	<0.02	5.77	0.01	92.34	<0.05		98.40
12	....Powder Horn Spring	CQ84IB77	<0.02	<0.01	0.07	0.31	2.32	0.01	96.30	<0.05		99.01
13	....Rico, Iron Draw	CQ87IB77	<0.02	<0.01	<0.02	<0.02	0.04	<0.005	99.23	<0.05		99.27
14	....Trimble Spring	CQ88IB77	<0.02	<0.01	0.02	0.04	0.74	<0.005	98.47	<0.05		99.27
15	....Dean artesian well	CQ79IB77	0.17	<0.01	0.36	<0.02	17.81	0.20	81.71	<0.05		100.25

[1] Approximate.

Table 3. Chemical and isotopic compositions of water from selected CO_2-rich springs of Colorado

[Concentrations are in milligrams per liter. Isotopic compositions are in per mil. Two hot springs (Hortense and Princeton) are given for comparison; --- no data]

Map no.	Name	Field number	$\delta^{18}O$	δD	T°C	pH	SiO_2	Ca	Mg
1	Steamboat Springs	CQ751B77	-17.77	-136.7	26.	6.55	24.	110.	31.
2	Juniper Spring	CQ741B77	-18.93	-141.3	37.	7.98	36.	3.0	0.33
3	Idaho Springs	CQ771B77	-15.90	-117.4	50.	6.33	68.	130.	39.
4	Glenwood Springs	CQ761B77	-17.73	-133.9	51.	6.32	33.	460.	88.
5	Manitou Iron Geyser.	CQ801B77	-12.11	- 84.5	10.	6.03	75.	185.	31.
6	Manitou 7-Minute Spring.	CQ811B77	-11.91	- 84.6	11.	6.28	22.	460.	125.
7	Mineral Spring	CQ861B77	-11.59	-108.5	15.	6.55	10.	170.	50.
8	Yellow Soda Spring ...	CQ781B77	-11.59	-86.0	8.	6.64	78.	240.	150.
9	Princeton Hot Spring.	CQ821B77	-15.65	-116.9	55.	8.50	63.	9.6	0.27
10	Hortense Hot Spring.	CQ831B77	-15.80	-118.8	83.	8.58	79.	4.1	<.1
11	Cimarron Spring	CQ851B77	-16.31	-126.6	13.	6.15	12.	130.	34.
12	Powder Horn Hot Spring.	CQ841B77	-15.89	-127.1	41.	6.53	80.	120.	49.
13	Rico, Iron Draw	CQ871B77	-15.86	-112.4	35.5	[4]6.65 / 6.0	120.	690.	98.
14	Trimble Spring	CQ881B77	-14.45	-106.2	43.	5.98	74.	470.	37.
15	Dean artesian well	CQ791B77	-10.90	-79.3	29.	5.98	22.	170.	71.

[1]Calculated.

[2]Total alkalinity as HCO_3.

[3]Present day sea water value is 3.48×10^{-3} (Wilson, 1975).

[4]Geysering spring: pH recorded after eruption and shortly before eruption, respectively.
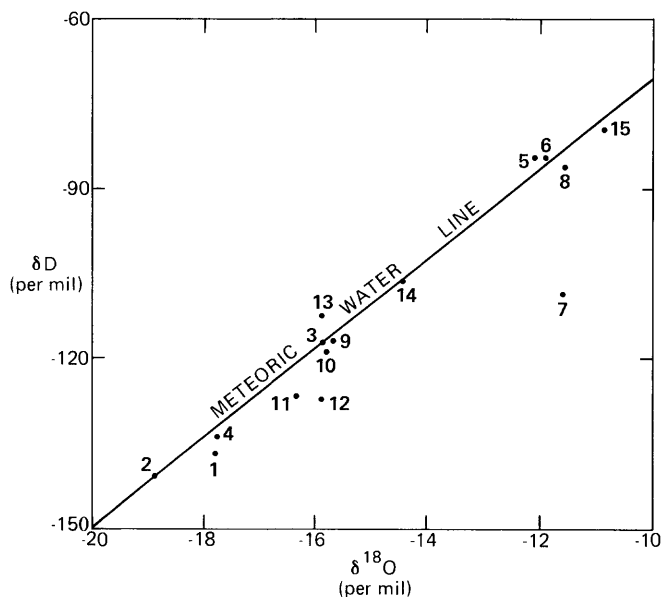

Figure 2. Stable isotope values of spring samples and their relation to the meteoric water line. Numbers refer to map numbers listed in table 1.

from the spring. The best explanation for the isotopic shift is that the local meteoric water is mixed with non-meteoric water richer in ^{18}O. Given the northerly trend in the deuterium depletion in the springs west of the Continental Divide (fig. 1), the nonmeteoric water is probably also enriched in deuterium relative to the local meteoric water.

The high chloride and bromide concentrations in Mineral Spring (table 3) identify the nonmeteoric component as being saline; most probably, an interstitial brine of marine origin. White and others (1963) showed that brines from marine clastic sediments are commonly high in bromide and that metamorphism of the sediments can yield brines rich in boron. Mineral Spring shows a slight boron enrichment. A small amount of mixing with such brines is also responsible for the elevated chloride and bromide contents of Steamboat and Yellow Soda Springs (table 3), although these springs plot very close to the meteoric water line (fig. 2). The high concentration of chloride in these springs, with such a slight shift in isotopic composition, requires that the brine be very concentrated. Because the isotopic compositions of the pure brines are not known, the rela-

Na	K	CO_2 (aqueous)[1] (as H_2CO_3)	HCO_3[2]	$\delta^{13}C$ $SrCO_3$	$\delta^{13}C$ CO_2(g)	Cl	SO_4	F	B	Br	I	Br/Cl[3] (x 10^3)
2,200.	130.	1,670.	3,430.	-4.41	-7.30	1,400.	540.	3.5	5.4	3.6	0.3	2.57
470.	2.0	21.	1,100.	-2.21	---	93.	2.	3.4	0.56	---	---	---
515.	73.	1,100.	1,470.	-4.66	-6.22	68.	400.	4.2	0.40	---	---	---
6,750.	160.	410.	782.	-5.72	-8.08	10,500.	1,100.	2.3	1.0	2.3	0.4	0.22
495.	82.	3,500.	1,600.	-3.30	-5.08	195.	210.	4.7	1.2	---	---	---
470.	50.	2,900.	2,540.	-2.87	-5.33	330.	240.	1.4	0.96	---	---	---
4,550.	120.	2,300.	4,570.	-4.70	-8.50	3,900.	1,400.	2.4	12.	13.0	0.6	3.33
1,500.	60.	1,600.	3,060.	-1.45	-7.07	1,300.	120.	2.5	1.0	6.0	<0.1	4.62
57.	1.9	0.31	68.	-11.5	---	5.1	61.	9.4	0.35	---	---	---
90.	2.8	0.24	80.	-8.54	---	8.4	95.	16.2	0.17	---	---	---
495.	71.	2,100.	1,320.	-6.43	-6.81	155.	340.	3.7	1.4	---	---	---
305.	63.	590.	1,170.	-3.42	-6.27	120.	120.	4.7	1.2	---	---	---
75.	29.	590. 2,670.	1,730.	-1.96	-6.13	3.0	890.	2.3	0.12	---	---	---
420.	40.	1,700.	1,090.	-5.80	-6.28	200.	1,100.	3.0	1.3	---	---	---
255.	31.	2,330.	1,200.	-6.78	-7.46	99.	200.	1.1	0.24	---	---	---

tive proportions of meteoric water and brine cannot be determined. It is surprising that a brine is still being flushed from a Proterozoic rock, as it is in Yellow Soda Spring, unless, of course, the brine has entered the Proterozoic rock from overlying Mesozoic rocks. White and others (1963) noted that the high chloride content and the low bromide to chloride ratio (see table 3) of Glenwood Springs were due to dissolution of salt from the evaporite of the Pennsylvanian Eagle Valley Formation. This formation crops out about 1 km south of the springs, is extensive in area, and contains thick salt lenses, anhydrite, and gypsum (Tweto and others, 1976). In accord with the observation of White and others (1963), figure 2 shows that, despite the high salt content, the water is essentially meteoric in origin.

Although the water discharged by the soda springs is mostly meteoric, concentrations of total dissolved CO_2 species (table 3) greatly exceed typical groundwater values given by White and others (1963). In the normal recharge process, CO_2 from plant-root respiration can react with feldspars to yield bicarbonate (Hem, 1970). This process can probably account for the bicarbonate concentrations of as much as 100 mg/L found in perennial spring water in granitic terranes (Feth and others, 1964; Miller, 1961) and in the two hot springs analyzed (table 3). Where limestone is present in the recharge zone, bicarbonate concentrations of ground water can reach several hundred milligrams per liter (White

and others, 1963). Hem (1970) showed that the bicarbonate concentrations reach these limits where the pressure of CO_2 from plant-root respiration approaches 0.1 atmosphere, generally the maximum CO_2 pressure attained in soil gases (Bolt and Bruggenwert, 1978, p. 97). It is difficult, however, to account for the greater than 1,000 mg/L bicarbonate in the soda springs (table 3) if only soil-horizon processes are considered.

Within certain aquifers, cation exchange (Freeze and Cherry, 1979):

$$H_2CO_3 + CaCO_3 + 2\,Na\,(clay)$$
$$\rightleftharpoons 2\,Na^+ + 2\,HCO_3^- + Ca\,(clay)\ ,$$
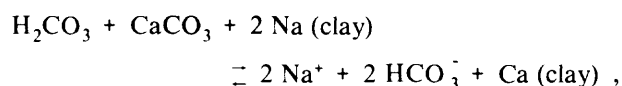
and sulfate reduction by buried organic material (Hem, 1970):

$$SO_4^= + CH_4 \rightleftharpoons HS^- + HCO_3^- + H_2O\ ,$$

can cause ground water bicarbonate concentrations to exceed 1,000 mg/L. Cation exchange leads to very high sodium to calcium ratios. Ground waters containing significant bicarbonate from sulfate reduction generally also contain appreciable CH_4 and H_2S and have low sulfate levels (Moran and others, 1978). When either

process occurs extensively within an aquifer, the resultant bicarbonate-rich ground water will have a slightly alkaline pH, between 7 and 9 (Freeze and Cherry, 1979; Groenewold and others, 1979). The pH and HCO_3^- (table 3) and elevated CH_4 (table 2) at Juniper Spring may reflect sulfate-reduction and cation-exchange processes in the aquifer. Irrigation wells in the vicinity yield water similar in composition to Juniper Spring from aquifers in the Cretaceous Mancos Shale (Brogden and Giles, 1977). The Mancos Shale overlies the Mesozoic sandstone in this area except at the site of Juniper Spring (Tweto, 1976a).

The other soda springs listed in table 3 have significantly lower pH values. Many have bicarbonate and CO_2 (aqueous) concentrations that are higher than can be attributed to either cation exchange or sulfate reduction, or to a combination of the two. Furthermore, all the soda springs discharge additional CO_2 in gas bubbles (table 2). The gas discharge in two of the springs is sufficient to cause geysering. The CO_2 (aqueous) values in table 3 represent the CO_2 in solution at the water surface. Concentrations of CO_2 (aqueous) at depth, where the hydrostatic pressure exceeds the gas pressure will be larger. [Note the effect of geysering (table 3) on the CO_2 (aqueous) at Rico.] Except at Juniper Spring and Glenwood Springs, which may derive much of its bicarbonate from evaporites, most of the bicarbonate and CO_2 in the springs must result from addition of CO_2 to the water at depth.

Irwin and Barnes (1980) have noted the abundance of CO_2-rich discharges in areas of seismicity where active faults allow CO_2 from depth to encounter ground water of meteoric origin, and they have also discussed sources and production at depth of CO_2. The three sources listed by these authors are mantle degassing, metamorphism of marine carbonate rocks, and decomposition of buried organic matter. Only Juniper Spring discharges appreciable quantities of methane and ethane (table 2), possibly from organic decomposition. The virtual absence of hydrocarbons rules out a significant contribution of organic carbon in the remaining springs. Whether the CO_2 is derived from the mantle or from marine carbonate rocks can best be deduced from the isotopic composition of the carbon.

The isotopic composition of the total CO_2 species is difficult, if not impossible, to measure if both gas and water are discharging because the proportions of gas and water are not known. Despite this difficulty, the upper and lower limits of the isotopic composition may be established by analyzing the dissolved CO_2 species and the CO_2 gas (table 3). The isotopic fractionations between the dissolved and gaseous CO_2 species are seldom the equilibrium values given by Friedman and O'Neil (1977). This is evidently a kinetic effect of the degassing process. The springs, producing bubbles of CO_2 ($pCO_2 \simeq 1$ atmosphere), are several orders of magnitude out of chemical equilibrium with the overlying air ($pCO_2 = 0.0003$ atmosphere). In this condition, the degassing process is apparently faster than the isotopic exchange reaction. Because the water discharges are usually greater than the discharge of CO_2 gas, the dissolved CO_2 species usually give a better indication of the source ^{13}C composition than does the gas. One can make a classification of CO_2 sources possible by assuming that a range of ^{13}C values for marine carbonates is +4 to -4 per mil and that mantle CO_2 is -4 to -8 per mil. The classification is somewhat approximate because highly metamorphosed carbonate rocks may be more than 4 per mil depleted in ^{13}C.

CONCLUSIONS

An exact division of the springs by carbon source is impossible. The amount of carbon from plant-root respiration and sulfate reduction will be different for each spring. These processes will contribute very little carbon in areas where Tertiary and Cretaceous sedimentary rocks are absent, and the bicarbonate concentrations of ground water are low (Freeze and Cherry, 1979; Repplier and others, 1981). There is thus strong evidence for the presence of mantle carbon at sites such as Idaho and Trimble Springs. The ^{13}C values (table 3) show that carbon from both mantle CO_2 and marine carbonate rocks is apparently found in the springs as a group. A mix of carbon from both sources may be present in any given spring as well. If intrusions are causing contact metamorphism of marine carbonate rocks at scattered localities in Colorado, then the paths by which intrusions are emplaced from depth may well be the same paths along which CO_2 may discharge from the mantle. In general, however, the relations in Colorado are very different from those generally found in Europe where the average $\delta^{13}C$ value in CO_2-rich springs is near 0 per mil (Barnes and others, 1984). There is a greater tendency for the Colorado springs to yield depleted (mantle) carbon, and the CO_2 discharges are far fewer and more scattered. Regional metamorphism may produce the CO_2 discharged by springs in Europe (Barnes and others, 1984), but the metamorphic CO_2 discharges from Colorado springs are more likely to be the result of contact metamorphism by local plutons.

REFERENCES CITED

Barnes, Ivan, Irwin, W.P., and White, D.E., 1984, Map showing world distribution of carbon-dioxide springs and major zones of seismicity: U.S. Geological Survey Miscellaneous Investigations Series Map I-1528, 10 p.

Barnes, Ivan, and O'Neil, J.R., 1974, Metamorphic reactions in flysch rocks, in Cadek, I., and Paces, T., eds., Proceedings of the International Symposium on Water-Rock Interaction, Czechoslovakia, p. 309-316.

Bolt, G.H., and Bruggenwert, M.G.M., 1978, Developments in soil science; soil chemistry: The Netherlands, Amsterdam, Elsevier Scientific Publishing Co., 281 p.

Brogden, R.E., and Giles, T.F., 1977, Reconnaissance of ground-water resources in a part of the Yampa River basin between Craig and Steamboat Springs, Moffat and Routt Counties, Colorado: U.S. Geological Survey Water-Resources Investigations Report 77-4, 1 plate.

Craig, Harmon, 1953, The geochemistry of the stable carbon isotopes: Geochimica et Cosmochimica Acta, v. 35, p. 53-92.

———1961, Isotopic variations in meteoric waters: Science, v. 133, p. 1702-1703.

Craig, Harmon, Boato, Giovani, and White, D.W., 1956, Isotope geochemistry of thermal waters, nuclear processes in geologic settings: National Academy of Sciences, National Research Council, 2d Conference Proceedings, Publication 400, p. 29-38.

Epis, R.C., Wobus, R.A., and Scott, G.R., 1979, Preliminary geologic map of the Black Mountain quadrangle, Fremont and Park Counties, Colorado: U.S. Geological Survey Open-File Report 79-652.

Feth, J.H., Roberson, C.E., and Polzer, W.L., 1964, Sources of mineral constituents in water from granitic rocks, Sierra Nevada, California and Nevada: U.S. Geological Survey Water-Supply Paper 1535-I, 70 p.

Freeze, A.R., and Cherry, J.A., 1979, Groundwater: Englewood Cliffs, N.J., Prentice-Hall, Inc., 604 p.

Friedman, Irving, and O'Neil, J.R., 1977, Compilation of stable isotope fractionation factors of geochemical interest, in Fleischer, Michael, ed., Data of Geochemistry (6th edition): U.S. Geological Survey Professional Paper 440-KK, 12 p.

George, R.D., Curtis, A., Lester, O.C., Crook, K., Yeo, J.B., and others, 1920, Mineral waters of Colorado: Colorado Geological Survey Bulletin 11, 474 p.

Groenewold, G.H., Hemish, L.A., Cherry, J.A., Rehm, B.W., Meyer, G.N., and Winczewski, L.M., 1979, Geology and geohydrology of the Knife River basin and adjacent areas of west-central North Dakota: North Dakota Geological Survey Report of Investigations 64, 402 p.

Hail, W.J., Jr., 1972, Reconnaissance geologic map of the Cedar Edge area, Delta County, Colorado: U.S. Geological Survey Miscellaneous Geologic Investigations Map I-697.

Hansen, W.R., 1971, Geologic map of the Black Canyon of the Gunnison River and vicinity, western Colorado: U.S. Geological Survey Miscellaneous Geologic Investigations Map I-584.

Hedlund, D.C., and Olson, J.C., 1975, Geologic map of the Powderhorn Quadrangle, Gunnison and Saguache Counties, Colorado: U.S. Geological Survey Geologic Quadrangle Map GQ-1178.

Hem, J.D., 1970, Study and interpretation of the chemical characteristics of natural water (2d edition): U.S. Geological Survey Water-Supply Paper 1473, 363 p.

Irwin, W.P., and Barnes, Ivan, 1975, Effect of geologic structure and metamorphic fluids on seismic behavior of the San Andreas fault system in central and northern California: Geology, v. 3, p. 713-716.

———1980, Tectonic relations of carbon dioxide discharges and earthquakes: Journal of Geophysical Research Special Collection Papers on Geochemical Measurements Pertinent to Earthquake Prediction, p. 3115-3121.

McKnight, E.T., 1974, Geology and ore deposits of the Rico district, Colorado: U.S. Geological Survey Professional Paper 723, 100 p.

Miller, J.P., 1961, Solutes in small streams draining single rock types, Sangre de Cristo Range, New Mexico: U.S. Geological Survey Water-Supply Paper 1535-F, 23 p.

Moore, J.G., Batchelder, J.N., and Cunningham, C.G., 1977, CO_2-filled vesicles in mid-Ocean basalt: Journal of Volcanology and Geothermal Research, v. 2, p. 309-327.

Moran, S.R., Cherry, J.A., Fritz, Peter, Peterson, W.M., Somerville, M.H., Stancel, S.A., and Ulmer, J.H., 1978, Geology, groundwater hydrology, and hydrogeochemistry of a proposed surface mine and lignite gasification plant site near Dunn Center, North Dakota: North Dakota Geological Survey Report of Investigations 61, 263 p.

National Oceanic and Atmospheric Administration, 1974, Climates of the States, v. 2, p. 604: Port Washington, N.Y., Water Information Center, 975 p.

Pineau, Francoise, Javoy, Marc, and Bottinga, Yan, 1976, $^{13}C/^{12}C$ ratios of rocks and inclusions in popping rocks of the Mid-Atlantic Ridge and their bearing on the problem of isotopic composition of deep seated carbon: Earth and Planetary Science Letters, v. 29, p. 413-421.

Presser, T.S., and Barnes, Ivan, 1974, Special techniques for determining chemical properties of geothermal water: U.S. Geological Survey Water-Resources Investigations Report 22-74, 11 p.

Repplier, F.N., Healy, F.C., Collins, D.B., and Longmire, P.A., 1981, Atlas of groundwater quality in Colorado: Colorado Geological Survey Map Series no. 16, 7 plates.

Rufner, J.A., 1977, The weather almanac: Detroit, Mich., Gale Research Company, 728 p.

Scott, G.R., Taylor, R.B., Epis, R.C., and Wobus, R.A., 1976, Geologic map of the Pueblo 1° X 2° quadrangle, south-central Colorado: U.S. Geological Survey Miscellaneous Field Studies Map MF-775.

Scott, G.R., Van Alstine, R.E., and Sharp, W.N., 1975, Geologic map of the Poncha Springs quadrangle, Chaffee County, Colorado: U.S. Geological Survey Miscellaneous Field Studies Map MF-658.

Scott, G.R., and Wobus, R.A., 1973, Reconnaissance geologic map of Colorado Springs and vicinity, Colorado: U.S. Geological Survey Miscellaneous Field Studies Map MF-482.

Steven, T.A., Lipman, P.W., Hail, W.J., Jr., Barker, Fred, and Luedke, R.G., 1974, Geologic map of the Durango quadrangle, southwestern Colorado: U.S. Geological Survey Miscellaneous Field Investigations Series Map I-764.

Tarr, A.C., 1974, World seismicity map, scale 1:39,000,000: Washington, D.C., U.S. Geological Survey.

Tweto, Ogden, 1976a, Geologic map of the Craig 1° × 2° quadrangle, northwestern Colorado: U.S. Geological Survey Miscellaneous Investigations Series Map I-972.

———1976b, Preliminary geologic map of Colorado: U.S. Geological Survey Miscellaneous Field Studies Map MF-788.

Tweto, Ogden, Moench, R.H., and Reed, J.C., Jr., 1976, Preliminary geologic map of the Leadville 1° × 2° quadrangle, northwestern Colorado: U.S. Geological Survey Miscellaneous Field Studies Map MF-760.

White, D.E., Hem, J.D., and Waring, G.A., 1963, Chemical composition of subsurface water, Chapter F, *in* Fleischer, Michael, ed., Data of Geochemistry, (6th edition): U.S. Geological Survey Professional Paper 440-F, 67 p.

Wilson, T.R.S., 1975, Salinity and the major elements of sea water, *in* Riley, J.P., and Skirrow, Geoffrey, eds., Chemical Oceanography, 2d edition: London, England, Academic Press, p. 366.

Errors in Estimating Ground-Water Components of Hydrologic and Phosphorus Budgets of Lakes

By Robin G. Brown

Abstract

Ground-water components in hydrologic budgets of seven Minnesota lakes were estimated as the residual of annual and seasonal budgets. Error analysis of these budgets indicated that the standard error of estimate associated with measured components of the budgets increases when seasonal budgets are used, but the error associated with the residual is generally the same when using either annual or seasonal budgets. The advantage of using seasonal budgets is that the residuals of these budgets provide information on seasonal patterns of ground-water inflow and outflow in the lakes. In contrast, annual budget residuals provide only information on the net annual ground-water inflow or outflow. Errors associated with the residuals of seasonal and annual budgets ranged from 12 to 196 percent.

Estimation of the ground-water component in annual phosphorus budgets was made with (1) hydrologic data derived from annual and seasonal hydrologic-budget residuals, and (2) estimates of phosphorus concentrations for ground-water inflow and outflow. An error analysis of the phosphorus budgets showed that the standard error of estimate associated with measured budget components can range from 20 to 30 percent, whereas the error associated with estimation of the ground-water component ranges from 54 to 202 percent. Estimation of the ground-water component in the phosphorus budget by means of seasonal hydrologic-budget residuals provides information on seasonal patterns of ground-water input and output of phosphorus over a year, whereas annual hydrologic-budget residuals provide only an annual net flux of phosphorus from the ground-water component.

INTRODUCTION

Background

Hydrologic (water) and phosphorus budgets of lakes commonly have been used to assess the input and output of water and chemicals in lakes (Scheider and others, 1979). The ground-water component of hydrologic budgets generally has been ignored or poorly understood and, as a result, has been estimated as the re-

sidual of hydrologic budgets (Winter, 1981). The ground-water component in phosphorus budgets generally is estimated or ignored also (Ayers and others, 1980; Tornes and Have, 1980).

Because calculations of phosphorus input and output in the phosphorus budget depend on data from the hydrologic budget, errors associated with the hydrologic budget are integrated into the phosphorus budget. Estimation of the ground-water component in the hydrologic budget as the residual of the budget, or as the balance between measured inputs and outputs, can result in large errors. Winter (1981) demonstrated that the residual of the budget may be nonzero solely because of errors in measurement of individual inputs and outputs in the water balance of a lake. Therefore, an analysis of the standard errors of estimate associated with budget components and residual values is essential to interpretation of the hydrologic budget.

The phosphorus budget is more complex than the hydrologic budget because the phosphorus budget has more than one unknown. Therefore, the ground-water component of phosphorus budgets must be estimated independently by means of whatever flow and concentration data are available. This estimation generally is poor because of the numerous errors in calculating ground-water inputs and outputs.

Purpose and Scope

We should examine estimates of the ground-water component in hydrologic and phosphorus budgets to determine the validity of the budgets. The purpose of this paper is to (1) examine the standard errors of estimate associated with measured components of the hydrologic budget, as well as the subsequent error associated with the residual, (2) examine the use of seasonal hydrologic budgets to isolate periods when lake inflows and outflows are predominantly ground water, (3) compare the standard errors and residual values of annual and seasonal hydrologic budgets with respect to advantages and disadvantages of using these two types of budgets

for estimating ground-water contribution to lake inflow and outflow, (4) assess the use of residuals from the annual and seasonal hydrologic budgets in estimating ground-water inputs and outputs in the phosphorus budget, and (5) determine the standard errors involved in estimating the ground-water component in the phosphorus budget, and how standard errors in both the hydrologic and phosphorus budgets affect interpretation of those budgets.

The hydrologic and phosphorus budgets discussed are the annual and seasonal budgets of seven selected lakes in Minnesota—Bryant Lake, Eagle Point Lake, Fish Lake, Lake Elmo, Lake Riley, Spring Lake, and Square Lake (fig. 1)—for 1982. The budgets were calculated as part of a study of lakes in the Twin Cities metropolitan area, Minnesota, which was a cooperative effort between the U.S. Geological Survey and the Metropolitan Council of the Twin Cities (Nelson and Brown, 1983).

DATA COLLECTION

Precipitation directly on the lake surface was measured daily throughout 1982 at each lake. Estimates of evaporation from the lakes were based on National Weather Service (NWS) Class A pan data from the St. Paul weather station; a pan-to-lake coefficient of 0.7 was used. Discharge at major surface-water inflows and at all outflows was calculated by use of continuous-stage recorders and stage-to-discharge relations; relations were based on 21 to 45 current-meter measurements at each gaging site. Discharge at minor lake inflows was estimated from current-meter measurements made during periods of flow. Changes in lake volume, measured by changes in lake level, were recorded daily by outflow stage recorders. Lake volumes were determined from 2- to 5-meter contour bathymetric maps prepared by the Metropolitan Council from lake surveys in 1981.

Atmospheric deposition of phosphorus to the lake surface was estimated from (1) atmospheric-deposition data collected in the metropolitan area in 1980 (Brown, 1983) and (2) atmospheric data from collectors installed at each lake during September and October of 1982. The atmospheric data for 1980 were used to adjust the atmospheric data from the 2 months in 1982 and to estimate atmospheric deposition during the unsampled 10 months. Phosphorus concentrations in major surface-water inflows to each lake were determined from samples taken during every flow event in 1982 by automatic water-quality samplers. Phosphorus concentrations in the surface-water outflows of each lake and minor surface-water inflows were obtained from weekly sampling. Phosphorus concentrations in ground water flowing into the lake were estimated from average phosphorus concentrations in ground water near these lakes.

Phosphorus concentrations in the epilimnion of each lake, determined by the Metropolitan Council, were used to estimate concentrations of phosphorus in ground-water outflow from the lake. A more detailed explanation of data-collection techniques is given by Nelson and Brown (1983).

Errors associated with data collection that have been identified in this paper are conservative estimates based on error values given by Winter (1981):

Precipitation - The error associated with collection of precipitation data is related to (1) gage calibration, (2) placement of the gage in the field, (3) areal extrapolation based on method used in averaging data collected in the gage network, and (4) density of gages in the network.

Evaporation - The error associated with collection of evaporation data is related to (1) NWS Class A pan calibration, (2) use of a pan-to-lake coefficient, and (3) areal extrapolation of data to lake area.

Surface-water discharge - The error associated with collection of surface-water-discharge data is related to (1) current-meter measurement, (2) development and use of stage-discharge relations or estimation of discharge based on periodic current-meter measurements, and (3) bias caused by measurements made in the channel.

Lake volume - The error associated with collection of lake-volume data is related to (1) accuracy of bathymetric map, and (2) definition of lake stage where daily readings of outflow-stage recorders are used.

Atmospheric deposition - The error associated with collection of atmospheric-deposition data is related to (1) gage calibration, (2) placement of gage in the field, (3) temporal and spatial extrapolation based on method used in averaging data from 1980 and 1982, and (4) accuracy of sample analyses by laboratory.

Surface-water quality - The error associated with collection of surface-water-quality data is related to (1) sampler placement and operation (only major inflows), (2) method, frequency, and timing of sampling, and (3) accuracy of sample analyses by laboratory.

Ground-water quality - The error associated with collection of ground-water-quality data is related to (1) sampling locations and methods, (2) the assumption that samples from wells estimate phosphorus concentrations in ground-water inflow to the lake, and samples from the epilimnion estimate phosphorus concentrations in ground-water outflow from the lake, and (3) accuracy of sample analyses by laboratory.
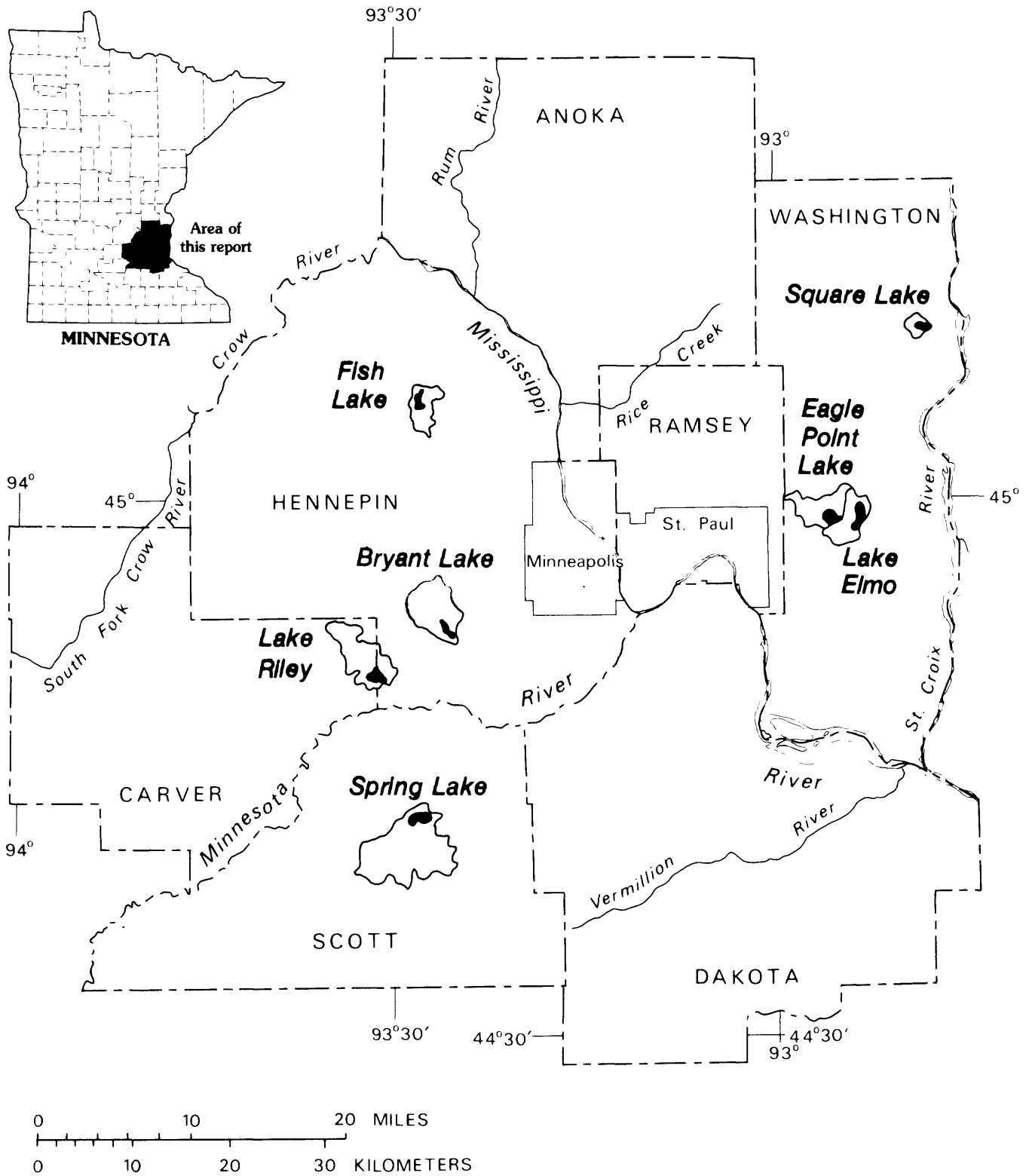
Figure 1. Location of study lakes and watersheds in the Twin Cities metropolitan area, Minn.

HYDROLOGIC BUDGETS

The annual and seasonal hydrologic budgets of each lake were arranged so that the ground-water component was the residual of the budget. The annual and seasonal hydrologic budgets are defined by the equation

$$R = P - E + SWI - SWO + LV ,\qquad (1)$$

where
- R is residual, assumed to be net ground-water inflow (negative value) or outflow (positive value),
- P is precipitation on the lake surface,
- E is evaporation from the lake surface,
- SWI is surface-water inflow (major and minor) to the lake,
- SWO is surface-water outflow from the lake, and
- LV is change in lake volume.

Errors in Estimating Ground-Water Component

Annual Budgets

The 1982 annual hydrologic budget and residual of each lake was calculated by means of equation 1. The values of each budget component for each lake are given in table 1. The ground-water component is calculated as the residual, which represents a net value of either inflow or outflow. Residuals of hydrologic budgets for five of the seven lakes showed an annual net ground-water inflow, whereas the other two lakes showed an annual net ground-water outflow. Ground-water inflow, as estimated from residuals, represents 15 to 76 percent of the total water input to the lakes and 13 to 29 percent of total outflow of the lakes, depending on the lake (table 1). Although these values represent only the annual net difference between inflow and outflow, the values for ground-water components in these budgets represent a substantial part of the total inflow or outflow in some of the lakes (table 1).

Standard error associated with each of the components in the annual hydrologic budget was determined according to methods presented by Winter (1981).The standard error is the standard error of estimate as 1 standard deviation of the budget value. The propagation of error for each component depends on the methods and instruments used, but the general equation can be written as

$$TEC_1 = \sqrt{(P_1 C_1)^2 + (P_2 C_1)^2 + \ldots (P_N C_1)^2} ,\qquad (2)$$

where

- TEC_1 is total standard error associated with the first budget component,
- P_1 is percent error for particular method or instrument used in calculating budget component, and
- C_1 is the value of the budget component.

For example, the standard error associated with the precipitation budget component in the hydrologic budget of Bryant Lake is 40,000 m^3.

$$TEC_{precipitation} =$$
$$\sqrt{(.02 \times 477)^2 + (.05 \times 477)^2 \div (.05 \times 477)^2 + (.04 \times 477)^2}$$
$$= 40.0 \text{ (in thousands of cubic meters)}.$$

The propagation of error for the budget residual is calculated with an equation similar to equation 2:

$$OE = \sqrt{(TEC_1)^2 + (TEC_2)^2 + \ldots (TEC_N)^2} ,\qquad (3)$$

where OE is overall standard error of hydrological budget, the standard error associated with the residual, and

- TEC_1 is the total standard error associated with budget components.

The overall standard error reflects the "typical" magnitude of the resulting error in estimating ground-water as the residual (Winter, 1981). The overall standard errors presented in table 1 show that the residual can have as much as 99 percent standard error, as for Eagle Point Lake, indicating that the residual in this example could consist entirely of budget error. Other lake budgets, such as Square Lake, have lower overall errors, and the residual standard error is as low as 12 percent. The standard error associated with the residual, in percent of the residual, is inversely related to the percentage of the budget represented by the residual. Eagle Point Lake residual standard error is 99 percent, whereas the residual represents only 13 percent of the total inflow in the budget. In contrast, Square Lake residual standard error is only 12 percent, whereas the residual represents 76 percent of the total inflow.

Seasonal Budgets

The 1982 year was divided into five seasons, and a hydrologic budget for each season was calculated for each lake. The seasons were January 1 through April 22 (season A), April 23 through June 1 (season B), June 2 through July 17 (season C), July 18 through September 4

Table 1. Annual hydrologic-budget components and associated standard errors

[Values in thousands of cubic meters, except as noted; ---, no data]

Component	Standard error[1] in percent	Quantity of water and associated standard error, by budget component						
		Bryant Lake	Eagle Point Lake	Fish Lake	Lake Elmo	Lake Riley	Spring Lake	Square Lake
PRECIPITATION		477	471	695	957	848	1,902	593
Gage	2	9.54	9.42	13.9	19.1	17.0	38.0	11.9
Placement	5	23.9	23.6	34.8	47.8	42.4	95.1	29.6
Areal averaging	5	23.9	23.6	34.8	47.8	42.4	95.1	29.6
Gage density	4	19.1	18.8	27.8	38.3	33.9	76.1	23.7
Total error[2]		40.0	39.4	58.2	80.1	70.9	159	49.6
EVAPORATION		555	476	725	968	958	2,011	669
NWS Class A pan	10	55.5	47.6	72.5	96.8	95.8	201	66.9
Pan to lake coefficient	15	83.2	71.4	109	145	144	302	100
Areal averaging	15	83.2	71.4	109	145	144	302	100
Total error		130	112	170	227	225	472	157
SURFACE-WATER INFLOW—MAJOR		229	335	214	400	1,380	2,540	0
Current-meter measurement	5	11.4	16.8	10.7	20.0	69.0	127	---
Stage-discharge relation	5	11.4	16.8	10.7	20.0	69.0	127	---
Channel bias	5	11.4	16.8	10.7	20.0	69.0	127	---
Total error		19.8	29.0	18.5	34.6	120	220	---
SURFACE-WATER INFLOW—MINOR		337	0	49	48	207	3,231	21
Current-meter measurement	5	16.8	---	2.45	2.40	10.4	161	1.05
Estimation of discharge	20	67.4	---	9.80	9.60	41.4	646	4.20
Channel bias	5	16.8	---	2.45	2.40	10.4	161	1.05
Total error		71.5	---	10.4	10.2	43.9	664	4.45
SURFACE-WATER OUTFLOW		703	400	1,096	1,440	1,250	8,910	1,940
Current-meter measurement	5	35.0	20.0	54.8	72.0	62.5	446	97.0
Stage-discharge relation	5	35.0	20.0	54.8	72.0	62.5	446	97.0
Channel bias	5	35.0	20.0	54.8	72.0	62.5	446	97.0
Total error		61.9	34.6	94.9	125	108	772	168
LAKE VOLUME[3]		-29	-200	-1	101	-658	310	-27
Bathymetric map	10	2.90	20.0	0.10	10.1	65.8	31.0	2.70
Stage gage	5	1.45	10.0	.05	5.05	32.9	15.5	1.35
Total error		3.24	22.4	.11	11.3	73.6	34.6	3.02
Overall error[4]		167(90)	129(99)	204(24)	274(25)	298(34)	1,155(33)	235(12)
RESIDUAL[5]		-186	130	-862	-1,104	885	-3,557	-1,968
Percent of budget[6]		15	13	47	44	29	32	76

[1] Percent error for methodology used based on error values reported by Winter (1981).

[2] Calculated standard error of estimate from the equivalent form of equation

[3] Lake-volume values that are negative represent an annual decrease in lake level, and positive values represent an annual increase in lake level.

[4] Calculated standard error of estimate from equation 3, number in parentheses represents percent of residual represented by the overall error.

[5] Residual value from equation 1, negative values represent ground-water inflow, and positive values represent ground-water outflow.

[6] Percent of total inflow or outflow in the lake represented by residual.

(season D), and September 5 through December 31 (season E). The divisions were based on inflow discharge; the dates of seasons show periods of stable inflow discharge or groupings of runoff events. We used equation 1 to calculate the seasonal budgets; an example of the seasonal budgets are given in table 2. The residual values for all seasons for all lakes is given in table 3.

As indicated in table 3, the net direction of ground-water flow in a lake may change with season. For example, Bryant Lake seasonal budget residuals are negative (ground-water inflow) during seasons A and B and are positive (ground-water outflow) during seasons C, D, and E. These seasonal budget residuals can be synthesized into one ground-water component made up of both ground-water inflow and outflow. For example, in Bryant Lake the seasonal budget residuals divide the annual residual (-186,000 m³) into ground-water inflow, 385,000 m³, and ground-water outflow, 199,000 m³.

Dividing the annual hydrologic budget into seasonal hydrologic budgets can change the interpretation of ground-water inflow and outflow in a lake. For example, estimate of ground-water inflow to Bryant Lake was 13 percent of the total input to the lake, based on annual budget data (table 1). However, based on seasonal budget data (table 2), estimate of ground-water inflow was 27 percent of the total input. Bryant Lake showed no ground-water outflow as calculated from annual budget data, but it was 14 percent of the total outflow on the basis of seasonal budget data. Standard errors associated with each component of the seasonal budgets were calculated by means of equation 2—the same equation described in the error analysis of annual budgets. The percent error associated with measurements in seasonal budgets generally is greater than that in annual budgets because the shorter timeframe increases the error (Winter, 1981). For example, the errors associated with precipitation measurement increase from values of 2, 5, 5, and 4 (table 1) to 2, 5, 10, and 8 (table 2). Increases in percent error of budget components result in increases in standard error associated with the residual in seasonal budgets (table 2). The standard error associated with the residual (overall error) was calculated with the use of equation 3, as described in the discussion of error analysis of annual budgets.

Standard errors associated with the annual negative, positive, or net residual in table 3 were calculated by means of an equation similar to equation 3:

$$ERS_T =$$

$$\sqrt{(ERS_A)^2 + (ERS_B)^2 + (ERS_C)^2 + (ERS_D)^2 + (ERS_E)^2} ,$$

(4)

where ERS_T is total standard error associated with the residual of the synthesis of either negative residuals, positive residuals, or all residuals (the net annual value) and

ERS_A is standard error associated with the residual of season A.

For example, the annual negative residual for Bryant Lake, -385,000 m³, has a total standard error of 100,000 m³, in which ERS_T of annual negative residual equals $\sqrt{(73.5)^2 + (68.1)^2} = 100$ (in thousands of cubic meters).

The positive annual residual is 199,000 m³ (table 3) and the total standard error associated with this residual is 142,000 m³, in which ERS_T of annual positive residual equals $\sqrt{(83.7)^2 + (84.0)^2 + (77.5)^2} = 142$ (in thousands of cubic meters).

The annual net is -186,000 m³ with a total standard error of 174,000 m³ (table 3), in which ERS_T of annual net residual equals

$$\sqrt{(73.5)^2 + (68.1)^2 + (83.7)^2 + (84.0)^2 + (77.5)^2}$$

$$= 174 \text{ (in thousands of cubic meters).}$$

Errors associated with the annual net residual as calculated above from seasonal-budget data are within a few percent of errors associated with the net annual residual determined from annual-budget data (tables 1 and 3). The similarity of these errors show that either method of estimating the net annual residual results in residuals of equal value and errors of nearly equal value.

PHOSPHORUS BUDGETS

We calculated the ground-water component of the phosphorus budget independently, using discharge data from the hydrologic budget and water-quality data. The phosphorus-budget residual consists of unknowns such as sedimentation, internal loading, and allochthonous inputs of phosphorus. The phosphorus budget is defined by the equation

$$R = A + SWI - SWO + GWI - GWO ,$$

(5)

where R is residual or unknown fluxes of phosphorus,

A is atmospheric deposition of phosphorus to lake,

SWI is surface-water input of phosphorus to lake,

Table 2. Example of seasonal hydrologic-budget components and associated standard errors for Bryant Lake

[Values in thousands of cubic meters, except as noted: ---, no data]

Component	Standard error[1] in percent	Quantity of water and associated standard error by budget component				
		Season A	Season B	Season C	Season D	Season E
PRECIPITATION		94	52	67	82	182
Gage	2	1.88	1.04	1.34	1.64	3.64
Placement	5	4.70	2.60	3.35	4.10	9.10
Areal averaging	10	9.40	5.20	6.70	8.20	18.2
Gage density	8	7.52	4.16	5.36	6.56	14.6
Total error[2]		13.1	7.23	9.31	11.4	25.3
EVAPORATION		19	112	150	154	120
NWS class A pan	10	1.90	11.2	15.0	15.4	12.0
Pan to lake coefficient	50	9.50	56.0	7.50	77.0	60.0
Areal averaging	15	2.85	16.8	22.5	23.1	18.0
Total error		10.1	59.5	79.7	81.8	63.8
SURFACE-WATER INFLOW—MAJOR		83	41	40	4	61
Current-meter measurement	5	4.15	2.05	2.00	0.20	3.05
Stage-discharge relation	10	8.30	4.10	4.00	0.40	6.10
Channel bias	5	4.15	2.05	2.00	0.20	3.05
Total error		10.2	5.02	4.90	0.49	7.47
SURFACE-WATER INFLOW—MINOR		122	60	59	6	90
Current-meter measurement	5	6.1	3.00	2.95	0.30	4.50
Estimation of discharge	30	36.6	18.0	17.7	1.80	27.0
Channel bias	5	6.1	3.00	2.95	0.30	4.50
Total error		37.6	18.5	18.2	1.85	27.7
SURFACE-WATER OUTFLOW		480	200	23	0	0
Current-meter measurement	5	24.0	10.0	1.15	---	---
Stage-discharge relation	10	48.0	20.0	2.30	---	---
Channel bias	5	24.0	10.0	1.15	---	---
Total error		58.8	24.5	2.82	---	---

Table 2. Example of seasonal hydrologic-budget components and associated standard errors for Bryant Lake—Continued

Component	Standard error[1] in percent	Quantity of water and associated standard error by budget component				
		Season A	Season B	Season C	Season D	Season E
LAKE VOLUME[3]		86	-60	-101	-108	154
Bathymetric map	10	8.6	6.0	10.1	10.8	15.4
Stage gage	10	8.6	6.0	10.1	10.8	15.4
Total error		12.2	8.48	14.3	15.3	21.8
Overall error[4]		73.5(26)	68.1(69)	83.7(89)	84.0(183)	77.5(131)
RESIDUAL[5]		-286	-99	94	46	59

[1] Percent error for methodology used based on error values reported by Winter (1981).

[2] Calculated standard error of estimate from the equivalent form of equation 2.

[3] Lake-volume values that are negative represent an annual decrease in lake level, and positive values represent an annual increase in lake level.

[4] Calculated standard error of estimate from equation 3, number in parentheses represents percent of residual represented by the overall error.

[5] Residual value from equation 1, negative values represent ground-water inflow and positive values represent ground-water outflow.

Table 3. Seasonal hydrologic-budget residuals and associated standard errors

[Values in thousands of cubic meters, except as noted; ---, no data]

Residual	Quantity of water and associated standard error by budget component						
	Bryant Lake	Eagle Point Lake	Fish Lake	Lake Elmo	Lake Riley	Spring Lake	Square Lake
Season A[1]	-286	-26	-219	-446	110	-1,172	-432
Error[2]	73.5(26)	62.6(241)	57.1(26)	92.6(21)	140(127)	856(73)	68.2(16)
Season B	-99	-17	-384	-242	247	-770	-233
Error	68.1(69)	56.4(332)	92.4(24)	128(53)	146(59)	342(44)	77.3(33)
Season C	94	116	-148	-121	362	197	-238
Error	83.7(89)	73.2(63)	106(72)	141(116)	147(41)	317(161)	97.1(41)
Season D	46	24	-64	-112	48	-45	
Error	84.0(183)	71.7(299)	108(169)	144(129)	144(300)	303(673)	199.6(58)
Season E	59	32	-47	-103	118	-1,767	-893
Error	77.5(131)	60.8(190)	91.1(194)	127(69)	118(100)	402(23)	149(17)
Annual negative.	-385	-43	-862	-1,104	0	-3,754	-1,968
Error[3]	100(26)	84.2(196)	207(24)	286(26)	---	1,050(28)	228(12)
Annual positive	199	172	0	0	885	197	0
Error	142(71)	119(69)	---	---	312(35)	317(161)	---
Annual net	-186	169	-862	-1,104	885	-3,557	-1,968
Error	174(94)	146(112)	207(24)	286(26)	312(35)	1,097(31)	228(12)

[1] Seasonal hydrologic budget residual; seasonal budgets are for the following periods: Season A—January 1-April 22; Season B—April 23-June 1; Season C—June 2-July 17; Season D—July 18-September 4; Season E—September 5-December 31.

[2] Calculated standard error from the equivalent form of equation 3; number in parentheses represents percent of residual.

[3] Calculated standard error from the equivalent form of equation 4; number in parentheses represents percent of residual represented by the overall standard error.

SWO is surface-water output of phosphorus from lake,

GWI is ground-water input of phosphorus to lake, and

GWO is ground-water output of phosphorus from lake.

Load Calculation

We calculated loads by using measured or estimated concentration data and discharge data from the annual and seasonal hydrologic budgets in the following equation:

$$L = CQ , \qquad (6)$$

where *L* is annual load of phosphorus for budget component, in kilograms,

C is mean annual concentration of phosphorus for budget component, in milligrams per liter, and

Q is annual discharge for budget component, in thousands of cubic meters.

An example of load calculations is given in table 4 for the annual phosphorus budget of Bryant Lake.

Loads calculated for the annual phosphorus budgets of the seven lakes with annual and seasonal budget residuals for ground-water components are given in table 5.

Errors in Estimating Ground-Water Component

Ground-water inflow and outflow can be a substantial component in the phosphorus budget, but the load attributed to ground-water inflow or outflow depends on whether annual or seasonal hydrologic-budget residuals are used in the calculation (table 5).

On the basis of annual hydrologic-budget data, ground-water input of phosphorus represents 3 to 91 percent of the total input of phosphorus to the lakes, and 27 to 29 percent of the total output of phosphorus from the lakes, depending on the lake (table 5). Differences in phosphorus loads in ground water that were calculated from annual versus seasonal hydrologic-budget data were evident only for lakes with different values for the ground-water component in the annual and seasonal hydrologic budgets (Bryant, Eagle Point, and Spring Lakes).

Error analysis of phosphorus-budget components is threefold; standard errors of estimate are calculated for (1) phosphorus concentration, (2) discharge associated with the concentration value, and (3) the load value. The phosphorus-concentration standard error is calculated

from an equivalent form of equation 2, given in the discussion on analysis of hydrologic-budget errors. The standard error associated with phosphorus-concentration data for each component includes all the errors associated with methodologies for obtaining the data (tables 4 and 5). Errors associated with discharge, given in tables 4 and 5, were obtained from the hydrologic-budget data given in table 1.

Standard errors of estimate associated with phosphorus load are comprised of errors from both the phosphorus-concentration data and the discharge data. The equation for the standard error associated with the phosphorus load is

$$E_L = \sqrt{[(E_C)^2 \mathrm{x}(Q)^2] + [(E_Q)^2 \mathrm{x}(C)^2]} , \qquad (7)$$

where E_L is standard error associated with phosphorus load,

E_C is standard error associated with phosphorus concentration value,

Q is quantity of water,

E_Q is standard error associated with quantity of water, and

C is concentration of phosphorus value.

For example, the standard error associated with the phosphorus load from atmospheric deposition at Bryant Lake (table 4) is obtained from the following calculation, in which E_L of atmospheric deposition equals $\sqrt{[(0.0051)^2 \mathrm{x}(477)^2] + [(40)^2 \mathrm{x}(0.0161)^2]} = 2.5$.

Errors associated with the ground-water component of the phosphorus budget generally are high, 2 to 5 times higher than those associated with other budget components, and range from 54 to 202 percent of the component value (table 5). The difference in errors associated with use of annual and seasonal hydrologic-budget data in computing the ground-water components of phosphorus budgets of lakes is evident only for lakes that seasonal hydrologic-budget data show have both ground-water inflow and outflow similar to the differences in errors associated with residuals of annual and seasonal hydrologic budgets.

The combination of the large standard error associated with estimating ground-water flow as a residual in the hydrologic budget and that associated with estimating phosphorus concentration in the ground-water flow into and out of a lake results in the large standard errors associated with the ground-water component of the phosphorus budget. If the estimated ground-water component of the phosphorus budget represents a substantial part of the total input or output of phosphorus in a lake, the standard error associated with this component can become so large that the validity of the budget calculation is questionable.

Table 4. Example of annual phosphorus-budget calculation and error analysis for Bryant Lake

[---. no data]

Component	Error[1] in percent	Phosphorus concentration (mg/L)	Quantity of water (thousands of m³)	Phosphorus load (kg)
ATMOSPHERIC DEPOSITION		0.0161	477	7.7
Gage	2	.0003	---	---
Placement	5	.0008	---	---
Temporal and spatial averaging	30	.0048	---	---
Gage density	5	.0008	---	---
Sample analysis	10	.0016	---	---
Total error[2]		.0051(32)	40(8)	2.5(33)
SURFACE-WATER INFLOW—MAJOR		.0829	229	19
Sampler	5	.004	---	---
Sampling method	10	.083	---	---
Sample analysis	10	.083	---	---
Total error		.012(14)	19.8(9)	3.9(20)
SURFACE-WATER INFLOW—MINOR		.0386	337	13
Sampling method	30	.012	---	---
Sampling analysis	10	.004	---	---
Total error		.012(32)	71.5(21)	4.9(38)
SURFACE-WATER OUTFLOW		.0398	703	28
Sampling method	15	.006	---	---
Sample analysis	10	.004	---	---
Total error		.007(18)	61.9(9)	7.4(26)
GROUND-WATER INFLOW......................		.0419	186	7.8
•Well sampling	15	.0063	---	---
Estimation method[3]	50	.021		
Sample analysis	10	.0042	---	---
Total error		.022(53)	167(90)	8.1(104)
GROUND-WATER OUTFLOW		---	0	0
Epilimnion sampling	15	---	---	---
Estimation method[3]	50	---	----	---
Sampling analysis	10	---	---	---
Total error		---	---	---

[1] Percent error based on methodology reported by Payne and others (1980) and Nelson and Brown (1983).

[2] Calculated standard error from equivalent form of equation 2 for phosphorus concentration, from table 1 for quantity of water, and from equation 7 for phosphorus load; number in parentheses represents percent of component represented by the error.

[3] Estimation-method error is the error in assuming that concentration represents the concentration in the water entering and leaving the lake by ground-water flow.

Table 5. Annual phosphorus load and associated standard error, by budget components

[Load values in kilograms except as noted; number in parentheses represents percent of component represented by standard error; ---, no data]

Component	Phosphorus load and associated standard error, by budget component						
	Bryant Lake	Eagle Point Lake	Fish Lake	Lake Elmo	Lake Riley	Spring Lake	Square Lake
Atmospheric deposition	7.7	26	20	27	41	218	9.2
Total error[1]	2.5(33)	8.4(33)	6.5(33)	8.8(33)	13(33)	71(33)	3.0(33)
Surface-water inflow—Major	19	52	37	64	298	819	0
Total error	3.9(20)	11(20)	7.6(20)	13(20)	61(20)	168(20)	---
Surface-water inflow—Minor	13	25	15	9	62	1.310	3.7
Total error	4.9(38)	9.4(38)	5.6(38)	3.4(38)	23(38)	493(38)	1.4(38)
Surface-water outflow	28	64	76	54	117	2.130	26
Total error	7.4(26)	17(26)	20(26)	14(26)	31(26)	564(26)	6.9(26)

Annual hydrologic-budget data[2]

Component	Bryant Lake	Eagle Point Lake	Fish Lake	Lake Elmo	Lake Riley	Spring Lake	Square Lake
Ground-water inflow	7.8	---	85	68	---	164	127
Total error	8.1(101)	---	49(58)	40(59)	---	102(62)	69(54)
Percent of budget[3]	16	---	54	40	---	6	91
Ground-water outflow	---	24	---	---	48	---	---
Total error	---	27(112)	---	---	30(63)	---	---
Percent of budget	---	27	---	---	29	---	---

Seasonal hydrologic-budget data[4]

Component	Bryant Lake	Eagle Point Lake	Fish Lake	Lake Elmo	Lake Riley	Spring Lake	Square Lake
Ground-water inflow	16	2.7	85	68	---	175	127
Total error	9.4(59)	5.5(202)	49(58)	40(59)	---	105(60)	69(54)
Percent of budget	29	3	54	40	---	7	91
Ground-water outflow	13	28	---	---	48	25	---
Total error	11.6(89)	24(87)	---	---	30(63)	42(169)	---
Percent of budget	32	30	---	---	27	1	---

[1] Calculated standard error of estimate from equivalent form of equation 7.

[2] Loads attributable to ground-water inflow and outflow based on annual hydrologic-budget data.

[3] Percent of total input or output of phosphorus in lake represented by ground-water input or output.

[4] Loads attributable to ground-water inflow and outflow based on seasonal hydrologic-budget data.

CONCLUSIONS

Estimates of the ground-water components in the hydrologic budget of a lake can be made from either annual or seasonal hydrologic data, but seasonal data provide more detailed information on ground-water interaction with the lake. The use of seasonal hydrologic-budget residuals to estimate annual ground-water inflow and outflow in a lake leads to approximately the same standard error associated with residuals as the use of annual hydrologic data, even though methodology errors can be greater. The advantage of using seasonal data is that distinct periods of net ground-water inflow or outflow can be identified, which aids understanding of the temporal and quantitative aspects of ground-water interaction with the lake. Estimating ground-water interaction from annual hydrologic budgets can be misleading where there are both ground-water inflow and outflow in the lake.

Estimation of the ground-water component in the phosphorus budget is only as accurate and precise as the estimation of ground-water flow and of the phosphorus concentration in the ground-water inflow and outflow. If ground-water flow is estimated in the hydrologic budget, the standard error associated with that estimate

is carried into the phosphorus budget and is multiplied by the errors associated with phosphorus concentrations. The use of seasonal hydrologic data to estimate ground-water components in the phosphorus budget was found to be an advantage because seasonal data provide better information on total input or output of phosphorus in ground water.

REFERENCES CITED

Ayers, M.A., Payne, G.A., and Have, M.R., 1980, Effects of urbanization on the water quality of lakes in Eagan, Minnesota: U.S. Geological Survey Water-Resources Investigations Report 80-71, 42 p.

Brown, R.G., 1983, Atmospheric deposition of selected chemicals and their effect on nonpoint-source pollution in the Twin Cities Metropolitan Area, Minnesota: U.S. Geological Survey Water-Resources Investigations Report 83-4195, 24 p.

Nelson, Luanne, and Brown, R.G., 1983, Streamflow and water-quality data for lake and wetland inflows and out-flows in the Twin Cities Metropolitan Area, Minnesota, 1981-82: U.S. Geological Survey Open-File Report 83-543, 182 p.

Payne, G.A., Ayers, M.A., and Brown, R.G., 1982, Quality of runoff from small watersheds in the Twin Cities Metro-politan Area, Minnesota—Hydrologic data for 1980: U.S. Geological Survey Open-File Report 82-504, 89 p.

Scheider, W.A., Moss, J.J., and Dillion, P.J., 1979, Measure-ment and uses of hydraulic and nutrient budgets, in Lake Restoration, Proceedings of a National Confer-ence, August 22-24, 1978, Minneapolis, Minnesota: U.S. Environmental Protection Agency, Ecological Research Series, EPA 440/5-79-001, 254 p.

Tornes, L.H., and Have, M.R., 1980, Water quality of four lakes in Lakeville, Minnesota: U.S. Geological Survey Water-Resources Investigations Report 80-66, 59 p.

Winter, T.C., 1981, Uncertainties in estimating the water balance of lakes: Water Resources Bulletin, v. 17, no. 1, p. 82-114.

Methodology for the Determination of Iodide in Saline Waters Using an Ion Chromatograph with an Electrochemical Detector

By H. Neil Elsheimer, LeRoy M. Law, *and* Yousif K. Kharaka

Abstract

An ion chromatographic method involving the use of an electrochemical detector was applied to the analysis of saline waters from gas wells in the Sacramento Valley, Calif. The saline solutions were diluted to bring the chloride level to approximately 1,000 milligrams per liter. A detection limit of 10 micrograms per liter I^- can be achieved. Other anions such as bromide do not interfere. An eluent of 0.02 M $NaNO_3$ and only a separator column were used; the time of elution was approximately 8 minutes. The values found by means of this method are compared with the values previously obtained by the classical method that includes bromine oxidation and a thiosulfate titration. The ion chromatographic method was found to be more precise, sensitive, and reliable than the titrimetric method.

INTRODUCTION

The classical titrimetric method for the determination of iodide in natural waters, and aqueous solutions in general, as reported by Kolthoff and Sandell (1952) is based on the oxidation of iodide to iodate through addition of excess bromine:

$$I^- + 3Br_2 + 3H_2O \rightarrow IO_3^- + 6HBr$$
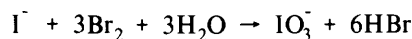
The excess bromine is subsequently decomposed by addition of sodium formate. The amount of iodide equivalent to the iodate is then liberated by the addition of an excess of potassium iodide to an acid solution:

$$IO_3^- + 5I^- + 6H^+ \rightarrow 3I_2 + 3H_2O$$
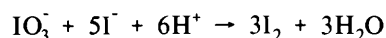
The titration of the liberated iodine is done with standard thiosulfate, and starch is used as the indicator:

$$I_2 + 2S_2O_3^{-2} \rightarrow S_4O_6^{-2} + 2I^-$$
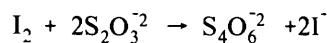
This titrimetric method was adopted by the American Society for Testing Materials (1966), and it has been used routinely by the Water Resources Division of the U.S. Geological Survey (Brown and others,

1979) and in particular on water samples from geopressured, geothermal zones and oil and gas fields (Lico and others, 1982). In this method, iodide is determined by itself or in combination with bromide, wherein bromide and iodide are oxidized by the addition of hypochlorite, and the resulting bromate and iodate converted to iodine and titrated as described above. The bromide is determined by difference.

Although the titrimetric method outlined above has been used successfully, it has certain disadvantages. These are, namely, (1) length and complexity of the procedure; (2) large sample volumes; (3) relatively high detection limits; and (4) subjectivity with regard to both removal of excess bromine and end-point detection. The fourth liability leads to inconsistent and inaccurate results, particularly where the original solutions are colored (usually yellow). The color phenomenon becomes critical at the point where sodium formate is added in slight excess to reduce excess bromine, and a clear solution supposedly results. If the solution has an initial yellow tinge (not uncommon in saline solutions) then excessive amounts of formate may be added, resulting in interference and causing low determinations. If the excess bromine is not completely removed, then the converse is true.

Alternative methods have included colorimetry (Black and Whittle, 1967; American Public Health Association and others, 1981), kinetic techniques (Rogina and Dubravcic, 1953; Dubravcic, 1955), and gas chromatography (Faigle and Klockow, 1982; Bachmann and Matusca, 1983). These approaches are limited either by sample impurities or by long preparation and analysis times.

An extensively used technique for the separation and determination of the halides and other ion species in solution has been ion chromatography, which was first developed by Small, Stevens, and Bauman (1975). They utilized a novel configuration of resins and columns to isolate the species of interest, supress the background electrolyte, and determine the individual species by means of a conductivity detector within a matter of

minutes. Applications of this technique for the determination of the halogens have been made by Evans, Tarter, and Moore (1981), Wang and Tarter (1983), and Williams (1983). Williams found a number of advantages in placing an ultraviolet (UV) detector in series with the conductivity detector.

Three disadvantages of the combination separator and suppressor column system in ion chromatography are (1) the need of periodic regeneration of the suppressor columns, (2) variations in peak retention times with suppressor column exhaustion, and (3) the necessity for background suppression of the eluent. Continuously generated fiber suppressor columns negate the first two disadvantages. Gjerde and others (1979, 1980) surmounted the third difficulty by eliminating the need of the suppressor column altogether through use of a lower capacity resin column and a more dilute eluent. Halides were determinable in the parts per billion range. Others reporting use of a single-column system for ion chromatography were Cochrane and Hillman (1982), who measured the decrease in UV absorption of the buffered eluent, and Reeve (1979) and Ivey (1983), who used a UV-transparent eluent. Increased sensitivity over a conductometric detection system was achieved in all studies. A potentiometric electrochemical detection system coupled to a single separator column was devised by Hershcovitz and others (1982) and applied to the halides.

Still other investigators have applied high-performance liquid chromatography (HPLC) with efficient single column separation systems to halide systems. These include Igawa and others (1981), Cassidy and Elchuck (1982), Skelly (1982), and Matsushita and others (1983).

Rocklin and Johnson (1983) developed an ion chromatographic method, based on an amperometric electrochemical method (Pihlar and others, 1979; Pihlar and Kosta, 1980) for cyanide analysis, for the separation and determination of cyanide, sulfide, iodide, and bromide, using 0.02 M NaNO$_3$ as eluent. The electrochemical detector is placed immediately following the separator column. The use of the electrochemical detector affords a greater selectivity for the halides and an increased sensitivity (10 μg/ L I$^-$). Because the E^0 (electrochemical potential) for the oxidation of Ag to AgCl is more positive than the E^0 for the oxidation of Ag to AgI at a potential on the diffusion controlled plateau for iodide, the current response for iodide will be much greater than for chloride. This affords the determination of iodide in the presence of excessive amounts of chloride to a ratio of 1,000:1 or more. Wang, Bunday, and Tarter (1983) combined the use of both an electrochemical and conductometric detector to determine all four halides quantitatively at the μg/ L level in a single injection.

Because the samples analyzed in this laboratory are generally high in chloride (several thousand to 200,000 mg/ L, and routinely as high as 20,000 mg/ L), and commonly 40 to 50 mg/ L or less in iodide, the Rocklin and Johnson (1983) method was adapted for our purposes. The high sensitivity and good resolution of the method gave promise of more accurate results than the titrimetric method, particularly at concentration levels of less than 1 mg/ L I$^-$.

ACKNOWLEDGMENTS

LABORATORY PROCEDURES

Apparatus

All chromatography was performed on a Dionex Model 14 ion Chromatograph equipped with an HPIC/ ASI separator column 220 mm in length, and a Dionex Electrochemical Detector, for which an amperometric system is used. The working electrode was Ag; the reference electrode was Ag/ AgCl; and the counter electrode was stainless steel. A Nafion (DuPont low equivalent weight polymer) cation exchange membrane separates the reference electrode from the flowing stream. A diagram of the working cell is displayed in figure 1. The normative working potential was approximately 0.2 V (volt) versus the Ag/ AgCl reference electrode, but in practice ranged from 0.1 to 0.33 V. The output range of the potentiostat varied inversely from 1 ηA/ V (nanoampere per volt) to 1 μA/ V (microampere per volt) as a function of the iodide concentration in solution. No suppressor column was used. The sample loop volume was 50 μL, and the eluent flow rate was 2.7 mL/ min. A Houston Instrument dual channel chart recorder was used to record the chromatograms.

Reagents

All standards and reagents were prepared from reagent-grade chemicals dissolved in distilled-deionized water. The eluent for the separator column was 0.020 M NaNO$_3$. Iodide standard solutions were prepared from a 1,000 mg/ L I$^-$ stock solution and ranged in concentration from 10 μg/ L to 10 mg/ L I$^-$. All working standards contained 1,000 Cl$^-$. All samples were collected and prepared by means of established field procedures, including filtration through a 0.45 μM filter (Lico and others, 1982). All samples were diluted appropriately so as to contain 1,000±100 mg/ L Cl$^-$. The reference electrode cavity was filled to capacity with several drops of a 1 M NaCl solution saturated with AgCl.
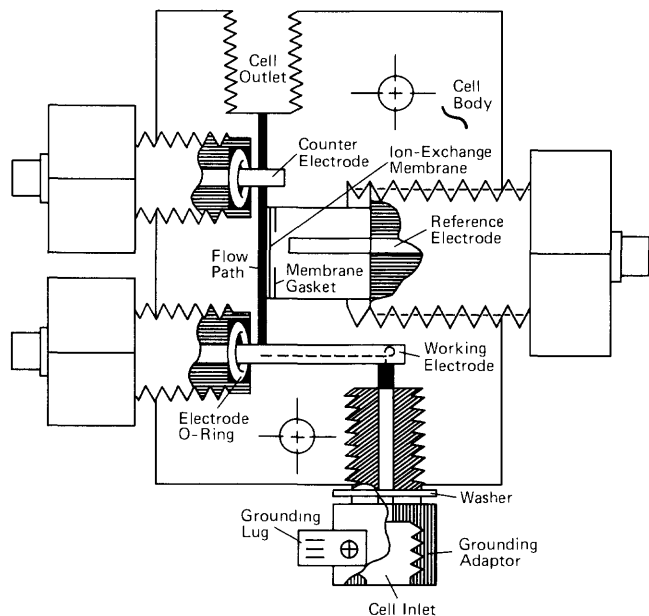
Figure 1. Diagram of amperometric flow-through cell (courtesy of Dionex Corp.).

Procedure

We cleaned the working electrode daily by polishing with either toothpaste or a silver-polishing compound, then thoroughly rinsing in distilled-deionized water. If prolonged system instability occurred after the cleaning of the working electrode, and no other reasons were self-evident, the internal filling solution of the reference electrode was replaced.

Before making a series of measurements, we turned on the eluent pump, recorder (1 in/min), and the electrochemical detector for a period of 30 to 60 minutes, or until a stable, relatively flat (except at high sensitivity levels) baseline was obtained. We determined optimum applied potential for a symmetrical peak with maximum height by repeated injections of an iodide standard solution appropriate to the output range setting of the potentiostat. There is a period of instability whenever the applied potentials are changed between decade ranges, that is, from 0.01 to 0.09 V range to the 0.10 to 0.19 V range. The optimum current output range was selected for the expected iodide concentration range. For example, the 300 ηA/V range was found satisfactory for 1 to 5 mg/L I⁻, whereas the 1 ηA/V range was appropriate for 10 to 90 μg/L I⁻.

Iodide standards in the concentration range of interest were repeatedly injected until acceptable reproducibility was achieved. We then injected increments of the sample solutions of interest and periodically checked the calibration curves by injecting additional standards. If the sample peaks are reasonably symmetrical, the digital readouts for the baseline and peak maximum signals will be as valid as the measured peak heights. When

operating in the μg/L I⁻ range, one should use only graphically measured peak heights because of peak spreading, significant tailing, and a markedly sloping baseline. At the more sensitive current range settings used for the microgram concentration ranges, one will find curvature of the standard plot for the lowest values. Where such curvature occurs, the concentration is obtained either from a curved line or by bracketing the sample with the appropriate standards. The lower limit of detection is approximately 10 μg/L I⁻. Electrode contamination is minimized where the electrochemical detector is turned off after operation each day.

RESULTS AND DISCUSSION

Initial investigations were made to determine the maximum chloride concentration that the detector and column system could accommodate without saturating the column or poisoning the electrode. Concentrations of chloride ranging from 5,000 to 100,000 mg/L, which contained 10 mg/L I⁻, were injected onto the column. The increasingly higher concentrations of chloride overloaded the column and were not readily eluted; this caused an erratic detector readout. The advantage of using high concentrations of chloride is the possible elimination of the dilution step. Not even the use of 2,000 mg/L Cl⁻ standards was found practical. However, a practical advantage of a large dilution step is that most samples are brought to a common iodide concentration level.

As was demonstrated earlier by Rocklin and Johnson (1983), the best procedure is to use 1,000 mg/L Cl⁻ solutions. The response was found to be linear over a concentration range of 1 to 5 mg/L I⁻, and the 300 ηA/V output showed the most appropriate sensitivity. Figure 2 illustrates the linearity achieved, and the y-axis values indicate the net electrochemical detector response. Figure 3 demonstrates the symmetry of the iodide peaks and their linearity over the 1 to 5 mg/L I⁻ concentration range. The maxima of the iodide peaks occurred after an elution time of approximately 8 minutes. As stated earlier, the optimum applied potential must be determined daily, or more particularly after each cleaning of the Ag electrode. An excessively positive potential results in a dip in the peak tailing, and too negative a potential will result in a sloping baseline. Occasionally, the optimum potential elicited a slightly dipping tail. When this happens, the minimum (valley) of the tail should be used as the baseline measurement. To shorten the time of analysis, we tested a more concentrated eluent than was used by Rocklin and Johnson (1983), namely 0.025 M NaNO₃, but the net gain in time was insignificant, and the results were inconsistent.

For samples in the 0.1 to 1 mg/L I⁻ concentration range, the optimum output range was 100 ηA/V. Figure 4 illustrates the linearity of the results. For samples in
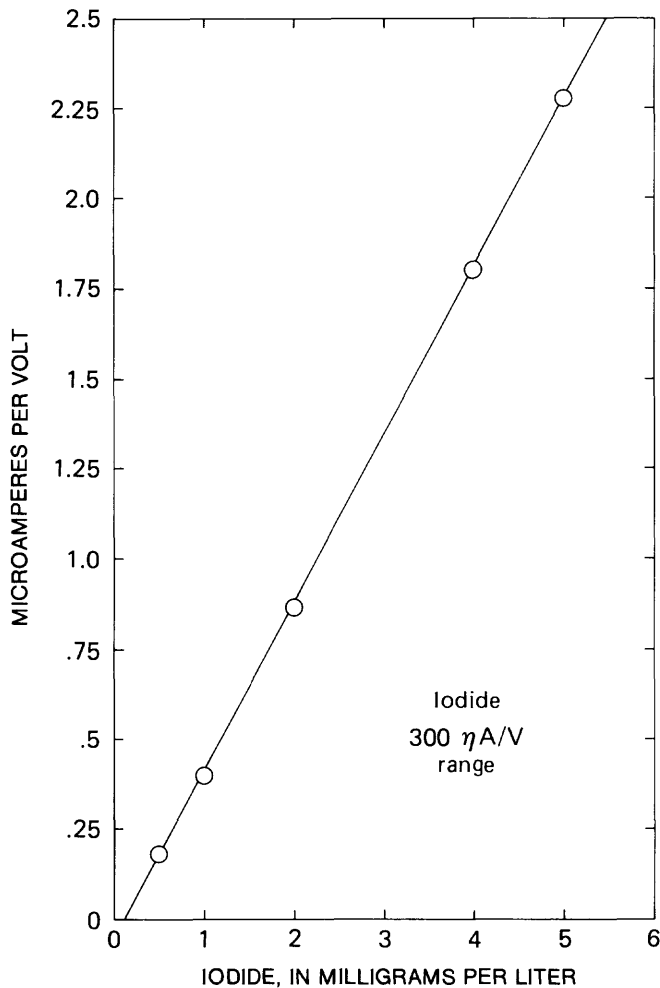
**Figure 2.** Calibration curve for high-level iodide samples (1 to 5 mg/L).
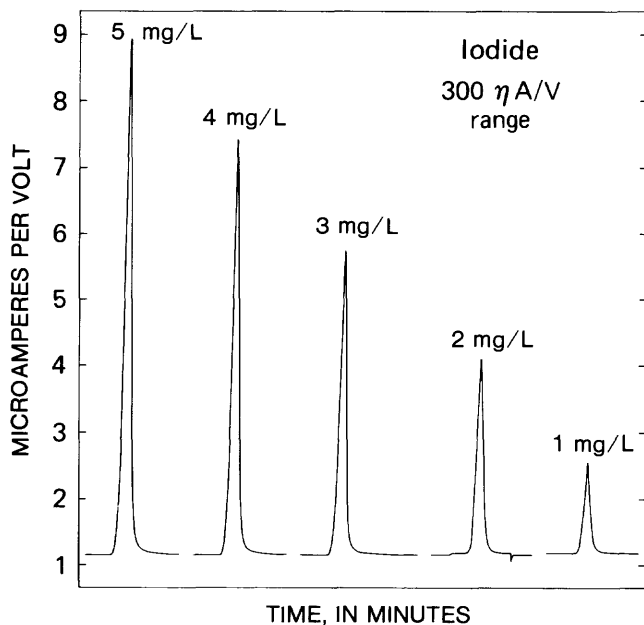
**Figure 3.** Ion chromatograph peaks for high-level iodide calibration standards.
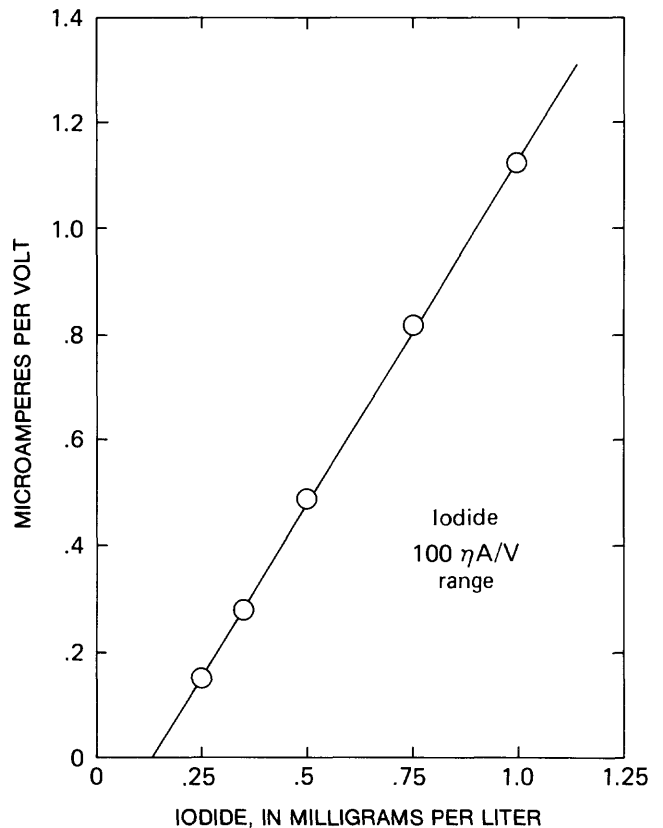
Figure 4. Calibration curve for medium-level iodide samples (0.1 to 1.0 mg/L).

the 10 to 100 μg/L I⁻ concentration ranges, greater amplitude is desirable to accurately measure peak height, and output ranges of 3 and 1 ηA/V are useful. Figures 5 and 6 illustrate typical calibration curves at these sensitivity levels. Curvature of the standard plots was shown below 20 and 50 μg/L I⁻, respectively. At these concentrations where such curvature occurs, the samples were treated as described in the "Procedure" section. The lower limit of detection is indicated as being 10 μg/L, which agrees with the work of Rocklin and Johnson (1983).

Table 1 documents the precision of the method. Approximately six measurements were made on each of three samples and one standard representing several concentration levels. The relative standard deviations (RSD) were less than 1 percent for both the graphical and the digital readout peak height data for the three samples and somewhat greater than 1 percent for the standard solution.

Two samples, diluted 1/10, were spiked with 3-, 1-, or 1/2-mL increments of a standard iodide solution and the chromatograms determined. These data are shown in table 2. The net concentrations of iodide for the original samples show ascending values as total concentration is increased; therefore slightly steeper slopes are indicated as iodide concentration is increased.
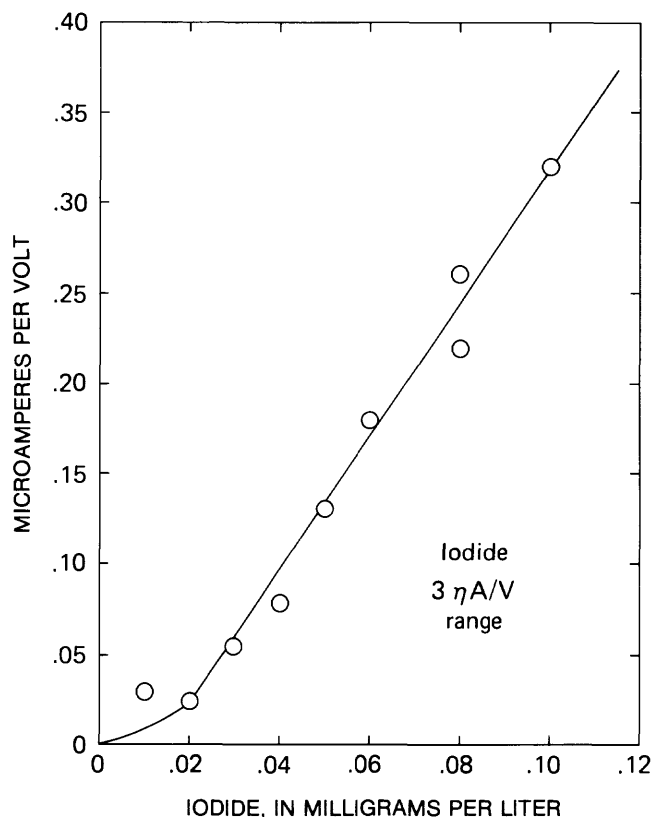
Figure 5. Calibration curve for low-level iodide samples (100 μg/L).
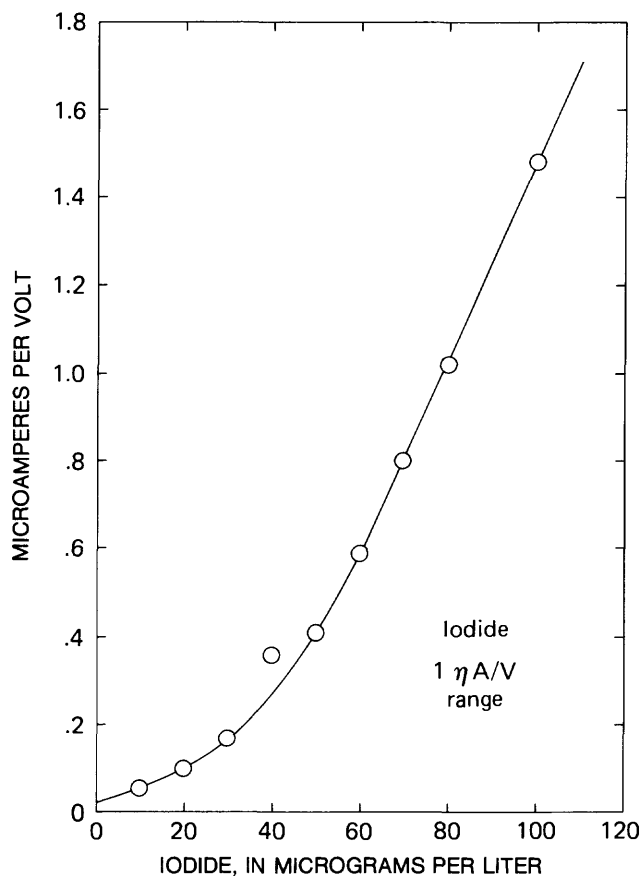
Figure 6. Calibration curve for iodide samples near the detection limit (10 μg/L).

Table 1. Precision of the ion chromatographic determination of iodide in saline samples from Sacramento Valley, Calif., gas wells

Sample	Dilution	Concentration (mg/L)	Detector range ($\eta A/V$)	Digital readout ($\mu A/V$)[1]	RSD[2]	Graphical readout (Div)[1]	RSD[2]
NSV-1	1/20	65.3	300	1.08	0.77	36.2	0.16
NSV-10	1/10	10.1	100	1.33	.45	45.8	.39
NSV-11	1/20	61.6	300	1.71	.58	58.6	.65
Standard	1/1	.1	3	.81	1.44	28.55	1.17

[1]Values shown represent means of approximately six determinations.

[2]Relative standard deviation in percent.

Table 2. Determination of iodide in spiked saline samples from Sacramento Valley, Calif., gas wells

Sample	Net sample concentration (mg/L)		Sample	Net Sample concentration (mg/L)	
	Digital	Graph		Digital	Graph
SSV-30 (1/10)	2.08	2.06	SSV-26 (1/10)	1.57	1.58
SSV-30+1.0 mg/L ...	2.07	2.06	SSV-26+1.0 mg/L ...	1.59	1.58
SSV-30+2.0 mg/L ...	2.14	2.13	SSV-26+2.0 mg/L ...	1.62	1.64
SSV-30+2.5 mg/L ...	2.17	2.17	SSV-26+3.0 mg/L ...	1.69	1.72
Mean value ...	2.11	2.10	Mean value ...	1.62	1.63

The mean concentration values have a relative deviation of 2 to 3 percent from the original values. These data further illustrate the comparability of the digital readout signal to the graphical measurement of peak height.

The principal application of this procedure was for the analysis of saline waters (solutions containing dissolved sodium chloride in amounts approximating seawater) from gas wells in the Sacramento Valley of California. Some typical chromatograms of northern and southern Sacramento Valley samples, illustrative of analysis at several concentration levels, are shown in figure 7. The iodide peak is well defined and segregated from most other anions. The chloride concentrations depicted are all approximately 1,000 mg/L, and the iodide concentrations range from 1 to 3 mg/L. The concentrations of bromide are two to three times those of the iodide, but could not be quantified under the conditions of the method. A 0.002 M Na_2CO_3 eluent is required to separate bromide from high concentrations of chloride. The large negative dips following the elution of the chloride and the bromide are caused by the reduction of AgCl and AgBr deposits, respectively, from the electrode, which satisfies the Nernst equation (Rocklin and Johnson, 1983).

Some typical data illustrative of the iodide concentrations found in the saline water samples from the Sacramento Valley gas wells are presented in table 3. The reciprocals of the dilution factors are approximately equivalent to the chloride concentrations of the original samples in grams per liter. The electrochemical detector results are compared with the titrimetric results, which were obtained earlier by means of the thiosulfate-starch method. For most samples, a positive bias was indi-

cated for the titration values. The differences were particularly magnified for low-level samples containing 0.5 mg/L I⁻. In these samples, the differences may be accounted for by the greater inherent sensitivity of the electrochemical detection of iodide by ion chromatography as opposed to the titrimetric method. For ex-
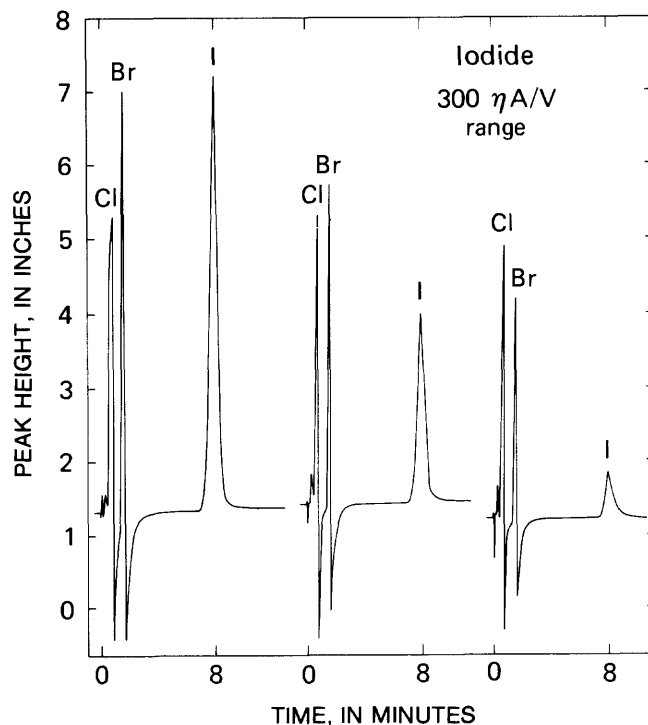
Figure 7. Typical ion chromatographs for Sacramento Valley, Calif., gas-well saline samples.

Table 3. Iodide determinations in saline samples from Sacramento Valley, Calif., gas wells
[ECD value and titration value in mg L, except as indicated]

Sample	Dilution factor	ECD[1] value	Titration value	Percent bias of titration value
NSV-1	(1/20)	65	66	+2
NSV-2	(1/4)	7.4	8.7	+18
NSV-4	(1/1)	10 µg/L	400 µg/L	+3900
NSV-5	(1/10)	9.5	9.8	+3
NSV-9	(1/10)	20	20	±0
NSV-13	(1/10)	18	17	-6
NSV-14	(1/1)	25 µg/L	100 µg/L	+400
NSV-16	(1/10)	26	29	+12
NSV-18	(1/20)	28	27	-4
NSV-19	(1/10)	30	44	+47
NSV-20	(1/4)	4.7	4.8	+2
NSV-24	(1/1)	20 µg/L	400 µg/L	+1900
SSV-1	(1/10)	18	25	+39
SSV-27	(1/4)	16	17	+6
SSV-29	(1/1)	0.5	0.8	+60

[1]ECD = Electrochemical detector.

ample, a 0.1 mL volume of 0.1 N thiosulfate titrant is equivalent to 0.2 mg/L I⁻, which amount would be at or near the detection limit for the method. The subsequent ion chromatographic determination of iodide in other saline water samples, which previously had been analyzed by several analysts, also showed significant variability from the ion chromatographic results. This emphasizes the subjectivity of the titration method.

CONCLUSIONS

An ion chromatographic method for determining iodide using an electrochemical detector has been successfully applied to saline samples containing high concentrations of chloride. All samples are diluted before analysis to approximately 1,000 mg/L Cl⁻, and then are passed through a single separator column. The method, which is precise, reliable, and highly sensitive, enables determinations as low as 10 μg/L I⁻ to be made. For these reasons, plus the savings in analytical time, the method offers some distinct advantages over the classical titrimetric method.

REFERENCES CITED

American Public Health Association, American Water Works Association, and Water Pollution Control Federation, 1981, Standard methods for the examination of water and wastewater (15th ed.): Washington, D.C., p. 342-46.

American Society for Testing and Materials, 1966, Manual on industrial water and industrial waste water (2d ed.): Philadelphia, Pa., p. 449-452.

Bachmann, K., and Matusca, P., 1983, Gas-chromatographische bestimmung von geringsten mengen Cl⁻, Br⁻, und I⁻ in wasser: Fresenius' Zeittschrift fur Analytische Chemie, v. 315, no. 3, p. 243-244.

Black, A.P., and Whittle, G.P., 1967, New methods for the colorimetric determination of halogen residuals. Part 1. Iodine, iodide, and iodate: Journal of the American Water Works Association, v. 59, p. 471-490.

Brown, E., Skougstad, M.W., and Fishman, M.J., 1979, Methods for collection and analysis of water samples for dissolved minerals and gases: U.S. Geological Survey (2d ed.), Techniques of Water-Resources Investigations Book 5, Chapt. A1, p. 98-101.

Cassidy, R.M., and Elchuk, Steven, 1982, Dynamically coated column for the separation of metal ions and anions by ion chromatography: Analytical Chemistry, v. 54, no. 9, p. 1558-1563.

Cochrane, R.A., and Hillman, D.E., 1982, Analysis of anions by ion chromatography using ultraviolet detection: Journal of Chromatography, v. 241, p. 392-394.

Dubravcic, M., 1955, Determination of iodine in natural waters (sodium chloride as a reagent in the catalytic reduction of ceric ions): Analyst, v. 80, p. 295-300.

Evans, K.L., Tarter, J.G., and Moore, C.B., 1981, Pyrohydrolytic-ion chromatographic determination of fluorine, chlorine, and sulfur in geological samples: Analytical Chemistry, v. 53, no. 6, p. 925-928.

Faigle, W., and Klockow, D., 1982, Gas-chromatographische bestimmung von spuren an chlorid, bromid, iodid, cyanid, thiocyanat and nitrat in wassrigen losungen nach derivatisierung mit hilfe der phasentransferkatalyse: Fresenius' Zeitsschrift fur Analytische Chemie, v. 310, p. 33-38.

Gjerde, D.T., Fritz, J.S., and Schmuckler, G., 1979, Anion chromatography with low-conductivity eluents. II.: Journal of Chromatography, v. 186, p. 509-519.

Gjerde, D.T., Schmuckler, G., and Fritz, J.S., 1980, Anion chromatography with low-conductivity eluents. II.: Journal of Chromatography, v. 187, p. 35-45.

Hershcovitz, H., Yarnitzky, C., and Schmuckler, G., 1982, Ion chromatography with potentiometric detection: Journal of Chromatography, v. 252, p. 113-119.

Igawa, Manabu, Saito, Kimiko, Tsukamoto, J., and Tanaka, Masao, 1981, Ion chromatographic separation of anions on silica-coated polyamide crown resin: Analytical Chemistry, v. 53, p. 1942-1944.

Ivey, J.P., 1983, Novel eluent for the UV and conductometric detection of anions in unsuppressed ion chromatography: Journal of Chromatography, v. 267, p. 218-221.

Kolthoff, I.M., and Sandell, E.B., 1952, Textbook of quantitative inorganic analysis (3rd ed.): New York, Macmillan Co., p. 585.

Lico, M.S., Kharaka, Y.K., Carothers, W.W., and Wright, V.A., 1982, Methods for collection and analysis of geopressured geothermal and oil field waters: U. S. Geological Survey Water-Supply Paper 2194, 21 p.

Matsushita, Susumu, Tada, Yoshimitsu, Baba, Nobuyuki, and Hosako, Keiichi, 1983, High-performance ion chromatography of anions: Journal of Chromatography, v. 259, p. 459-464.

Pihlar, B., and Kosta, L., 1980, Determination of cyanides by continuous distillation and flow analysis with cylindrical amperometric electrodes: Analytica Chimica Acta, v. 114, p. 275-281.

Pihlar, B., Kosta, L., and Hristovski, B., 1979, Amperometric determination of cyanide by use of a flow-through electrode: Talanta, v. 26, p. 805-810.

Reeve, R.N., 1979, Determination of inorganic main group anions by high-performance liquid chromatography: Journal of Chromatography, v. 177, no. 2, p. 393-397.

Rocklin, R.D., and Johnson, E.L., 1983, Determination of cyanide, sulfide, iodide, and bromide by ion chromatography with electrochemical detection: Analytical Chemistry, v. 55, no. 4, p. 4-7.

Rogina, B., and Dubravcic, M., 1953, Micro-determination of iodides by arresting the catalytic reduction of ceric ions: Analyst, v. 78, p. 594-599.

Skelly, N.E., 1982, Separation of inorganic and organic anions on reversed-phase liquid chromatography column: Analytical Chemistry, v. 54, no. 4, p. 712-715.

Small, Hamish, Stevens, T.S., and Bauman, W.C., 1975, Novel ion exchange chromatographic method using conductimetric detection: Analytical Chemistry, v. 47, no. 11, p. 1801-1809.

Wang, Chuyng-Yu, Bunday, S.D., and Tarter, J.G., 1983, Ion chromatographic determination of fluorine, chlorine, bromine, and iodine with sequential electrochemical and conductometric detection: Analytical Chemistry, v. 55, no. 9, p. 1617-1619.

Wang, Chung-Yu, and Tarter, J. G., 1983, Determination of halogens in organic compounds by ion chromatography after sodium fusion: Analytical Chemistry, v. 55, no. 11, p. 1775-1778.

Williams, R.J.. 1983, Determination of inorganic anions by ion chromatography with ultraviolet absorbance detection: Analytical Chemistry, v. 55, no. 6, p. 851-854.

Cascade-Sieve Shaker for Rapid Particle-Size Analysis of Coarse Sediment

By David W. Hubbell *and* Herbert H. Stevens, Jr.

Abstract

A new sieving apparatus and an analytical method have been developed and used for rapidly defining the particle-size distribution of sediment coarser than 0 millimeter. The apparatus consists of inner and outer support frames, a series of rectangular sieve screens that are arranged in an alternating cascade fashion, and a mechanism for vibrating the inner frame and screens vertically at a frequency of 3.7 Hertz. Sediment introduced on the topmost sieve is vibrated through the system. Particles that pass through a sieve are directed to the next finer sieve, whereas particles that are retained are shunted off into a collection container. Size separates in the collection containers are weighed cumulatively on an electronic balance, and the particle-size distribution is calculated automatically by computer. The size distribution of a predried 1,500-gram sample that is composed of no more than 60-percent sand (material finer than 2.0 millimeter) ordinarily can be determined in about 5 minutes. Percent-in-class values compare within 1 percent of comparable values obtained by conventional nested-sieve (rotap) analysis. Because percent-finer values are derived by summing percent-in-class values, percentages finer than 2.0 and 1.0 millimeters differ from comparable rotap values by 2 and 3 percent, respectively.

INTRODUCTION

In sedimentation studies, one of the most fundamental analytical procedures is the determination of the size of sediment particles. A knowledge of particle size is required to understand and predict all phases of sedimentation phenomena, including weathering, erosion, transport, deposition, and diagenesis. The mode and extent of transport and deposition of sediment particles particularly depend on their size. In recent sediment-transport studies that were undertaken for the purpose of calibrating bedload samplers, it was necessary to define the particle-size distribution of several thousand bedload samples. Because the analysis of this number of samples in a short time by means of conventional sizing procedures would have required an extremely intensive and expensive effort, a rapid-sieving apparatus and automated computational procedure were developed and used to expedite the task. This report describes the new apparatus and analytical method and compares results of analysis obtained by means of the new and the traditional methods.

PARTICLE-SIZE ANALYSIS METHODS

Particle sizes commonly are defined in several different ways. Most often, the size of an individual particle is characterized in terms of (1) the diameter of a sphere having the same fall velocity as that of the particle, (2) a linear dimension expressing the size of the smallest opening through which the particle can pass, or (3) a linear dimension that typifies the dimensions of a projection of the particle on a measurement grid. Analytical methods that utilize these different means to characterize size are generally categorized, respectively, as sedimentation, sieving or aperture, and image-analyzing methods. Because each of these general methods is based on different geometric and mass criteria, and because the shape, angularity, and density of natural particles differ considerably, defined particle sizes are somewhat method dependent.

Usually, the actual physical sizes of sediment particles are characterized most accurately by means of sieving or image-analyzing methods. Therefore, these methods are most appropriate when the geometrical or bulk (other than mass-related) properties of the sediment are of interest. Sedimentation methods yield sizes that are derived from the hydrodynamic characteristics of particles. Therefore, methods that define particle size on this basis are useful when transport phenomena are of primary concern. However, even though each method tends to be preferable for certain purposes, owing to the complexities of sedimentation processes, none of the methods provide results that are completely satisfactory for characterizing either the properties of deposited particles or the dynamic behavior of particles subject to transport. Further, duplicate analyses usually can be used to relate results of one method of analysis to results of another method of analysis. For this reason, the ease and expense of analysis also must be considered in determining how sediment particles are analyzed.

Because of the susceptibility of small particles to be transported and the difficulty and expense of constructing and maintaining fine-mesh sieves, such particles usually are sized by means of sedimentation methods. Fall velocities are affected by the three-dimensional geometry and the density of the particles; hence, for standardization between sediments, it is mandatory to express results from sedimentation-method analyses in terms of "standard fall diameters." The standard fall diameter of a particle is the diameter of a sphere that has a specific gravity of 2.65 and the same standard fall velocity as the particle. The standard fall velocity is the average rate of fall that a particle will finally attain when falling alone in quiescent distilled water of infinite extent at a temperature of 24 °C (Inter-Agency Committee on Water Resources, 1957a).

Large particles, particularly those larger than 2 mm in diameter, because of their relatively high fall velocities, usually are sieved. In this method, sizes are expressed as sieve diameters. The sieve diameter is the length of the side of the smallest square mesh through which the particle will pass. Sieve diameters are unaffected by particle densities and depend only on the cross-sectional geometry of the particles.

The difference between fall and sieve diameters of regularly shaped particles (particles having a shape factor of 0.7 or greater) that are 62 μm (0.062 mm) or smaller is negligible. However, for particles larger than 62 μm, the difference between fall and sieve diameters increases as size increases and shape factor decreases; for natural particles larger than 2.0 mm (except spheres), the differences are substantial (Inter-Agency Committee on Water Resources, 1957a, fig. 7). Because of the discrepancy, it is important to always specify the method of analysis.

Bed-material and bedload samples from sand-bed streams usually are analyzed by either the visual-accumulation (VA) tube method (VA method, Inter-Agency Committee on Water Resources, 1957b) or sieving, or a combination of both. The VA method, which is a sedimentation method, is suitable and recommended for analyzing particles in a sample that are smaller than 2.0 mm in diameter; the larger particles are sized by sieving. Samples from gravel-bed streams almost always are sieved.

The results of a size analysis ordinarily are expressed either as a frequency distribution or as a cumulative frequency distribution. Both types of distributions can be computed on the basis of mass, volume, or number of particles; normally, distributions are computed on the basis of mass. A frequency distribution expresses the fractions (percentages) of the total sample that are within specified size ranges (classes). The cumulative distribution indicates the fractions (percentages) of the total sample that are either smaller (finer) or larger (coarser) than a series of specified sizes. Cumulative distributions in this report give the percentages of a sample, by mass, that are finer than specified sizes.

SIEVE ANALYSES

In the laboratory, most sieve analyses of dried stream sediments entail performed use of sieves in a circular frame, either 76 or 203 mm in diameter, that supports the sieve screen (mesh). For the analysis, the sample is deposited on the topmost sieve of a stack of nested sieves, arranged so that the finest mesh sieve is at the bottom and progressively larger mesh sieves are stacked on top. The sieve stack is then mounted in a shaker mechanism that imparts a low-frequency horizontal rotary motion to the stack while, simultaneously, a hammer mechanism delivers a vertical blow to the top of the stack during each horizontal cycle. After a 15-minute sieving most particles pass through all sieves having larger meshes than the minimum cross-section dimensions of the particle (Guy, 1969, p. 50). In this report, the apparatus is called a rotap, and the sieving method is termed a "rotap analysis."

Rotap analyses provide reasonably accurate size distributions. Repeated analyses of the same sample ordinarily gives frequency distributions that are within about 2 percent of each other in every size class. As such, rotap analyses constitute the standard against which other sieving methods are evaluated.

Commercial continuous-feed sieving systems are used to separate large volumes of particles into size classes. Typically, these systems contain several large rectangular sieves that are arranged so that sediment can be fed continuously onto the topmost (coarsest) sieve. Particles smaller than any given sieve pass through to the next smaller sieve, and particles retained on any sieve are continuously shunted off to a repository of some sort. The sieves, which vibrate continuously, are positioned at an angle so that particles larger than the sieve openings will move along the length of the sieve. The sieve mesh openings, which are rectangular rather than square, facilitate rapid sieving; the wires that form the long side of each opening are parallel to the downslope sides of the sieve. Normally, owing to the high rates of sediment inflow onto the sieves and the short residence time for particles on the sieves, size separations are not as precise as they are in a rotap analysis.

Although rotap analyses insure accurate and consistent results, the analytical method involves several time-consuming manual operations. About 30 minutes is required to prepare, sieve, and weigh each sample, and another 10 minutes is spent in computing and tabulating the analysis results. Because of the current increase in sampling and analyzing bedload and bed and bank materials from coarse-bedded streams, a need now exists for systems and methods for defining the particle-size

distribution of sediment particles larger than 1 or 2 mm with about the same accuracy as rotap analysis, but with more speed and efficiency.

NEW APPARATUS AND ANALYTICAL METHOD

Size distributions determined in connection with most previous field and laboratory studies of sedimentation phenomena in coarse-bedded streams are expressed in terms of sieve diameters, which must be retained for continuity in any new method of size analysis. Where continuity is maintained, all size data can be treated, adjusted, or modified similarly. With this criteria in mind, we designed and constructed a sieving apparatus that incorporates selected features from both the rotap and the continuous-feed systems. Particles separated into size classes by the apparatus are weighed cumulatively on an electronic balance that is interfaced to a microcomputer. The computer is programmed to accept digital weight values directly from the balance and to calculate, store, and tabulate particle-size distributions.

The sieving apparatus (figs. 1 and 2) consists of (1) an outer metal frame with wooden sides and base, (2) an inner metal frame that supports rectangular sieves arranged in an alternating cascade fashion, in which the lower end of each sieve is approximately aligned with the upper end of the next finer sieve below, and (3) a motor-pillow-block-cam mechanism. The inner frame is attached to the outer frame at the top by four vertical springs (fig. 3). Two cam wheels, which are fixed by pillow blocks to the outer frame base, ride on the inside of horizontal members on the inner frame (fig. 4). Rotation of the cam wheels imparts a downward force. Hence, continuous rotation of the cam wheels causes the frame and sieves to vibrate vertically. The unit oscillates at 3.7 Hz (220 r/min) and has a vertical displacement of 32 mm. The cam wheels also give the inner frame a slight horizontal motion; metal uprights attached to the pillow-block-support bracket stop the motion and impart a jolting vibration in the horizontal direction. Metal troughs are located at the lower end of each sieve. Flexible hoses attached to drain spouts on the bottom of the troughs pass directly downward into the open end of removable plastic collection containers located at floor level. A metal tray, which has no side at its lower end, is attached directly below and parallel to the upper two-thirds of each sieve. Flexible plastic sheeting covers each sieve surface. Slopes of the sieves are individually adjustable. A "feed" pan (not shown in the photographs), located outside the outer frame near the top, is supported at its outer end by a rigid threaded rod fastened to the top of the outer frame. The inner end of the feed pan rests on a horizontal bar attached to the sides of the outer frame. The slope of the feed pan can be adjusted by moving the

support point for the pan up or down along the threaded rod. A plastic sleeve, which surrounds the inner end (lip) of the feed pan, connects to the underside of the upper end of the plastic sieve cover on the topmost sieve; the sleeve provides a slidelike pathway from the feed pan to the upper end of the sieve (see figs. 1 and 3).

The unit is constructed to accommodate six 305-by 356-mm rectangular sieve screens. L-shaped hook strips crimped onto the two long edges of the screens decrease the effective screen area to about 254 by 356 mm and serve to secure the screens to their support brackets. Sieve sizes in the prototype were 11.3, 8.0, 5.6, 4.0, 2.0, and 1.0 mm; however, any sequence of sizes coarser than 1.0 mm could be used. An enclosed pan beneath the lowest sieve intercepts all material that passes through the finest sieve.

Operation

Sediment is introduced into the feed pan at the top of the unit, and then the mechanism is turned on. As much as about 3,500 g of sediment can be dumped into the present feed pan. Although only the inner frame oscillates, sufficient motion is transmitted to the outer frame to cause the feed pan to vibrate. The vibration causes sediment to slide out of the slightly sloping pan into the sleeve, and, thence, onto the upper end of the topmost sieve. The oscillatory motion of the inner frame and sieves is almost vertical; hence, the particles on the sieves tend to bounce up and down. The sieve covers are reflecting barriers and continually direct the particles back to the sieves. Through this action, and because particle distributions on the sieves are generally only one grain layer thick, each particle bounces against the mesh many times as it slowly progresses down the length of the sieve. Particles larger than the sieve mesh eventually reach the lower end of the sieve and fall into the trough. Once in the trough, they move to the drain hole and slide down the hose to the collection containers. Particles that pass through a sieve are intercepted by the tray beneath the sieve and deposited onto the upper one-third of the next finer sieve. This action proceeds until every particle either has been retained by a sieve (and directed to a collection container) or has passed through all sieves. Particles that pass through all sieves are collected in the closed section beneath the smallest sieve and directed to the "pan" collection container.

After the sieving operation is completed, the collection containers are removed manually from the unit, and the sized material from each container is progressively added, beginning with the pan material, to a tared container on an electronic balance that is connected through an RS-232 interface directly to a microcom-
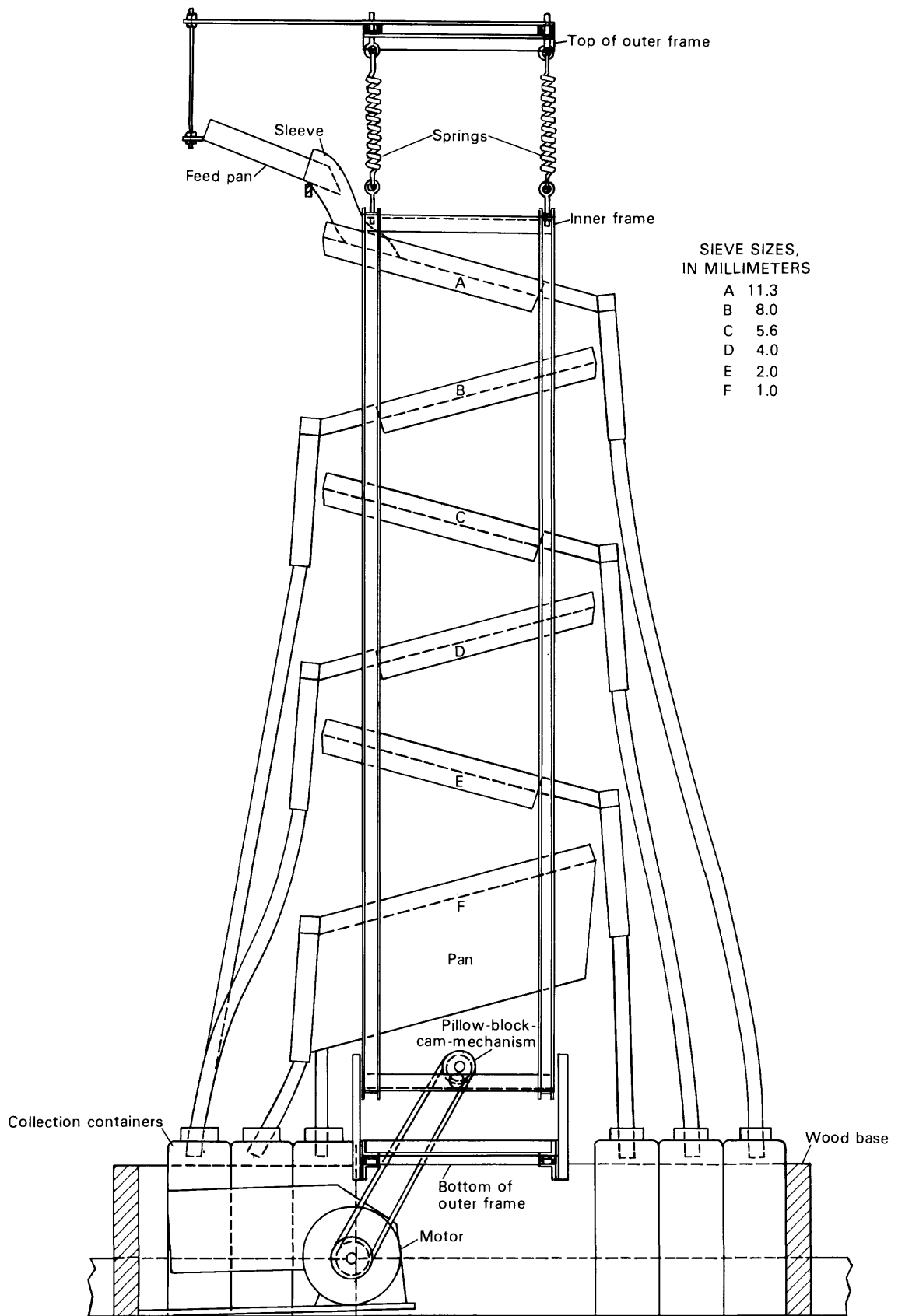
Figure 1. Schematic drawing of cascade-sieve shaker. The sketch does not show a complete view of the outer frame.

SIEVE SIZES,
IN MILLIMETERS

A	11.3
B	8.0
C	5.6
D	4.0
E	2.0
F	1.0

puter. The computer is programmed to accumulate the weights of the size fractions and then to compute, store, and print the particle-size distribution.

A typical sample of about 1,500 g that is composed of 30 to 50 percent sand can be sieved and have its particle-size distribution determined in about 5 minutes. Samples that have lower sand content, as well as small-volume samples, can be analyzed more rapidly. Ordinarily, the slope of the feed pan is adjusted to provide a feed rate of about 1,000 g/min, and sieving is continued for 3 minutes after all particles have been shaken from the feed pan. However, samples that have a high sand content must be sieved for much longer periods; samples composed of 90 percent sand typically require sieving times of 10 to 12 minutes.

Some particles finer than a given sieve may be collected in the size fraction for that sieve, some very fine particles may be retained on the trays beneath each sieve, and some particles may inadvertently be ejected from the system; however, the quantities misplaced are relatively small. To identify changes in sample weight during analysis, the analyst must weigh all samples on the electronic balance before they are sieved. In the computer program for calculating the particle-size distribution, any difference between the preanalysis (initial) weight of the sample and the postanalysis cumulative weight is assumed to have resulted from a "loss" of very fine material within the system. The loss, which usually, but not always, is a positive value, is added to the pan weight before computation of the particle-size distribution. An example of the computer output, which demonstrates the computational procedures, is shown in figure 5. Data in the figure are from a large set of analyses of bedload samples. The analyses were selected to illustrate typical results, and they are not arranged in the order in which the samples actually were sieved. A further explanation of the weight-adjustment procedure is given in the following section.

Accuracy

We have evaluated the accuracy of the sieving operation and the validity of the weight-adjustment procedures by subjecting individual test samples to both a conventional rotap analysis and a cascade-sieve shaker analysis. Test samples having different weights and size distributions were dry sieved first by means of the rotap method. For this procedure, samples heavier than 400 g (see Guy, 1969, p. 50) were split into subsamples weighing less than 400 g, and each subsample was sieved separately in 203-mm sieves; common size fractions from all subsamples then were combined for determination of the sample size distribution. Later, we recombined all size

fractions from each sample and analyzed the samples by using the cascade-sieve shaker. Particle-size distributions defined by these analyses are given in table 1. As indicated in the table, many of the analyses by the cascade-sieve shaker method showed a loss during the analysis; that is, the preanalysis sample weight differed from the postanalysis weight. Losses (or gains) during analysis, whether they are from one size class or several classes, adversely affect the accuracy of all computed percent-in-class values (and consequently, all percent-finer values). To remedy such a situation, one must apply some corrective procedure. To correct the analyses in table 1, and all other cascade-sieve shaker analyses, we added the loss to the weight of material in the less-than-1.0-mm class before determining percent-in-class values. This procedure was adopted as the best practical means to account for the errors because of the manner in which losses (and gains) were observed to occur.

In the cascade-sieve shaker, losses result when small quantities of material adhere to the trays beneath the sieves or escape from underside of the sieve covers. Results from many analyses have shown that, generally, losses increase as the sample size increases, and that all the adhering material and most of the escaping material is finer than 1.0 mm. Also, that material lost by adhesion from one sample ultimately is added to the material in the finer-than-1.0-mm size separate of a subsequently sieved sample; in these cases, the loss is a negative value (a gain).

Differences between the percent-in-class values defined by the two methods are shown in table 2. (Negative values indicate that more material was retained in a class by the cascade-sieve shaker than by the rotap.) For most samples, the cascade-sieve shaker retained slightly more material than the rotap in all size classes except the 4.0- to 5.6-mm and less than 1.0-mm classes. This indicates that a small quantity of the material retained by every sieve, except the 4.0-mm sieve, actually was finer than the sieve size. The apparent deviation from this trend shown by the 4.0-mm sieve may have resulted because of slight differences in the actual mesh sizes of the 4.0-mm cascade-sieve shaker and rotap sieves or because of the loss of 4.0- to 5.6-mm particles from the system. The two finest sieves retained the largest proportions of material finer than the sieve mesh.

Statistics shown in table 2 below the matrix of difference values give the mean difference for each size separate and the interval within which the true mean difference can be expected to lie for confidence levels of 90 and 95 percent. These statistics are based on 25 of the 27 comparisons listed in table 1, and were determined with the following relations:
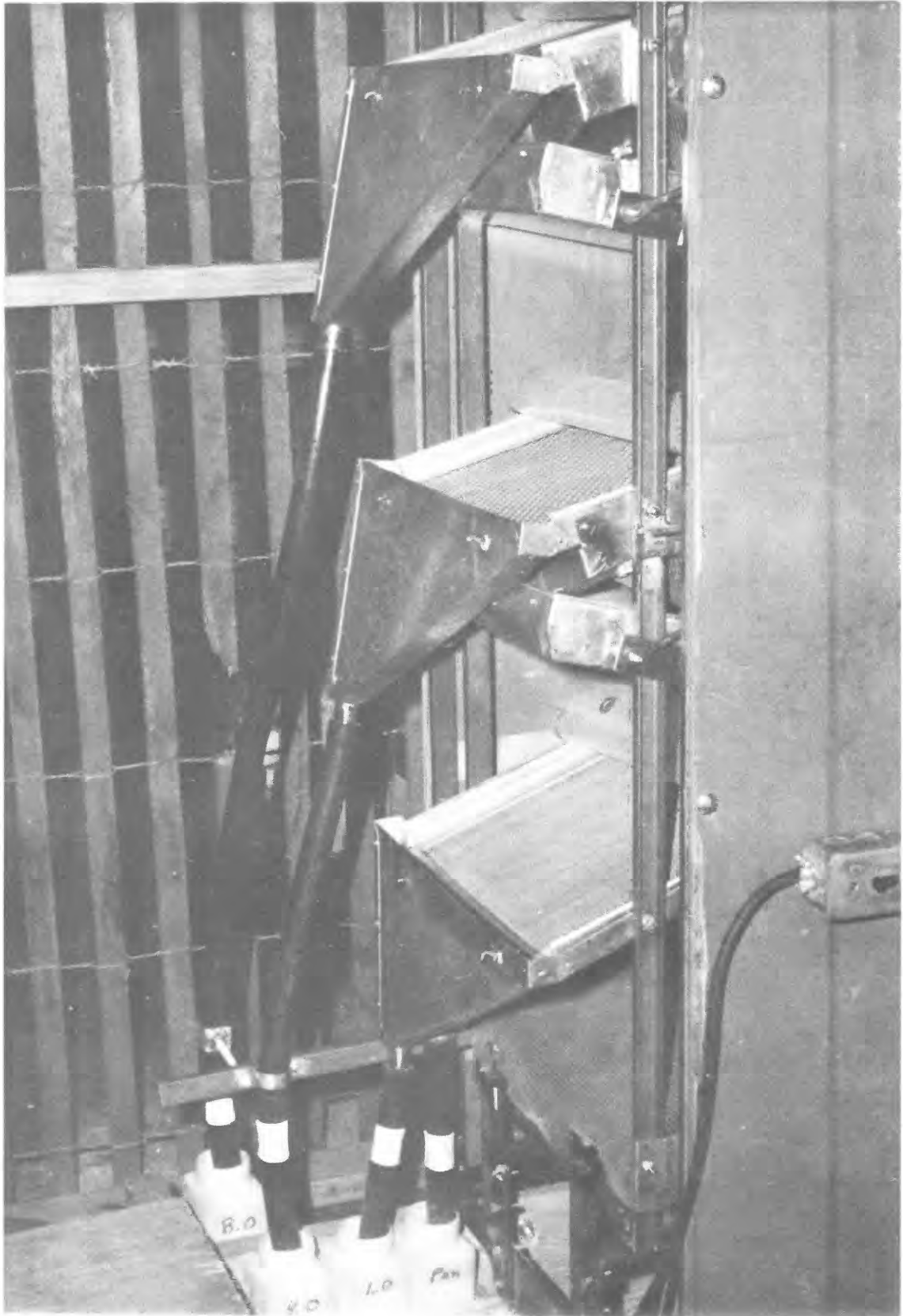
Figure 2. Exterior view of cascade-sieve shaker. The right side of the shaker (not shown) is virtually the same as the left side (shown).
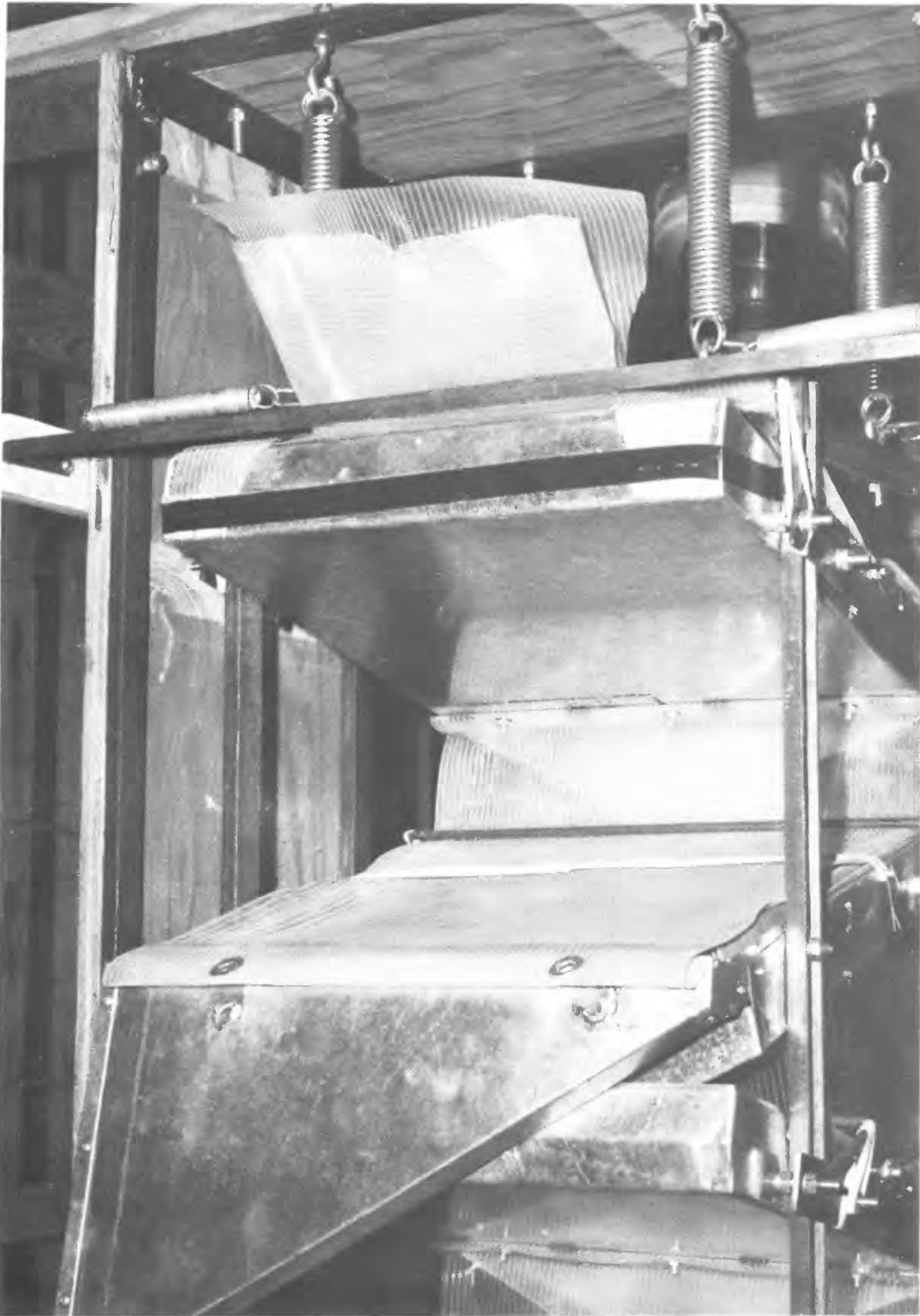
Figure 3. Inner-frame support springs. Vertical springs suspend the inner frame beneath the outer frame and provide a reactive force against the cam-wheel rotation. Horizontal springs restrain lateral motion of the inner frame.
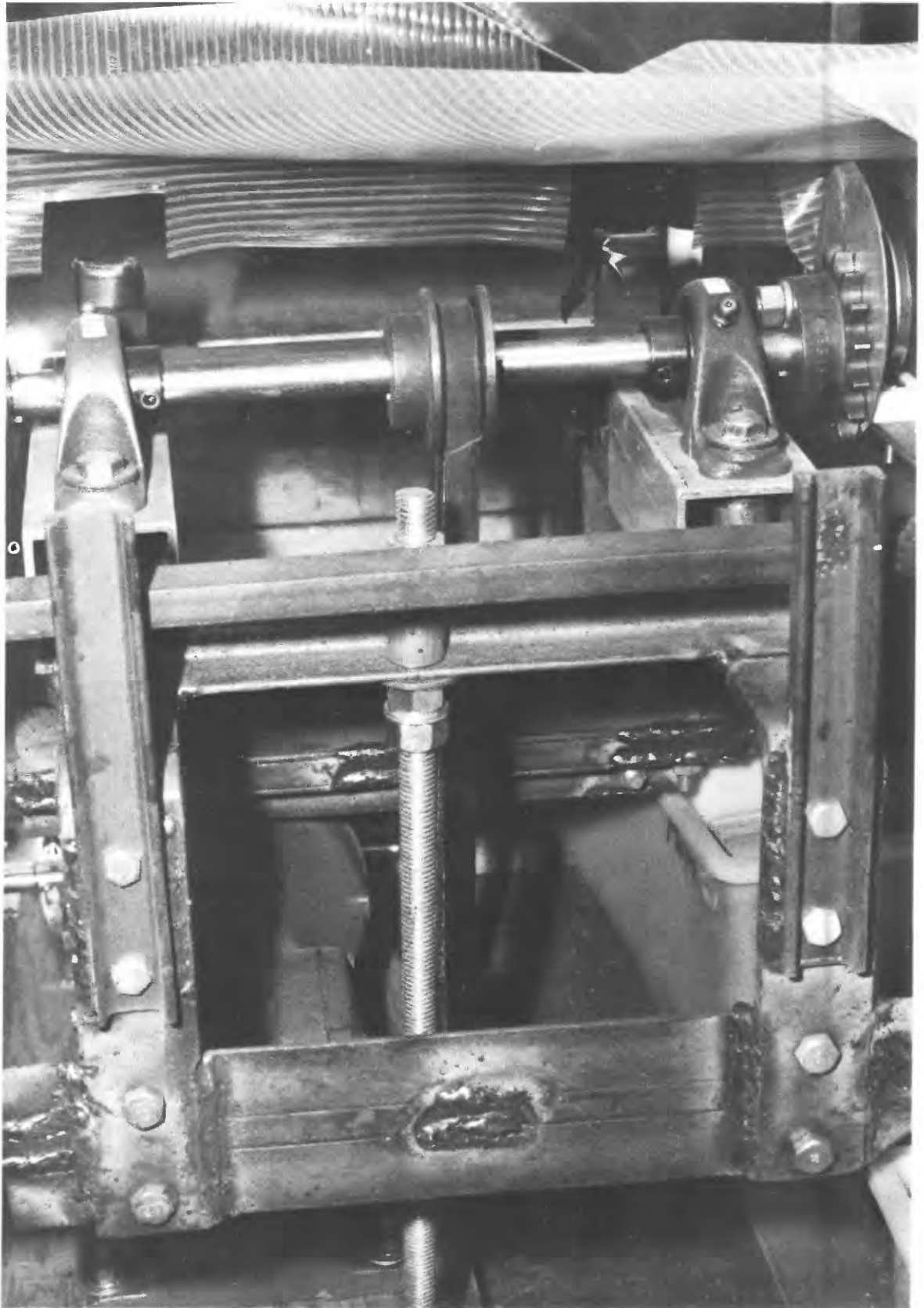
Figure 4. Cam-wheel drive mechanism. Rotation of the shaft causes the inner frame to oscillate vertically.

Table 1. Particle-size distributions of test samples as defined by rotap and cascade-sieve shaker analyses
[Method of analysis: R, rotap; C, cascade-sieve shaker]

Sample number	Total weight (g)	Method of analysis	Loss[1] (g)	Percent finer than indicated size (mm)					
				1.0	2.0	4.0	5.6	8.0	11.3
1	2,263	R		16.1	31.6	44.5	59.1	96.7	98.7
		C	9	13.3	29.7	43.0	58.0	96.0	98.6
2	1,825	R		15.8	34.2	49.1	64.5	97.7	99.5
		C	8	13.6	32.4	47.8	63.6	96.2	99.2
3	753	R		24.3	35.9	45.7	60.3	97.1	98.3
		C	1	21.5	33.8	44.5	58.6	96.1	98.4
4	344	R		31.1	42.7	52.0	67.1	98.5	100.0
		C	1	28.4	40.6	50.5	65.1	98.0	100.0
5	1,659	R		14.9	31.0	43.9	60.1	97.6	99.3
		C	5	12.6	28.7	42.4	58.2	95.8	98.6
6	2,014	R		9.1	22.9	37.8	54.4	96.9	99.3
		C	14	8.3	21.2	36.3	53.3	95.9	98.5
7	1,515	R		41.5	54.2	60.7	68.7	94.2	96.4
		C	14	38.1	52.7	60.0	67.6	92.8	96.0
8	533	R		30.9	43.5	51.2	62.3	95.7	97.0
		C	4	28.2	41.8	50.2	60.3	94.2	96.8
9	1,734	R		32.0	47.3	56.4	65.6	93.8	95.6
		C	15	29.5	45.5	55.4	64.6	92.5	95.4
10	926	R		52.8	65.0	71.5	78.6	98.3	99.4
		C	8	49.2	63.0	70.3	77.6	97.3	99.0
11	664	R		32.0	45.6	53.9	63.5	97.8	99.5
		C	5	29.1	43.7	53.0	61.5	95.4	99.3
12	143	R		32.8	48.9	59.4	73.4	96.5	98.6
		C	-1	28.6	46.1	58.0	71.3	92.3	97.2
13	127	R		20.6	32.4	41.8	57.5	96.9	100.0
		C	0	19.0	30.0	40.2	55.2	96.1	99.2
14	162	R		45.2	60.0	68.6	76.6	98.8	100.0
		C	2	41.5	58.6	67.7	75.0	98.2	100.0
15	794	R		28.2	43.8	53.6	64.9	96.1	98.4
		C	6	25.2	41.7	52.2	63.1	94.1	97.6
16	1,075	R		26.6	36.6	43.9	57.1	95.9	98.0
		C	8	24.1	35.5	42.9	55.0	94.2	97.2
17	122	R		25.4	41.0	50.8	55.7	86.0	92.6
		C	2	23.4	40.3	50.0	55.6	82.2	91.9
18	994	R		49.0	62.6	72.5	80.7	98.7	100.0
		C	14	45.8	60.3	71.3	78.9	97.5	98.9
19	1,270	R		44.4	72.1	84.8	90.2	99.5	99.8
		C	9	39.7	68.2	82.7	88.1	97.9	99.2
20	938	R		60.8	83.0	90.8	94.6	99.8	100.0
		C	14	53.7	79.2	88.7	92.5	98.6	99.5
21	1,031	R		42.2	57.1	68.6	77.3	98.3	99.3
		C	13	39.9	55.0	67.5	75.9	97.5	98.7
22	1,964	R		27.2	42.3	54.4	66.6	96.8	98.8
		C	0	24.1	39.4	52.8	64.3	95.4	97.8
23	1,581	R		53.2	86.6	93.3	95.7	99.7	100.0
		C	6	42.7	81.4	91.1	93.9	98.4	99.4
24	924	R		55.2	66.1	74.6	82.0	99.1	99.9
		C	-2	49.9	62.8	72.5	80.0	98.0	99.2
25	368	R		75.8	92.1	96.2	98.1	100.0	100.0
		C	4	65.8	88.3	94.7	97.1	99.5	100.0
26	248	R		64.2	73.9	78.7	84.3	98.4	100.0
		C	2	59.5	70.7	77.1	81.9	96.8	98.8
27	739	R		58.4	68.5	75.7	82.6	96.9	99.1
		C	3	52.6	65.5	73.3	80.2	96.0	98.7

[1]Preanalysis total weight minus postanalysis cumulative weight. The loss is assumed to result from fine material being retained within the shaker or lost to the outside or both. Before calculation of percent-finer values, the loss is added to the weight of material finer than 1.0 mm. A negative loss indicates an addition to the sample of material previously retained within the shaker.

Table 2. Differences between percent-in-class values defined by rotap and cascade-sieve shaker analyses

Sample number	Size class (mm)						
	>11.3	11.3-8.0	8.0-5.6	5.6-4.0	4.0-2.0	2.0-1.0	<1.0
1	-0.10	-0.60	-0.40	-0.40	-0.40	-0.90	2.80
2	-.30	-1.20	.60	-.40	-.50	-.40	2.20
3	.10	-1.10	-.70	.50	-.90	-.70	2.70
4	.00	-.50	-1.50	.50	-.60	-.60	2.80
5	-.70	-1.10	-.10	.40	-.80	.00	2.30
6	-.80	-.20	-.10	-.40	-.20	.90	.70
7	-.40	-1.00	.30	.40	-.80	-1.90	3.30
8	-.20	-1.30	-.50	1.00	-.70	-1.00	2.70
9	-.20	-1.10	.30	.00	-.80	-.70	2.50
10	-.40	-.60	.00	-.20	-.80	-1.60	3.40
11	-.20	-2.20	.40	1.10	-1.00	-1.00	3.10
12	-1.40	-2.80	2.10	.70	-1.40	-1.40	4.20
13	-.80	.00	-1.50	.70	-.80	.80	1.60
14	.00	-.60	-1.00	.70	-.50	-2.30	3.60
15	-.80	-1.20	.20	.40	-.70	-.90	2.80
16	-.80	-.90	-.40	1.10	-.10	-1.40	2.30
17	-.70	-3.10	3.70	-.70	.10	-1.30	2.00
18	-1.10	-.10	-.60	.60	-1.10	-.90	3.20
19	-.60	-1.00	-.50	.00	-1.80	-.80	4.60
20	-.50	-.70	-.90	.00	-1.70	-3.30	7.10
21	-0.60	-0.20	-0.60	0.30	-1.00	-0.20	2.40
22	-1.00	-.40	-.90	.70	-1.30	-.20	3.20
24	-.70	-.40	-.90	-.10	-1.20	-2.00	5.30
26	-1.20	-.40	-.80	.80	-1.60	-1.50	4.70
27	-.40	-.50	-1.50	.00	-.60	-2.80	5.70

Statistical summary of differences

Sample size	25	25	25	25	25	25	25
Mean	-0.55	-0.93	-0.21	0.31	-0.85	-1.04	3.25
s	.39	.77	1.13	.50	.48	.98	1.39

90-percent confidence-level interval limits

Minimum	-0.69	-1.19	-0.60	0.14	-1.01	-1.38	2.77
Maximum	-.42	-.66	.17	.48	-.69	-.71	3.72

95-percent confidence-level interval limits

Minimum	-0.71	-1.25	-0.68	0.10	-1.04	-1.45	2.68
Maximum	-.39	-.61	.25	.52	-.65	-.64	3.82

$$s^2 = \Sigma(x-m)^2 / (n-1) , \quad (1)$$

where s is the standard deviation,

x is an individual difference between the percent-in-class values defined by a rotap analysis and a cascade-sieve shaker analysis,

m is the mean of all values in the sample of size n; and

$$\mu = m \pm \frac{ts}{\sqrt{n}} \quad (2)$$

where μ is mean of all possible x values (the population mean),

t is the value from the t-distribution for $n-1$ degrees of freedom and a specified confidence level.

	16.0	11.3	8.0	5.6	4.0	2.0	1.0	<1.0
SAMPLE NO: 20	DATE: 8/17/82		INIT WT: 551 g			LOSS: 3 g		
ACCUM WT (g)		348	320	313	226	191	146	90
ADJ ACC WT (g)		351	323	316	229	194	149	93
PERCENT FINER	100	92	90	65	55	42	26	
SAMPLE NO: 25	DATE: 8/18/82		INIT WT: 1202 g			LOSS: 13 g		
ACCUM WT (g)		1189	1141	1106	659	471	306	141
ADJ ACC WT (g)		1202	1154	1119	672	484	319	154
PERCENT FINER	100	96	93	56	40	27	13	
SAMPLE NO: 30	DATE: 8/19/82		INIT WT: 367 g			LOSS: -7 g		
ACCUM WT (g)		374	334	327	236	196	160	105
ADJ ACC WT (g)		367	327	320	229	189	153	98
PERCENT FINER	100	89	87	62	51	42	27	
SAMPLE NO: 35	DATE: 8/20/82		INIT WT: 164 g			LOSS: 2 g		
ACCUM WT (g)		162	162	159	122	109	94	66
ADJ ACC WT (g)		164	164	161	124	111	96	68
PERCENT FINER	100	100	98	76	68	59	41	
SAMPLE NO: 40	DATE: 8/20/82		INIT WT: 2721 g			LOSS: 20 g		
ACCUM WT (g)		2701	2565	2512	1710	1336	962	454
ADJ ACC WT (g)		2721	2585	2532	1730	1356	982	474
PERCENT FINER	100	95	93	64	50	36	17	

Figure 5. Example of computer printout of cascade-sieve shaker analysis results.

The statistical analysis shows that for all size classes, except the finer-than-1.0-mm class, percent-in-class values defined by cascade-sieve shaker analysis can be expected to be within about 1 percentage point of values defined by rotap analysis.

Samples 23 and 25 were not included in the statistical computations because of excessively large percent-in-class differences (values) in the size classes of 1.0 to 2.0 mm and less than 1.0 mm. These two samples had the largest proportions of material less than 2.0 mm of all test samples. The data in figure 6 illustrate that differences in percent-in-class values defined by rotap and cascade-sieve shaker analyses are more or less constant for samples in which the percentage of material less than 2.0 mm is no greater than 60 percent; however, the differences increase markedly where more than 60 percent of the sample is finer than 2.0 mm. For this reason, the accuracies indicated in table 2 are applicable only to samples for which about 60 percent or less of the sample is finer than 2.0 mm.

Differences between the percent-finer values defined by rotap analysis and cascade-sieve shaker analysis are presented in table 3. Data in the table are based on the same sample analyses shown in table 2. Percent-finer values at different sizes are obtained by summation of percent-in-class values for the intervening classes. Inasmuch as most of the percent-in-class values defined by cascade-sieve shaker analysis, except those for classes 4.0 to 5.6 mm and less than 1.0 mm, are larger than comparable rotap-analysis values, the differences in percent-finer values in table 3 generally increase as the particle size decreases. Statistics given at the bottom of the table, which we derived by using equations 1 and 2,
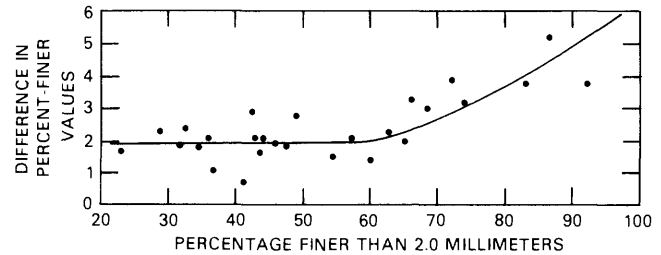
Figure 6. Difference in values of percent finer than 2.0 mm defined by the rotap and cascade-sieve shaker methods as a function of the percentage of material finer than 2.0 mm.

show the mean difference in percent-finer values by size, standard deviations of the differences, and the intervals within which the true mean differences can be expected to be for confidence levels of 90 and 95 percent. The statistics show that, on the average, we can adjust percent-finer values defined by cascade-sieve shaker analyses to correspond to comparable rotap-analysis values by applying the following percentage factors:

Size (mm)	11.3	8.0	5.6	4.0	2.0	1.0
Adjustment factor	+1	+1	+2	+2	+2	+3

Because of the relative sensitivity of percent-finer values, these adjustment factors may not be applicable for samples having gradations substantially different from the test samples, and they would not be applicable for any samples in which more than about 60 percent of the material is finer than 2.0 mm.

SUMMARY AND CONCLUSIONS

The cascade-sieve shaker method of particle-size analysis significantly reduces the time and effort required to size coarse bedload and bed-material samples. Manual operations associated with the method, in addition to drying the sample, consist of (1) obtaining a preanalysis total sample weight by means of electronic balance, (2) depositing the sample into the feed pan and turning on the shaker, (3) removing the size-fraction collection containers from their support trays, and (4) pouring the contents of the collection containers progressively, by size ranges, into a single container situated on the electronic balance. All other operations are automatic. Required sieving times depend primarily on the sand (material finer than 2.0 mm) content of the samples; sieving time increases as the proportion of sand increases. For samples containing about 30 to 50 percent sand, a complete analysis including sieving, weighing, and computing can be finished in 5 to 6 minutes. Samples that have less sand content can be analyzed more quickly, but 10 to 12 minutes sieving time is required for samples containing 90 percent sand.

Table 3. Differences between percent-finer values defined by rotap and cascade-sieve shaker analyses

Sample number	Particle size (mm)					
	11.3	8.0	5.6	4.0	2.0	1.0
1	0.10	0.70	1.10	1.50	1.90	2.80
2	.30	1.50	.90	1.30	1.80	2.20
3	-.10	1.00	1.70	1.20	2.10	2.80
4	.00	.50	2.00	1.50	2.10	2.70
5	.70	1.80	1.90	1.50	2.30	2.30
6	.80	1.00	1.10	1.50	1.70	.80
7	.40	1.40	1.10	.70	1.50	3.40
8	.20	1.50	2.00	1.00	1.70	2.70
9	.20	1.30	1.00	1.00	1.80	2.50
10	.40	1.00	1.00	1.20	2.00	3.60
11	.20	2.40	2.00	.90	1.90	2.90
12	1.40	4.20	2.10	1.40	2.80	4.20
13	.80	.80	2.30	1.60	2.40	1.60
14	.00	.60	1.60	.90	1.40	3.70
15	.80	2.00	1.80	1.40	2.10	3.00
16	.80	1.70	2.10	1.00	1.10	2.50
17	.70	3.80	.10	.80	.70	2.00
18	1.10	1.20	1.80	1.20	2.30	3.20
19	.60	1.60	2.10	2.10	3.90	4.70
20	.50	1.20	2.10	2.10	3.80	7.10
21	0.60	0.80	1.40	1.10	2.10	2.30
22	1.00	1.40	2.30	1.60	2.90	3.10
24	.70	1.10	2.00	2.10	3.30	5.30
26	1.20	1.60	2.40	1.60	3.20	4.70
27	.40	.90	2.40	2.40	3.00	5.80

Statistical summary of differences

	11.3	8.0	5.6	4.0	2.0	1.0
Sample size	25	25	25	25	25	25
Mean	0.55	1.48	1.69	1.38	2.23	3.28
	.39	.88	.58	.44	.79	1.39

90-percent confidence-level interval limits

	11.3	8.0	5.6	4.0	2.0	1.0
Minimum	0.42	1.18	1.49	1.23	1.96	2.80
Maximum.....	.69	1.78	1.89	1.54	2.50	3.75

95-percent confidence-level interval limits

	11.3	8.0	5.6	4.0	2.0	1.0
Minimum	0.39	1.12	1.45	1.20	1.91	2.70
Maximum.....	.71	1.84	1.93	1.57	2.56	3.85

Comparisons of particle-size distributions defined by the standard rotap method and the cascade-sieve shaker method show that size separations by means of the cascade-sieve shaker method are very slightly less accurate than those by the rotap method. For samples containing less than about 60 percent sand, values of the percentage of material finer than 2.0 mm differ from those for rotap analysis by an average of 2 percentage points. Average differences in percent-in-class values for all size classes except less than 1.0 mm, are within 1 percentage point for samples that have sand content of 60 percent or less. Differences of this magnitude are within the range of accuracy of rotap analyses; hence, the existence of real differences can be questioned. However, because virtually all percent-in-class differences in any given size class are in the same direction, it appears that small differences do exist. Although cumulative particle-size distributions (percent-finer distributions) by

the rotap and cascade-sieve shaker methods also differ only slightly, average adjustment factors can be applied to the percent-finer values from cascade-sieve shaker analyses to achieve parity.

Use of the existing prototype cascade-sieve shaker increases sieving times and decreases accuracy in analyses of samples that contain more than about 80 percent material finer than 2.0 mm or 60 percent finer than 1.0 mm; for this reason, its use is not recommended for analyzing such samples.

The cascade-sieve shaker must be developed further before the full benefits of the method can be realized.

REFERENCES CITED

Guy, H.P., 1969, Laboratory theory and methods for sediment analysis: U.S. Geological Survey Techniques of Water-Resources Investigations, Book 5, Chapter C1, 58 p.

Inter-Agency Committee on Water Resources, 1957a, Report No. 12, Some fundamentals of particle size analysis, in A study of methods used in measurement and analysis of sediment loads in streams: Minneapolis, Minnesota, St. Anthony Falls Hydraulic Laboratory, 55 p.

———1957b, Report No. 11, The development and calibration of the visual-accumulation tube, in A study of methods used in measurement and analysis of sediment loads in streams: Minneapolis, Minnesota, St. Anthony Falls Hydraulic Laboratory, 109 p.

The Stability of Rhodamine WT Dye in Trial Studies of Solute Transport in an Acidic and Metal-Rich Stream

By Kenneth E. Bencala, Diana M. McKnight, Gary W. Zellweger, *and* Julie Goad

Abstract

Rhodamine WT and sodium chloride were concurrently injected for a period of 24 hours into the naturally acidic water of the Snake River (Montezuma, Colo.). The experimental reach included the confluence with the pristine water of Deer Creek. The experiment was a trial study of field techniques and solute-transport characteristics of the stream. Spatial variations in the concentrations of chloride, sodium, sulfate, and fluoride were observed. The variations are slight; however, they are qualitative indicators of inflow and (or) reactivity in this metal-rich stream.

Water samples collected for rhodamine WT determination were stored for several days before analysis. A decrease in fluorescence associated with the water chemistry occurred in the samples obtained in the Snake River above the confluence with Deer Creek. This observation is based on comparisons between samples obtained above and below the confluence and supported by comparisons with the assumed conservative tracer chloride. The transport experiment was followed by subsequent batch experiments conducted in bulk water samples from the stream. Results obtained in batch experiments support the conclusions of the solute-transport experiment. The apparent stability of the rhodamine WT was time dependent and related to the location of the source of the bulk water from the stream and to whether or not the dye was added immediately after collection of the bulk water.

INTRODUCTION

The concentrations of metal contaminants and micronutrients in streams are determined by complex interactions of physical, chemical, and biotic processes. One approach to understanding and quantifying these processes and their interactions has been to perform reactive-metal-transport experiments in natural streams. Recent uses of this approach include studies of aluminum, copper, zinc, and iron by Chapman (1982), copper by Kuwabara and others (1984), and lead by Kennedy and others (1984/1985). In these studies, chloride or sodium was used as the assumed conservative tracer for the evaluation of basic transport properties. Spatial variations, both natural and experimental, in solute concentrations indicate inflow and (or) reactivity. Where inflows are highly contaminated but small and ill-defined, direct measurements of either inflow rates or solute concentrations may be difficult to obtain. As recently demonstrated by Chapman and others (1983), in-stream chemical data can be used to identify sources of inflow and extent of reactivity. The reliability of information on the extent of solute tracer reactions is crucial to such investigations.

Metal chemistry and therefore transport are sensitive to the acidity of the stream. Effective tracers for use in reactive-metal-transport experiments must be relatively insensitive to variations in the acidity and metal chemistry that occur naturally within the stream reach or during the experiment. Knowledge of the time-dependent properties of tracers at field conditions is also required. Bencala and others (1983) compared rhodamine WT and chloride in a 15-hour reactive-transport experiment. A subsequent laboratory study showed a time-dependent sorption of dye onto sediment as the probable mechanism for attentuation of the rhodamine WT concentration in the field experiment. The stability of a tracer over periods of several days to weeks, even months, can be significant in transport studies for two reasons. First, in extreme situations, solute residence times within the hydrologic system may reach several days (for an example, see Kennedy and others, 1984/1985). Second, our experience has shown that complex reactive-transport experiments entail the collection of hundreds to thousands of water samples, each of which may be analyzed later for numerous chemical constituents. A knowledge of the stability of the experimental tracers over the time period required for the entire chemical analyses is desirable.

Smart and Laidlaw (1977) presented an extensive evaluation of eight fluorescent dyes "to assess their utility in quantitative tracing work." They recommended rhodamine WT as a dye appropriate for water tracing. One factor influencing the fluorescence of rhodamine WT was the presence of acid in the dye solution. They

performed laboratory studies using three acids (HCL, HNO₃, and H₂SO₄) and a phosphate buffer. Their work demonstrated that the lowering of dye fluorescence accompanied decreased pH. Each acid lowered the dye fluorescence to a different degree. Thus, they suggested that, where natural water is acidic, the fluorescence of rhodamine WT should be determined in the natural water samples. Smart and Laidlaw (1977) did not assess the influence of metal concentrations on the fluorescence of rhodamine WT. There is a possibility that reactive metals such as copper would interact with the fluorophores in rhodamine WT to quench fluorescence, as has been observed for naturally occurring dissolved organic material (Saar and Weber, 1980). High concentrations of metals such as iron, aluminum, and manganese are generally associated with acid conditions in streams.

Purpose of Study

The solute-transport experiment was a trial run for the evaluation of experimental techniques and logistics. In this study, we report results concerning solute-transport experiments in acidic and metal-rich streams. Physical and chemical data are presented to define the transport environment. Chemical data from the experiment include summaries of the variations of solute concentrations within the Snake River. These sets of data provide the background information for our discussion of the stability of rhodamine WT in naturally acidic stream water. The chloride analyses presented in this paper were provided by R. J. Avanzino (U.S. Geological Survey, Menlo Park, Calif.).

Location of Study Area

The experiments encompassed the acidic waters of a small mountain stream, the Snake River, near Montezuma, Colo. A sketch of the experimental reach is shown in figure 1. Near its headwaters, the Snake River is joined by a second stream of approximately equal flow, Deer Creek. Deer Creek is a pristine, typical Rocky Mountain stream. In contrast, the Snake River is characterized by high metal concentrations and low pH. Because of the inflow from Deer Creek, the water chemistry of the Snake River is markedly different above and below the confluence. Concentrations of aluminum and iron and pH in the Snake River above and below the confluence are shown in figure 2. At both sites, the iron, which may interact with the dye, is generally present as ferrous iron (McKnight, unpublished data, 1983). In Deer Creek, the pH was 6.6, and the metal concentrations very low compared with those in the Snake River. Geochemical and ecological characteristics of the site

have been studied by Theobald and others (1963) and McKnight and Feder (1984). Detailed sketches of the site are also contained in those reports. The stream was also included in a survey by Moran and Wentz (1974) of the effects of metal-mine drainage on water quality.

In early August 1982, the discharge in the Snake River, as estimated by means of chloride dilution, was 0.34 m³/s above the confluence and 0.68 m³/s below. Sketches of three cross sections, in Deer Creek and
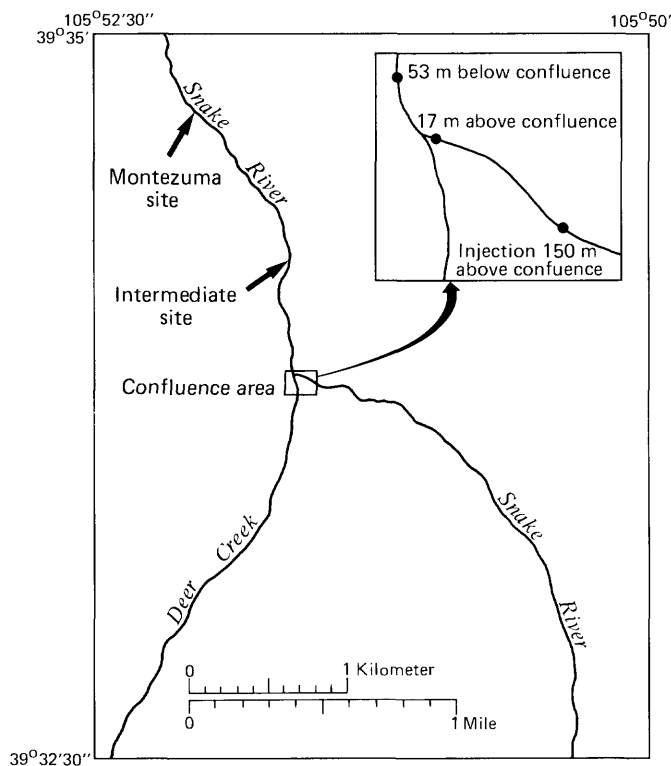
Figure 1. Experimental reach of the Snake River (Montezuma, Colo.) near the confluence with Deer Creek. Injection and monitoring stations are noted.
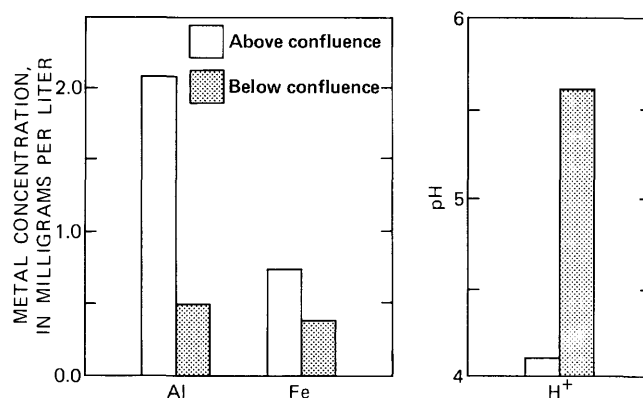
Figure 2. Concentrations of aluminum and iron and pH in the Snake River during early August 1982. Open bars represent samples taken above the confluence with Deer Creek. Shaded bars represent samples taken below the confluence with Deer Creek.

above and below the confluence in the Snake River, are shown in figure 3. The various reaches of this stream system are about 2 to 4 m in width and 0.2 to 0.5 m in depth.

In the transport experiment, incomplete lateral mixing of Deer Creek and Snake River waters could have led to misleading results for the samples obtained below the confluence. In October 1983, water samples were obtained in Deer Creek, in the upstream reach of the Snake River, and across four transects of the Snake River. The first transect was within the area where the two streams join. The next three transects were above, at, and below the regular downstream sampling site used in the August 1982 transport experiment. In figure 4, profiles are shown for sodium, sulfate, and silica concentrations, and pH. Within the confluence, the gradients in chemical composition are clear. The transects from the three downstream sites all indicate that mixing is virtually complete over the distance to the 1982 sampling site. This conclusion is consistent with transverse pH measurements in October 1957 by Theobald and others (1963). In October 1963, the flow was not necessarily identical with the flow in August 1982; however, both sampling days occurred during the low-flow regime. The data from these transects support the results of the transport study.

METHOD OF STUDY

Transport Experiment

In the transport experiment, an aqueous solution of sodium chloride and rhodamine WT was continuously injected into the Snake River 150 m above the Deer Creek confluence for 24 hours, starting at 1245 hours on August 3, 1982. Below the injection point, water samples were taken from the Snake River at sampling locations above and below confluence (fig. 1). In addition to the monitoring location directly below the confluence, water samples were obtained from two sites farther downstream in the Snake River. In figure 1 these are labeled as the Intermediate and Montezuma sites. Most samples were taken manually and stored immediately. Some samples from the Montezuma site were collected overnight automatically and retrieved the following day. Concentration differences between manual and automatic samples were judged insignificant. Water samples for anion and cation determinations were filtered through 0.45 μm filter membranes and stored in polyethylene bottles. Water samples for dye determinations were stored directly in glass bottles.

Rhodamine WT concentrations were measured within 2 weeks of the experiment. Those samples to be anlayzed for rhodamine WT were divided into two groups—samples obtained above the confluence and
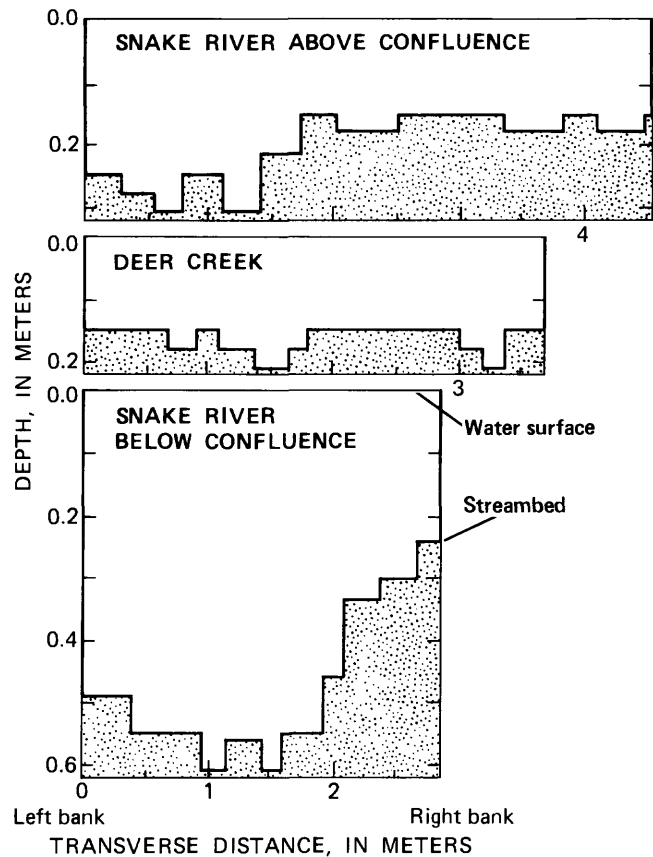
Figure 3. Cross sections of the streams in the experimental area.

samples obtained below. Following procedures suggested by Smart and Laidlaw (1977), we prepared (1) a set of dye-calibration standards with Snake River water obtained above the confluence, which was used in the analysis of the samples from above the confluence; and (2) a set with water below the confluence, which was used in analysis of samples from below the confluence.

Complete time series of normalized rhodamine WT concentrations are illustrated in figures 5A and 5B. A concentration decrease of roughly 30 percent occurred about one-half hour after the start of the injection. This was the result of the temporary failure of one of the three injection pumps. We normalized data by dividing measured concentrations (minus background) by concentrations at the "plateau" (minus background). The "plateau" concentrations used in this normalization were the averages of concentrations from below the confluence over a plateau period midway through the experiment from 1800 hours August 3 through 0900 hours August 4.

For reference, concentrations of four solutes were determined in addition to the concentrations of rhodamine WT. These data help to define the solute-transport environment of the rhodamine WT experiment. The
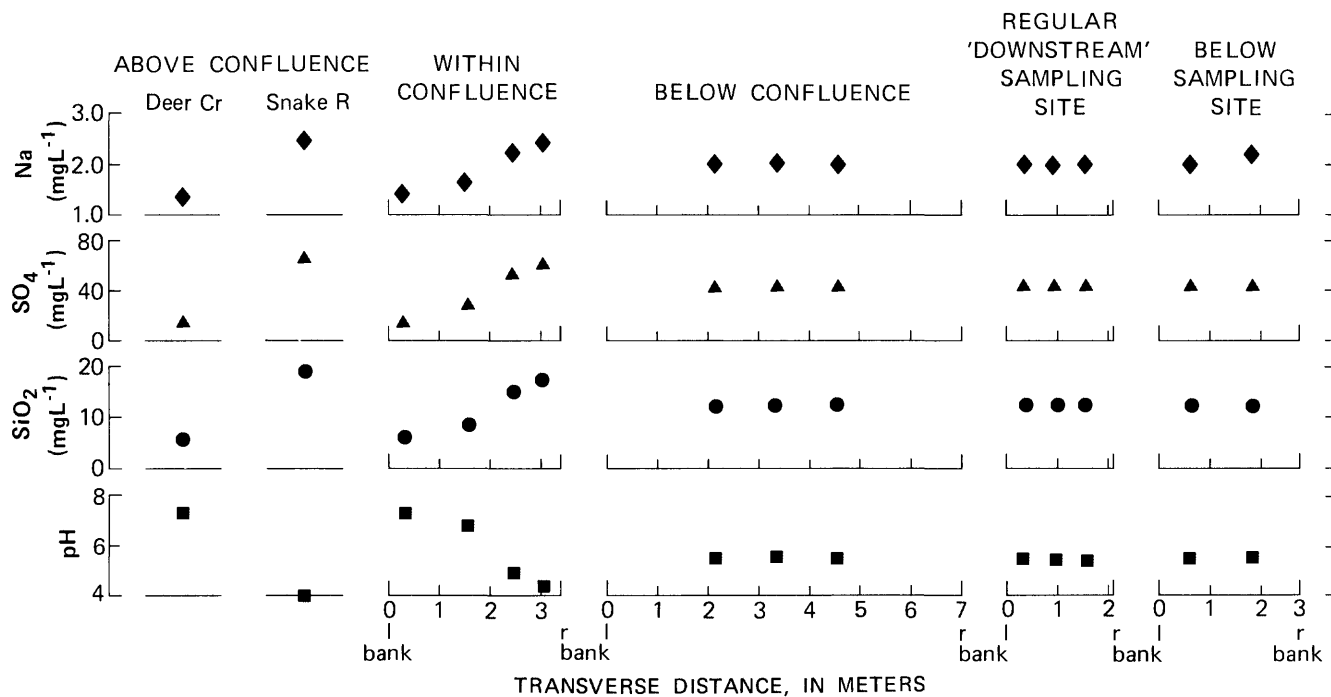
Figure 4. Transects of pH and sodium, sulfate, and silica concentrations at sampling sites of Snake River and Deer Creek.
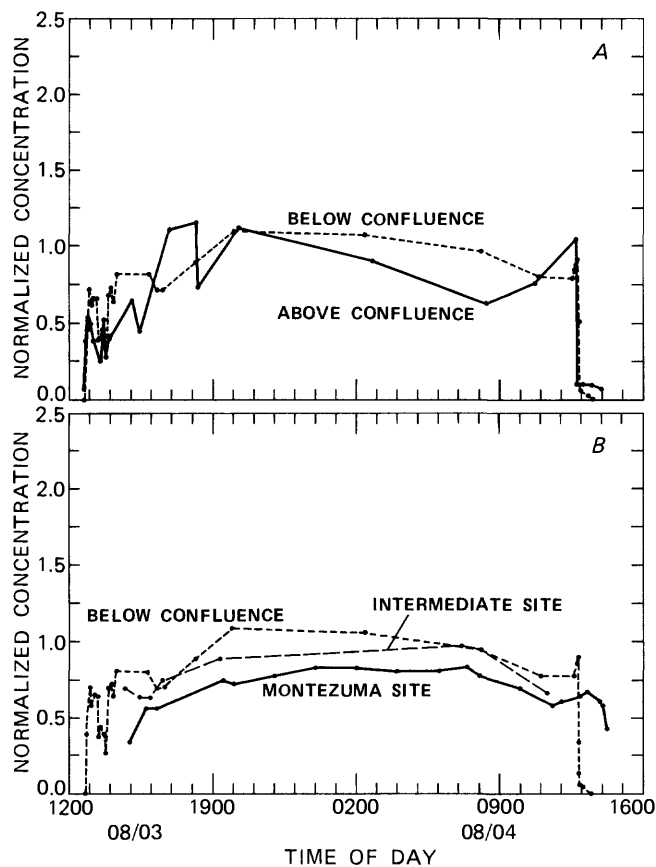

Figure 5. Rhodamine WT concentrations for injection into the Snake River. A, Concentrations above and below the confluence. B, Concentrations at three stations below the confluence.

normalized chloride concentrations above and below the confluence are compared in figure 6A. The concentrations above the confluence are consistently higher, by about a factor of 2, than those below the confluence. The time series in the downstream reach are represented in figure 6B. The values at the Montezuma site are consistently lower than values at the site below the confluence. With only a few exceptions, the values at the Intermediate site fall between those at the other two sites. The data presented in figure 6B provide an experimental indication of a declining chloride concentration along the Snake River below the confluence. Chloride is generally considered to be one of the least reactive solutes in natural systems (Feth, 1981). Thus, the decline in concentration along the downstream direction is presumably caused by inflows from seeps along the streambanks.

The concentration data for sodium, sulfate, and fluoride also provide indications of inflow and (or) reactivity along the downstream direction. From the August 1982 transport experiment, median concentrations of chloride, sodium, sulfate, and fluoride at six sampling sites are presented in figures 7A-D respectively. Four chloride and sodium plateau levels are shown along with the corresponding background levels observed before and after the passage of the injected pulse. Four sulfate and fluoride natural background levels are shown. Median concentrations are presented as summaries of the entire data sets. The median experimental plateau concentrations for chloride (fig. 7A) indicate the trend described above for the complete time series (fig.
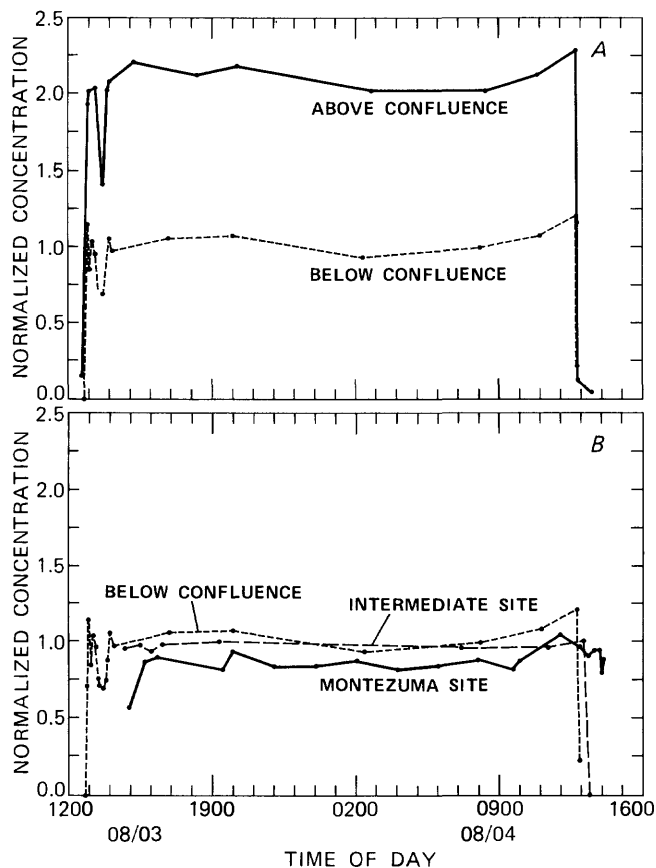
Figure 6. Chloride concentrations for injection into the Snake River. Injections started at 1245 hours August 3, 1982, and ended at 1245 hours the following day. *A*, Concentrations above and below the confluence. *B*, Concentrations at three stations below the confluence.

6*B*). The median experimental plateau concentrations for sodium (fig. 7*B*) increase along the downstream reach of the Snake River. The increase is slight but is also present in the median background concentrations. These trends support the conclusion drawn from the chloride data that there are solute inflows from seeps along the streambank. Apparently, the seeps would need to carry sodium at a concentration higher than the median level in the stream. The median sulfate (fig. 7*C*) and fluoride (fig. 7*D*) levels vary spatially in both the sets of samples taken above and below the confluence. Potentially, both inflows and in-stream reactivity could be the cause of these variations.

The chloride, sodium, sulfate, and fluoride data presented from this trial study of solute transport provide only an indication of the spatial variability of solute concentrations in the Snake River. The summarized
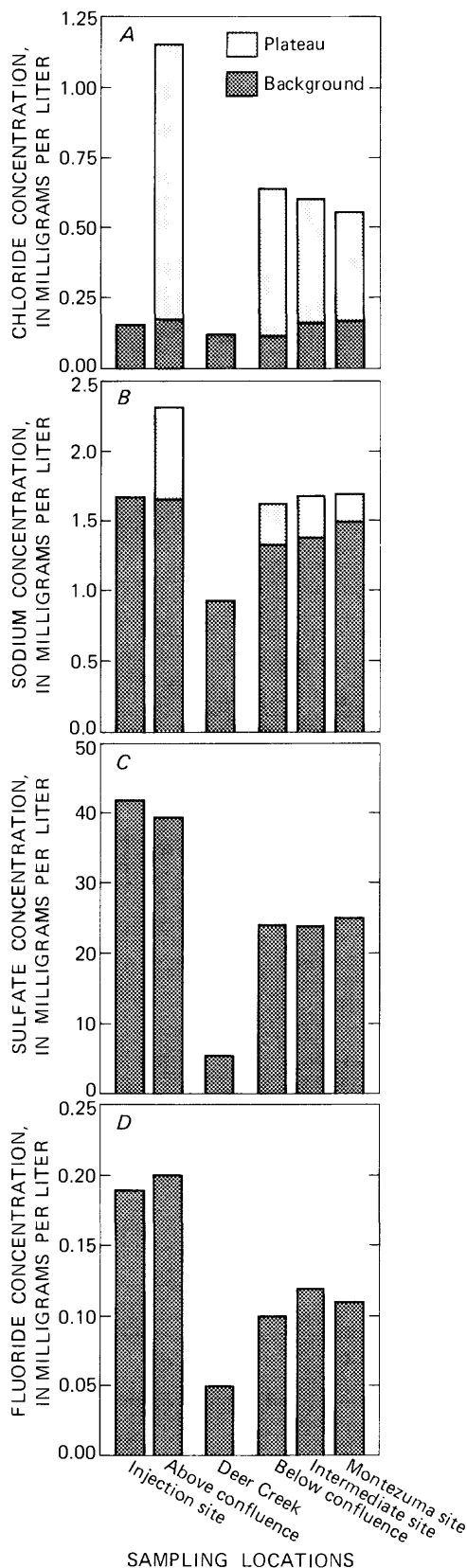
Figure 7. Median solute concentrations in Deer Creek and → along the Snake River. Background and experimental plateau levels are illustrated for chloride and sodium. *A*, chloride; *B*, sodium; *C*, sulfate; and *D*, fluoride.

SAMPLING LOCATIONS

results presented here indicate (1) the probable presence of seeps of sufficient extent to influence solute concentration and (2) the possibility of in-stream reactivity. The concentration of rhodamine WT will clearly be attenuated by inflows. In-stream reactivity of other solutes (specifically trace metals) may further influence the fluorescent properties of rhodamine WT.

Batch Experiment

In January 1984, water samples were collected from the Snake River, above and below the confluence with Deer Creek. The pH of the Snake River water was 3.8 and 5.3, above and below the confluence, respectively. Five samples from each site were immediately spiked with known amounts of rhodamine WT. Additional bulk samples of stream water were also obtained. A delayed addition of known amounts of rhodamine WT was made 9 days later to this stored bulk water. Determinations of apparent recovery were subsequently made over a period of several months. The results are presented as time series in figure 8. The recoveries were computed relative to a set of five standards prepared with distilled water.

DYE STABILITY

The time series (fig. 5A and B) of rhodamine WT concentrations are noisy and there appear to be three somewhat distinct periods of plateau concentrations (as will be shown in the figures to follow). Thus, we have averaged the normalized concentrations over initial-, mid-, and final-plateau periods. The normalization is computed in the same manner as described previously; that is, the normalization is with reference to back-

ground concentrations and the average midplateau concentrations at the site below the confluence with Deer Creek. Thus, the normalized midplateau concentrations at the site below the confluence are equal to one for both chloride and rhodamine WT. The normalized plateau concentrations are shown in figure 9.
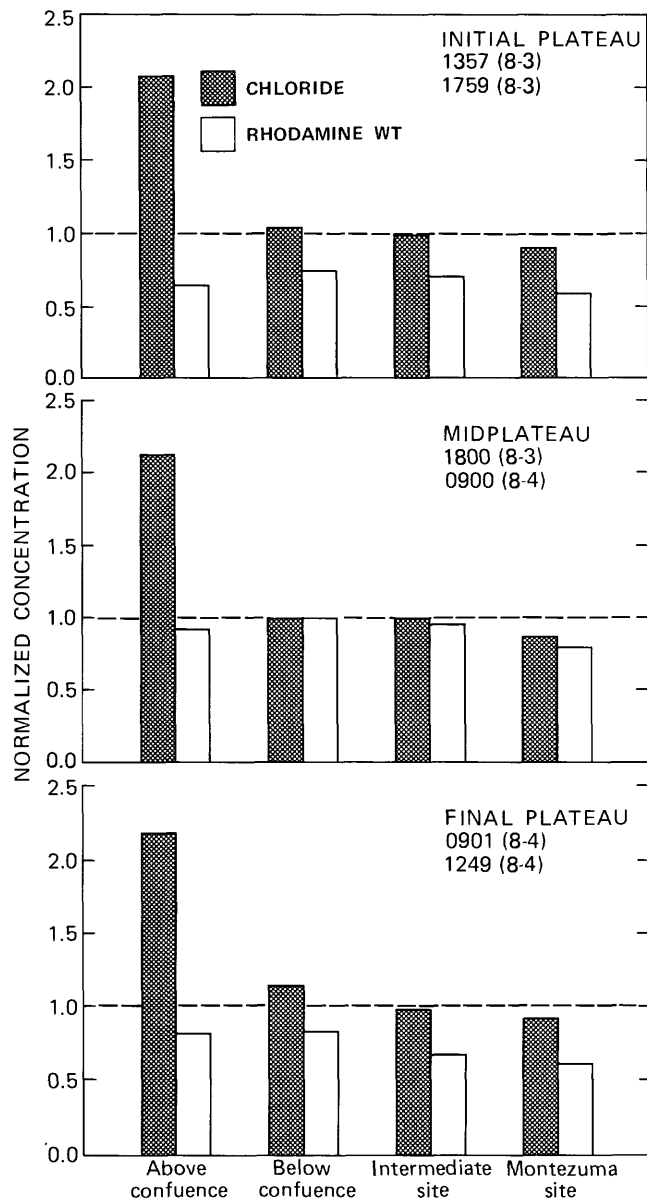
Figure 9. Normalized concentration of chloride and rhodamine WT during plateau periods. Open bars represent average rhodamine WT concentrations. Shaded bars represent average chloride concentrations. Immediately below the confluence, the surmised periods are as follows: initial plateau period, from 1357 hours to 1759 hours August 3; midplateau period, from 1800 hours August 3 to 0900 August 4; final plateau period from 0901 hours to 1249 hours August 4. To allow for time of travel, subtract 1 minute from these times for the site above confluence, add 30 minutes for the intermediate site, and add 75 minutes for the Montezuma site.

Figure 8. Recovery of rhodamine WT after addition to bulk water samples from the Snake River. Four sets of additions were completed. Immediate and delayed additions of rhodamine WT were made to samples from above and below the confluence.

In the samples obtained above the confluence, the dye apparently was not stable. All three plateau periods represented in figure 9 illustrate similar trends. On a normalized scale, the chloride concentration above the confluence was approximately double the chloride concentration below the confluence. The higher concentration upstream is as expected given the relatively "clean" water inflow of Deer Creek in the confluence. The rhodamine WT responded in a markedly different manner. On the normalized scale, the apparent rhodamine WT concentration above the confluence was approximately equal to the apparent rhodamine WT concentration below the confluence. Figure 9 shows comparisons of rhodamine WT and chloride at the Intermediate and Montezuma sites. The pattern of downstream attenuation observed in the chloride data is also present in the dye data.

Taken by itself, the rhodamine WT data suggest that the dye was not stable in the upstream acidic water over the period of time from the experiment to the dye analysis. The upstream water cannot be diluted by the Deer Creek inflow and still retain its concentration level below the confluence. In comparison with the chloride data, the upstream rhodamine WT samples were attenuated by approximately 50 percent. The laboratory experiments of Smart and Laidlaw (1977) suggested that the acidity of the solution influences the fluorescent properties of the dye. Those earlier experiments did not consider the possible influence of sample acidity on apparent dye stability in samples analyzed against calibration standards prepared in natural water samples.

A limited set of real-time-fluorescence data were also obtained at the sites above and below the confluence. These data are presented in figure 10. The direct meter readings from the fluorometer were normalized for comparison with all other data. The overall response
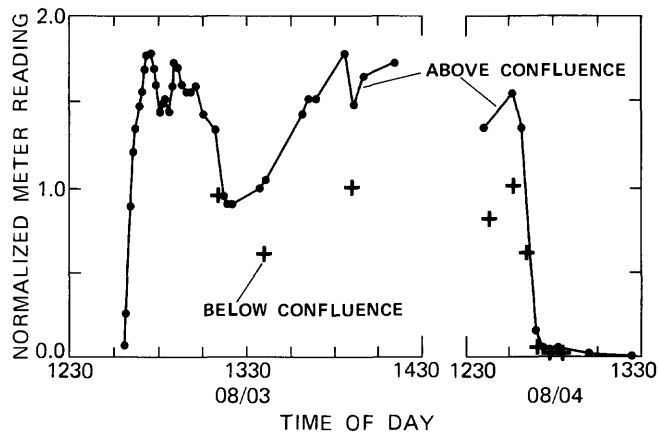
is consistent with the appearance of the chloride response. At the time of the experiment, the fluorescence in the stream above the confluence was approximately 1 1/2 times greater than the fluorescence below the confluence. On the basis of the chloride data, the actual dye concentrations above and below the confluence would have differed by a factor of 2. As expected from the work of Smart and Laidlaw (1977), an immediate decrease in dye fluorescence occurred in the more acidic upstream water.

Results of the batch experiments are summarized in figure 11. (Refer to fig. 6 for the detailed time series.) Apparent dye recovery in the Snake River samples was determined relative to the distilled water standards. From the batch experiments, the summary in three trends is shown in figure 11.

First, recovery is lower in the samples from above the confluence. In figure 11, the open bars are lower than the corresponding shaded bars. The difference in recovery between samples taken above and below confluence is not stable over relatively long periods of storage. Second, recovery was typically lower in the samples to which dye was added immediately. In figure 11A, bars representing samples from above the confluence are lower than bars in figure 11B. The difference in recovery between immediate and delayed addition is not stable over relatively long periods of storage. Finally, there is
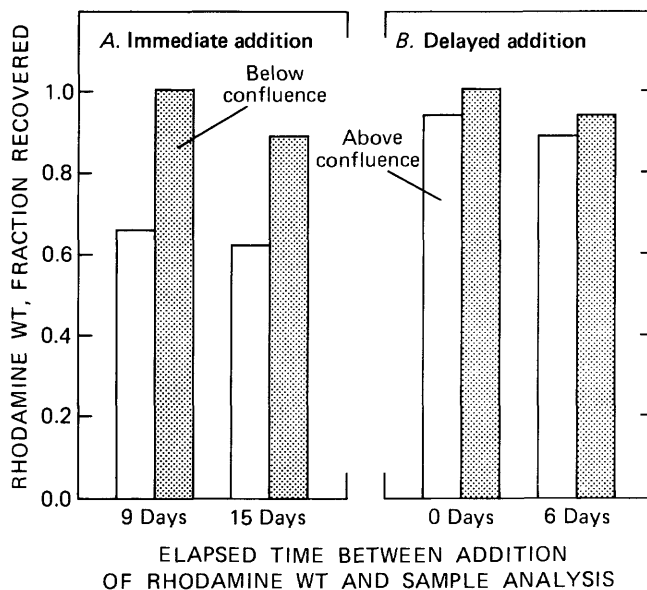
Figure 11. Recovery of dye in bulk samples of Snake River water. Open bars represent samples taken above the confluence. Shaded bars represent samples taken below the confluence. A, Rhodamine WT immediately added to bulk stream water samples. Nine and fifteen days later, dye concentrations were determined relative to distilled water standards. B, Rhodamine WT added to bulk stream water 9 days after collection of water. On the day of the addition and 6 days later, dye concentrations were determined relative to distilled water standards.

Figure 10. Normalized meter readings of fluorescence. The readings were obtained in real-time above and below the confluence. The normalization is with respect to the maximum value read below the confluence on each day.

an overall trend for the apparent concentration of the dye to decay. Within each of figures 11*A* and 11*B*, the bars for the second analysis are lower than those for the first analysis. On the basis of the results of Smart and Laidlaw (1977) this water was expected to have a lower recovery. However, the decrease in recovery observed in this stream experiment is greater (50 percent) than would have been predicted from data based on differences in pH. This suggests that differences in other chemical constituents, such as iron, may also contribute to the lower recovery at the upstream site. The apparent recovery was also influenced by the timing of the dye addition to the stream water. Recovery in the samples from above the confluence is clearly lower in those samples to which dye was added immediately after collection of the water. Changes in the metal chemistry with time, such as oxidation or precipitation of iron, are possible explanations for these results. Finally, there was an apparent time-dependent decay in the dye recovery. In the bar graphs (fig. 11), each of the second set of bars represents recovery determined 6 days after the first set. The decay over this period was nominally 5 percent. The findings of these batch experiments illustrate trends in dye stability in acidic water consistent with those of the field experiment.

SUMMARY

An apparent chemical attentuation of rhodamine WT was found in the samples obtained above the confluence of Deer Creek and Snake River. The observations are based on comparisons between samples from different locations in the stream and comparisons with the assumed conservative tracer chloride. Normalized chloride concentrations above the confluence were approximately double the concentrations below the confluence. Normalized rhodamine WT concentrations above the confluence were approximately equal to the concentrations below the confluence, and thus were attenuated by a factor of one-half.

The concentrations of rhodamine WT below the confluence area were generally consistent with those of the other solutes. The indications of spatial variability of solute concentration determined from this trial study are slight. However, the implications for further solute-transport studies in the Snake River system are clear. The metals iron and aluminum are present in the Snake River system in concentrations on the order of a mg/L (Theobald and others, 1963, McKnight and Feder, 1984). Seeps that are small in their volumetric contribution to flow could contain levels of trace metals large enough to influence in-stream concentrations. An understanding of this hydrologic influence from the in-stream reactivity of these metals will be necessary for further analysis of solute transport in this system. The reaction

mechanisms for rhodamine WT in this acidic environment are not well understood. Thus, discrimination of physical versus chemical processes would be difficult to evaluate with transport experiments based on rhodamine WT.

Results obtained in batch experiments support the conclusions of the solute-transport experiment. The apparent stability of the rhodamine WT was time dependent and related to the location of the source of the bulk water from the stream and to whether or not the dye was added immediately upon collection of the bulk water. These results support conclusions from the transport experiment.

Rhodamine WT was injected because the high sensitivity of field-portable fluorometers makes fluorescent dyes leading candidates for water tracing. The laboratory studies of Smart and Laidlaw (1977) showed that various acids have different effects on the fluorescence of rhodamine WT. Other chemical constituents of stream water may also influence fluorescence. The results presented in this study supplement those earlier results by showing (1) that differences in stream chemistry within an experimental stream reach in a field transport experiment result in major (50 percent) changes in fluorescence, which, in turn, limit the utility of rhodamine WT data for solute-transport calculations, and (2) that the fluorescence of rhodamine WT continues to decrease with time in naturally acidic stream water.

REFERENCES CITED

Bencala, K.E., Rathbun, R.E., Jackman, A.P., Kennedy, V.C., Zellweger, G.W., and Avanzino, R.J., 1983, Rhodamine WT dye losses in a mountain stream environment: Water Resources Bulletin, v. 19, no. 6, p. 943-950.

Chapman, B.M., 1982, Numerical simulation of the transport and speciation of nonconservative chemical reactants in rivers: Water Resources Research, v. 18, no. 1, p. 155-167..

Chapman, B.M., Jones, D.R., and Jung, R.F., 1983, Processes controlling metal ion attenuation in acid mine drainage: Geochimica et Cosmochimica Acta, v. 47, p. 1957-1973.

Feth, J.H., 1981, Chloride in natural continental water—a review: U.S. Geological Survey Water-Supply Paper 2176, 30 p.

Kennedy, V.C., Jackman, A.P., Zand, S.M., Zellweger, G.W., and Avanzino, R.J., 1984/1985, Transport and concentration controls for chlorine, strontium, potassium, and lead in Uvas Creek, a small cobble-bed stream in Santa Clara County, California, Part 1, Conceptual model: Journal of Hydrology, v. 75, p. 67-110.

Kuwabara, J.S., Leland, H.V., and Bencala, K.E., 1984, Copper transport along a Sierra Nevada stream: Journal of Environmental Engineering, v. 110, no. 3, p. 646-655.

McKnight, D.M., and Feder, G.L., 1984, The ecological effect of acid conditions and precipitation of hydrous metal oxides in a Rocky Mountain stream in Colorado: Hydrobiologia, v. 119, no. 2, p. 129-138.

Moran, R.E., and Wentz, D.E., 1974, Effects of metal-mine drainage on water quality in selected areas of Colorado, 1972-73: Colorado Water Conservation Board, Colorado Water Resources Circular 25, 250 p.

Saar, R.A., and Weber, J.H., 1980, Comparison of spectrofluorometry and ion-selective electrode potentiometry for determination of complexes between fulvic acid and heavy-metal ions: Analytical Chemistry, v. 52, no. 13, p. 2095-2100.

Smart, P.L., and Laidlaw, I.M.S., 1977, An evaluation of some fluorescent dyes for water tracing: Water Resources Research, v. 13, no. 1, p. 15-33.

Theobald, P.K., Lakin, H.W., and Hawkins, D.B., 1963, The precipitation of aluminum, iron, and manganese, at the junction of Deer Creek with the Snake River in Summit County, Colorado: Geochimica et Cosmochimica Acta, v. 27, no. 2, p. 121-132.

Susceptibility to Mudflows in the Vicinity of Lassen Peak, California

By Donna C. Marron *and* Julie A. Laudon

Abstract

Mudflow deposits emplaced during eruptions of Lassen Peak in 1915 and those that predate the 1915 eruptions indicate that stream valleys in the vicinity of Lassen Peak, northeastern California, are susceptible to mudflows. Mudflows related to eruptions in 1915 traveled approximately 20 kilometers down Lost Creek, approximately 7 kilometers down Hat Creek, and less than 3 kilometers down Manzanita Creek. A different sequence of eruptive events in 1915 could have generated larger mudflows. Pre-1915 mudflow deposits possibly related to the extrusion of Lassen Peak are exposed in the headwaters of Manzanita Creek. The summit morphology and fracture patterns before and during the 1914-15 eruptions indicate that stream valleys that drain Lassen Peak to the northwest and southeast are most likely to be affected by eruption-related mudflows should future eruptions of Lassen Peak occur. Damage reports and existing 1915 mudflow deposits indicate that much of the apparent mudflow damage in 1915 was caused by hyperconcentrated streamflow downstream from a mudflow. An ancient landslide on a glacially undercut slope underlain by hydrothermally altered rocks in the valley of Mill Creek is temporally correlated with a 3,860 ± 50-year old mudflow deposit approximately 4 kilometers downstream; this finding indicates that landslides resulting from a combination of steep slopes and the low shear strength of hydrothermally altered rocks can generate mudflows in some stream valleys near Lassen Peak.

INTRODUCTION

Purpose and Scope

Recent study at Mount St. Helens (Janda and others, 1981; Waitt and others, 1983) in addition to research conducted at other Cascade volcanoes (Crandell, 1971; Miller, 1980) indicates that mudflows are the most laterally extensive and perhaps the most severe hydrologic hazard associated with volcanic activity in the Pacific Northwest. Lassen Peak, as a large volcanic dome, has a considerably more limited eruptive history than the stratovolcanoes that are more common in the Cascade Range. Volcanic domes are steep-sided features formed by the extrusion of viscous lava. Stratovolcanoes are built by the accumulation of alternating layers of lava, pyroclastic flow deposits, and mudflow deposits. Mudflows caused by eruptive activity at Lassen Peak in 1915 show that, despite these differences, the Lassen area is susceptible to mudflow hazards. The purpose of this study was to look for evidence of mudflows in the geologic record in the vicinity of Lassen Peak, and to examine the implications of recent work on volcanic-mudflow generation and movement with regard to future mudflow hazards in the Lassen area. An understanding of the geologic history of the Lassen area is stressed as being a critical part of evaluating both the susceptibility of stream valleys near Lassen Peak to mudflows and the degree to which mudflow hazards near Lassen Peak resemble mudflow hazards near other volcanoes.

Previous Work

Potential geologic hazards in Lassen Volcanic National Park were studied by D.R. Crandell and D.R. Mullineaux (U.S. Geological Survey, written commun., 1970). Their report discusses hazards associated with eruptive activity, landslides, mudflows, and floods. Statements regarding mudflow hazards are general, and indicate that stream valleys draining Lassen Peak are most susceptible to mudflow activity. Crandell and Mullineaux suggested that mudflows associated with future eruptive activity at Lassen Peak could be as large or larger than the mudflows that occurred in 1915.

The 1914-15 eruptions and associated mudflows at Lassen Peak were described and discussed by Day and Allen (1925), Finch (1930), and Williams (1932). Loomis (1926) provided excellent photography of the 1914-15 eruptions and mudflows. Eppler (1984) described the deposits left by the 1915 Lassen Peak mudflows and discussed the mechanics of the emplacement of the deposits.

Studies of mudflow deposits in the vicinity of several Cascade volcanoes provided the framework for the stratigraphic evaluation of mudflow deposits used in this study. To assess mudflow hazards near the Cascade volcanoes, Crandell and Mullineaux (1975) pointed out that stratigraphy and extent of mudflow deposits must be

studied. Mullineaux and Crandell (1962) and Crandell and Mullineaux (1973, 1978) studied mudflow deposits from Mount St. Helens in Washington. Crandell (1971) studied mudflow deposits from Mount Rainier in Washington, and Miller (1980) studied mudflow deposits from Mount Shasta in California.

Observations of mudflow generation and movement caused by recent eruptions at Mount St. Helens also have been helpful in understanding modern mudflow hazards at Lassen Peak. Cummans (1981) and Janda and others (1981) discussed mudflows caused by the May 18, 1980, eruption of Mount St. Helens. Waitt and others (1983) discussed mudflows caused by a subsequent smaller eruption at Mount St. Helens. Pierson and Scott (1985) discussed the downstream dilution of a volcanic mudflow to a hyperconcentrated streamflow near Mount St. Helens. Hyperconcentrated streamflows have sediment loads of 40 to 80 percent by weight and have rheologic properties that are intermediate between those of mudflows and those of flowing water (Beverage and Culbertson, 1964).

ACKNOWLEDGMENTS

VOLCANIC MUDFLOW GENERATION

The generation of a volcanic mudflow requires a source of water and a large volume of easily mobilized sediment. Loose debris is commonly present on the flanks of volcanoes; hence, the sudden availability of water in volcanic areas commonly is the controlling condition in mudflow generation. The great relief common near volcanoes causes mudflows to increase or maintain their speed and to flow long distances downstream.

Crandell (1971) described a variety of conditions that have caused mudflows on and near various volcanoes. Conditions directly related to volcanic eruptions include the expulsion of a crater lake, the direct extrusion of mud from a vent or fissure, the temporary damming of a river by rock debris from an eruption, the melting of snow and ice by a volcanic blast or pyroclastic flow, the collapse of hydrothermally altered volcanic

dome rocks as a result of volcanic or phreatic explosions, and the melting of snow and ice by contact with a lava flow. Conditions unrelated or indirectly related to volcanic eruptions include the breaching of large lakes on or near volcanoes, the release of water stored in or behind glacial ice, and the mobilization of loose pyroclastic deposits or other volcanic materials on steep slopes by intense rains or rapidly melting snow. Landslides that are common in hydrothermally altered areas near some volcanoes can generate mudflows by incorporating streamflow and mobilizing downstream into mudflows (Johnson and Rahn, 1970) or by damming a stream, creating a small lake that incorporates sediment and that flows downstream as a mudflow when the dam breaches.

GEOLOGIC HISTORY OF THE STUDY AREA

Lassen Peak is one of the southernmost Cascade volcanoes (fig. 1). Eruptions in the vicinity of Lassen Peak date back to the late Pliocene. Lavas, pyroclastic flow deposits, and mudflow deposits that form a large
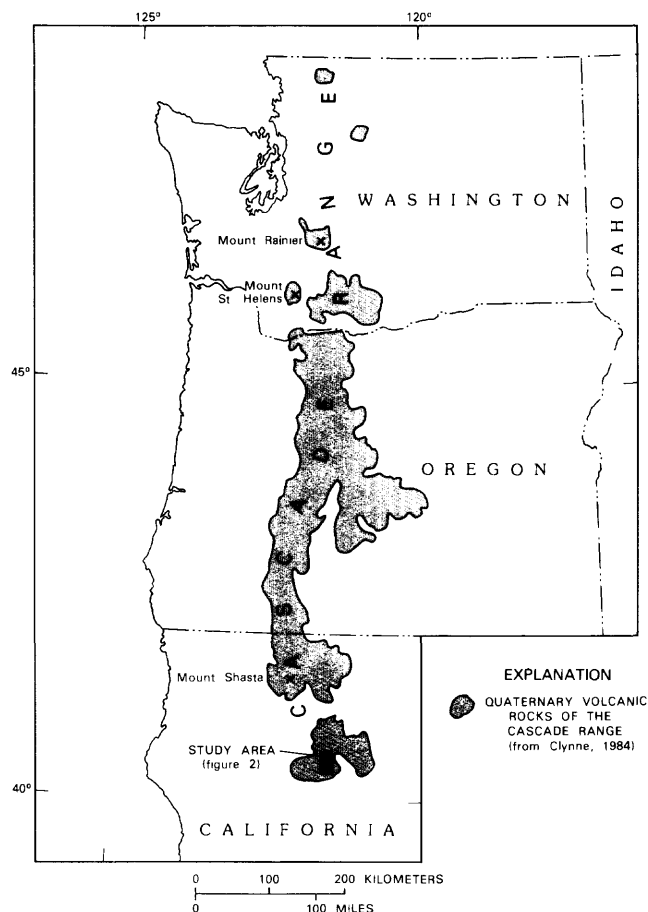

Figure 1. Location of the study area and Quaternary volcanic rocks in the Cascade Range.

plateau in the area have been attributed to three volcanic centers, each of which had a cone-building stage followed by a period of silicic dome building, lava flow extrusion, and pyroclastic flow emplacement (Clynne, 1984). The most recent of the three centers is called the Lassen volcanic center (Williams, 1932). Remnants of the stratovolcano created during the cone-building stage of this center (Brokeoff volcano) include Brokeoff Mountain, Mount Diller, and Mount Conard (fig. 2). Brokeoff volcano was constructed during the period between 0.35 and 0.70 million years ago (Clynne, 1984), after which the massive volcano was largely destroyed by glaciers that extensively eroded the hydrothermally altered cone (Williams, 1932). The long-lived volcanic centers are within an area of basaltic volcanism of a regional nature that has produced shield volcanoes, lava flows, and cinder cones (Clynne, 1984).

Crandell (1972) estimated the age of Lassen Peak to be about 11,000 years, based on glacial evidence and the geometry of the mountain. In particular, the lack of major well-defined cirques on Lassen Peak, the talus cone that could not have survived glaciation but that presently surrounds Lassen Peak, and glacial striations on rock surfaces close to Lassen Peak that are in orientations that do not parallel likely flow directions for glaciers that originated on Lassen Peak indicated to Crandell (1972) that the extrusion of Lassen Peak postdated the most recent major glaciation (11,000 to 15,000 years B.P.) in the area. Small glacial cirques and moraines on Lassen Peak were attributed by Crandell (1972) to minor glaciation (5,000 to 11,000 years B.P.) that corresponds to a late Tioga age glacial advance in the Sierra Nevada.

New evidence suggests that a part of Lassen Peak predates major glaciation in the Lassen area. Clasts, which have a lithology that is indistinguishable in hand specimen from the lithology of the Lassen Peak dome, are widespread in glacial deposits that extend more than 10 km downstream from Lassen Peak in the Lost Creek valley. Hand-specimen clasts in glacial material are considered to have the same lithology as Lassen Peak rocks if they have a silicic, glassy groundmass; abundant phenocrysts of feldspar, quartz, biotite, and hornblende; and distinctive emerald-green phenocrysts of augite. The groundmass, where fresh, is light gray to medium gray, the darker color indicating a higher glass content. Where oxidized, the groundmass appears pink to red. Phenocrysts consist of about 70 to 80 percent feldspar, 10 percent or more quartz, at least 5 percent biotite, 5 percent hornblende, and traces of augite (M.A. Clynne, U.S. Geological Survey, oral commun., 1984). Although none of these mineralogical characteristics alone is unique, together they produce a unique lithology that can be distinguished from other lithologies in the area.

The apparently unglaciated appearance of much of Lassen Peak contrasts with a bowl-shaped valley on the northeast side of Lassen Peak (the headwaters of Lost Creek), which resembles a glacial cirque more than the side of an unglaciated volcanic dome. Lassen Peak may have been extruded during more than one dome-building period—one preceding major glaciation, and another in postglacial times that obscured most of the glacial features of the older dome. Chemical data for Lassen Peak rocks show two distinct groups within the dome (M.A. Clynne, U.S. Geological Survey, written commun., 1985).

Known eruptive activity in the Lassen Peak area that postdates the extrusion of Lassen Peak includes the extrusion of Chaos Crags and associated pyroclastic flows, multiple eruptions of a small cinder cone about 18 km northeast of Lassen Peak (James, 1966), and the
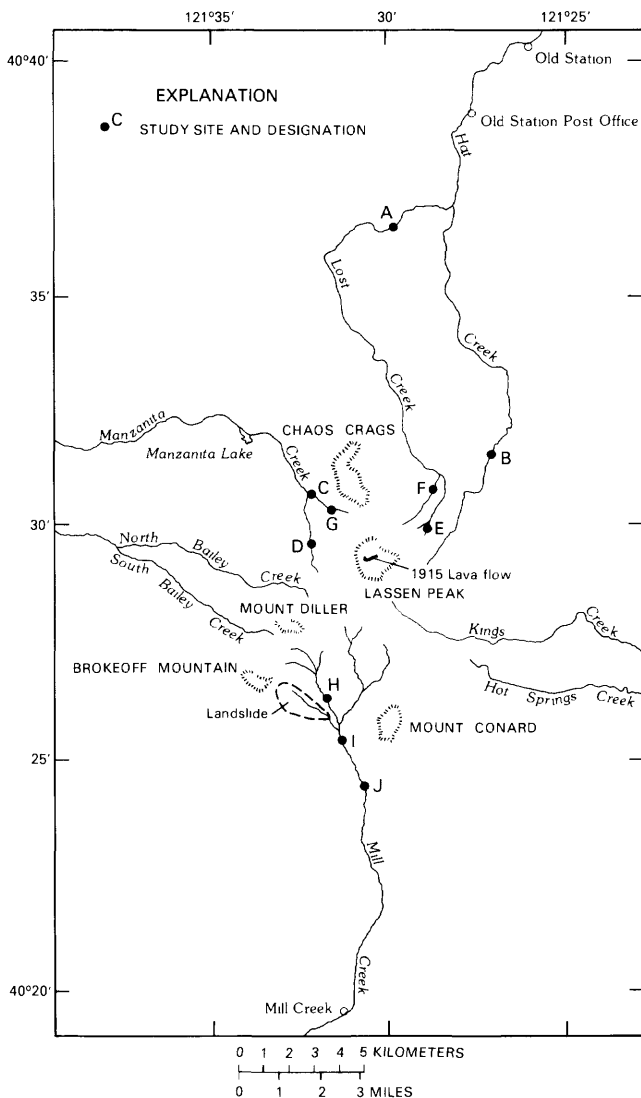
Figure 2. Location of study sites. Sites A-D mark the downstream extent of 1915 mudflow deposits. Locations of sites A and B from Eppler (1984).

1914-15 eruptions at Lassen Peak. The Chaos Crags dome-forming and pyroclastic events, dated at 1,050 years B.P. (Clynne, 1984), resemble other episodes of the silicic volcanism that characterizes the present stage of the Lassen volcanic center. The cinder-cone eruptions, which included the extrusion of lava flows and the formation of a small cinder cone, resemble other episodes of the hybrid andesite volcanism that also is characteristic of the present stage of the Lassen volcanic center (Clynne, 1984). The hybrid andesite volcanism is the result of mafic magma from deep in the Earth's crust mixing with a shallower body of silicic magma, from which nearby silicic domes and associated pyroclastic flows were derived (Clynne, 1984). Neither the Chaos Crags nor the cinder-cone eruptions apparently were associated with significant mudflows. Relief in the area was not sufficient to give potential mudflows much momentum. Also, the geometry and the cooling history of Chaos Crags and the cinder cone during the period of volcanism probably were not conducive to the collection of a large snowpack, which is an important source of water for mudflow generation.

1914-17 ERUPTIONS AND MUDFLOWS AT LASSEN PEAK

Until the May 1980 eruptions at Mount St. Helens, Lassen Peak was the site of the most recent volcanic eruption in the conterminous United States. The 1914-17 eruptions of Lassen Peak started with an eruption of clouds of ash and water in May 1914, and continued with similar mild eruptions until May 1915. A lava flow became visible at the summit of Lassen Peak on May 19, 1915. On that night, a sediment-rich flood carrying pieces of the new lava damaged property in the valleys of Lost and Hat Creek valleys. A volcanic blast on May 22, 1915, destroyed part of the forest on the northeast flank of Lassen Peak, and generated a large mudflow in the valley of Lost Creek and a smaller mudflow in the valley of Hat Creek (fig. 2). Smaller mudflows were emplaced in the valley of Manzanita Creek at an undetermined time on May 22, and on the northeast flank of Lassen Peak on May 22 after the large blast and its associated mudflows. Eruptions of ash and water vapor continued intermittently until June 1917.

The specific conditions that caused the first of the two large mudflows at Lassen Peak in 1915 are controversial. Diller (1916) and Day and Allen (1925) attributed the snowmelt, which provided the water for the mudflow, to a laterally directed volcanic blast. Finch (1930) reinterpreted the events and decided that contact with newly extruded lava melted the snow. The lava-flow hypothesis became widely accepted (Williams, 1932; Crandell, 1971) but has recently been contested by

Eppler (1984) who supported the volcanic-blast hypothesis.

Because the May 19 mudflow and its presumed initiating event occurred at night, and because the May 22 blast and mudflows covered much of the area affected by the May 19 mudflow and possible volcanic blast, indirect evidence must be used to test the different hypotheses. Calculations by Eppler (1984) indicate that the heat transfer resulting from contact of the May 19 lava flow with underlying snow was not sufficient to melt the water required for the rather large May 19 mudflow. Eppler (1984) also made calculations indicating that the steam released by juvenile magma was not an adequate source of water for the May 19 mudflow. Photographs of the crater taken before the May 19 mudflow show a small lake; however, its apparent volume is orders of magnitude smaller than the estimated water requirement for the May 19 mudflow. Tentative evidence of a small May 19 volcanic blast is seen in photographs taken before May 19 and between May 19 and May 22. According to Eppler (1984), these photographs show the denudation, probably by a small volcanic blast, of a small, previously forested area that lies outside the path of the May 19 mudflow. A volcanic explosion may have broken up the lava flow, facilitating more efficient heat transfer between lava and snow. A major eruption, during which a laterally directed volcanic blast denuded considerable parts of the northeastern flank of Lassen Peak, was associated in time with the first May 22 mudflow in Lost Creek. Although the May 22 blast covered a larger area in the headwaters of Lost and Hat Creeks than did the May 19 mudflow and possible blast, the volumes of the May 22 mudflow deposits were smaller than the volume of the May 19 deposit. Possibly, the May 19 mudflow had greatly depleted sources of water and sediment before the May 22 mudflows. The second May 22 mudflow in the Lost Creek valley and the mudflows in the Manzanita Creek valley were not obviously associated with explosive volcanic activity.

During the 1915 eruptions of Lassen Peak, a hybrid andesite magma, which was more mafic than the parent magma of Lassen Peak, reached the Earth's surface through a conduit in the Lassen Peak dome. It is unlikely that the 1915 magma was extruded from the magma chamber that produced the Lassen Peak dome (MacDonald and Katsura, 1965). Lava flows that have lithologies different from those of surrounding rocks are not found on other silicic domes in the Lassen Peak area.

METHODS OF STUDY

Initial field investigations were conducted in stream valleys that contain 1915 mudflow deposits, in-

cluding the valleys of Lost Creek, Hat Creek, and Manzanita Creek (fig. 2). These valleys were of particular concern because the geologic, climatic, and topographic factors that controlled mudflow occurrence in 1915 might also control mudflow occurrence during possible future eruptions. Subsequent investigations were conducted in the valleys of North and South Bailey Creeks because of their proximity to Lassen Peak. Finally, the valley of Mill Creek was examined because of its proximity to Lassen Peak and its potential for landsliding in the extensively hydrothermally altered rocks in the northern part of the basin. Time did not permit an examination of the valleys of Kings Creek and Warner Creek, which were given low priorities because of the complex topography between the main parts of those valleys and Lassen Peak.

Field investigations entailed walking stream valleys and looking for mudflow deposits. The distinction between mudflow deposits and glacial and volcaniclastic deposits commonly was ambiguous. Distinctive but not universal features of volcanic mudflows include abundant void spaces within the matrix, crude inverse grading, and an outcrop pattern consisting of a thin veneer on terraces or benches within stream valleys (Crandell, 1971). Where exposed and preserved, a bedded sandy layer at the base of some mudflow deposits (Schmincke, 1967) is helpful in distinguishing mudflow from glacial deposits. Although striated and faceted clasts are distinctive of glacial till, the possibility that mudflows could have incorporated glacial material enroute down-valley prevents the use of such clasts as indicators of glacial origin (Crandell, 1971). Distinctive characteristics of pyroclastic flows include the presence of a pumiceous matrix, welding (which may or may not be present in the pyroclastic materials), abundant charcoal at the bases of deposits, and uniform rather than random directions of thermoremnant magnetism (Crandell, 1971). Mudflow deposits of 1915 or later were distinguished from all other deposits by their inclusion of pieces of the distinctive black, glassy dacite that was extruded in 1915.

MUDFLOW STRATIGRAPHY IN STREAM VALLEYS

1915 Deposits

Mudflow deposits were emplaced in the valleys of Lost Creek, Hat Creek, and Manzanita Creek during the eruptions of Lassen Peak in May of 1915. The deposits were mapped by Williams (1932) and MacDonald (1963), and were examined in more detail in the valleys of Lost and Hat Creeks by Eppler (1984). The following discussion summarizes and augments previous work on the 1915 deposits.

Lost Creek

The Lost Creek valley received the largest mudflows generated during the 1915 eruptions of Lassen Peak. Deposits left by the 1915 mudflows extend approximately 20 km downstream from the peak (site A in fig. 2). Eppler (1984) distinguished three mudflow deposits in the Lost Creek valley—one emplaced on May 19, and two on May 22. According to Eppler, the May 19 deposit ranges from 0.15 to 1.5 m in thickness and contains about 6×10^6 m^3 of material; the first May 22 deposit ranges from 0.1 to 1.0 m in thickness and contains about 2×10^6 m^3 of material; and the second May 22 deposit is thicker than the first May 22 deposit, contains about 1×10^6 m^3 of material, and is found only in the southern parts of the Hat Creek and Lost Creek valleys.

The three mudflow deposits differ considerably in their average thickness, their morphology as deposits, and their grain-size distribution (Eppler, 1984). The May 19 and the second May 22 mudflow deposits are thick, very poorly sorted, coarse grained, and have steep-sided margins, leveed channels, and an uneven surface morphology. The first May 22 deposit, in contrast, is finer grained, better sorted, and has thin margins and a flat surface morphology. Differences between the deposits may reflect differences in the velocity and water content of the mudflows during emplacement and grain-size distribution of the sediment entrained in the flows.

Hat Creek

Williams (1932) and MacDonald (1963) mapped 1915 mudflow deposits along the entire reach of Hat Creek upstream from its junction with Lost Creek. Eppler's (1984) map and our investigation show 1915 mudflows extending only about 7 km downstream from Lassen Peak along Hat Creek to a point well upstream from the junction of Hat and Lost Creeks (site B in fig. 2). The greater extent of 1915 mudflow deposits in the Lost Creek as opposed to the upper Hat Creek valley probably reflected the orientation of the volcanic blasts and the deflection of mudflows by the low ridge that separates the headwaters of Lost and Hat Creeks (D.B. Eppler, Arizona State University, oral commun., 1984).

Manzanita Creek

Williams' (1932) map of the Lassen Peak area shows 1915 mudflow deposits extending down both headwater forks of Manzanita Creek to just downstream from their junction. Our field investigation, however, revealed a more limited extent of 1915 mudflow deposits in the Manzanita Creek drainage (sites C and

D in fig. 2). Photographs taken before and after the May 22 eruptions indicate that the bulk of the 1915 mudflow deposits in the Manzanita Creek drainage were emplaced on May 22 (Day and Allen, 1925). The deposits in both the unnamed north and south forks of Manzanita Creek resemble the May 19 and particularly the second May 22 mudflow deposits in Lost Creek in their coarse texture, poor sorting, and well-defined levees and flow margins.

Deposits Not Related to 1915 Eruptions

We attempted to identify and map pre-1915 mudflow deposits in the Lassen Peak area in order to assess the present-day susceptibility of the stream valleys there to mudflows. Ancient mudflows that apparently originated from the now-extinct Brokeoff volcano therefore were not considered in this investigation. Mudflows related to glacial activity on Lassen Peak are mentioned but not emphasized. Postglacial mudflow deposits that occur in hydrothermally altered areas and that appear unrelated to eruptions of Lassen Peak are discussed. References to pre-1915 mudflows originating from Lassen Peak in the valleys of Lost and Hat Creeks have been made by Finch (1929), Williams (1932), and Crandell (1972). No evidence of mudflow activity was found in the valley of Bailey Creek.

Lost Creek

Two mudflow sequences are exposed in steep walls of gullies near the headwaters of Lost Creek. The exposure at site E (fig. 2) is at least 2.5 m thick and consists of 0.5- to 1.2-m thick, poorly sorted layers interbedded with 7- to 10-cm thick, moderately to well-sorted sandy layers. Charcoal from one of the sandy layers yielded a radiocarbon age of 7,980 ± 50 years (M.A. Clynne, U.S. Geological Survey, oral commun., 1985). A 13- to 17-m thick sequence of mudflows interbedded with alluvium is exposed at site F (see fig. 2) (Crandell, 1972). These deposits differ from other mudflow deposits in the Lassen Peak area in their extensive association with alluvium. Although the deposits described by Crandell (1972) could not be dated directly, a tentative correlation with a sand-and-gravel deposit downstream that underlies a 5,400-year-old peat deposit, and the similarity of the weathering profile on the mudflows to the weathering profile on moraines of late Tioga age, indicated to Crandell (1972) that the deposits resulted from the mobilization of debris by meltwater during the late Tioga glacial retreat. There is no evidence that either of the mudflow sequences extended beyond the flanks of Lassen Peak. The apparent limited extent of the mudflows, and their likely temporal association

with late Tioga glacial activity, diminishes their importance from a modern hazards perspective.

Williams (1932) described pre-1915 mudflow deposits in the form of "moraine-like mounds" adjacent to and outside the 1915 mudflow deposits in Lost Creek. Williams (1932) believed that the older mudflows were associated with the formation of Lassen Peak and were more extensive than the 1915 mudflows. Finch (1929) also described pre-1915 deposits along Lost Creek, some of which he believed were emplaced within the last 500 years.

Our field investigation along Lost Creek was conducted between 1 and 30 km from the summit of Lassen Peak (fig. 2). Beyond the flanks of Lassen Peak, most exposures in the banks of the creek consist of 1915 mudflow deposits, underlain in places by Chaos Crags pyroclastic flow deposits, and glacial deposits beneath and on streambanks adjacent to and outside the younger deposits. Exposures, mentioned as pre-1915 mudflow deposits by Williams (1932) and Finch (1929), appear to be glacial deposits and 1915 mudflow deposits.

Hat Creek

Williams' (1932) geologic map of the Lassen Peak area shows about 1 km^2 of pre-1915 mudflow deposits along the headwaters of Hat Creek. More recent field studies indicate that, rather than older mudflow deposits, a thin, unsorted deposit containing solidified pieces of 1915 lava is widespread in that area (R.L. Christianson, U.S. Geological Survey, oral commun., 1984). Our investigation along the upstream reaches of Hat Creek for the present study was conducted between 1 and 10 km from the summit of Lassen Peak (fig. 2). The pre-1915 exposures in the banks of the creek consists of pyroclastic flow deposits, fluvial deposits, glacial deposits, and lava flows.

Manzanita Creek

Mudflow deposits that pre-date the Chaos Crags pyroclastic flows are exposed in gully walls at the head of the unnamed north fork of Manzanita Creek (site G in fig. 2). At least two mudflow deposits, each of which is approximately 0.3 and 0.5 m thick, overlie a deposit that consists of considerably weathered, angular clasts with a lithology that appears identical in hand specimen to that of Lassen Peak. Clasts in the mudflow deposits also are exclusively of the Lassen Peak lithology. In contrast to mudflow deposits identified by Crandell (1972) in the headwaters of Lost Creek, the Manzanita Creek deposits contain very angular clasts and are not associated with fluvial deposits. Bedded basal layers distinguish the mudflow deposits from

glacial till; a lack of pumiceous matrix distinguishes the mudflow deposits from pyroclastic deposits. These pre-1915 mudflows may have been related to the initial extrusion of the Lassen Peak dome. No evidence of these mudflows was found farther downstream. Between site G (fig. 2) and Manzanita Lake, stream cuts expose Chaos Crags pyroclastic flows, glacial deposits, and the considerably weathered deposit consisting exclusively of angular fragments of Lassen Peak lithology. Downstream from Manzanita Lake, the course of Manzanita Creek was disrupted by the collapse of a part of the Chaos Crags dacite dome field about 300 years ago (Crandell and others, 1974). Glacial deposits and various volcanic units are exposed along the abandoned course of Manzanita Creek, but there is no evidence of mudflow activity.

Mill Creek

Mudflow hazards in the Mill Creek valley differ from those in the valleys discussed previously because (1) the Mill Creek valley is separated from Lassen Peak by complex topography that could deflect or dissipate mudflows, and (2) landslides on the streamside hillslopes that have been glacially steepened and extensively altered hydrothermally can mobilize into mudflows. Mudflows generated directly from volcanic activity are less likely here than in other stream valleys draining Lassen Peak, as indicated by the lack of 1915 mudflow activity in the Mill Creek valley. Mudflows generated by mass-movements on steep slopes underlain by hydrothermally altered bedrock, however, are a significant hazard, as indicated by the mudflow deposits discussed below.

Mudflow deposits that postdate glacial activity were observed at several locations in the Mill Creek valley (fig. 2). At site H, about 4 m of fluvial deposits interbedded with more poorly sorted layers, which may be mudflow deposits, are overlain by a mudflow deposit about 1 m thick. This uppermost mudflow deposit is unsorted; contains rounded, subangular, and angular clasts; does not contain clasts of Lassen Peak lithology; and is underlain by a sandy, bedded layer. At site I, about 1 km downstream from site H, a poorly sorted, roughly bedded deposit containing charred logs is exposed in steep streambanks about 10 m above the present level of Mill Creek. One of these logs has been dated at 3,310 ± 55 years B.P. (Clynne, 1984). The land surface along the left bank of the creek at that location is hummocky and contains elongated boulder ridges that may have resulted from mudflows.

About 3 km farther downstream, a continuous deposit extends 240 m along both sides of Mill Creek (site J in fig. 2). Streambed exposures of the deposit are unbedded, and 5 to 8 m thick (fig. 3). Clasts are angular

to subangular, and both clasts and matrix appear hydrothermally altered. The matrix is considerably more clayey than mudflow deposits observed in the valleys of

A

B

Figure 3. Mudflow deposit at site J (fig. 2) in the Mill Creek valley. Deposit is 5 m thick at this location. A, Downstream view of deposit on right bank. B, In-channel view of deposit on right bank.

Lost, Hat, and Manzanita Creeks. The deposit slopes away from Mill Creek toward both valley walls, thins downstream, and ends abruptly on both sides of the valley. Charcoal collected from a continuous organic-enriched layer at the base of the deposit on the left bank was dated at 3,860 ± 50 years B.P.

Similar radiocarbon ages of the deposits at sites I and J (fig. 2) indicate that the deposits resulted from a single mudflow. Active streamside landsliding along Mill Creek may have removed intermediate parts of the deposit. Clynne (1984) correlated the deposit that he dated with a large landslide identified by D.R. Crandell and D.R. Mullineaux (U.S. Geological Survey, written commun., 1970) adjacent to one of the headwater tributaries of Mill Creek (fig. 2). The correlation was based on clasts of similar lithologies in the deposits and, in the lower deposit, the inclusion of a log from a tree species that grows only at the higher altitudes where the landslide occurred. The landslide identified by Crandell and Mullineaux may have incorporated streamflow and mobilized into a mudflow. This mudflow apparently traveled about 4 km downstream, leaving the deposits dated by Clynne (1984) and by the present study.

RELATION BETWEEN MUDFLOW DEPOSITS AND DAMAGE

Reports of damage caused by the May 19, 1915, mudflows and related floods near Lassen Peak, although inconsistent and difficult to interpret, indicate that damage extended downstream from the present (1985) extent of May 19, 1915, mudflow deposits. Accounts from Loomis (1926) indicate that cabins on Hat Creek owned by Wilcox, Sorenson, and Hall were severely damaged or destroyed on the night of May 19, 1915. Accounts of cabins filled with mud indicate that the damage was done by mudflows or extremely sediment-rich streamflows. A sketch map of homestead and ranch locations in a 1915 account of mudflow damage (Richard L. Vance, U.S. National Park Service, written commun., 1985) and descriptions of the location of cabins and ranches by Willendrup (1976) indicate that (1) the Wilcox and Sorenson cabins were part of homesteads located between the junction of Lost and Hat Creeks and the present (1985) Old Station Post Office; (2) the Hall ranch was between the Old Station Post Office and Old Station (fig. 2); and (3) the Wilcox Ranch was downstream from the Hall ranch. A report in Loomis (1926) of damage to a Wilcox cabin downstream from the Hall ranch possibly is a confused account of damage to a cabin on the Wilcox homestead upstream from the junction of Lost and Hat Creeks. Eppler (1984) mapped the downstream extent of the May 19, 1915, mudflow deposit at about 2.5 km up-

stream from the junction of Lost and Hat Creeks (fig. 2). Much of the damage attributed to the May 19, 1915, mudflow in the Hat Creek valley, therefore, probably was caused by hyperconcentrated streamflow downstream from the mudflow.

Accounts of the May 19, 1915, mudflow also indicate that the height of the flow was well above the height of the resulting deposit. Mud lines on trees in the valley of Lost Creek about 7 km downstream from Lassen Peak were an estimated 4 to 6 m above the top of the mudflow deposit (Loomis, 1926). The thickness of the deposit in that area is commonly less than 1 m.

POSSIBLE FUTURE MUDFLOWS

Mudflows Related to Eruption

Mudflows directly related to eruptions of Lassen Peak are the most significant mudflow hazard in most stream valleys draining the peak. Therefore, the probability of future large mudflows in these valleys is a function of the probability of future eruptive activity on Lassen Peak. Although no volcanic domes in the Lassen area except for Lassen Peak show evidence of eruptions long after their period of formation, the 1915 and possible prior eruptions indicate that future eruptions of Lassen Peak are possible.

Conditions controlling the magnitude and direction of mudflows that could be caused by future eruptions are variable, and some are difficult to predict. Such conditions include the depth of the snowpack and the direction and area affected by blast or pyroclastic flows. There is general consensus that the snowpack was unusually thick before the May 1915 eruptions of Lassen Peak. Day and Allen (1925) reported that snow depths ranged from 5 to 13 m in the bowl at the head of Lost Creek in May 1914, and also that the cumulative snowfall during the winter of 1914-15 at nearby weather stations was similar or greater than that during the winter of 1913-14.

Although a thicker snowpack could provide a greater source of water and thus increase the size of potential mudflows, the effects of recent volcanic activity on glaciers at Mount St. Helens indicate that a single pyroclastic flow or volcanic blast does not always melt all the snow and ice in its path. Brugman and Meier (1981) reported the melting and erosion of about 6 m of snow and ice on glaciers in the paths of pyroclastic flows at Mount St. Helens. They also reported a change from 45 to 20 m—in the estimated average thickness of a glacier in the area affected by the May 18, 1980, volcanic blast. This change may overestimate the thickness of snow and ice actually removed by the blast because the original thickness is an average of the

thickness of the entire glacier, whereas the posteruption thickness is an average of the lower part of the glacier (the upper part having been removed by a massive landslide), which most likely was thinner than the upper part even before the eruption. The capacity of a pyroclastic flow to erode a snowpack may exceed the potential of such a flow to erode more densely packed glacial snow and ice.

The size of the snow-covered area affected by a pyroclastic flow or volcanic blast can affect the volume of snow melted and hence the size of a resulting mudflow. Day and Allen (1925) concluded from an examination of photographs taken in May 1915, that the May 22, 1915, blast at Lassen Peak covered a larger area on the flanks of Lassen Peak than did the mudflow and possible blast of May 19, 1915. If the May 22 blast had occurred before the May 19 mudflow and possible blast had removed much of the snow in the headwaters of Lost Creek, the resulting mudflow in that valley may have been larger than the one that occurred on May 19, 1915.

Although controls on the eastern orientation of the May 22 blast and the possible May 19 blast are not understood, several lines of evidence indicate that the east and west sides of Lassen Peak have a greater probability of being affected by eruptions than other sides; therefore, the valleys of Lost, Hat, and Manzanita Creeks have a relatively greater probability of being affected by mudflows related to eruptive activity. Before the 1914-15 eruptions of Lassen Peak, notches on the east and west sides of the summit indicated a zone of weakness and possible earlier eruptions oriented along an east-west-trending line (Day and Allen, 1925). During the early stages of the 1914-15 eruptions, fractures extending from the crater and the elongation of the crater itself also were oriented in an east-west direction (Day and Allen, 1925). During the May 19-22, 1915, eruptions, lava was extruded down the northeast and west flanks of Lassen Peak (fig. 2).

Mudflows Not Related to Eruption

Mudflow deposits in Mill Creek indicate that hydrothermally altered areas near Lassen Peak are susceptible to large mudflows that are not directly related to eruptions. The most likely mechanism for generating these mudflows involves the occurrence of landslides on glacially oversteepened valley walls underlain by the weak, hydrothermally altered rocks. These landslides can mobilize downstream into mudflows or can dam streams; when the dam breaches, the collected water and incorporated sediment can flow downstream as a mudflow. The significance of rapid mass-movement and clayey mudflows in hydrothermally altered areas near

volcanoes was recognized by Crandell (1971). Substantial clay contents of such mudflows add to their mobility (Rodine and Johnson, 1976) and consequent destructive potential.

SUMMARY

Mudflow deposits in stream valleys draining Lassen Peak demonstrate a potential for mudflows in this area. Mudflow deposits that resulted from eruptions in May 1915 extend about 20 km down the valley of Lost Creek, about 7 km down the valley of Hat Creek, and less than 3 km down the valleys of two unnamed headwater tributaries of Manzanita Creek. Deposits left by mudflows unrelated to the 1915 eruptions of Lassen Peak were found in the valleys of Lost, Manzanita, and Mill Creeks.

Mudflows resulting from eruptions of Lassen Peak are the most significant mudflow hazard in most valleys in that area. Although repetitive eruptive activity does not appear typical of volcanic domes in the Lassen Peak area, the 1914-15 eruptions of Lassen Peak demonstrate that future eruptions of that dome are possible. The summit morphology before the 1914-15 eruptions, summit fractures created during the 1914-15 eruptions, and the orientation of lava flows extruded in 1915 indicate that the valleys of Hat, Lost, and Manzanita Creeks are particularly susceptible to the effects of volcanic activity on Lassen Peak. A different sequence of eruptive activity in May 1915 could have generated a larger mudflow than the one that travelled about 20 km down the valley of Lost Creek. Much of the damage attributed to May 1915 mudflows in the valleys of Hat and Lost Creek was probably caused by hyperconcentrated streamflows.

Mudflow deposits in the Mill Creek valley indicate that glaciated stream valleys draining hydrothermally altered rocks are susceptible to large mudflows that are not directly related to volcanic activity. A likely correlation of two dated deposits along Mill Creek with a large streamside landslide upstream indicate that the landslide incorporated water and flowed about 4 km down the valley of Mill Creek as a mudflow.

REFERENCES CITED

Beverage, J.P., and Culbertson, J.K., 1964, Hyperconcentrations of suspended sediment: Proceedings, American Society of Civil Engineers, Journal of Hydraulics Division, 4136, HY6, p. 117-1.

Brugman, M.M., and Meier, M.F., 1981, Response of glaciers to the eruptions of Mt. St. Helens, in Lipman, P.W., and Mullineaux, D.R., eds., The 1980 eruptions of Mount St. Helens, Washington: U.S. Geological Survey Professional Paper 1250, p. 743-756.

Clynne, M.A., 1984, Stratigraphy and major element geo-chemistry of the Lassen volcanic center, California: U.S. Geological Survey Open-File Report 84-224, 168 p.

Crandell, D.R., 1971, Postglacial lahars from Mount Rainier volcano, Washington: U.S. Geological Survey Professional Paper 677, 75 p.

———1972, Glaciation near Lassen Peak, northern California, in Geological Survey Research 1972: U.S. Geological Survey Professional Paper 800-C, p. C179-C188.

Crandell, D.R., and Mullineaux, D.R., 1973, Pine Creek volcanic assemblage at Mount St. Helens, Washington: U.S. Geological Survey Bulletin 1383-A, 23 p.

———1975, Technique and rationale of volcanic-hazards appraisals in the Cascade Range, northwestern United States: Environmental Geology, v. 1, no. 1, p. 23-32.

———1978, Potential hazards from future eruptions of Mount St. Helens volcano, Washington: U.S. Geological Survey Bulletin 1383-C, 26 p.

Crandell, D.R., Mullineaux, D.R., Sigafoos, R.S., and Rubin, Meyer, 1974, Chaos Crags eruptions and rock-fall avalanches, Lassen Volcanic National Park, California: U.S. Geological Survey Journal of Research, v. 2, no. 1, p. 49-61.

Cummans, John, 1981, Mudflows resulting from the May 18, 1980, eruption of Mt. St. Helens, Washington: U.S. Geological Survey Circular 850-B, 16 p.

Day, A.L., and Allen, E.T., 1925, The volcanic activity and hot springs of Lassen Peak: Washington, D.C., Carnegie Institution of Washington Publication 360, 190 p.

Diller, J.S., 1916, Volcanic history of Lassen Peak: Science (new series), v. 43, p. 727-733.

Eppler, D.B., 1984, Characteristics of volcanic blasts, mud-flows, and rock-fall avalanches in Lassen Volcanic National Park, California: Tempe, Arizona State University, unpublished Ph.D. dissertation, 261 p.

Finch, R.H., 1929, Lassen Report No. 19: The Volcano Letter, no. 237, p. 1.

———.1930, Mudflow eruption of Lassen Volcano: The Volcano Letter, no. 266, p. 1-4.

James, D.E., 1966, Geology and rock magnetism of Cinder Cone lava flows, Lassen Volcanic National Park, California: Geological Society of America Bulletin, v. 77, no. 3, p. 303-312.

Janda, R.J., Scott, K.M., Nolan, K.M., and Martinson, H.A., 1981, Lahar movement, effects, and deposits, in Lipman,

P.W., and Mullineaux, D.R., eds., The 1980 eruptions of Mt. St. Helens, Washington: U.S. Geological Survey Professional Paper 1250, p. 461-478.

Johnson, A.M., and Rahn, P.H., 1970, Mobilization of debris flows: Zeitschrift fur Geomorphologie, v. 9, p. 168-186.

Loomis, B.F., 1926, Pictoral history of the Lassen volcano: Mineral, Calif., Loomis Museum Association, Lassen Volcanic National Park, 110 p.

MacDonald, G.A., 1963, Geology of the Prospect Peak Quadrangle, California: U.S. Geological Survey Geologic Quadrangle Map GQ-345, scale 1:62,500.

MacDonald, G.A., and Katsura, Takashi, 1965, Eruption of Lassen Peak, Cascade Range, California, in 1915—Example of mixed magmas: Geological Society of America Bulletin, v. 76, p. 475-482.

Miller, C.D., 1980, Potential hazards from eruptions of Mt. Shasta, California: U.S. Geological Survey Bulletin 1503, 43 p.

Mullineaux, D.R., and Crandell, D.R., 1962, Recent lahars from Mount St. Helens, Washington: Geological Society of America Bulletin, v. 73, no. 7, p. 855-870.

Pierson, T.C., and Scott, K.M., 1985, Downstream dilution of a lahar—Transition from debris flow to hyperconcentrated streamflow: Water Resources Research, v. 21, no. 10, p. 1511-1524.

Rodine, J.D., and Johnson, A.M., 1976, The ability of debris, heavily freighted with coarse clastic materials, to flow on gentle slopes: Sedimentology, v. 23, no. 2, p. 213-234.

Schmincke, H.V., 1967, Graded lahars in the type sections of the Ellensburg Formation, south-central Washington: Journal of Sedimentary Petrology, v. 37, no. 2, p. 438-448.

Waitt, R.B., Jr., Pierson, T.C., MacLeod, N.S., Janda, R.J., Voight, Barry, and Holcomb, R.T., 1983, Eruption-triggered avalanche, flood, and lahar at Mt. St. Helens—Effects of a winter snowpack: Science, v. 221, no. 4618, p. 1394-1397.

Willendrup, A.W., 1976, The Lassen Peak eruptions and their lingering legacy: Chico, Calif., Chico State University, unpublished M.A. thesis, 229 p.

Williams, Howell, 1932, Geology of the Lassen Volcanic National Park, California: University of California, Department of Geological Sciences Bulletin, v. 21, no. 8, p. 195-385.

Application of Generalized Least Squares in Regional Hydrologic Regression Analysis

By Gary D. Tasker, James H. Eychaner, and Jery R. Stedinger[1]

Abstract

Alternative methods for estimating parameters of a regional regression of the 100-year peak discharge are considered. A generalized least-squares (GLS) technique that accounts for cross-correlated data of different record length was compared with the commonly used ordinary least-squares (OLS) method. The GLS technique is shown to be better than the OLS technique in terms of average variance of prediction on the basis of a split-sample study of 89 gages in Pima County, Ariz.

INTRODUCTION

Streamflow records are collected at only a very few of the many sites at which hydrologic information is needed. A regional regression model commonly provides a method of transferring streamflow information collected at gaged sites to the ungaged sites where information is needed. It also can be used to improve at-site estimates of streamflow characteristics at gaged locations by incorporating information from nearby sites.

Recently, Stedinger and Tasker (1985) proposed a new method for estimating the parameters of regional regression models that takes into account the length of record available at gaged sites and the between-site cross correlation among concurrent flows. In this new method, a generalized least-squares (GLS) estimator of the regression model's parameters is used. By contrast, hydrologists commonly use ordinary least-squares (OLS) estimators that are appropriate and statistically efficient if the flow records are equally reliable (of equal length) and if concurrent flows at any pair of stations are independent. Stedinger and Tasker (1985) showed, in a Monte Carlo simulation, that the proposed GLS method (1) provided estimates of regression parameters with smaller mean-square errors than did the OLS estimates, (2) provided relatively unbiased estimates of the vari-

ance of the regression parameters compared with those of OLS, and (3) provided a more accurate estimate of the regression model error than did OLS.

In this report, the GLS estimation technique of Stedinger and Tasker (1985) is compared with OLS estimation in a split-sample experiment, in which real data from Pima County, Ariz., are used. A brief description of the methods precedes the description of data used in the comparison and the results of the split-sample experiment.

ORDINARY LEAST-SQUARES-GENERALIZED LEAST-SQUARES THEORY

We discuss here how to estimate the parameters of a linear model specifying the value of the T-year flow event (such as the 100-year peak) as a function of various drainage-basin characteristics (such as the drainage area, or channel slope, and (or) percent forest and lakes). The data available at each of N sites in a region are summarized by vectors of basin characteristics, x_i, and a streamflow record of n_i values

$$\{ y_{i,1}, y_{i,2}, \ldots y_{i,n_i} \}$$

available for each site i. These may be the annual maximum flow or a transform thereof so that the y's are normally distributed. The normality assumption is adopted to facilitate this explanation. Other distribution, such as the log-Pearson III, could be used with appropriate adjustments in the explanation that follows. The normal assumption worked well in Monte Carlo experiments reported by Stedinger and Tasker (U.S. Geological Survey, written commun., 1984) even when the actual distribution was Pearson III.

Let $\hat{Y} = (\bar{y}_1 + z_p s_1, \ldots, \bar{y}_N + z_p s_N)^T$ (1)

be the vector of at-site estimates of the $(1/p)$-year flow, where $\bar{y}_i$ and s_i are the usual sample estimates of mean

[1] Department of Environmental Engineering, Cornell University, Ithaca, NY 14853.

and standard deviation of the flows at site i, and z_p is the standard normal deviate with exceedance probability p. Also, let $Y = (\mu_1 + z_p \delta_1 , ..., \mu_N + z_p \delta_N{}^T$ be the vector of true $(1/p)$-year flows, where μ_i and δ_i are the true mean and standard deviation of the $y_{i,t}$ at site i.

The ordinary least-squares regional regression model can be written

$$Y = X\beta + e , \qquad (2)$$

where X is an $(N \times k)$ matrix of basin characteristics augmented by a column of ones, β is a $(k \times 1)$ vector of regression coefficients, and e is an $(N \times 1)$ vector of random errors with expected values of zero and a covariance matrix that is assumed to be of the form $I_N \delta^2$; here I_N is an N-dimensional identity matrix, and δ^2 is a constant. The OLS estimate of β is

$$\hat{\beta}_{\mathrm{OLS}} = (X^T X)^{-1} X^T Y \qquad (3)$$

The estimators sampling covariance matrix, given the stated assumptions, is

$$\mathrm{Var}\,(\hat{\beta}_{\mathrm{OLS}}) = \sigma^2 (X^T X)^{-1} \qquad (4)$$

The OLS model is appropriate where all estimates of T-year events have equal variance, and concurrent flows at different sites are uncorrelated or independently distributed. In general, these two conditions are not met because gaged records are of different length and concurrent annual floods are often cross correlated.

A more appropriate model for use in hydrologic regression is the GLS model. In the GLS model, the assumptions of equal variance of the T-year events and zero cross-correlation for concurrent flows are relaxed. The covariance matrix for the errors in the GLS model is organized in a matrix Σ whose elements are

$$\Sigma_{ij} = \begin{cases} \gamma^2 + n_i^{-1} \sigma_1^2 \,(1+0.5z_p) & \text{for } i=j \\ \rho_{ij}{}^{n^{-1}} m_{ij} \,(1+0.5\rho_{ij}z_p^2) & \text{for } i\neq j \end{cases} \qquad (5)$$

where ρ_{ij} is the estimated cross correlation between annual flood flows at sites i and j, m_{ij} is the number of concurrent years of record, and γ^2 is the model-error variance. The model-error variance ia a measure of the precision of the true regression model and is defined by

$$\gamma^2 = E \,(Y - X\beta)^2 \qquad (6)$$

The value γ^2 is assumed to be independent of x_i, where x_i is a vector of basin characteristics at site i. The GLS estimate of β is

$$\beta_{\mathrm{GLS}} = (X^T \Sigma^{-1} X)^{-1} X^T \Sigma^{-1} Y \qquad (7)$$

This estimator has a sampling covariance matrix, given the assumptions, equal to

$$\mathrm{Var}(\hat{\beta}_{\mathrm{GLS}}) = (X^T \Sigma^{-1} X)^{-1} \qquad (8)$$

The greatest barrier to the use of GLS methods has been that the value of the convariance matrix Σ is unknown because it depends on the population values of γ^2, σ_i, and ρ_{ij}. Stedinger and Tasker (1985) proposed use of a reasonable estimator of Σ. Their Monte Carlo simulations showed that use of the estimator of Σ in equation 7 led to an improved estimator of β (in terms of mean-square error) and more accurate estimates of the model variance γ^2 than did use of competing ordinary and weighted least-squares procedures.

The method used to estimate Σ is briefly described; Stedinger and Tasker (1985) provide a more detailed description. If Σ were known, then

$$E\{ (Y - X\beta_{\mathrm{GLS}})^{\mathrm{T}} \Sigma(\gamma^2, \rho_{ij}, \sigma_i)^{-1} (Y - X\beta_{\mathrm{GLS}})\}= N\text{-}k , \qquad (9)$$

where Σ is written as $\Sigma(\gamma^2, \rho_{ij}, \sigma_i)$ to emphasize its dependence on γ^2, ρ_{ij}, and σ_i. The problem is to estimate γ^2, ρ_{ij}, and σ_i for equation 5 so that we can obtain an estimate of Σ.

Reliable estimations of the cross correlation between flows at each pair of stations, ρ_{ij}, where only short concurrent records are avaiable, are difficult. We can best make such estimations subjectively by using good judgment based on hydrologic principles. Our goal in estimating the ρ_{ij}'s is to capture the essential underlying cross-correlation structure among the streamflows within a region. If values for ρ_{ij} are subjectively assigned, one should consider the distance between the two stations and whether the stations are affected by the same rainfall events. One suggestion for estimating the ρ's is to classify each pair (i, j) of stations as likely to have a high, medium, or low cross correlation; such classification is based on the sample cross correlation for the pair and on good judgment. If classifying pairs of stations, one could consider the proximity of the stations, their drainage areas, any tributary relation between them, the type of storms that cause peak flows in each basin, and other factors.

At first, one may consider estimating the σ_i's in equation 9 by their usual sample estimate s_i. However, this leads to poor estimates of β (Stedinger and Tasker, 1985). A better approach is to first regress the s_i against basin characteristics and then use the regression estimate of $E(\sigma_i | x_i)$. Finally, one can estimate γ^2 by iteratively solving equation 9 to obtain an estimate, $\hat{\gamma}^2$, of γ^2 for the specified values of ρ_{ij} and $E(\sigma | x)$.

Some refinements in the procedure actually result in an algorithm that is slightly more involved than the

procedure outlined here. A Fortran 77 computer program that estimates regression-model parameters using the GLS procedure described here is available from the first author.

SPLIT-SAMPLE EXPERIMENT

To compare the OLS and GLS methods, we selected data for 89 stations that had been used in a flood-frequency study of Pima County, Ariz. (Eychaner, 1984). Pima County is in the Basin and Range lowlands water province of southern Arizona (fig. 1) and includes about 24,000 km^2 of the upper Sonoran Desert. Wide valley floors receive an average rainfall of 150 to 300 mm/yr at altitudes of less than 1,000 m above sea level. Average precipitation in scattered areas above 2,300 m is as much as 750 mm/yr. Most floods are the result of intense summer thunderstorms, although tropical storms and widespread winter storms can produce
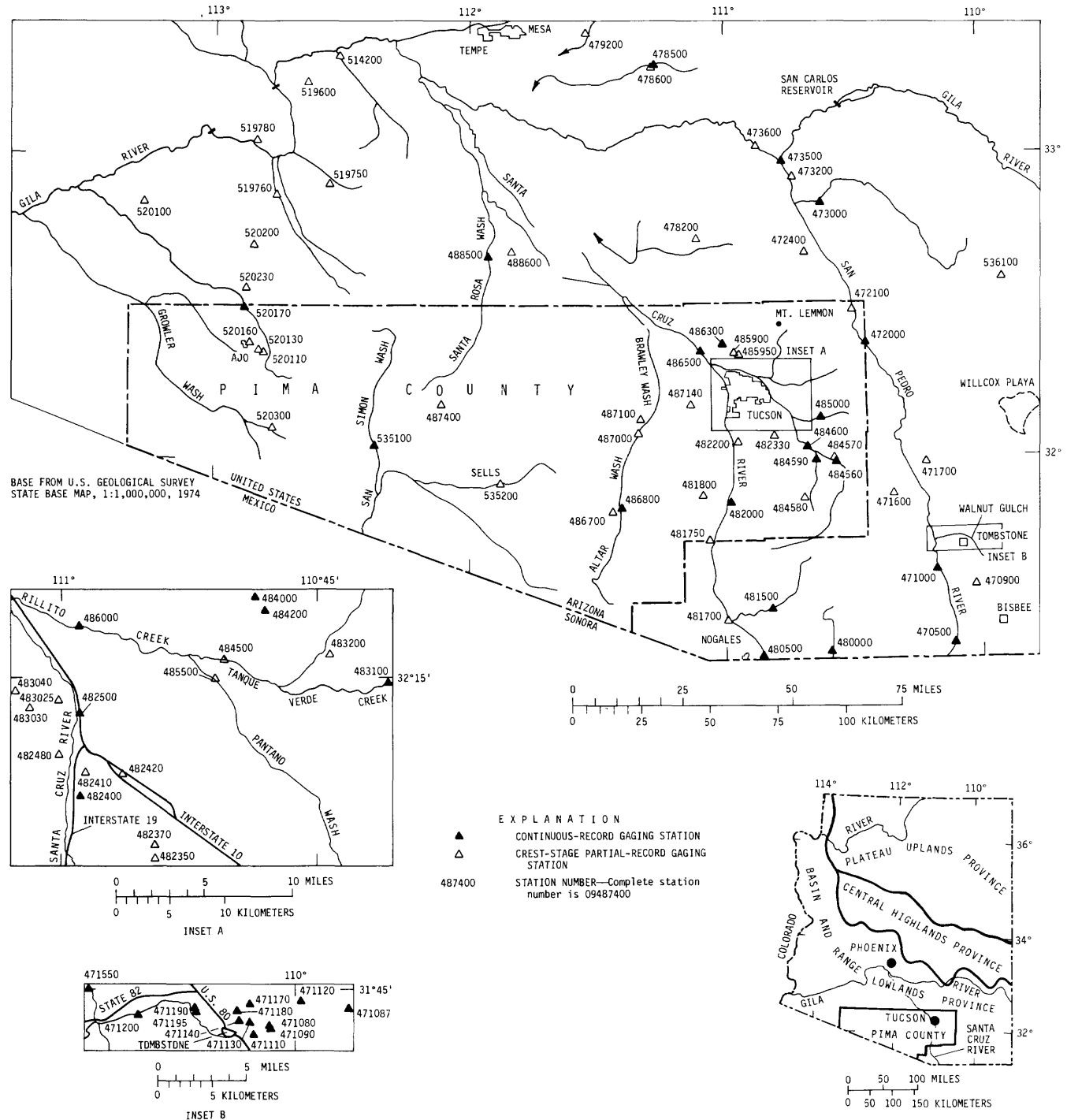
Figure 1. Study area and locations of gaging stations.

serious flooding in the largest basins. Flood-frequency estimates in the region generally have large uncertainties.

The 89 stations (fig. 1) represent rural basins that have drainage areas of 0.39-11,580 km², channel slopes of 0.29-13 percent, average annual precipitation of 127-574 mm, and mean altitudes of 205-1,920 m. The stations were divided into four mutually exclusive subsets of 22 or 23 stations; each subset had approximately the same range of basin characteristics. The data used in this experiment are listed in table 1.

Table 1. Data used in regression analyses

Station	Years of record	Subset	ln(A)	A^{-0.125}	Mean of ln(Q)	Std dev of ln(Q)	Regional skew	ln(Q_{100})
470500	43	2	6.6080	0.43780	8.76203	0.55861	-0.1	10.0204
470900	16	3	1.6583	.81278	5.96024	1.02603	-.1	8.2716
471000	66	1	7.1058	.41139	8.91607	.65532	-.1	10.3923
471080	14	2	1.8593	.79262	5.63903	1.25813	-.1	8.4732
471087	19	1	-1.5141	1.20836	4.54162	1.18836	-.1	7.2187
471090	15	4	2.2094	.75868	6.33050	1.20955	-.1	9.0553
471110	26	1	2.2235	.75734	6.20063	1.12735	-.1	8.7402
471120	19	3	1.1568	.86537	6.33994	.97514	-.1	8.5367
471130	19	1	1.7884	.79967	6.43688	.89709	-.1	8.4578
471140	20	2	3.6029	.63740	7.11729	1.03754	-.1	9.4546
471170	24	2	-.1278	1.01610	4.23353	1.48563	-.1	7.5802
471180	28	4	1.2442	.85597	5.04059	1.39537	-.1	`8.1839
471190	28	1	3.7819	.62329	7.22137	1.17086	-.1	9.8590
471195	16	2	1.6526	.81337	5.53357	1.72717	-.1	9.4244
471200	24	4	4.0553	.60235	7.38531	.85104	-.1	9.3024
471550	15	3	7.4615	.39349	8.94554	.69607	-.1	10.5136
471600	10	3	-.2358	1.02991	1.22958	2.06427	-.1	5.8798
471700	16	4	.9970	.88283	5.04865	1.12642	-.1	7.5862
472000	51	2	7.9858	.36853	9.03880	.79508	-.1	10.8299
472100	14	2	2.0820	.77086	4.83267	1.40964	-.1	8.0082
472400	15	1	.8755	.89634	4.98325	1.91713	-.1	9.3020
473000	31	3	6.2934	.45535	8.38394	.75640	-.1	10.0879
473200	14	1	1.2892	.85116	6.21468	1.19665	-.1	8.9104
473500	23	4	8.4054	.34970	8.90133	.75272	-.1	10.5970
473600	14	2	1.4748	.83164	5.92294	.52982	-.1	7.1165
478200	19	1	2.7473	.70935	6.08320	1.32491	-.1	9.0678
478500	17	4	4.9698	.53729	8.04938	1.01245	-.1	10.3301
478600	13	2	-.9943	1.13234	4.26623	.76100	-.1	5.9806
479200	15	2	-.6733	1.08780	3.84785	1.10386	-.1	6.3345
480000	33	2	4.4092	.57629	7.26604	.85564	-.1	9.1935
480500	52	2	6.2785	.45621	8.37128	.70321	-.1	9.9554
481500	44	2	5.3422	.51285	7.87392	.83814	-.1	9.7620
481700	14	2	2.3321	.74714	5.68715	.97445	-.1	7.8823
481750	20	1	5.1705	.52398	7.24278	1.26435	-.1	10.0910
481800	14	4	-1.8971	1.26762	3.21740	.97123	-.1	5.4053
482000	38	2	7.4157	.39575	8.40973	.68755	-.1	9.9586
482200	18	3	1.8946	.78913	6.34984	.76745	-.1	8.0787
482330	16	1	-.2095	1.02653	4.57800	.83331	-.1	6.4552
482350	14	3	1.4771	.83140	5.24989	1.16165	-.1	7.8668
482370	16	4	1.6639	.81222	5.12578	1.26734	-.1	7.9807
482400	16	2	2.7850	.70601	5.95034	.79946	-.1	7.7513
482410	12	1	1.9796	.78079	5.53334	.65301	-.1	7.0044
482420	12	4	3.2772	.66389	6.02886	.79508	-.1	7.8200
482480	13	2	1.0783	.87390	3.98370	1.91759	-.1	8.3035
482500	65	1	7.7062	.38164	8.55572	.65808	-.1	10.0382
483025	14	1	1.0080	.88162	4.67678	1.57128	-.1	8.2164
483030	16	2	.7467	.91088	6.77421	.66084	-.1	8.2629

We computed at-site estimates of the 10-year flood for each station from the log-Pearson III distribution (Hydrology Subcommittee, 1982) using a fixed coefficient of skewness of -0.1 for all stations. The cross correlation of individual peaks at different sites in this region tends to be small because of the localized nature of the summer thunderstorms. The correlation coefficients p_{ij} were estimated on the basis of computed sample correlations and good judgment. From the total 947 pairs of stations, correlation coefficients p_{ij} were estimated on the basis of computed sample correlations and good judgment. From the total 947 pairs of stations, 3 were classified as having high correlation, 41 as having medium correlation, and 903 as having slight correlations. The assigned coefficients were 0.7 (for high correlation), 0.4 (for medium), and 0.15 (for low).

Table 1. Data used in regression analyses—Continued

Station	Years of record	Subset	ln (A)	(A)$^{-0.125}$	Mean of ln(Q)	Std dev of ln(Q)	Regional skew	ln (Q$_{100}$)
483040	17	1	-.7765	1.10193	4.44813	1.00324	-.1	6.7081
483100	23	4	3.7612	.62491	7.08459	.88005	-.1	9.0671
483200	16	1	.7129	.91474	4.57478	.90883	-.1	6.6221
484000	51	1	3.5695	.64006	6.96048	1.02189	-.1	9.2625
484200	16	3	2.7912	.70546	5.72354	1.00162	-.1	7.9799
484500	21	3	5.3890	.50986	7.53774	1.24662	-.1	10.3460
484560	15	2	5.6664	.49248	7.59208	.86163	-.1	9.5331
484570	18	3	3.6480	.63381	6.68993	1.14531	-.1	9.2700
484580	15	4	2.6462	.71837	6.16080	1.08245	-.1	8.5992
484590	14	3	3.92199	.61247	7.25153	1.21392	-.1	9.9861
484600	25	4	6.12469	.46506	8.11592	1.06103	-.1	10.5061
485000	30	2	3.80226	.62171	6.81542	1.29912	-.1	9.7420
485500	17	1	6.40027	.44931	7.55386	1.25859	-.1	10.3891
485900	18	1	1.59535	.81921	4.10827	1.09557	-.1	6.5763
485950	18	3	.76584	.90871	4.77050	.98044	-.1	6.9791
486000	67	4	6.82219	.42623	8.48134	.76423	-.1	10.2029
486300	19	1	5.52146	.50148	7.83547	1.04906	-.1	10.1987
486500	40	3	8.16128	.36054	9.04386	.51923	-.1	10.2135
486700	13	4	1.96431	.78228	4.95056	.60719	-.1	6.3184
486800	15	1	6.13772	.46430	8.39592	.75318	-.1	10.0926
487000	18	3	6.65424	.43527	8.25016	.60328	-.1	9.6092
487100	14	3	2.47643	.73377	6.65355	.75248	-.1	8.3487
487140	12	4	-.79851	1.10497	5.23262	.75571	-.1	6.9350
487400	11	3	.89202	.89449	5.08088	.97607	-.1	7.2797
488500	26	4	7.48550	.39232	7.06963	1.08866	-.1	9.5221
488600	13	2	2.54942	.72711	5.59482	1.07277	-.1	8.0115
514200	16	3	5.99892	.47243	7.23610	.91735	-.1	9.3026
519600	17	2	.88788	.89495	5.96231	.82179	-.1	7.8136
519750	17	1	4.23121	.58925	6.03738	1.66592	-.1	9.7902
519760	16	3	4.83635	.54632	6.18290	1.63000	-.1	9.8548
519780	14	3	2.55725	.72640	7.63422	.55124	-.1	8.8760
520100	17	3	2.16328	.76307	4.84464	1.55632	-.1	8.3506
520110	16	3	-.82087	1.10806	4.79628	.56621	-.1	6.0718
520130	16	4	1.55180	.82368	6.23056	.74811	-.1	7.9158
520160	15	4	.77933	.90718	5.43364	.86117	-.1	7.3736
520170	13	4	5.49307	.50327	8.01898	.56045	-.1	9.2815
520200	15	4	2.49322	.73224	5.96485	.61940	-.1	7.3602
520230	16	4	.39878	.95137	4.56925	1.44165	-.1	7.8169
520300	15	3	-.10546	1.01327	5.09907	.72554	-.1	6.7335
535100	11	4	6.34388	.45249	6.99848	1.25376	-.1	9.8228
535200	15	1	2.50144	.73148	7.41340	.46927	-.1	8.4705
536100	12	4	-.21073	1.02669	4.74102	.95350'	-.1	6.8890

Hydrologic Models

Our objective is to estimate the 100-year flood peak at ungaged sites for which only drainage-basin characteristics are available. The most commonly used basin characteristic is drainage area, or contributing drainage area. The logarithms of the variables in question commonly are assumed to be linearly related, so that a simple model is

$$\ln Q_{100,i} = a + b \ln A_i + e_i , \qquad (10)$$

where $Q_{100,i}$ is the 100-year peak at station i, A_i is the contributing drainage area at station i, e_i is an error term, and a and b are constants to be estimated. This model assumes that $\ln Q_{100,i}$ and $\ln A_i$ are linearly related. Unfortunately, even at gaged sites, only an estimate $\hat{Q}_{100,i}$ of the 100-year flood $Q_{100,i}$ is available; therefore, the former values must be used to select a model and estimate its parameters. Substitution of $\hat{Q}_{100,i}$ in equation 10 results in a need for GLS estimation procedure because each $\hat{Q}_{100,i}$ may not have the same variance, and cross correlation between pairs of sites is likely.

A plot of $\ln Q_{100,i}$ versus $\ln A_i$ (fig. 2) for the 89 stations suggests a relation that is slightly curvilinear, rather than the straight line implied by equation 10. Such a pattern might result from differences in channel slope—for example, if slope were correlated with drainage area. The relation could then be adequately described by a multiple linear regression among the logarithms of the data. For this region, however, Eychaner (1984) found that additional linear variables were insuf-

ficient to describe the nonlinearity; he found a better OLS fit to the data using the second-order polynomial:

$$\ln Q_{100,i} = a + b \ln A_i + b_2 (\ln A_i)^2 + e_i . \quad (11)$$

A second method is to use a transformation other than logs to deal with the nonlinearity. Figure 3 shows a plot of $\ln(Q_{100,i})$ against $(A)_i^{-0.125}$.
This plot shows an approximately linear relationship

$$\ln Q_{100,i} = a^* + b^* A_i^{-0.125} + e_i^* . \qquad (12)$$

We selected the exponent -0.125 by iteratively selecting exponents and plotting until the plot appeared approximately linear.

One can estimate the parameters of either the model in equation (11) or that in equation (12) by using the GLS method described above.

Measures of Model Error

If a regression model is used for prediction, we are interested in how well the regression estimate, $x_o\beta$, at site with basin characteristics x_o predicts the true value, y_o, at that site. We may think of the variance of prediction γ_p^2 as made up of model-error variance (the variance of the values of $\mu_i + z_p\sigma_i$ values about the true regression line) and the sampling-error variance (the variance of the sample regression line about the true regression line). This follows from the relationship:

$$\gamma_p^2 = E(y_0 - x_0\hat{\beta})^2 = E(y_0 - x_0\beta)^2 +$$
$$E(x_0\beta - x_0\hat{\beta})^2 . \qquad (13)$$

Figure 2. Relation of $\ln Q_{100}$ to $\ln A$ for 89 stations in Pima, County, Ariz.
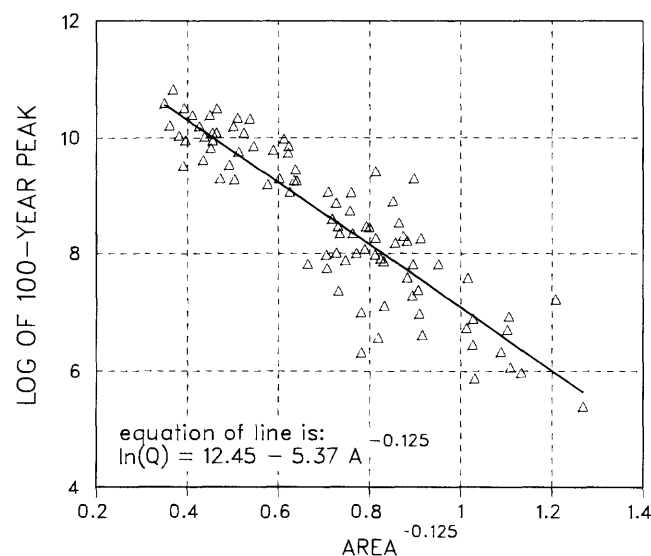
Figure 3. Relation of $\ln Q_{100}$ to $A^{-0.125}$ for 89 stations in Pima County, Ariz.

In an ordinary least-squares analysis, the true model-error variance $E(y_o - x_o\beta)^2$ is assumed to be VAR(e_i), which is estimated by the sample regression residual mean-square error s_r^2. The sampling-error variance

$$E(x_0\beta - x_0\hat{\beta})^2 = x_0 \text{Var}(\hat{\beta}) x_0^T \qquad (14)$$

would be estimated by $s_r^2 (x_o (X^TX)^{-1} x_o^T)$. Thus, an OLS estimate of the prediction error (13) would be (Draper and Smith, 1981, p. 83)

$$\hat{\gamma}_{P\text{-OLS}} = s_r^2 (1 + x_0 (X^TX)^{-1} x_0) \qquad (15a)$$

Hardison (1971) recognized that this estimate (equation 15a) of γ_p^2 could be seriously in error when applied to a regression of streamflow characteristics based on relatively short and correlated records. He suggested, in different notation, that when all the sites have equal record length, γ_p^2 could be estimated as

$$\hat{\gamma}_{P\text{-HARD}} = s_r^2 (1 + x_0 (X^TX)^{-1} x_0^T) -$$
$$(1 - 2\rho) \bar{V}_T , \qquad (15b)$$

where ρ is the average interstation correlation coefficient of the dependent variables and $\bar{V}_T$ is the average variance of the time-sampling error at the stations used in regression.

In a generalized least-squares analysis, we obtain an estimator, $\hat{\gamma}^2$, of the model-error variance, γ^2, by solving equation 9, and the covariance of $\bar{\beta}$ is estimated by equation 8. As a consequence, a GLS procedures estimate of the variance of prediction becomes

$$\hat{\gamma}^2_{P\text{-GLS}} = \hat{\gamma}^2 + x_0 (X^T\hat{\Sigma}^{-1}X)^{-1} x_0^T . \qquad (16)$$

Stedinger and Tasker (1985) showed, by Monte Carlo experiments, that the GLS procedure (1) provided estimates of β with smaller prediction variances than the OLS procedure and (2) provided more realistic estimates of model error variance than the simple OLS procedure, equation 15a. The conclusions from that study are supported by the results of this split-sample experiment in which real data were used.

RESULTS

For each of the four subsets, parameter estimates were determined by means of OLS and GLS procedures for model 1 (equation 11) and model 2 (equation 12). Then for each subset, the 66 or 67 stations not used to estimate parameters were used as verification sets. The model's prediction of the average variance of prediction, $\bar{\gamma}_p$, based on the estimation data sets, was calculated in three ways. First, for OLS regression,

$$\bar{V}_{P\text{-OLS}} = s_r^2/n' \{n' ++ \sum_i x_i (X^TX)^{-1} x_i^T\} , \qquad (17)$$

where the summation is over the data in the estimation sets, and n' is the number of sites in the estimation sets. Second, also for OLS, Hardison's (1971) adjustment was calculated, so that

$$\bar{V}_{p\text{-HARD}} = \bar{V}_{p\text{-OLS}} - (1 - 2\bar{\rho})\bar{V}_T , \qquad (18)$$

where $\bar{\rho}$, the average interstation correlation coefficient was taken to be 0.1. For this analysis, $\bar{\rho}$ was calculated by first estimating the average cross correlation of the transformed flood-peak series, r, and converting it to $\bar{\rho}$ by the relationship

$$\bar{\rho} = \frac{\bar{r}(1 + 0.5K_p^2\bar{r})}{1 + 0.5K_p^2} , \qquad \text{(Stedinger and Tasker, 1985)} \quad (19)$$

where K_p is frequency factor for a Pearson III distribution. The $\bar{r}$ was estimated as 0.2 and K_p as 2.25, yielding $\bar{\rho}$ of 0.085, rounded to 0.1. $\bar{V}_T$, the average sampling error of at-site estimates, calculated as:

$$\bar{V}_T = \frac{1}{n} \sum_i [s_i^2/n_i(1 + 0.5K_p^2 (1 + .75G) + GK_p)] , \qquad (20)$$

where G is the skewness coefficient used to calculate Q_{100}, s_i is the sample standard deviation of annual peaks at site i, and n is the years of record i at site i. For the four subsets, $\bar{V}_T$ was 0.237, 0.222, 0.255, and 0.196, respectively. Finally, for GLS, the predicted average variance of prediction is

$$\bar{V}_{P\text{-GLS}} = \hat{\gamma}^2 + \frac{1}{n} \sum_i \{x_i (X^T\hat{\Sigma}^{-1}X)^{-1} x_i^T\} . \qquad (21)$$

For each of 4 sets, the parameter estimates are shown for model 1 in table 2 and for model 2 in table 3. For each model and verification set, the average mean-square error (mse) of prediction was calculated as

$$\hat{\text{mse}}_j = \frac{1}{n} \sum_i (\hat{y}_i - \hat{x}_i\beta)^2 , \qquad (22)$$

where the summation is over all stations not used in estimating $\hat{\beta}$, and N' is the number of such stations. To obtain an independent estimate of the model error γ^2, we subtracted the average time-sampling error for the verification sets from the estimated mean-square error to obtain an estimate of just the average variance of prediction for each verification $\hat{V}_{p\text{-VAL}}$.

On the basis of verification sets, the average variance of prediction for model 1 over all four sets was 0.200 natural log units squared for OLS and 0.190 natural log units squared for GLS. Similarly, for model

Table 2. Summary of results for model 1, $\ln(Q_{100}) = a + b_1 \ln(A) + b_2\{\ln(A)\}^2$
[---, no data]

| Subset | Method | Coefficients | | | Estimation set | | Verification set | |
		a	b_1	b_2	Average V_p	Adjusted V_p	n	Average V_p
1	OLS	7.3303	0.5899	-0.0217	0.681	0.491	67	0.152
	GLS	7.2657	.6498	-.0307	.456	---	67	.134
2	OLS	7.1480	.6210	-.0270	.392	.214	67	.168
	GLS	7.2403	.5842	-.0232	.208	---	67	.178
3	OLS	6.6540	.9342	-.0623	.219	.019	67	.315
	GLS	6.7185	.9120	-.0606	.149	---	67	.294
4	OLS	6.9812	.5881	-.0202	.487	.330	66	.163
	GLS	7.0197	.5864	-.0202	.309	---	66	.152

Table 3. Summary of results for model 2, $\ln(Q_{100}) = a + b\,(A)^{-0.125}$
[---, no data]

| Subset | Method | Coefficients | | Estimation set | | Verification set | |
		a	b	Average V_p	Adjusted V_p	n	Average V_p
1	OLS	12.4840	-5.1537	0.635	0.445	67	0.149
	GLS	12.4897	-5.1969	.414	---	67	.136
2	OLS	12.3330	-5.1849	.401	.223	67	.172
	GLS	12.2940	-5.0680	.173	---	67	.180
3	OLS	12.8254	-6.0072	.245	.041	67	.245
	GLS	12.7390	-5.8631	.138	---	67	.231
4	OLS	12.2198	-5.2389	.451	.294	66	.158
	GLS	12.2766	-5.2659	.276	---	66	.145

2, the average variance of prediction over all four sets was 0.181 for OLS and 0.173 for GLS. It is sometimes helpful to convert from square log units to percent by the transformation.

$$\overline{SEp} = 100\,(\text{Exp}(\overline{V}_p)\,-1)^{1\cdot2}\,, \qquad (23)$$

where $\overline{SEp}$ is the average standard error of prediction, in percent. On the basis of the verification sets, $\overline{SEp}$ for OLS and model 1 is 47 percent, $\overline{SEp}$ for GLS and model 1 is 46 percent, $\overline{SEp}$ for OLS and model 2 is 45 percent, and for GLS and model 2 is 43 percent. These results indicate that, regardless of which model was used, the GLS method yielded, on the average, slightly smaller standard errors of prediction. This is the same conclusion drawn by Stedinger and Tasker (1985) from the Monte Carlo results.

Another important issue to examine is which of the three methods (OLS, OLS with Hardison's adjustment, or GLS) estimates the respective model's predictive ability most accurately. To answer this question, compare the $\overline{V}_p$ computed from the estimation data sets with $\overline{V}_p$ computed from the verification data sets. The average difference and average absolute difference between these $\overline{V}_p$'s were calculated for each model and each method (table 4).

Results in table 4 indicate that the GLS method provides the best estimate of a model's predictive ability. The results also indicate that Hardison's adjustment is preferred where OLS regression is used. In subset 3, $\overline{V}_{p\text{-OLS}}$ and $\overline{V}_{p\text{-GLS}}$ achieve their smallest values, and $\overline{V}_{p\text{-VAL}}$ achieves its largest values. Thus, apparently subset 3 contains a set of sites that the models fit relatively well, leaving sites that the models fit less well to the verification set.

Table 4. Differences between V_p computed from estimation datasets and V_p computed from verification datasets

Method	Model 1		Model 2	
	Average difference	Average absolute difference	Average difference	Average absolute difference
OLS	0.245	0.293	0.252	0.252
Adjusted OLS[1]	.064	.212	.070	.172
GLS	.091	.164	.077	.127

[1] V_p computed by method suggested by Hardison (1971).

CONCLUSIONS

Two conclusions can be made from this example. First, of the data sets considered, the differences between the model-parameter estimates (the values of β, or more specifically, a, b_1, b_2 and a^*, b^*) obtained with the OLS and GLS procedures are very modest. This reflects the fact that all sites had at least 11 years of data, and most had more than 20 years. This, coupled with the large model-error variance γ^2, meant that the sampling-error terms in equation 5 had relatively little effect on the analysis. In addition, most of the cross correlations seemed to be very small. Large differences can be expected where many (but not all) of the n_i are small and perhaps some cross correlations are larger (more than 0.8).

The second conclusion is that only GLS provides a nearly unbiased estimate of the true variance of prediction. By neglecting the time-sampling error present in available estimates of the 100-year flood peak, the OLS procedure substantially overestimates the true prediction variance. Nevertheless, with only 22 to 23 observations, all estimators of the variance of prediction are highly unstable. This is consistent with the results in Stedinger and Tasker (1985) which showed that the variance of their $\hat{\gamma}^2$ estimator is generally greater than would be the variance of a residual variance estimator with the corresponding number of degrees of freedom in an ordinary least squares analysis.

Stedinger and Tasker (1985) proposed a procedure to use GLS regression for regional hydrologic regressions. From a statistical standpoint, the method is satisfying because it deals with the problem of cross-correlated data and unequal variance between sites in a logical and sound manner. Limited application to real data reported herein indicates that the method has the potential to be satisfying from a practical standpoint as well.

REFERENCES CITED

Draper, N.R., and Smith, H., 1981, Applied Regression Analysis, (2nd ed.): New York, John Wiley and Sons, 709 p.

Eychaner, J.H., 1984, Estimation of magnitude and frequency of floods in Pima County, Arizona, with comparisons of alternative methods: U.S. Geological Survey Water-Resources Investigations Report 84-4142, 69 p.

Hardison, C.H., 1971, Prediction error of regression estimates of streamflow characteristics at ungaged sites: U.S. Geological Survey Professional Paper 750-C, p. C228-C236.

Hydrology Subcommittee, 1982, Guidelines for Determining Flood Flow Frequency Interagency Advisory Committee on Water Data: U.S. Geological Survey, Reston, Virginia.

Stedinger, J.R., and Tasker, G.D., 1985, Regional hydrologic analysis 1—ordinary, weighted, and generalized least squares compared: Water Resources Research, v. 21, no. 9, p. 1421-1432.

Application of Stable Isotopes to the Origin and Migration of Oil-Field Waters In Pleistocene Reservoir Rocks, Offshore Texas

By William W. Carothers, Joshua D. Cocker,[1] LeRoy M. Law, *and* Yousif K. Kharaka

Abstract

The stable isotope ratios of formation waters from Pleistocene reservoir rocks of the High Island 573 Field result from mixing of the original marine waters of deposition and a highly modified brine originating at depth. The original waters of deposition have isotopic compositions and concentrations of conservative dissolved inorganic constituents similar to those of ocean waters. The δD value for the deep brine (-18.8 per mil) indicates a water-rock isotope equilibration temperature of about 125 °C that originates from a depth of 4,500 meters below the sea floor. The concentration of chloride (99,000 milligrams per liter) and the Br/Cl ratio for this brine indicate dissolution of halite structures in the Louann Salt underlying the High Island Field.

Mixing of these two types of waters resulted from the migration of the deep brine updip and along faults in the field and into the shallower reservoirs. Concentrations of sodium, calcium, lithium, and chloride for these waters generally indicate that these constituents have acted essentially as conservative elements since middle Pleistocene time. These constituents are used, together with the δ^{18}O and δD values of the waters, to give approximately the same mixing proportions between the two end members.

INTRODUCTION

Studies of the origin and migration of oil-field waters are important for understanding the possible source rocks and migration of the associated petroleum. These studies are particularly important for determining the source of oil and gas from Pleistocene and other relatively young reservoir rocks located in the Gulf of Mexico. The age of the reservoir rocks and the temperature and pressure environments in these fields are clearly inadequate for generating their petroleum, which must have originated in deeper sediments.

_____

[1]Mobil Research and Development Corp., Dallas, Tex.

Stable isotope ratios of formation waters provide valuable information for interpreting their origins and the processes that modify their chemical compositions following deposition. The values of δ^{18}O and δD subsurface waters have been used to distinguish waters of meteoric origin from connate waters that were entrapped in sediments at the time of deposition. A number of processes, however, may modify the original isotopic composition of the subsurface waters, and we must take them into account in interpreting origin of waters. Significant modifying processes include mixing by influx of waters of different origins, isotope exchange reactions between rock and water, and isotope fractionations that result from shale membrane filtration effects (Kharaka and Carothers, 1985).

Clayton and others (1966) used isotopic compositions of oil-field brines from the Illinois, Michigan, Alberta, and gulf coast sedimentary basins to show that the original connate waters have been flushed and replaced by recent meteoric waters. The δ^{18}O and δD values of the waters in these basins show both oxygen and hydrogen isotope shifts, but the line best fitting the isotope values from each basin intersects the meteoric water line (Craig, 1961) at a point equal to isotope compositions of present-day meteoric water of recharge.

Mixing of marine connate water and meteoric water was reported by Hitchon and Friedman (1969) to have produced the isotope ratios for the brines from the western Canadian sedimentary basin. This mixing interpretation was supported by mass-balance calculations for deuterium as well as concentrations of dissolved inorganic constituents. Kharaka and others (1973) reported that δ^{18}O values of oil-field brines from Kettleman North Dome, Calif., resulted from isotope-exchange reactions with carbonate cement and dissolved carbonate species. The δD values for the Kettleman brines suggest that two types of waters are produced at Kettleman; namely, shallow-meteoric waters concentrated in deuterium by shale membranes and deeper marine connate waters expelled from siltstones and shales that are depleted in deuterium.

The $\delta^{18}O$ values of marine connate waters from early and middle Cenozoic reservoirs of onshore northern Gulf of Mexico (Kharaka and others, 1977 and 1979) increase with increasing depth, whereas the δD values decrease with depth. The increase in $\delta^{18}O$ values with depth results from a greater degree of isotope exchange with the enclosing rocks. The decrease of δD values with depth was interpreted to result mainly from isotope exchange between the connate water and detrital clay minerals that have very light original δD values of about -70 per mil (Kharaka and Carothers, 1985).

Results of oxygen and hydrogen isotope studies for formation-water samples from the offshore Gulf of Mexico High Island 573 Field are described in this report. The reservoir rocks in this field are sandstones of early and middle Pleistocene age. The isotope data are combined with selected chemical data to show that the composition of waters in the study area result from the mixing of the original marine connate waters of deposition and a more saline brine that has migrated updip and upward along faults into the producing reservoirs.

ACKNOWLEDGMENTS

GEOLOGIC SETTING OF THE HIGH ISLAND FIELD

The water samples for this study were collected from sandstone reservoir rocks of Pleistocene age in the High Island 573 Field (fig. 1). The field is stratigraphically and structurally complex, and each of the water samples is from a different reservoir.

The field is approximately 200 km southeast of Houston, Tex., near the edge of the continental shelf. The well locations and their relationship to the field's major fault are shown in figure 1. The major fault (fig. 1) is a growth fault with hundreds of meters of throw. The larger part of the field's petroleum reserves are in a complex, faulted rollover structure downthrown to this major fault. There are also reserves in a faulted anticlinal structure on the upthrown side. The Pleistocene sediments in the area consist of interbedded sands and shales that were deposited in a deltaic environment (Caughey, 1975). The Jurassic Louann Salt mass is beneath the field (fig. 2) at a depth of about 5 km below sea level.

CHEMICAL ISOTOPIC ANALYTICAL TECHNIQUES

Stable oxygen and hydrogen isotopes of the water were determined after the samples, collected in the field, were filtered through 0.45 mm membranes. We used the method described by Epstein and Mayeda (1953) to obtain oxygen isotope ratios. Hydrogen released by passing the waters over uranium (Friedman, 1953) and also by reaction of the waters with zinc at 430 °C was analyzed for D/H (deuterium/hydrogen) ratios. Isotope abundances were determined by means of conventional isotope ratio mass spectrometry. The δ values are reported in per mil relative to SMOW (Standard Mean Ocean Water) with oxygen and deuterium δ values reproducible within -0.1 and -1 per mil, respectively. The δD values that we obtained using the zinc method are concordant (± 1 per mil) with those obtained using the uranium method. Samples for chemical analyses were collected, treated, and analyzed by means of the methods outlined by Lico and others (1982).

RESULTS OF CHEMICAL AND ISOTOPIC COMPOSITIONS OF HIGH ISLAND WATERS

The $\delta^{18}O$ and δD values for the waters of this study (table 1) range from -0.9 to 2.8 per mil and -1.2 to -18.8 per mil, respectively. The producing zones have measured subsurface temperatures that range from 49 to 98 °C (table 1). The chemical compositions of sampled waters and of average seawater are shown in table 2. Sample 83-TX-5 has the highest salinity (159,800 mg/L), which is more than four times that of seawater, whereas the salinity of the most dilute formation water is 38,600 mg/L, only about 10 percent higher than average seawater.

The variation of temperature with depth (fig. 3) shows a geothermal gradient of approximately 28 °C/km for the High Island Field. This gradient is similar to the gradient observed for the normally pressured zone (29 °C/km) in the Houston-Galveston area (Kharaka and others, 1977). The δD values versus subsurface temperatures for the samples of this study shown on figure 4 indicate extensive scatter of points, especially when compared with the δD values and subsurface temperatures (including regression line) for the deep formation waters from the Houston-Galveston gas and oil fields (Kharaka and others, 1977) also shown on figure 4. The δD values decrease (become isotopically lighter) as the $\delta^{18}O$ values increase (fig. 5). Figure 5 also shows the proportional mixing line between formation water sample 83-TX-5 and sample 83-TX-7.

Sodium concentrations for the High Island formation waters increase linearly as chloride concentrations
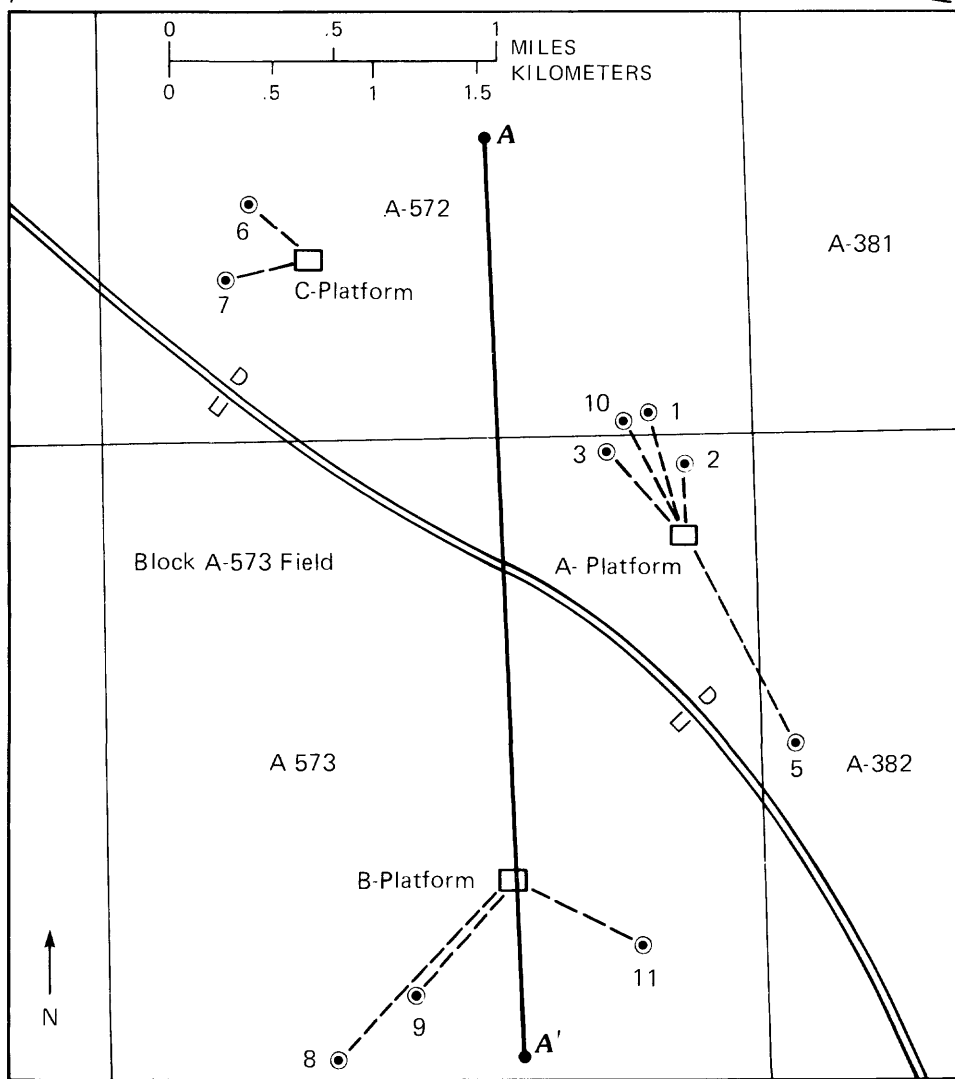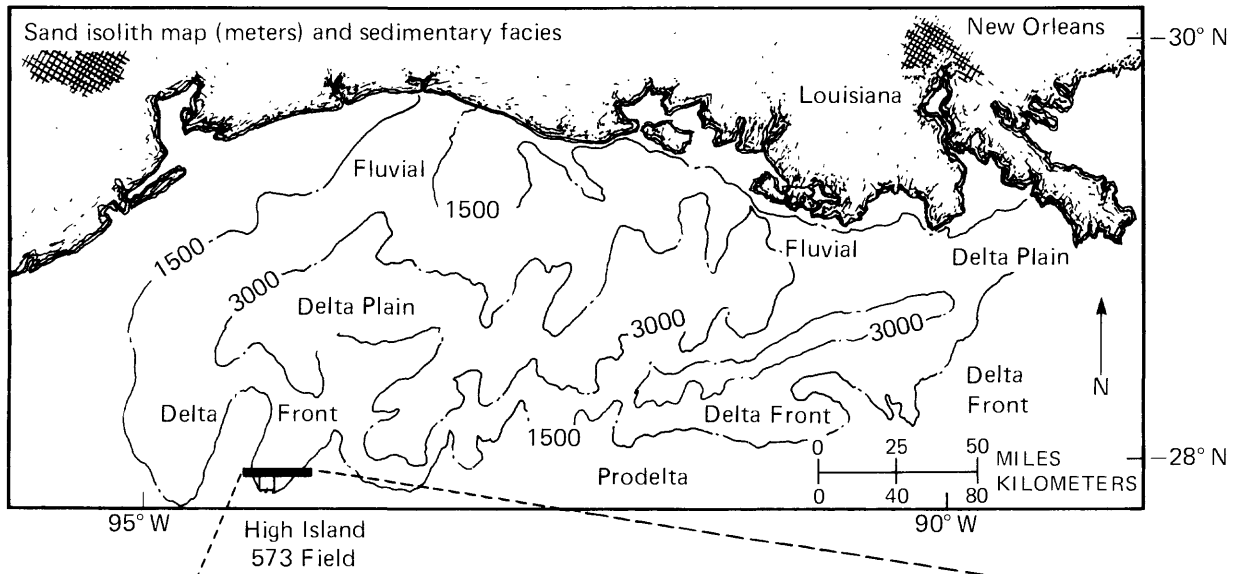
Figure 1. Location of High Island 573 Field. Well locations are shown in relation to the major faulting trend, indicated by the double line (sample 83-TX-12 from Block 571A not shown). Sand isolith (thickness in meters) and facies map modified from Caughey (1975). Cross section A-A' shown in figure 2.
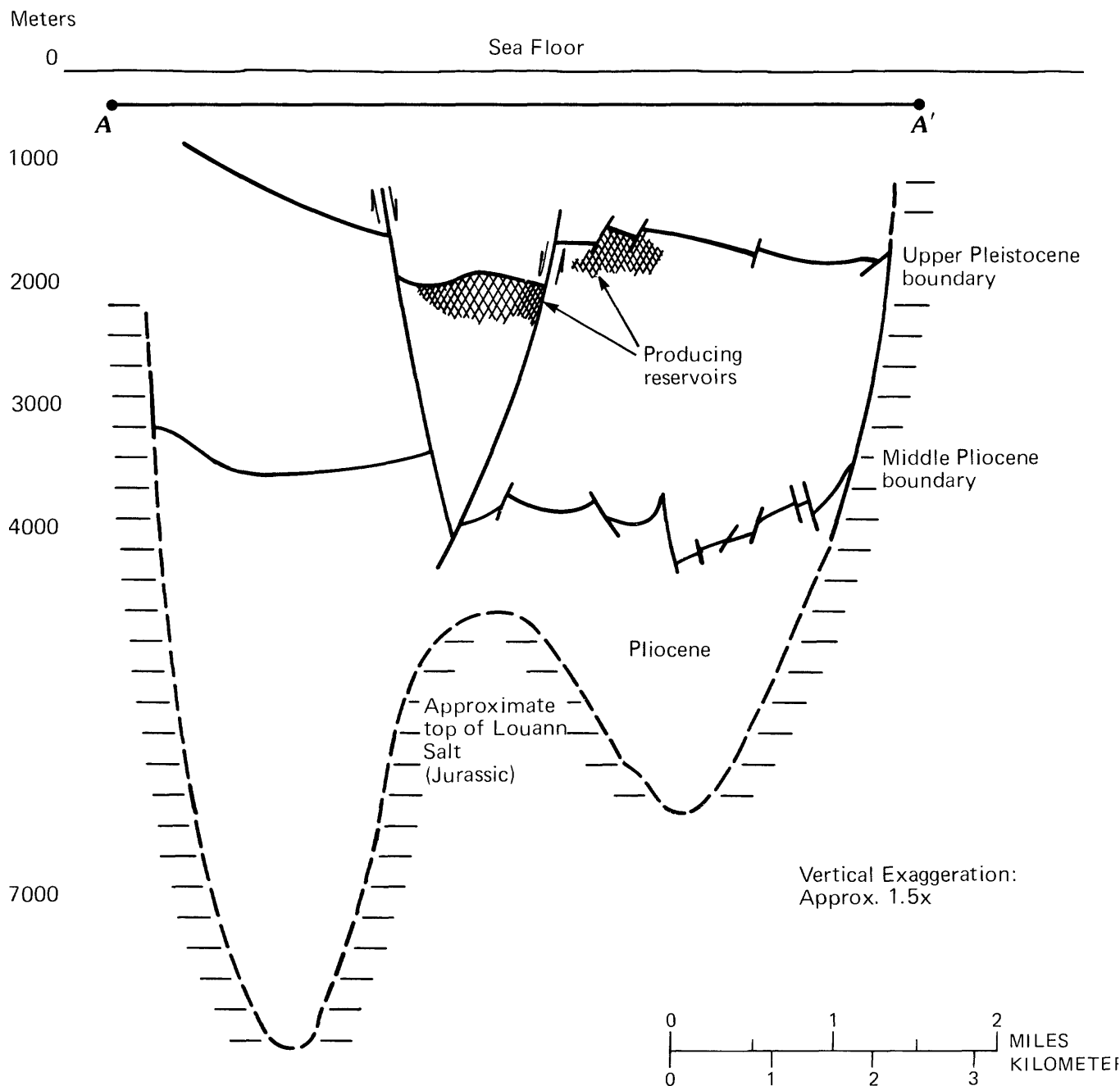
Figure 2. Schematic cross section through High Island 573 Field showing reservoir locations, faulted upper Pleistocene boundary, paleontologic markers (upper Pleistocene middle *Primosina* and middle Pliocene *Globoquadrina altispira*), and seismically estimated top of Louann Salt below sea floor. Trend of cross section A-A' shown in figure 1.

increase (fig. 6). Also shown on figure 6 are the proportions of sample 83-TX-5 that have mixed with the remaining samples. The $\delta^{18}O$ values of waters generally increase as chloride concentration increases (fig. 7). The linear relationship of decreasing δD values with in-

creasing chloride concentrations is shown on figure 8. The plots of chloride and bromide concentrations for these waters show generally that bromide is depleted relative to chloride compared to the seawater evaporation line (fig. 9).

Table 1. Well data and stable isotope ratios of formation waters from High Island 573 Field

Sample no.	Well name[1]	Depth (m)[2]	Temperature[3] (°C)	$\delta^{18}O$	δD
83-TX-1	A-11A	2,045	70	-0.1	-8.1
83-TX-2	A-11B	1,876	55	.4	-9.0
83-TX-3	A-10A	2,184	66	-.7	-7.0
83-TX-5	A-9A	2,140	67	2.8	-18.8
83-TX-6	C-8A	1,849	53	-.9	-1.2
83-TX-7	C-14A	1,838	52	-.9	-2.0
83-TX-8	B-14A	1,789	50	2.4	-15.2
83-TX-9	B-2A	1,741	49	-.2	-7.6
83-TX-10	A-14B	2,216	77	.3	-10.1
83-TX-11	B-12A	2,052	64	.1	-8.0
83-TX-12[4]	A-45-1	3,719	98	1.4	-11.7

[1] All water samples were taken from wells that primarily produce oil. All wells have water production greater than 50 barrels per day (50-850 bbl/d), and the range of gas/water ratios is low. Consequently, condensed water problems were specifically avoided.

[2] Depth is below sea level. Depth of water column approximately 75 meters.

[3] Temperatures were measured during bottom hole pressure surveys.

[4] Columbia Natural Gas Co. (Block 571A).

DISCUSSION

The original waters of deposition for the Pleistocene reservoirs of this study were marine (Caughey, 1975). The precise isotopic composition of the northern Gulf of Mexico deepwater mass of Pleistocene age is uncertain because of glacial effects. The mean $\delta^{18}O$ value of the ocean during the time of maximum Pleistocene glaciation has been reported (Emiliani and Shackleton, 1974; Williams and others, 1981) to vary from 0.4 to 1.6 per mil. Craig (1966) reports that during maximum Pleistocene glaciation ocean wide $\delta^{18}O$ and δD values would have increased by 1.0 and 7.4 per mil, respectively, from present day values. If all glacial ice were to melt, present $\delta^{18}O$ and δD values of the ocean waters would decrease by about 0.5 and 4.0 per mil, respectively (Craig, 1966).

Sample 83-TX-7 of this study represents water that has retained its near zero values for $\delta^{18}O$ and δD since entrapment during deposition (table 1). Also, the total dissolved solids, as well as the concentrations of sodium and chloride, for this sample are about equal to the concentrations of seawater (table 2), indicating only a small change in the concentrations of these elements since deposition.

However, major differences in chemical compositions exist between sample 83-TX-7 and seawater. The concentration of sulfate for 83-TX-7 is lower by about three orders of magnitude than that for seawater, and concentration of magnesium is about one third that of seawater. On the other hand, sample 83-TX-7 is enriched in calcium, strontium, barium, boron, bromide, iodide, and many other dissolved species relative to seawater

(table 2). Many of these differences, however, are those that would be expected from early stages of diagenesis of marine waters and some (including sulfate and magnesium depletions) are observed for interstitial waters from shallow cores of the Deep Sea Drilling Program (DSDP) (Gieskes, 1981). Other differences, such as bromide and iodide enrichment, can be attributed to bioconcentrators (seaweeds and corals) that were buried with the sediments and later leached by the surrounding waters to release bromide and iodide.

The sample that shows the maximum differences in isotopic and dissolved inorganic constituents from the original water of deposition is 83-TX-5 (table 1). Both the isotopic values and concentrations of dissolved constituents indicate that this brine has been produced from water in contact with the underlying salt deposits. Evidence from seismic data indicates that salt structures underlie the High Island area at a depth of about 5,000 m (fig. 2). The subsurface temperature at a depth of 5,000 m would be about 140 °C as shown from the geothermal gradient for High Island (fig. 3).

Both the $\delta^{18}O$ and δD values for the waters of sample 83-TX-5 are similar to the isotope values of deep formation waters from onshore Gulf of Mexico wells (Kharaka and Carothers, 1985). Results from these wells showed enrichment in ^{18}O and depletion in D for waters as depth of producing wells increased. Isotope-exchange reactions between the reservoir rocks and waters were cited to have modified the isotopic values of the marine waters of deposition. The plot of δD values versus subsurface temperature for their study of the Houston-Galveston deep formation waters (fig. 4) shows the

Table 2. Chemical analyses of formation waters from the High Island 573 Field

[Concentrations in milligrams/liter; alkalinity as HCO_3^-]

Sample no.	Total dissolved solids	Li	K	Na	Mg	Ca	Sr	Ba	B	Cl	Br	I	SO₄	Alkalinity
83-TX-1	74,000	1.8	160	26,300	788	1,320	97	77	23	44,400	143	4.0	12	494
83-TX-2	80,300	2.0	172	28,400	869	1,370	119	102	25	48,400	89	4.7	9.9	546
83-TX-3	60,700	1.7	139	19,800	287	1,030	59	75	31	33,400	102	4.5	16	568
83-TX-5	159,800	5.0	244	53,700	1,270	3,810	346	316	33	99,000	177	3.1	7.4	308
83-TX-6	43,700	0.6	110	15,400	499	679	36	40	16	26,200	102	5.1	9.9	480
83-TX-7	38,600	0.6	103	13,300	349	850	27	52	16	23,000	287	4.3	9.9	443
83-TX-8	137,800	4.9	250	47,700	1,040	2,840	238	256	40	84,600	91	4.6	0.5	293
83-TX-9	92,600	2.2	167	31,800	1,010	2,250	147	171	18	52,600	108	4.4	0.4	350
83-TX-10	62,800	1.8	143	22,300	365	1,130	66	90	37	37,700	185	5.6	15	460
83-TX-11	88,400	2.3	183	30,400	873	2,010	129	113	24	53,800	113	4.3	15	402
83-TX-12	90,700	5.5	271	30,900	482	2,690	146	200	42	53,300	118	6.2	12	2,140
Seawater[1]	35,000	0.2	380	10,500	1,350	400	8	0.03	4.6	19,000	65	0.06	2,700	142

[1] Composition of seawater from Goldberg (1963)
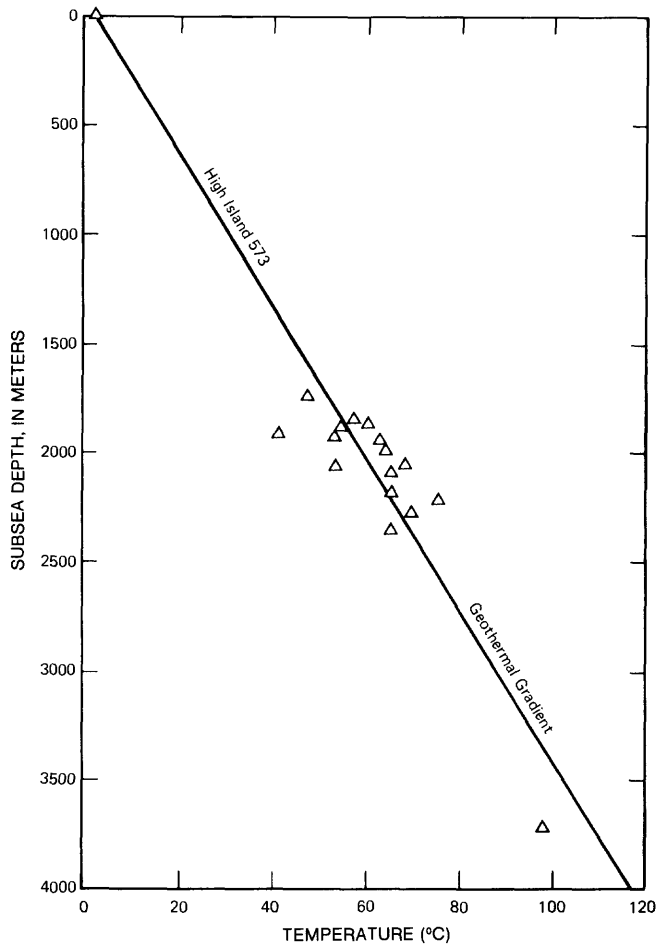
Figure 3. Geothermal gradient for the High Island 573 Field. Data points are from table 1 and selected producing wells (J.D. Cocker, Mobil Research and Development Corp., oral commun., 1984).

Figure 4. δD values of formation waters relative to Standard Mean Ocean Water (SMOW) plotted against subsurface temperatures. Solid line shows the Houston-Galveston δD isotope gradient.

linear regression line of decreasing δD values with increasing temperatures. Extrapolation of a δD value of -18.8 per mil for sample 83-TX-5 to the regression line of figure 4 shows a subsurface temperature of about 125 °C assuming 100 percent influx of water interacted with rocks at depth.

The chemical composition of sample 83-TX-5 indicates a water that has been modified by dissolution of evaporites; this finding supports the conclusion drawn from the isotope and seismic data presented above. The concentrations of sodium and chloride for sample 83-TX-5 are the highest values for these formation waters. These concentrations are similar to values reported for waters analyzed from deep wells and from reservoirs in contact with salt structures from onshore coastal Gulf of Mexico (Kharaka and Carothers, 1985). The Br/Cl ratio for sample 83-TX-5 also indicates dissolution of halite because the ratio is much lower (falls above the evaporation line) than that expected from evaporation of seawater (fig. 9).

MIXING OF FORMATION WATERS FROM HIGH ISLAND FIELD

Using the isotopic ratios and dissolved chemical compositions of sample 83-TX-7 (least modified water) and 83-TX-5 (highly modified water) as end members, we can explain the Pleistocene High Island reservoir formation waters as a mixture of these two types of waters.

The linear relationship between $\delta^{18}O$ and δD values for these waters (fig. 5) results from proportional mixing between the two end members mentioned above. The isotopic ratios for the waters are not temperature dependent because there is no correlation between δD or $\delta^{18}O$ values and subsurface temperatures
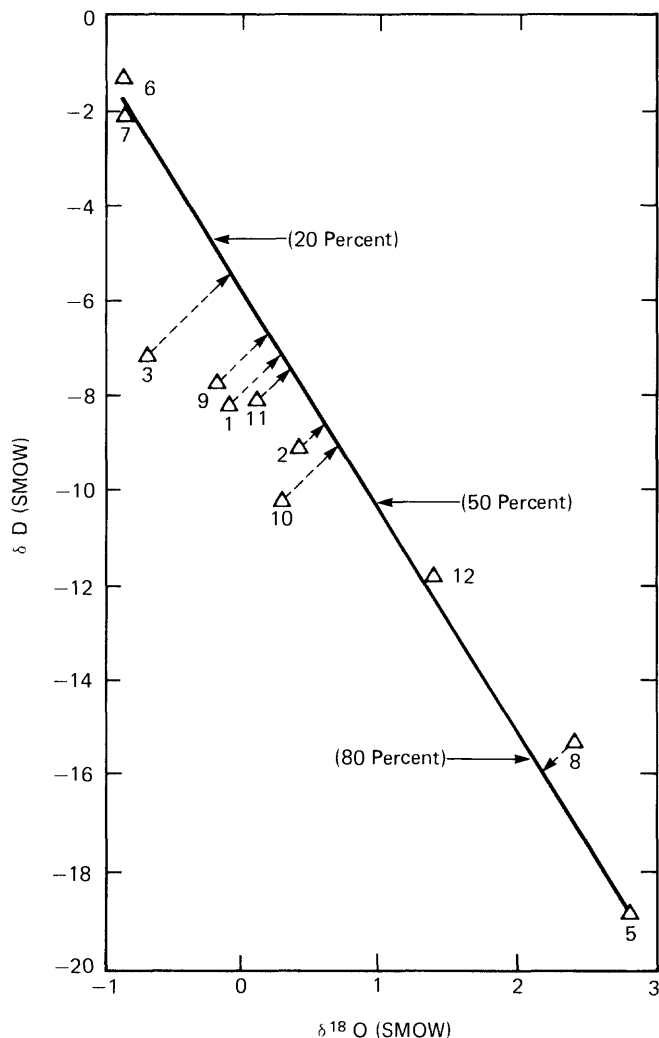
Figure 5. Plot of measured $\delta^{18}O$ and δD values relative to Standard Mean Ocean Water (SMOW). Solid line connects end members. Intermediate points, projected onto the mixing line, show percent mixing of deep brine (5) with original water of deposition (7).


Figure 6. Concentrations of sodium versus chloride. Solid line connects end members. Intermediate points, projected onto the mixing line, show percent mixing of deep water with water of deposition.

(fig. 4, table 1). The scatter shown in these figures results from mixing rather than possible exchange reactions between water and sediment. The reservoirs of the High Island area are all essentially similar in lithology and water-rock ratios (J.D. Cocker, Mobil Research Corp., oral commun., 1984). These facts suggest that extensive exchange reactions between sediment and water are not responsible for producing such a wide scatter of isotope ratios for the waters of the High Island area.

Analyses of dissolved chemical constituents for these waters also indicate mixing between the same end members. The concentrations of chloride, and to some extent sodium, are probably the best indicators of mixing in subsurface waters because of their high concen-

trations (least affected by minor changes) and their behavior as the most conservative elements in diagenetic reactions. As stated previously, chloride and sodium concentrations for sample 83-TX-7 are only slightly higher than concentrations of these ions in seawater (table 2). The highest concentrations of chloride and sodium, on the other hand, are observed for sample 83-TX-5 (table 2). An excellent mixing line is obtained for the remaining samples where concentrations of sodium and chloride are plotted together (fig. 6). The proportions of sample 83-TX-5 type water that has mixed with each of the remaining sampled waters are also shown on figure 6. The $\delta^{18}O$ and δD values for the waters and their concentrations of chloride plot in a linear manner with virtually the same amounts (-10 percent) of proportional
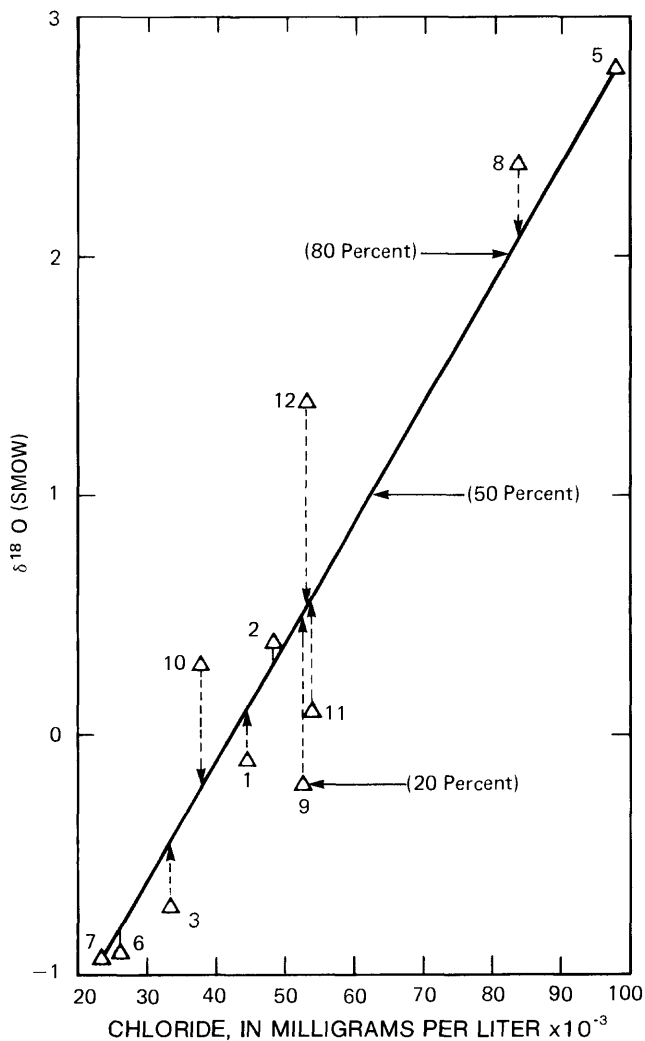
Figure 7. $\delta^{18}O$ values relative to Standard Mean Ocean Water (SMOW) and concentrations of chloride. Solid line connects end members. Intermediate points, projected onto the mixing line, show percent mixing of deep brine (5) with original water of deposition (7).

Figure 8. δD values relative to Standard Mean Ocean Water (SMOW) and concentrations of chloride. Solid line connects end members. Intermediate points, projected onto the mixing line, show percent mixing of deep brine (5) with original water of deposition (7).

mixing of the end members (figs. 7 and 8, respectively) as derived from the $\delta^{18}O$ versus δD plot (fig. 5). Furthermore, mixing lines with about the same proportions of the two end members are also obtained from plots of other inorganic constituents—namely, total dissolved solids, calcium, and lithium (table 2), where $\delta^{18}O$ and δD values indicate further evidence for the origin of the waters.

The fact that $\delta^{18}O$ and δD values and a number of chemical constituents can be used to calculate mixing between two end members indicates minimal isotopic exchange between water and sediments after migration. Note that $\delta^{18}O$ values for samples 83-TX-10 and 83-TX-12 plot above the line on figure 7; this indicates a posi-

tive shift in $\delta^{18}O$ values possibly due to some isotopic exchange. Figure 8 also shows that these two samples have δD values that plot farthest from the mixing line. Samples 83-TX-10 and 83-TX-12 showed the highest temperatures for the sampled waters of this study (77 and 98 °C, respectively), and this temperature range may be the lower limit where isotope exchange begins in these reservoirs. Isotopic exchange between rock and water probably produces the observed scatter for both $\delta^{18}O$ and δD values versus chloride concentrations; however, the results indicate that more time and higher temperatures are required for isotopic exchange between these waters and sediments.
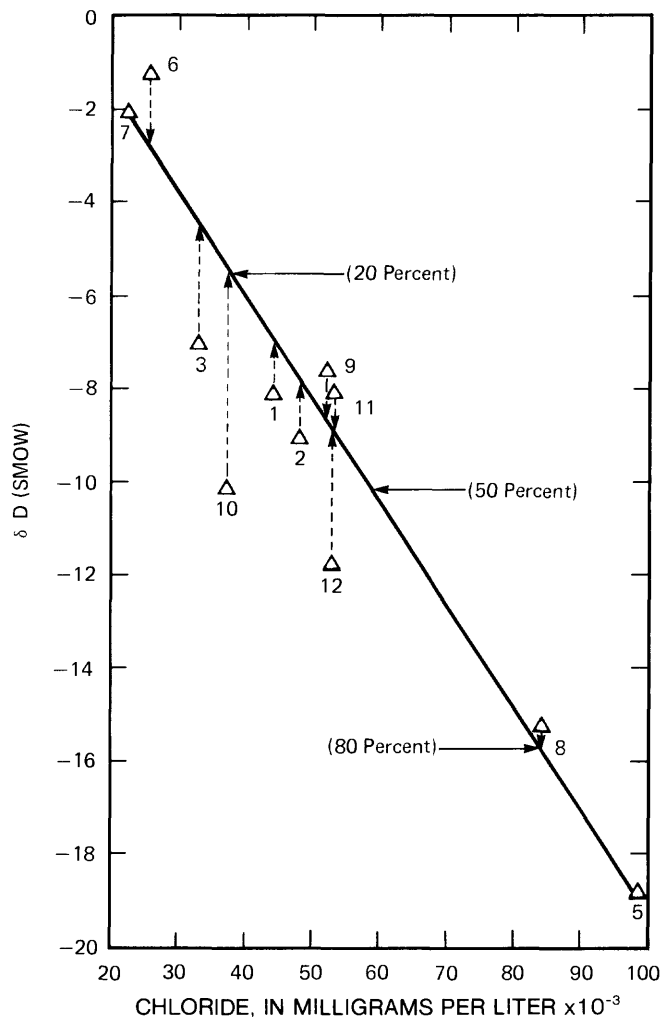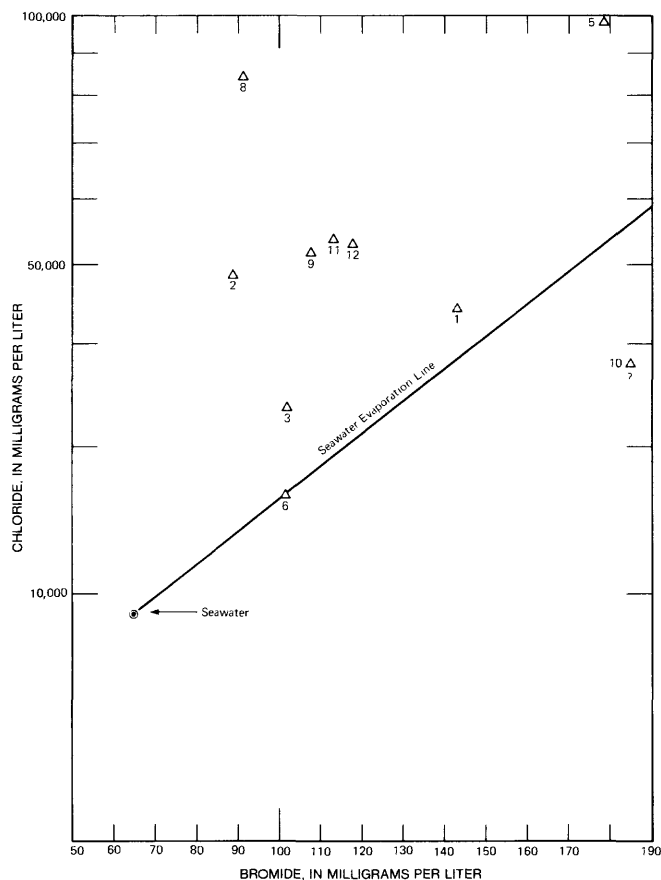
Figure 9. Plot of concentrations of chloride and bromide. The solid line is the evaporation line for ocean water. Values for sample 83-TX-7 not plotted (23,000 mg/L chloride and 287 mg/L bromide). High concentrations of bromide for this sample are not fully understood.

CONCLUSIONS

The stable isotope ratios for the formation waters of the High Island 573 Field result from proportional mixing of the original marine waters of deposition and deeper upward migrating connate brine that had interacted with halite deposits at depth. The isotopic compositions of mixtures of these two types of waters describe a straight mixing line for the plots of $\delta^{18}O$ and δD values for the remaining samples. Analyses of conservative dissolved chemical constituents of these waters also indicate mixing between the same end members of this study: concentrations of chloride, sodium, calcium, and lithium provide excellent mixing lines. The isotopic ratios for these waters are not temperature dependent and the retained isotopic signature of the water from depth suggests a minimum water-sediment isotope equilibration temperature of about 125 °C. The geothermal gradient for the High Island 573 Field indicates that this temperature correlates with a depth of about 4,500 meters below sea floor as the source for this deep brine.

REFERENCES CITED

Caughey,C.A., 1975, Pleistocene depositional trends and most valuable gulf oil reserves: Oil and Gas Journal, parts 1 and 2, September 8, p. 90-94, September 15, p. 240-243.

Clayton, R.N., Friedman, Irving, Graf, D.L., Mayeda, T.K., Meents, W.F., and Shimp, N.F., 1966, The origin of saline formation waters. I. Isotopic composition: Journal of Geophysical Resources, v. 71, p. 3869-3882.

Craig, Harmon, 1961, Isotopic variations in meteoric waters: Science, v. 133, p. 1702.

——— 1966, Isotopic composition and origin of the Red Sea and Salton Sea geothermal brines: Science, v. 154, p. 1544-1548.

Emiliani, Cesare, and Shackleton, N.J., 1974, The Brunhes epoch: isotopic paleotemperatures and geochronology: Science, v. 183, p. 511-514.

Epstein, Samuel, and Mayeda, Toshiko, 1953, Variations of $\delta^{18}O$ content of waters from natural sources: Geochimica et Cosmochimica Acta, v. 4, p. 213.

Friedman, Irving, 1953, Deuterium content of natural waters and other substances: Geochimica et Cosmochimica Acta, v. 4, p. 89.

Gieskes, J.M., 1981, Deep sea drilling interstitial water studies—Implications for chemical alteration of the ocean crust, layers I and II, in Warme, J.E., Douglas, R.G., and Winterer, E.L., eds., The Deep Sea Drilling Project, A Decade of Progress; 149-168.

Goldberg, E.D., 1963, Chemistry—the oceans as a chemical system, in Hill, M.N., ed., Composition of seawater, comparative and descriptive oceanography, v. 2, of The sea: New York, Interscience Publishers, p. 3-25.

Hitchon, Brian, and Friedman, Irving, 1969, Geochemistry and origin of formation waters in the western Canada sedimentary basin. I. Stable isotopes of hydrogen and oxygen: Geochimica et Cosmochimica Acta, v. 33, p. 1321-1349.

Kharaka, Y.K., Berry, F.A.F., and Friedman, Irving, 1973, Isotopic composition of oil-field brines from Kettleman North Dome oil field California, and their geologic implications: Geochimica et Cosmochimica Acta, v. 37, p. 1899-1908.

Kharaka, Y.K., Callender, E., and Carothers, W.W., 1977, Geochemistry of geopressured, geothermal waters from the Texas Gulf coast: Geopressured-Geothermal Energy Conference, 3rd Proceedings, University of Southwestern Louisiana, v. 1, p. 121-165.

Kharaka, Y.K., and Carothers, W.W., 1985, Oxygen and hydrogen isotope geochemistry of deep basin brines, in Fontes, J. Ch., and Fritz, P., eds., Handbook of environmental isotopes, v. 2: Amsterdam, Elsevier.

Kharaka, Y.K., Lico, M.S., Wright, V.A., and Carothers, W.W., 1979, Geochemistry of formation waters from Pleasant Bayou No. 2 well and adjacent areas in Coastal Texas: Geopressured Geothermal Resources Conference, 4th, Proceedings, Austin, Texas, p. 168-193.

Lico, M.S., Kharaka, Y.K., Carothers, W.W., and Wright, V.A., 1982, Methods for collection and analysis of geopressured geothermal and oil field waters: U.S. Geological Survey Water-Supply Paper 2194, 21 p.

Williams, F.D., Moore, W.S., and Fillon, R.H., 1981, Role of glacial Arctic Ocean ice sheets in Pleistocene oxygen isotope and sea level records: Earth Planetary Science Letters, v. 56, p. 157-166.

A Technique for Analysis of Ground-Water Systems at Regional and Subregional Scales Applied on Long Island, New York

By Herbert T. Buxton *and* Thomas E. Reilly

Abstract

A technique of ground-water flow modeling that enables representation of a ground-water system's hydrologic characteristics and applied stresses at regional and local scales is described in this report. The technique couples a regional model of an entire ground-water system, including its natural hydrologic boundaries, and a subregional representation designed to provide fine detail in and near the local area of concern. The regional model generates the water budget for the subregional area; the distribution of flow across the subregional boundary defines the boundary conditions for the subregional representation. The result, referred to as a coupled regional-subregional model, (1) predicts regional changes in ground-water levels and the distribution of water derived from natural boundaries, and (2) provides detailed prediction of changes in ground-water levels and the distribution of discharge to natural boundaries within the subregion.

An application of the technique to Long Island, N.Y., where it was used to estimate the effects of decreased recharge resulting from the installation of sanitary sewers, is discussed in detail. The results of steady-state and transient-state calibrations are presented. The coupled regional-subregional simulations give detailed response of ground-water levels and seepage to streams in the area of the sewer districts and still maintain an accurate representation of ground-water flow on an islandwide scale.

INTRODUCTION

Computer simulation, generally referred to as modeling, allows quantitative analysis of the effects of stresses on a ground-water flow system. Modeling requires representation of the characteristics of the continuous natural system with discrete numerical values. If the natural system is accurately represented in the numerical model, the simulation of specific hydrologic events or stresses will yield an approximation of the response of the natural system in terms of headwater and ground-water flow.

The model grid should, with a fully three-dimensional perspective, correctly represent the geometry of the ground-water system in a discrete form. In many places, this becomes complicated by aquifer heterogeneities and irregularly shaped boundaries found in natural systems. A conflict often arises where the investigation of a local problem requires a detailed representation of the ground-water system near the stress (subregional scale) because accurate simulation of ground-water flow rates and directions can be obtained only by representing the entire ground-water system to its natural boundaries (regional scale).

This report describes a ground-water flow-modeling technique that can be applied in the analysis of a problem that requires representation of hydrologic characteristics of regional and subregional scales. The technique offers an alternative to large variable-grid models that can be cumbersome both computationally and in terms of data handling, and that are less useful in applications other than the specific one for which they were designed. The technique was applied to estimate the hydrologic effects of decreased recharge in Long Island expected to result from the installation of an extensive network of sanitary sewers. The report, prepared in cooperation with the Nassau County Department of Public Works and Suffolk County Department of Health Services, New York, discusses the theory and methods used and some advantages and disadvantages of the technique as demonstrated by the Long Island application.

MODELING TECHNIQUE

The response of a ground-water system to stresses is controlled largely by its internal and external geometry and boundary conditions. On the local scale, however, its response is affected by irregularities in local geometry typically found in natural systems. In modeling analyses, the desired detail of response determines the scale of representation.

This technique allows model analysis of a ground-water system in which the hydrologic characteristics, the applied stress, and the desired detail of prediction require representation at both regional and subregional scales. Use of the technique requires a regional model of the entire ground-water system (fig. 1A) extending to its natural hydrologic boundaries and a subregion model represented at a finer scale to give detail in a local area of concern. The coupling of numerical simulations at these two scales combines the benefits of both by providing a generalized indication of the hydrologic response throughout the system and by estimating the response of ground-water levels and flow in detail within the area of concern.

Model Design

The design of the regional model must be consistent with its regional perspective (fig. 1B). The regional model can be used alone to assess the general effects of a stress applied anywhere in the system and gives the amount and distribution of water derived from natural hydrologic boundaries, which may be near or far from the stress.

The subregion in or surrounding the stressed area is substantially smaller (fig. 1A). The model grid for this subregion (fig. 1C) can incorporate the local details of the ground-water system and the distribution of the induced stress, thereby yielding a more detailed response. The subregional grid in this example has nine blocks for every regional grid block and can represent individual streams and the shoreline in greater detail than the regional grid.

The subregion contains only part of the hydrologic system. Although some of its boundaries may coincide with the natural boundaries that are represented in the regional model, others are artificial. (Artificial model boundaries do not coincide with real hydrologic boundaries; they are arbitrarily assigned and may align with geographic or other boundaries that have little or no relation to the hydrologic system.) The hydrologic conditions at an artificial boundary respond to changing aquifer conditions both within and beyond the boundary, which makes them difficult to approximate. Thus, the subregional representation by itself is not a model; it cannot accurately predict the system's response to natural or induced stresses by itself and is therefore referred to herein as a "subregional representation."

Method of Coupling

The coupling procedure uses a regional simulation to approximate the water budget for the subregional area; that is, it computes the quantity and distribution

of flow to both the natural and artificial boundaries in the subregional area. Water crossing the artificial boundaries of the subregion is derived from natural boundaries or storage outside the area. Conservation of the volume of water within the entire system and within the subregion is maintained by the regional simulation. The procedure for coupled simulations is summarized step by step as follows.

For steady-state conditions, the regional model simulates the hydrologic condition of interest to provide a coarse-scale estimate of ground-water levels and the distribution of flow within the system. The results are then used to calculate the distribution of flow (or change in flow), block by block, across the artificial boundaries of the subregion. The flow from each regional block is divided among the corresponding smaller blocks along the subregion boundary. The coupled regional-subre-
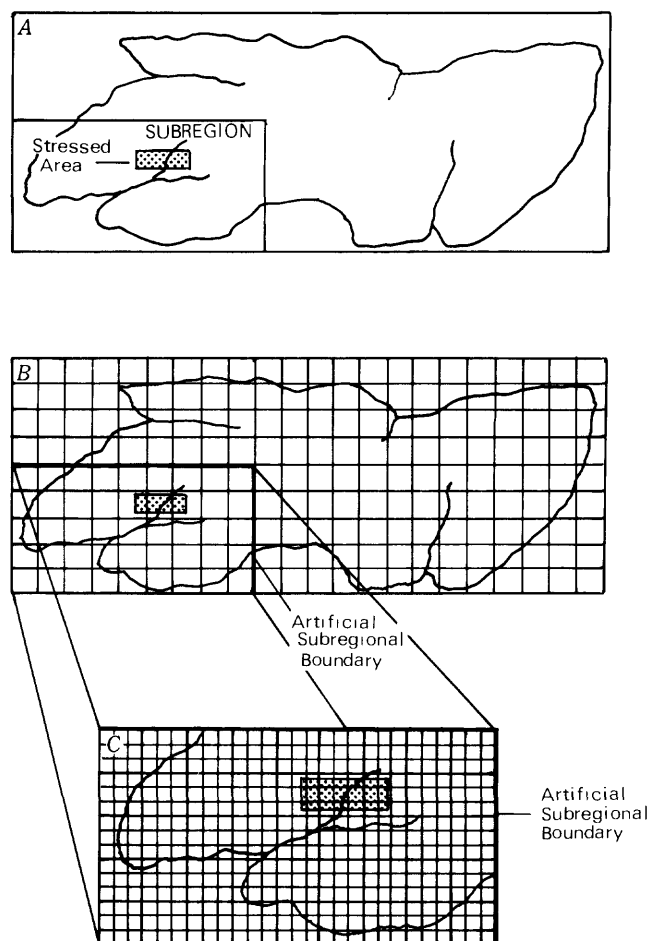

Figure 1. Conceptual representation of a hypothetical ground-water system: A, Location of induced stress and of subregion to be represented in detail. B, Regional-scale model grid for simulation of the entire ground-water system. C, Finer scale subregional grid for coupled regional-subregional simulation. Dark lines show coinciding regional grid.

gional simulation is then made from the subregional representation with the specified-flow boundary conditions predicted by the regional model.

In transient-state simulations, the procedure outlined above must be applied for each time step of the simulation and requires considerable care because both the rate and direction of ground-water flow across the subregion boundaries change through time. A regional simulation is made with appropriate time steps, generating the changes in water levels and flow at the end of each time step. The distribution of flow crossing the subregion boundary is then calculated, and the flow values are averaged over the time step and applied to a subregional simulation with the same time steps.

Grid Alignment

To facilitate the coupling procedure, we designed the subregion to correspond to a specific group of regional grid blocks, as shown in figure 1C. A major consideration in defining the coupled simulation is preserving the water balance developed by the regional model. Specifically, a balance must be kept between the total volumes of defined fluxes, either recharge or stress, in the subregional representation and in the coinciding area of the regional model. The finer detail in the subregion gives a better definition of the distribution of flow within the area, but the total volumes of flow must be equal or the basic concept of using the regional model to estimate the water budget for the subregion breaks down. If the subregion is defined as a specific part of the regional model, flow-boundary conditions for the artificial subregion boundaries can be estimated, and a consistent water budget can be maintained more easily.

The alignment of the regional and subregional grids is depicted in figure 2. The amount of ground-water flow between nodes A and B of the regional model flows through the vector volume, shaded in figure 2A. The finite-difference method used in this numerical representation approximates this flow at the face of the model block (the midpoint between the nodes). The subregional grid is aligned with the regional grid, as shown in figure 2B, such that the midpoint between nodes A and B of the regional model coincides with the border of active blocks in the subregional representation. This is consistent with the finite-difference approximation of flow entering the subregional area, where the flow is approximated at the midpoint between the outermost active node of the subregional grid and the next node if the grid were extended farther.

This alignment of regional and subregional grids allows the flow between nodes A and B of the regional model to be distributed among corresponding nodes in the subregional grid (fig. 2B).
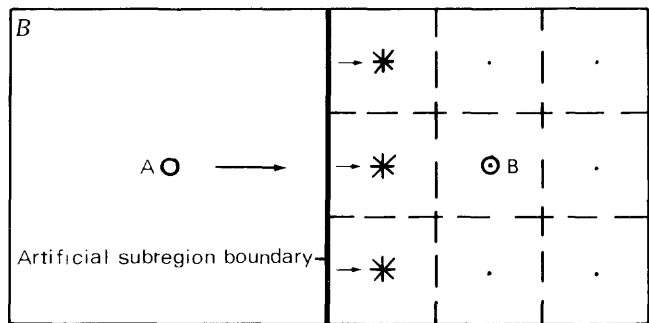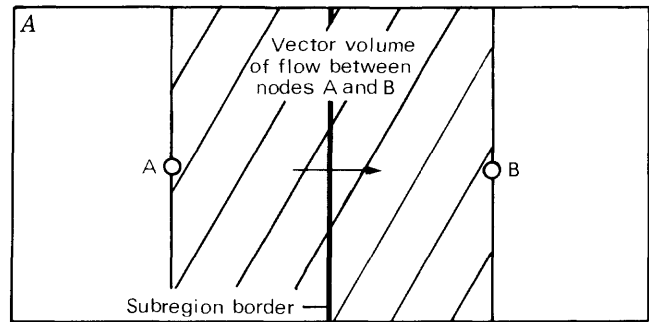

EXPLANATION

- Subregional grid nodes

O Regional grid nodes

✳ Subregional grid nodes among which flow between regional nodes A and B is distributed

⟶ Direction of ground-water flow

Figure 2. Comparison of regional and subregional grids: A, Part of regional model grid along border of subregion. B, Corresponding part of subregional grid showing alignment of grids.

APPLICATION OF TECHNIQUE TO LONG ISLAND

The ground-water reservoir on Long Island is the primary source of water for public supply and for industrial and agricultural use. Ground water also sustains the island's streams and wetlands, which are important for recreation and wildlife; ground-water discharge to the bays preserves a salinity necessary for the shellfish habitat. Continued development and urbanization over the past century have placed an increasing stress on the ground-water system.

Sanitary sewers have long been used in western Long Island to limit the amount of contamination entering the ground-water system through septic tanks and

similar domestic waste-disposal systems. The sewer networks collect a large amount of water, which after treatment is discharged to the ocean. This process diverts a large volume of water that provided substantial recharge to the ground-water system. The reduction in recharge has caused a lowering of ground-water levels and an attendant decrease in streamflow and subsea outflow to surrounding saltwater bodies (Reilly and others, 1983).

Construction of an extensive sanitary-sewer network in southern Nassau County Sewage Disposal Districts 2 and 3 (SDD-2, SDD-3) and Suffolk County Southwest Sewer District (SWSD) (fig. 3) is nearing completion (1986). The U.S. Geological Survey, in cooperation with Nassau and Suffolk Counties, undertook a modeling analysis to predict the hydrologic effects of sewering. The model discussed herein supplies detail in and around SDD-2 and SDD-3 in southern Nassau County, the location of the major part of the stress and its most severe effects. The results of the complete study are presented in a series of three reports (Reilly and others, 1983; Buxton and Reilly, 1985; Reilly and Buxton, 1985).

Hydrologic Considerations

The complete understanding of a hydrologic system necessary for the development of the ground-water

flow model includes definition of the system geometry, the natural hydrologic boundaries, the hydrologic coefficients of the major units, and the general patterns of ground-water movement. The Long Island hydrologic system has been described in many publications, for example, Franke and McClymonds (1972) and Franke and Cohen (1972).

System Geometry and Hydrologic Boundaries

The Long Island ground-water system consists of a layered sequence of aquifers and confining units that dips gently to the south and east (fig. 4). Crystalline bedrock forms the bottom of the ground-water system and is virtually impermeable. Overlying the bedrock are Cretaceous formations classified in the following hydrogeologic units in ascending order: the Lloyd aquifer, the Raritan confining unit, and the Magothy aquifer. Above the Cretaceous deposits is a series of interglacial and interstadial marine clays referred to herein as the south-shore confining unit. Overlying these units are glacial deposits consisting primarily of moraine and outwash. Several minor hydrogeologic units are also present but are not essential to this discussion.

The aquifers are units that have sufficient permeability to yield significant quantities of water to wells. The confining units, whose vertical hydraulic conduc-
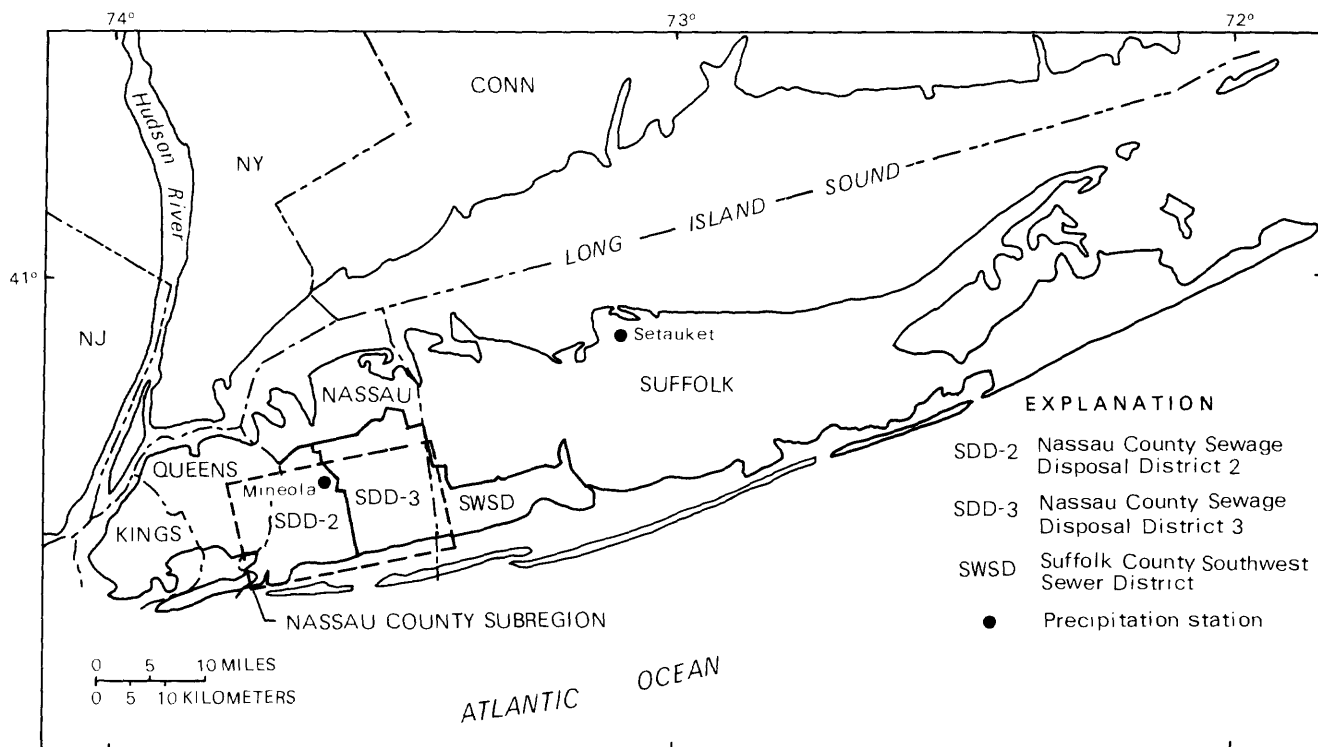
Figure 3. Location of sewer districts and Nassau County subregion.

tivity is three to four orders of magnitude lower than that of the aquifer units, separate the three major aquifers (fig. 4).

The fresh saturated ground-water system is bounded on the top by the water table and fresh surface-water bodies, on the bottom by impermeable bedrock, and on the sides by salty ground water or the saltwater bodies that surround the island.

Patterns of Ground-Water Movement

Precipitation infiltrating through the unsaturated zone to the water table is the only source of natural recharge on Long Island. Upon entering the ground-water system, the water remains in continuous motion. The path of flow from the water table to a point of discharge

is determined by the rate and areal distribution of recharge, the geometry and hydraulic characteristics of the aquifers and confining units, and the proximity and nature of the discharge boundaries. These factors together determine the three-dimensional distribution of hydraulic head and the actual paths of ground-water flow. Vertical patterns of ground-water flow are depicted in figure 4.

Much of the water that enters the ground-water system remains in the upper glacial aquifer, moves laterally, and discharges to surrounding saltwater bodies. The local configuration of the water table is influenced by patterns of shallow ground-water movement reflecting interaction with surface-water bodies. For example, where the water table intersects stream channels, they act as ground-water drains resulting in shallow,
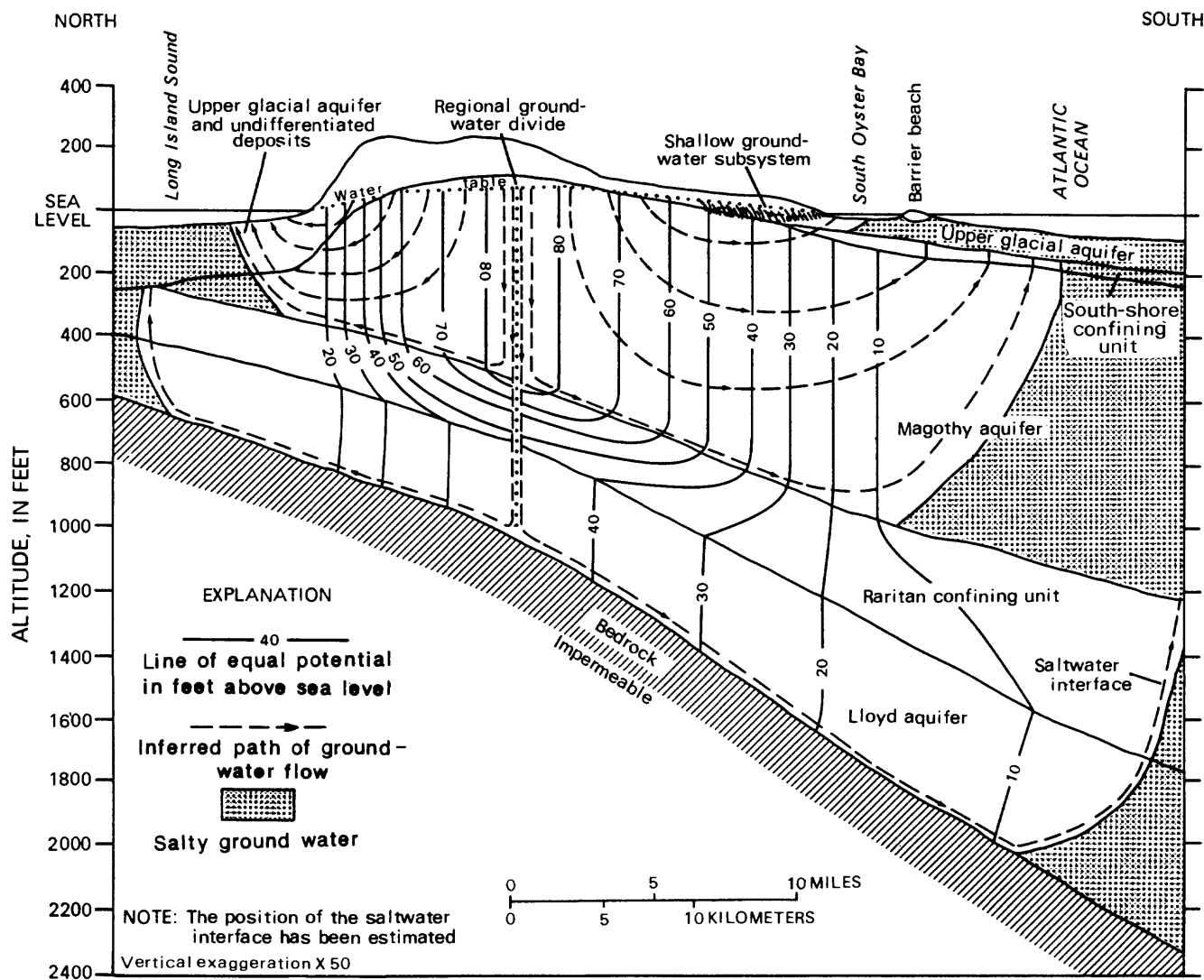
Figure 4. Generalized hydrologic cross section of ground-water system of Long Island under predevelopment conditions; located near Nassau-Suffolk border. (Modified from Franke and Cohen, 1972.)

small-scale ground-water flow systems (Prince, 1980; Harbaugh and Getzen, 1977; Franke and Cohen, 1972).

Some of the water that enters the system flows downward into the deeper aquifers (fig. 4). In areas of continuity between aquifers, the water moves freely, but in confining units it moves more slowly and is refracted toward the vertical. Water in the deeper aquifers generally moves toward the shore, where vertical gradients cause upward flow through the confining layer to the overlying aquifer. Where the overlying aquifer contains freshwater, the water remains in the ground-water system. Where the overlying aquifer contains salty water, the freshwater mixes with the salty water and is thus lost from the fresh ground-water reservoir. The resulting layered system, where fresh ground water extends farther seaward in the deeper aquifers, is depicted in figure 4.

Model Design

The area of primary interest in this investigation is in and adjacent to the area of the sewer network (fig. 3). The loss of recharge due to the sewer network is expected to cause a decline in ground-water levels and streamflow both within and considerably beyond the sewer districts.

To predict the magnitude and extent of these declines, a ground-water model must realistically represent the natural hydrologic boundaries yet supply local detail in the immediate area of the stress, especially near the shoreline and around the numerous gaining streams that flow to the south shore. The regional and subregional grids described in the following sections are intended to adequately represent both these scales.

Regional Design

A regional model (Reilly and Harbaugh, 1980; Getzen, 1977) represents the entire Long Island ground-water system including its natural hydrologic boundaries. The model grid has 29 rows and 76 columns, each block representing 6,000 ft in both horizontal dimensions (fig. 5A). The model divides the aquifer system into five separate layers (fig. 6B); the bottom three represent the Magothy aquifer (layers 1, 2, and 3), and the upper two represent the upper glacial aquifer (layers 4 and 5). The south-shore confining unit, where present, restricts flow between the upper glacial and Magothy aquifers (between layers 3 and 4, from the bottom).

The boundary conditions used in the Long Island regional model are approximations of the natural system boundaries, described previously; these boundaries are discussed in detail in Getzen (1977, p. 27-31) and Reilly and Harbaugh (1980, p. 24-26). A brief summary follows.

The upper (water table) layer is represented using the Dupuit assumptions for unconfined flow, a constant inflow rate equal to the appropriate recharge from precipitation. Streams, which are fed primarily by ground water, are represented as nonlinear head-dependent discharge boundaries. The amount of ground water seeping to the stream is determined by the head in the aquifer until the water table drops below the streambed altitude, when seepage stops and the stream dries up.

Ground-water discharge at the shore and upward from the Magothy aquifer through the south-shore confining unit (subsea outflow) is controlled by the head of surrounding coastal waters. Mean sea level is represented as a constant hydraulic head of zero. The lateral interface between fresh and salty ground water is represented as a no-flow (streamline) boundary. It is assumed that the abrupt difference in density across this boundary tends to keep the two fluids separate.

The top of the Raritan confining unit (fig. 4) is also represented as a no-flow boundary. The average thickness of this unit is 200 to 250 ft, and its vertical hydraulic conductivity is 3 to 4 orders of magnitude lower than that of overlying aquifers; therefore, only negligible quantities of ground water move through it (Franke and Getzen, 1976).

Subregional Design

The subregion comprises an area of almost 200 mi^2 in and around SDD-2 and SDD-3 in southern Nassau County (fig. 5). The horizontal grid pattern consists of a 54- by 51-block rectangle in which each block represents an area of 2,000 by 1,000 ft. Each regional grid block is represented by 18 (3 by 6) subregional grid blocks.

The vertical dimension is represented in four layers (fig. 6C), which is largely the same as the regional design except that the Magothy aquifer is represented by only two layers. Natural boundaries within the subregion include the water table, streams, the shore, and subsea boundaries. These boundaries are represented just as in the regional model. The top of the Raritan confining unit is considered a no-flow boundary, as in the regional model.

The remaining lateral boundaries do not coincide with natural hydrologic boundaries. The values of specified flow crossing these artificial boundaries are calculated from results of the regional model.

The fine subregional grid allows a more detailed representation of (1) the distribution of the sewering stress, (2) the irregular shoreline, (3) the many small gaining streams, and (4) the irregular thickness and northern limit of the south-shore confining unit, than does the coarse regional model grid (fig. 5). This in turn
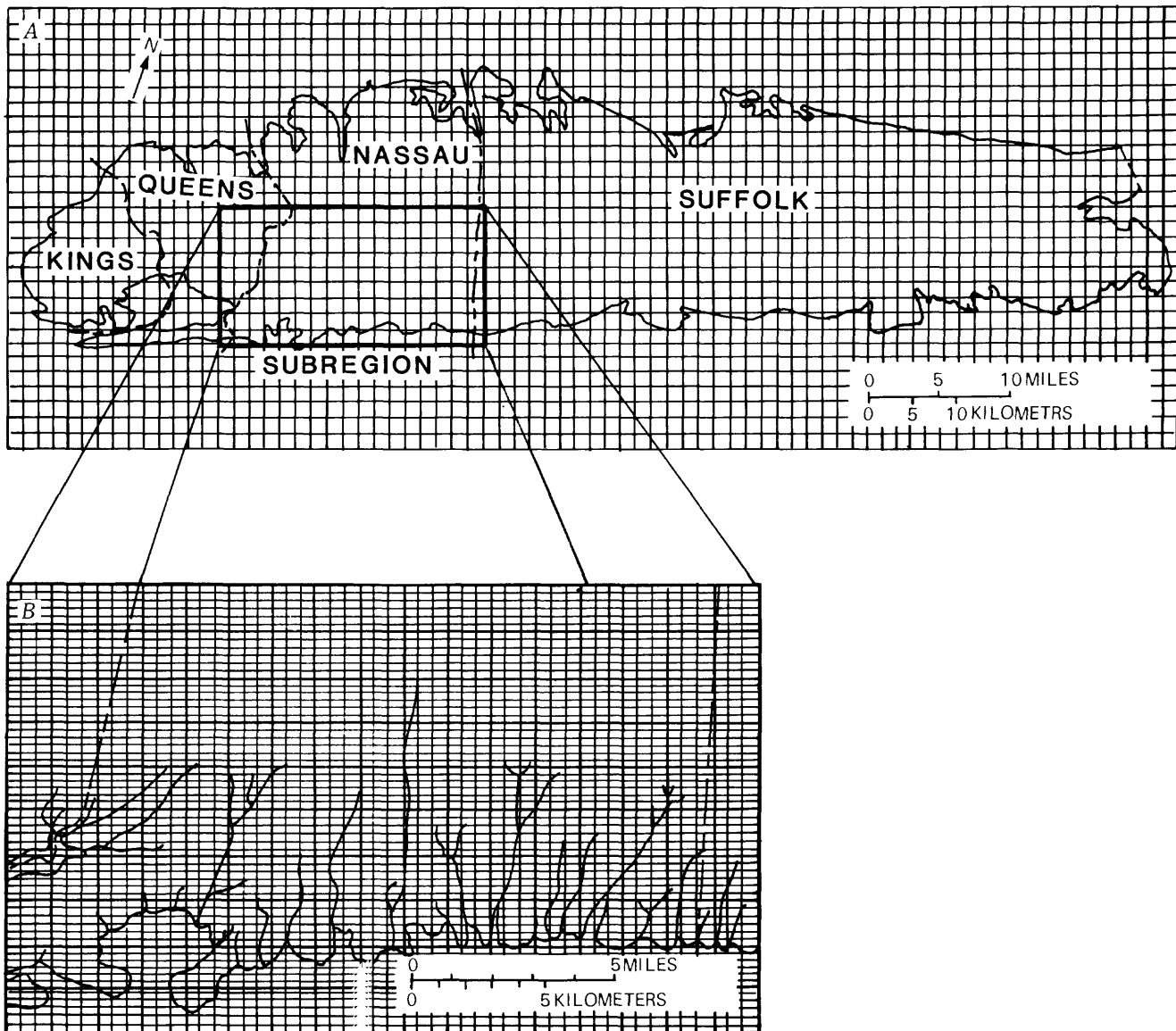
Figure 5. Model grids. *A*, The Long Island regional ground-water model. *B*, Nassau County subregion.

enables detailed predictions of local decreases in ground-water levels and base flow.

A data-collection program was conducted during 1978-79 to measure the magnitude and distribution of ground-water seepage to streams and to delineate the configuration of the south-shore confining unit; these data provided the information necessary to give the added detail within the subregion.

Model Calibration

Calibration entails the refinement of data that are used in the model to represent sources and sinks, boundary conditions, initial conditions, and aquifer properties. Continued comparisons between simulated results and observed data are used to assess the values that give the best representation of the system modeled. Basic to calibration is the assumption that when the model accurately represents the hydrologic system, simulation of a historic stress should accurately reproduce the observed water-level response.

The calibration strategy for the coupled regional-subregional model included two steady-state simulations and a transient-state simulation. The model was not used for prediction until the hydrologic conditions of both steady-state and transient-state simulations were correctly reproduced.

Steady-State Calibration

The steady-state calibration had two purposes. The first was to calibrate the model to a selected equi-

librium hydrologic condition in which the stress and response characteristics of the system are well documented. The second was to provide the steady-state simulation needed as the initial condition for subsequent transient-state simulations.

The steady-state calibration included the simulation of two separate conditions—those before the effects of man (predevelopment) and those during 1968-75. The predevelopment period represents the natural groundwater flow system without the effects of pumping, and the 1968-75 period represents present conditions. Only the latter simulation is discussed here.

The 1968-75 period was chosen for several reasons. (1) It is the only recent period during which the hydrologic system maintained a temporary equilibrium condition; (2) sufficient data on precipitation, pumpage, and base flow were available to define these components of the hydrologic budget; and (3) data on the configuration of the water table and potentiometric surface of the confined Magothy aquifer were available for comparison with model results.
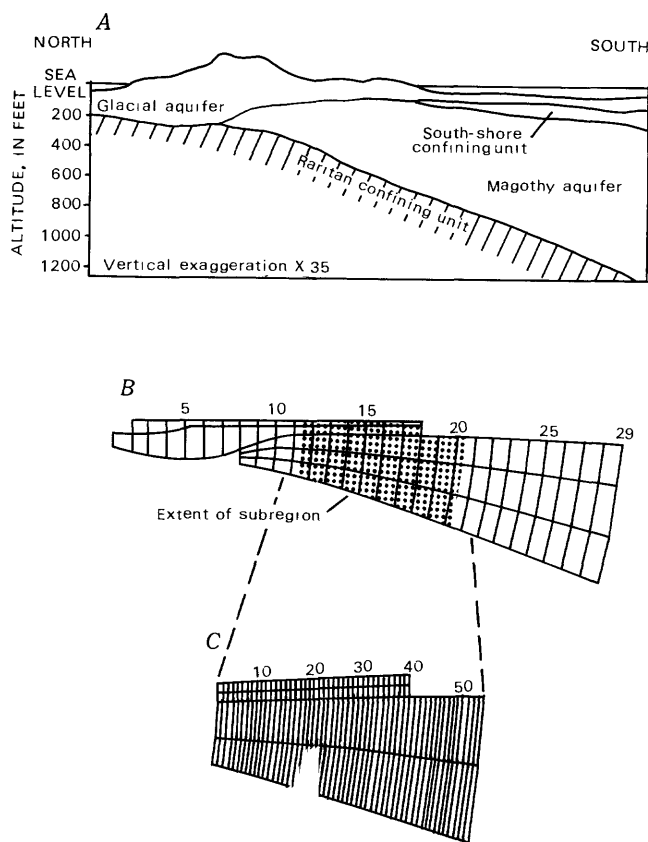
During the steady-state calibration, accuracy was assessed through comparison of heads in the upper model layer (layer 4, water table) with a water-table map for March 1972 (Vaupel and others, 1977), and by comparison of heads in the bottom model layer (layer 1, base of the Magothy aquifer) with a potentiometric-surface map of the Magothy aquifer for March 1972 (Vaupel and others, 1977). A comparison of model results with observed water levels in the upper glacial (water-table) aquifer (fig. 7) shows predicted groundwater levels and gradients similar to observed values. The effect of seepage to streams in the subregional area (fig. 7B) is apparent as V-shaped notches in the simulated water-table contours.

Discrepancy between simulated and observed water levels may in part be attributed to the flow boundaries calculated from the regional model. These errors may arise from either (1) differences between the scale of the regional and subregional grids or (2) differences in the coefficient values used in each.

Errors resulting from the difference in grid scale appear minor and are evident only close to the border of the subregional area, where discretization error from the coarse regional grid is transmitted via specified flow values. Errors resulting from the difference in hydrologic coefficients are more difficult to evaluate. The most significant refinements made in the subregional representation were in the delineation of the south-shore confining unit and the shore- and stream-discharge boundaries. The regional model accurately simulated the quantity and distribution of ground water crossing the artificial lateral boundaries of the subregion. It is assumed that the refinement of coefficients in the subregional representation refined the distribution of head and ground-water flow within the subregion but did not introduce error.

Transient-State Calibration

The transient-state calibration had three main goals. The first was to verify the data used in the steady-state calibration; the second was to evaluate data specific to transient model simulations, and the third was to evaluate the technique of using the regional model to calculate flux-boundary conditions for the subregional model during short-term transient simulations.

In the transient-state calibration, the model simulates fluctuations in saturated thickness, in confined and unconfined ground-water storage, and in ground-water seepage to streams.

The transient-state calibration entailed simulation of the response of the ground-water system to a severe decline in natural recharge in the early 1960's. During 1962-66, the cumulative deficiency below long-term mean annual precipitation (44.6 inches) totaled 41.7 inches, as measured at Setauket in Suffolk County (see

Figure 6. Vertical representation of aquifer system. A, Generalized hydrogeologic cross section of Long Island. B, Layered representation in regional model grid showing extent of subregion. C, Layered representation in subregional grid.
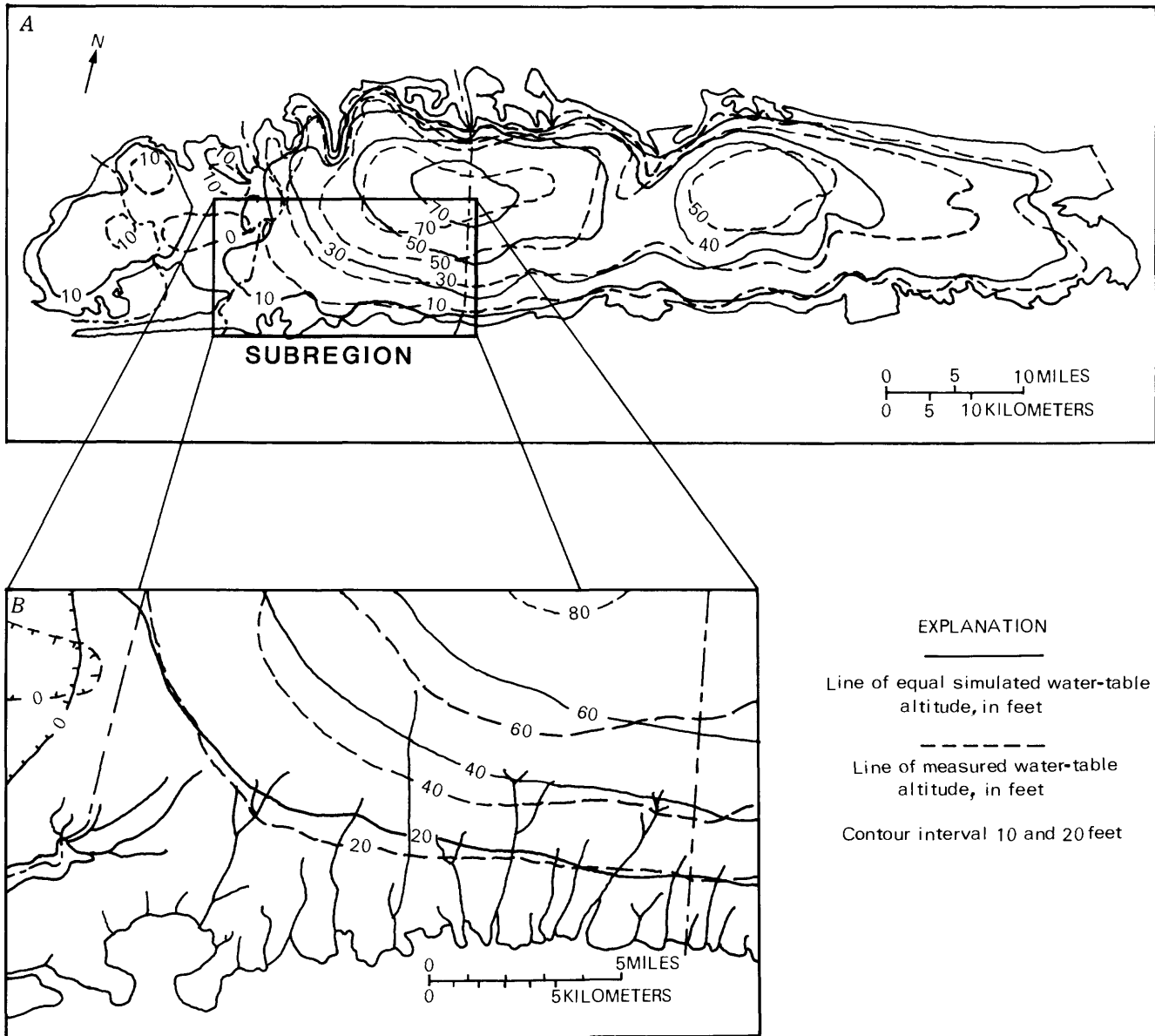
Figure 7. Comparison of water-table configuration as measured in March 1972 (from Vaupel and others, 1977) with that simulated for equilibrium period 1968-75: A, As simulated by regional model. B, As simulated by coupled regional-subregional model.

fig. 3). This decrease had a severe effect on the ground-water system. Flow in many Long Island streams was the lowest of record, and ground-water levels declined throughout the island; the maximum decline was about 10 ft in the central part of the island (Cohen, Franke, and McClymonds, 1969). The magnitude of this stress and the documentation of the response of water levels and streamflow through recovery made this hydrologic event ideal for testing the predictive capability of the model.

The predevelopment equilibrium condition simulated during the steady-state calibration was used as the

initial condition for this transient-state simulation. The 3 years (1959-61) preceding the drought were simulated to synchronize the computer simulation with the real system.

Because long-term average recharge from precipitation was used to define the initial condition for this simulation, changes from long-term average recharge were used as the stress. Changes in natural recharge during 1959-67 (fig. 8A) were calculated from a simple but consistent water-budget approach (Reilly and others, 1983). Factors considered in these calculations were monthly precipitation as recorded at Setauket and

Mineola (see fig. 3), estimated average monthly evapotranspiration, and estimated antecedent soil-moisture deficiency.

We assessed the accuracy of the simulation of the 1962-66 drought by comparing predicted and measured changes in ground-water levels and ground-water seepage to streams. Figure 8 compares simulated and observed changes in the average of water levels in seven key wells in the Nassau County subregion, the water level in an individual well (N1263), and the base flow of a major stream (Massapequa Creek, see fig. 9). The simulated changes in water levels and base flow reflect seasonal fluctuations as well as the general effect of the drought. Discrepancies are the result of small errors in defining initial conditions and some stresses that were affecting the system but were not applied to the simulation.

Model Application

After calibration, the coupled regional-subregional model closely reproduced both steady-state and the transient-state calibration conditions. The accuracy
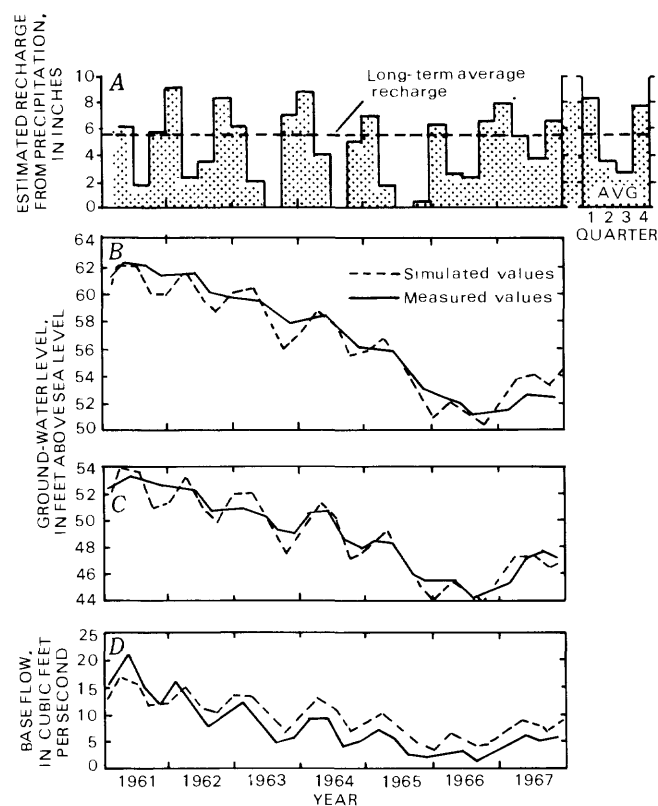
Figure 8. Graphs of hydrologic changes, 1961-67: *A*, Ground-water recharge. *B*, Average of water levels in seven key wells in the subregion. *C*, Water level in well N1263 (model row 24, column 40). *D*, Base flow in Massapequa Creek. (Locations shown in fig. 9.)

demonstrated in these simulations is an indication of the confidence that should be given to subsequent predictive simulations. The coupled model was then applied to predict the effects of proposed sanitary sewering in the vicinity of Nassau County SDD-2 and SDD-3 (fig. 3).

Description of Simulation

The stress being studied is the loss of ground-water recharge by the implementation of sanitary sewers, which intercept water that would otherwise be returned to the ground-water system through septic tanks and similar waste-disposal systems. The loss was estimated by county agencies to be 15.5 ft^3/s in Nassau County SDD-2, 80.9 ft^3/s in Nassau County SDD-3, and 43.3 ft^3/s in Suffolk County SWSD.

The total loss of 139.7 ft^3/s, or about 65 percent of the recharge from precipitation in the 200 mi^2 area of the sewer districts, was distributed according to population density.

The initial condition used for this predictive simulation was the 1968-75 steady-state calibration simulation. Thus, all predicted changes are relative to the conditions prevailing during 1968-75.

Results of Simulation

The predicted equilibrium effects of the sewering stress are presented in terms of ground-water levels and seepage to streams (base flow). The water-level decline predicted by the regional model is shown in figure 9*A*. The drawdown extends well beyond the subregion and is quite severe in its northeast corner. The calculated changes in flow across the subregion's artificial boundaries are large, as indicated by the large gradients along its border.

Results of the coupled regional-subregional model (fig. 9*B*) show that the most severe drawdown is in the eastern part of Nassau County, where it attains a maximum of 18 ft. The effect of streams is also evident; drawdown along stream boundaries is smaller because of reduced ground-water discharge to the stream.

The predicted decreases in base flow of the major streams in the subregional area, depicted in figure 10, are relatively uniform throughout the area; the total predicted decrease is 49.5 ft^3/s—an average decrease of more than 75 percent per stream. As a result, the streams will have a much lower average flow and will be shortened considerably.

EVALUATION OF TECHNIQUE

The application of the technique to Long Island demonstrates the importance of evaluating the regional characteristics and regional response of a ground-water
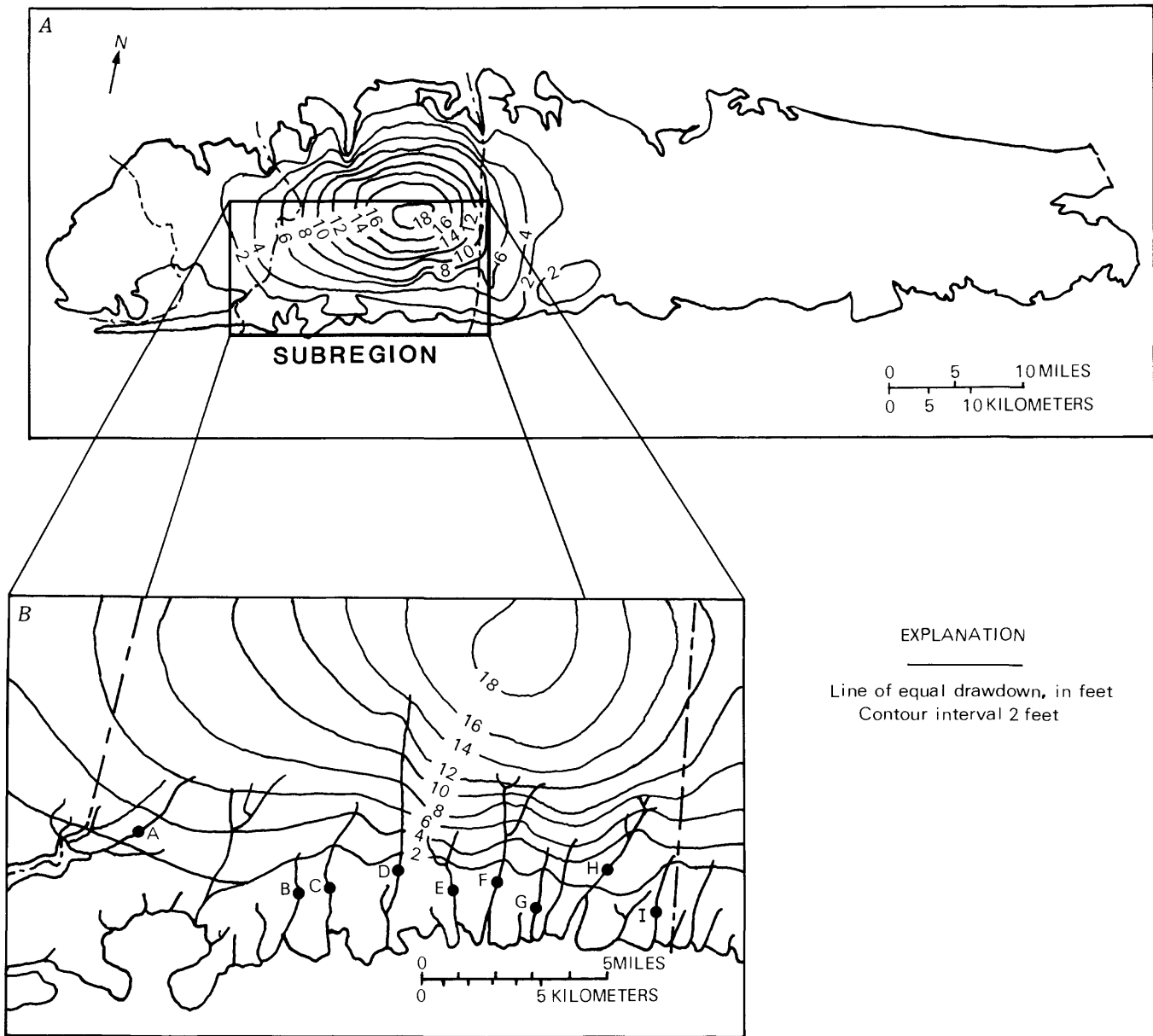
Figure 9. Predicted drawdown of the water table resulting from the loss of ground-water recharge through sewering: A, As simulated by regional model; B, As simulated by coupled regional-subregional model. Gaging stations on major streams: A, Motts Creek; B, Parsonage Creek; C, Milburn Creek; D, East Meadow Brook; E, Cedar Swamp Creek; F, Bellmore Creek; G, Seamans Creek; H, Massapequa Creek; and I, Carmans Creek.

system even though the primary interest is local. De-signing a single model grid that would extend far enough to include all boundaries affected by the stress and, at the same time, give the desired detail in the area of primary concern would be difficult, if not impossible. A variable-spaced finite-difference grid that gives the fine grid size of the subregional grid and expands to the area and block size of the regional grid would have considerably more than 8,000 nodes per layer and would introduce more error than a uniform grid. The Long Island regional model grid has only 2,204 nodes per layer, and the subregional grid has 2,754 nodes per layer,

which are both more manageable sizes. Even a finite-element grid, although more easily adapted to irregular problems, would probably become computationally cumbersome when applied to a problem such as the one presented. In addition, the usefulness of such variable grid models for other applications would be greatly reduced.

The Long Island regional model was designed to predict the regional effect of stresses applied at any location in the system. If a preliminary regional assessment indicates that the stress will have a severe effect, then a subregional or site-specific analysis can be made
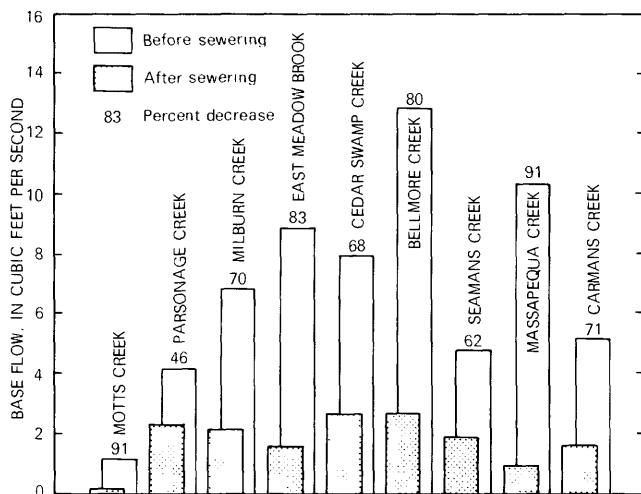
Figure 10. Predicted reduction in base flow due to sewering. (Stream locations are shown in fig. 9.)

which could lead to development of another subregional representation to be coupled with the regional model.

The regional model is used to calculate the distribution of boundary flows (budget) for the subregion. Great care was taken in the Long Island application to maintain an equivalent budget for the subregional representation and the same area of the regional model. The total water loss due to sewering, total recharge from precipitation, and the initial total base flow were the same; however, the distribution of these fluxes was refined in the subregional representation. The finer grid scale and additional data collection within the subregion justify a more detailed representation of irregular natural boundaries, internal hydrogeologic geometry, and complicated stresses, as well as limited refinement in hydrologic coefficients. However, caution should be taken to avoid discrepancy between coefficient values, which could produce a basic inconsistency in the representation of the system.

The degree of refinement allowed in the subregional representation (including the contrast in grid scales) is dependent upon the characteristics of the system being investigated and should be given careful consideration.

Refinement in Representation

In the Long Island application, the greater refinement provided in the subregion is evident by comparison of the regional and subregional grid (fig. 11). In the regional model (fig. 11*A*), an entire stream may be "lumped" into the equation for one or two nodes. Where

several streams must be represented in the same nodal equation, regional predictions of changes in ground-water seepage to streams must be combined for groups of streams or over a large area of the model. In contrast, the subregional grid network (fig. 11*B*) allows the seepage to short lengths of a stream to be represented in each nodal equation, and segments from different streams are never represented in the same model block. As a result, parts of a stream can "dry up" as ground-water levels decline, which enables prediction of changes in base flow and stream length of individual streams.

The collection of additional hydrogeologic data in the subregion during this study enabled some refinements in the thickness and northern extent of the south-shore confining unit; during calibration, these irregularities were found to affect simulated ground-water levels locally. A comparison between the regional and subregional representations of the extent of this unit is given in figure 12. The subregional representation incorporates refinements based on the additional data and the detail allowed by the finer grid. However, both representations are consistent with their respective scales, and, although coarser, the regional representation probably does not cause significant error in prediction of the water budget for the subregional area. If the data warranted, the regional-model coefficients could have been adjusted and the model recalibrated, but this was not considered necessary for this application.

Refinement in Predicted Response

Both the regional and coupled regional-subregional models have been used to predict the hydrologic response to the stress of sewering in Nassau County SDD-2 and SDD-3 and in Suffolk County SWSD. Because these two models represent the same hydrologic system, we sought consistent results by means of model construction and calibration of the coupled model. The equilibrium response of the water table as predicted by both models is shown in figure 13. The coupled simulation shows greater detail, especially near the shore and stream boundaries. The similarity of magnitude and general configuration of the predicted water tables, however, indicate a generally consistent representation of the ground-water system in both models.

SUMMARY AND CONCLUSIONS

This report describes a ground-water flow modeling technique that facilitates analysis of a hydrologic system controlled by hydrologic factors that range from regional to local scale. A regional model represents the entire ground-water system, and a local (subregional) model represents a particular area of concern.

The regional model, designed to give a general representation of the system as far as its natural boundaries, is used to (1) assess the regional response of the system to stresses in terms of ground-water levels and flow and (2) predict the flow budget (the magnitude and distribution of ground water crossing the subregion's artificial boundaries) for the subregion in which a more detailed investigation is desired. The subregional representation is designed in a finer scale and allows detailed representation of specific hydrologic characteristics. A coupled regional-subregional simulation combines to predict the system-wide effects of a stress and yet to give a detailed prediction of ground-water levels and flow in the immediate area of the stress.

The technique was applied to evaluate the effects of a large network of sanitary sewers that is nearing completion (1986) in central Long Island. A previously developed islandwide ground-water model was coupled with a finer scaled subregional representation developed to represent the irregular stream and shoreline boundaries and internal geometry in the immediate area of the sewering stress. The coupled model was calibrated (1) in steady state by simulating predevelopment and present equilibrium conditions, and (2) in transient state by simulating a period of severe drought (1962-66). The coupled model was then used to predict the effects of the sewering stress.
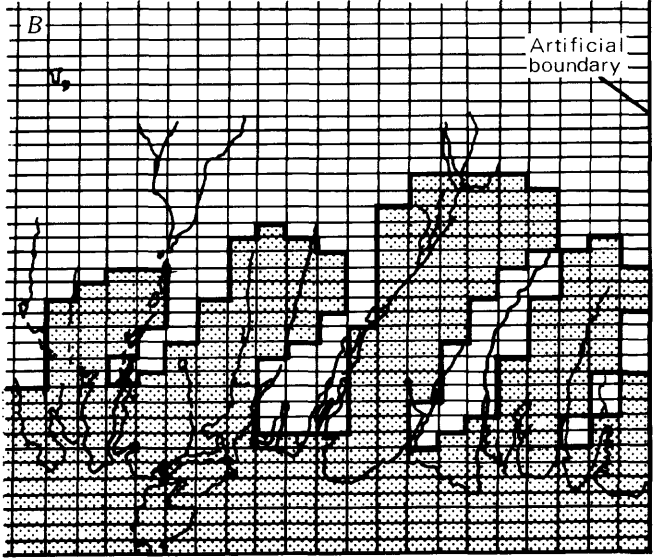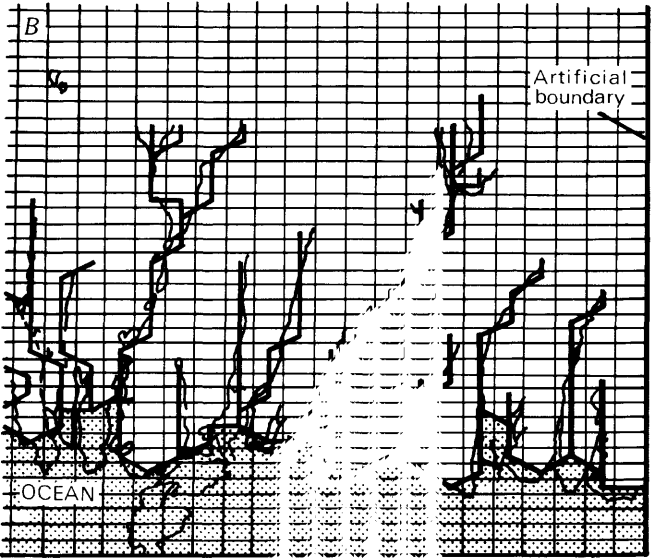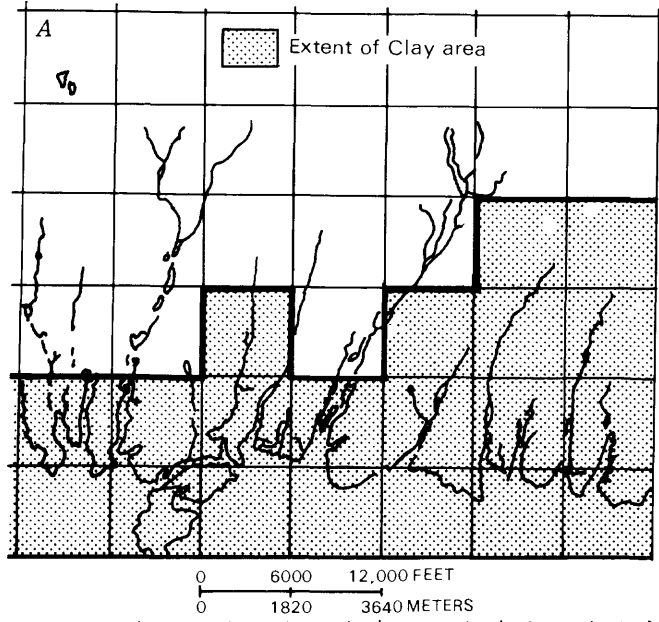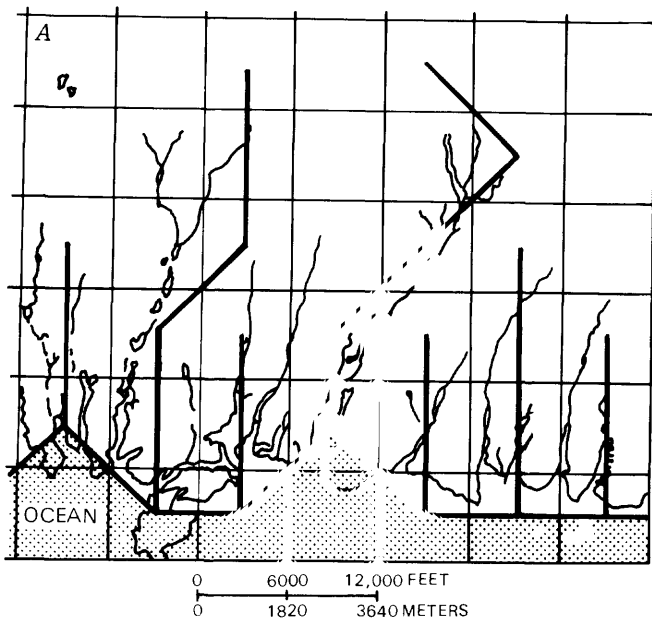
Figure 11. Representation of stream and shoreline boundaries for same area. A, In the regional grid. B, In the subregional grid.


Figure 12. Extent of south-shore confining unit. A, As represented in the regional grid. B, As represented in the subregional grid.

— 6 — Coupled model prediction, in feet

— — 6 — — Regional model prediction, in feet
Contour interval 2 and 4 feet
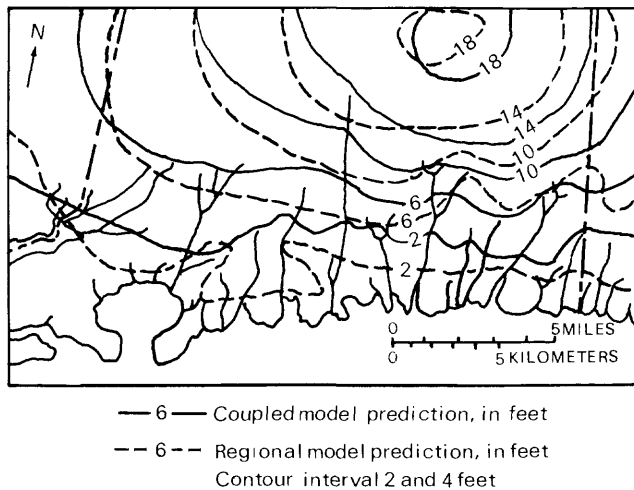
Figure 13. Water-table decline due to loss of recharge from sewering as predicted by regional and coupled regional-subregional models.

This technique has several advantages. Both the regional model and subregional representation can be designed specifically to the intended scale. The regional model can be used to study the mechanics of the entire ground-water system, to make regional assessments of possible future resource-management or development plans, and to calculate boundary conditions for other coupled models.

This technique has proved valuable in analyzing a ground-water system in which both regional and local hydrologic factors control the system's response to stress and where the need for continued analysis for future resource management and development seems likely.

REFERENCES CITED

Buxton, H.T., and Reilly, T.E., 1985, Effects of sanitary sewers on ground-water levels and streams in Nassau and Suffolk Counties, New York—Part 2—Development and application of southwest Suffolk County model: U.S. Geological Survey Water-Resources Investigations Report 83-4209, 39 p.

Cohen, Philip, Franke, O.L., and McClymonds, N.E., 1969, Hydrologic effects of the 1962-66 drought on Long Island, New York: U.S. Geological Survey Water-Supply Paper 1879-F, 18 p.

Franke, O.L., and Cohen, Philip, 1972, Regional rates of ground-water movement on Long Island, New York, *in*

Geological Survey Research 1972: U.S. Geological Survey Professional Paper 800-C, p. C271-C277.

Franke, O.L., and Getzen, R.T., 1976, Evaluation of hydrologic properties of the Long Island ground-water reservoir using cross-sectional electric-analog models: U.S. Geological Survey Open-File Report 75-679, 80 p.

Franke, O.L., and McClymonds, N.E., 1972, Summary of the hydrologic situation on Long Island, New York, as a guide to water-management alternatives: U.S. Geological Survey Professional Paper 627-F, 59 p.

Getzen, R.T., 1977, Analog-model analysis of regional three-dimensional flow in the ground-water reservoir of Long Island, New York: U.S. Geological Survey Professional Paper 982, 49 p.

Harbaugh, A.W., and Getzen, R.T., 1977, Stream simulation in an analog model of the ground-water system on Long Island, New York: U.S. Geological Survey Water-Resources Investigations Report 77-58, 15 p.

Pluhowski, E.J., and Spinello, A.G., 1978, Impact of sewerage systems on stream base flow and ground-water recharge on Long Island, New York: U.S. Geological Survey Journal of Research, v. 6, no. 2, p. 263-271.

Prince, K.R., 1980, Preliminary investigation of a shallow ground-water flow system associated with Connetquot Brook, Long Island, New York, in March 1975: U.S. Geological Survey Water-Resources Investigations Report 80-47, 37 p.

Reilly, T.E., and Buxton, H.T., 1985, Effects of sanitary sewers on ground-water levels and streams in Nassau and Suffolk Counties, New York, Part 3—Development and application of southern Nassau County model: U.S. Geological Survey Water-Resources Investigations Report 83-4210, 41 p.

Reilly, T.E., Buxton, H.T., Franke, O.L., and Wait, R.L., 1983, Effects of sanitary sewers on ground-water levels and streams in Nassau and Suffolk Counties, New York, Part 1—Geohydrology, modeling strategy, and regional evaluation: U.S. Geological Survey Water-Resources Investigations Report 82-4045, 45 p.

Reilly, T.E., and Harbaugh, A.W., 1980, A comparison of analog and digital modeling techniques for simulating three-dimensional ground-water flow on Long Island, New York: U.S. Geological Survey Water-Resources Investigations Report 80-14, 40 p.

Trescott, P.C., 1975, Documentation of finite-difference model for simulation of three-dimensional ground-water flow: U.S. Geological Survey Open-File Report 75-438, 32 p.

Vaupel, D.E., Prince, K.R., Koehler, A.J., and Runco, Mario, 1977, Potentiometric surfaces of the upper glacial and Magothy aquifers and selected streamflow statistics, 1943-72, on Long Island, New York: U.S. Geological Survey Open-File Report 77-528, 18 p., 8 pls.